

THE UNIVERSITY OF CALGARY

KINETICS OF MONOCLONAL ANTIBODY PRODUCTION
IN CHEMOSTAT HYBRIDOMA CULTURES

by

THEODOROS I. LINARDOS

A THESIS

SUBMITTED TO THE FACULTY OF GRADUATE STUDIES
IN PARTIAL FULFILLMENT OF THE REQUIREMENTS FOR THE
DEGREE OF
DOCTOR OF PHILOSOPHY

DEPARTMENT OF CHEMICAL AND PETROLEUM ENGINEERING

CALGARY, ALBERTA

JUNE, 1991

© THEODOROS LINARDOS 1991



National Library
of Canada

Bibliothèque nationale
du Canada

Canadian Theses Service Service des thèses canadiennes

Ottawa, Canada
K1A 0N4

The author has granted an irrevocable non-exclusive licence allowing the National Library of Canada to reproduce, loan, distribute or sell copies of his/her thesis by any means and in any form or format, making this thesis available to interested persons.

L'auteur a accordé une licence irrévocable et non exclusive permettant à la Bibliothèque nationale du Canada de reproduire, prêter, distribuer ou vendre des copies de sa thèse de quelque manière et sous quelque forme que ce soit pour mettre des exemplaires de cette thèse à la disposition des personnes intéressées.

The author retains ownership of the copyright in his/her thesis. Neither the thesis nor substantial extracts from it may be printed or otherwise reproduced without his/her permission.

L'auteur conserve la propriété du droit d'auteur qui protège sa thèse. Ni la thèse ni des extraits substantiels de celle-ci ne doivent être imprimés ou autrement reproduits sans son autorisation.

ISBN 0-315-71141-8

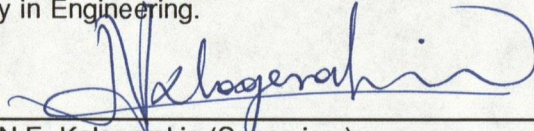
Canada

THE UNIVERSITY OF CALGARY
FACULTY OF GRADUATE STUDIES

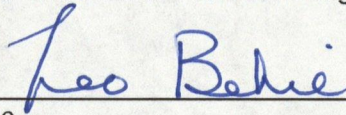
The undersigned certify that they have read, and recommend to the Faculty of Graduate Studies for Acceptance, a thesis entitled,

"Kinetics of Monoclonal Antibody Production in Chemostat Hybridoma Cultures"

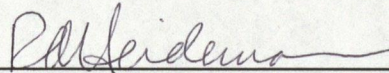
submitted by Theodoros I. Linardos in partial fulfillment of the requirements for the degree of Doctor of Philosophy in Engineering.



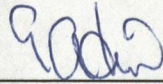
Dr. N.E. Kalogerakis (Supervisor)
Department of Chemical & Petroleum Engineering



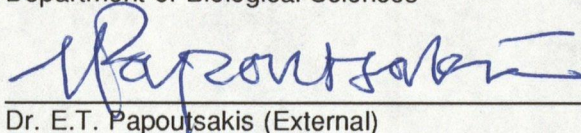
Dr. L.A. Behie
Department of Chemical & Petroleum Engineering



Dr. R.A. Heidemann
Department of Chemical & Petroleum Engineering



Dr. G.A. Din
Department of Biological Sciences



Dr. E.T. Papoutsakis (External)
Northwestern University

Date

June 3, 1991

ABSTRACT

Monoclonal antibodies (MAb) are protein molecules produced in culture by hybridoma cells. The scientists' ability to generate MAb that bind specifically to biological molecules of interest has opened a wide field of applications mainly in the areas of diagnostic and therapeutic medicine. The study of hybridoma culture kinetics has intensified in the recent years, since increasing demand is forcing many companies to turn to bioreactors for the production of their high priced antibodies. The present work sheds light on the kinetics of MAb production with emphasis on chemostat cultures. A commercially important mouse-mouse hybridoma cell line was employed as a model system.

In preparation for the chemostat experiments in stirred tank bioreactors, two sets of batch spinner flask runs were performed. The underlying theme in the first series of experiments was the effort to partially replace glutamine with an alternative nutrient in order to curb the production of growth inhibiting ammonia. Glutamate and α -ketoglutarate, intermediates of glutamine oxidation, were examined first. The effect of varying glucose to glutamine ratio was examined next, since glucose and glutamine are complementary nutrients. Finally, since growth inhibition by shear stress can become significant in stirred tank bioreactors, a second set of spinner flask experiments were performed to investigate the use of methylcellulose in eliminating growth inhibition by shear stress.

Experiments on continuous cultures, although lengthy, are indispensable in kinetic studies as they allow independent examination of the effect of important culture parameters. In the presented chemostat runs in 1.5 L Celligen bioreactors, time lengths up to 4 weeks were required for each steady state and certain experiments exceeded three months in duration. Data collected included viable cell density and cell viability, MAb titer and concentrations of key nutrients and waste byproducts in the reactor. In the first series of chemostat experiments the effect of dilution rate was examined. The values of specific growth and death rate, nutrient uptake and product formation quotients were calculated for each steady state. The effect of pH and dissolved oxygen

concentration (DO) was also examined in chemostat cultures. Cell growth properties varied significantly with pH but no DO effect was found in the range examined. As a continuation of the batch experiments, the effect of glucose to glutamine ratio in the feed was also studied in chemostat cultures. In contrast to the batch culture results, glutamine addition was found to have a negative effect on growth and MAb production in chemostat cultures due to the accumulation of ammonia. Dialyzed chemostat experiments showed that MAb productivity and cell density increased by 40% when ammonia and other low molecular weight inhibitors were removed through the wall of dialysis tubing coiled in the bioreactor. Low cost medium, free of serum or serum replacements was passing through the dialysis tubing at rates up to 5 L/d.

The experimental data from the chemostat cultures were used for the development of a steady state empirical model for cell growth and MAb production. The specific MAb productivity was shown to be a linear function of the specific death rate. In turn, the specific death rate was modeled as an exponential function of the cell age. The effect of stress on nutrient uptake by the cells was modeled by the proposed Generalized Maintenance Energy Model. The underlying idea in the proposed model was that the measured specific death rate can be used to quantify the effects of stress on the cell functions. Excellent agreement was observed with experimental data from this work and from the recent literature.

Further valuable insight on the kinetics of chemostat hybridoma cultures was gained with the development of the cell cycle model. In the proposed model, the specific death rate was shown to be a linear function of the cell fraction arrested in the G₁ phase of the cell cycle. Experimental results from chemostat cultures were successfully described using the cell cycle model. The model can be conveniently incorporated in further cell cycle modeling efforts.

The presented experimental data and the proposed models can form the basis for future research objectives. Moreover, the results of this study can be directly applied to the commercial MAb production by continuous hybridoma cultures.

ACKNOWLEDGEMENTS

My supervisor Dr. Nicolas Kalogerakis offered me the opportunity to work in this exciting project and I sincerely thank him for that. Moreover, I would like to thank him for providing help and inspiration in difficult times. I would also like to recognize Dr. Leo Behie's constant support throughout my years in this University.

I am greatly indebted to Chembiomed Ltd. (Edmonton) for allowing use of their excellent facilities and for backing up financially my experiments. During my work in Edmonton everybody from the administrative staff to the scientists and research directors were always very accessible and extremely helpful and I always felt a part of the team. I would like to thank each one of them and in particular, Dr. Louis Lamontagne who was in charge of this project.

From the Chembiomed staff I would like to mention separately Andrew Graham and Laurie Mallabone for taking the time to teach me the basics in mammalian culture. Narges Djafargoli was always willing to provide expert technical assistance and Heather Good always responded to my requests for advice but also for cell culture equipment and materials. Special thanks to David Lowen for his invaluable help in computer matters. I would also like to thank John Coffin for his assistance with setting up the dialyzed chemostat.

I would like to thank Dieter Moebest for the excellent cooperation during the six months we worked together and for being a good friend. John Iatrou also helped me in the last stages of the work at the Pharmaceutical Production Research Facility, in Calgary. I would also like to take the opportunity to thank the secretaries of the Chemical Engineering Department and especially Norma Wilson, Jeannie Streets and Linda Jeffery for being always friendly and helpful with my frequent requests.

Finally, I would like to express my deepest gratitude to my family for their love, support and patience during the seemingly endless years of my studies in Canada.

DEDICATED TO MY FAMILY

TABLE OF CONTENTS

	Page
APPROVAL PAGE	ii
ABSTRACT	iii
ACKNOWLEDGEMENTS	v
DEDICATION	vii
TABLE OF CONTENTS	viii
LIST OF TABLES	xii
LIST OF FIGURES	xiv
LIST OF SYMBOLS	xxiv
1. INTRODUCTION	1
2. BACKGROUND INFORMATION	5
2.1 ANTIBODIES	5
2.1.1 The immune response	5
2.1.2 Antibody structure and function	6
2.1.3 Biosynthesis of antibodies	8
2.1.4 Monoclonal antibodies	10
2.2 HYBRIDOMAS	11
2.2.1 Formation and properties	11
2.2.2 Metabolism of hybridoma cells in culture	12
2.2.3 Reproduction cycle of hybridoma cells	14
3. KINETICS OF HYBRIDOMA GROWTH AND MA_b PRODUCTION	18
3.1 EXPERIMENTAL STUDIES - LITERATURE REVIEW	18
3.1.1 Effect of nutrient levels on cell metabolism	18
3.1.2 Toxic effect of waste products	19
3.1.3 Effect of pH, dissolved oxygen and temperature	20

3.1.4	Effect of shear stress	22
3.1.5	Effect of growth rate on MAb production	24
3.2	BRIEF REVIEW OF MODELING EFFORTS IN THE LITERATURE	25
3.2.1	MAb production	25
3.2.2	Specific growth and death rate	26
3.2.3	Uptake of nutrients and waste production	27
3.3	SCOPE OF THE STUDY	27
4.	EXPERIMENTAL APPARATUS AND PROCEDURES	29
4.1	MATERIALS AND METHODS	29
4.1.1	Cell line	29
4.1.2	Culture medium	29
4.1.3	Sampling and sample storage	30
4.1.4	Enzymatic methods of analysis	30
4.1.5	HPLC analysis	31
4.1.6	Monoclonal antibody assay	32
4.2	CELL CULTURE EQUIPMENT	32
4.2.1	Spinner flasks	32
4.2.2	Celligen bioreactor	34
4.2.3	Dialyzed chemostat	36
5.	EXPERIMENTAL RESULTS - BATCH CULTURES	38
5.1	EFFECT OF GLUTAMINE TO GLUTAMATE RATIO	38
5.1.1	Non-adapted cells	38
5.1.2	Partially adapted cells	40
5.2	EFFECT OF GLUTAMINE TO α -KETOGLUTARATE RATIO	49
5.3	EFFECT OF GLUCOSE TO GLUTAMINE RATIO	75
5.4	SHEAR PROTECTION BY METHYLCELLULOSE	84

6.	EXPERIMENTAL RESULTS - CHEMOSTAT CULTURES	103
6.1	EFFECT OF DILUTION RATE	103
6.1.1	Viable cell density and viability	105
6.1.2	Growth rate and death rate	105
6.1.3	Nutrient and waste concentrations	107
6.1.4	Monoclonal antibody production	110
6.1.5	Nutrient uptake and by-product formation	114
6.2	EFFECT OF pH AND DISSOLVED OXYGEN	117
6.3	EFFECT OF GLUCOSE TO GLUTAMINE RATIO	129
7.	EXPERIMENTAL RESULTS - DIALYZED CHEMOSTAT	144
7.1	CONTROL CHEMOSTAT RUN	145
7.2	DIALYZED RUNS - BATCH START-UP	145
7.3	DIALYZED RUNS - CHEMOSTAT OPERATION	148
7.4	DISCUSSION	150
7.4.1	Comparison of steady state measurements	150
7.4.2	Effect of dialysis on cell growth	153
7.4.3	Effect of dialysis on the MAb production	155
7.4.4	Concluding remarks	155
8.	DEVELOPMENT OF A STEADY STATE MODEL	157
8.1	MAb PRODUCTION	157
8.2	CELL DEATH	159
8.3	GLUCOSE AND GLUTAMINE UPTAKE	162
8.4	STEADY STATE BEHAVIOR OF THE CHEMOSTAT	165
8.5	CONCLUDING REMARKS	168
9.	DEVELOPMENT OF A CELL CYCLE MODEL	170
9.1	CELL CYCLE REPRESENTATION	170
9.2	PROPOSED MODEL	170

9.2.1	Steady-state death rate	172
9.2.2	Cell age distributions in state A	172
9.2.3	Calculation of cell fractions	175
9.2.4	Steady state growth rate and cycle time	176
9.3	MODEL PARAMETERS	176
9.3.1	Calculation of f_0	177
9.3.2	Calculation of k_c and k_0	178
9.3.3	Calculation of t_B	181
9.3.4	Estimation of T_C and model predictions	181
9.4	RESULTS AND DISCUSSION	181
9.5	CONCLUDING REMARKS	189
10.	CONCLUSIONS AND RECOMMENDATIONS	194
10.1	CONCLUSIONS	194
10.2	RECOMMENDATIONS	196
11.	REFERENCES	197
12.	APPENDIX A: DMEM COMPOSITION	208

LIST OF TABLES

Table	Title	Page
5.1.	Effect of varying glutamine to glutamate ratio on spinner flask cultures of non-adapted cells.	48
5.2	Effect of varying glutamine to glutamate ratio on spinner flask cultures of partially adapted cells.	53
5.3	Effect of varying glutamine to α -ketoglutarate ratio. Results from Experiment 1.	69
5.4	Effect of varying glutamine to α -ketoglutarate ratio. Results from Experiment 2.	79
5.5	Effect of varying glucose to glutamine ratio in batch spinner flask cultures.	80
5.6	Effect of stirring speed on batch spinner flask cultures. No methylcellulose was added in the medium.	85
5.7	Effect of stirring speed on batch spinner flask cultures supplemented with 0.3% <i>w/v</i> methylcellulose.	93
5.8	Effect of methylcellulose concentration on shear protection at a stirring speed of 430 <i>RPM</i> .	98
5.9	Effect of methylcellulose concentration on shear protection at a stirring speed of 560 <i>RPM</i> .	99
6.1	Effect of pH on chemostat hybridoma cultures. Steady state measurements.	120
6.2	Effect of pH on chemostat hybridoma cultures. Steady state	127

	measurements.	
6.3	Effect of glucose to glutamine ratio in the feed medium of a chemostat culture.	130
7.1	Comparison of steady state measurements in dialyzed chemostat cultures with varying dialysis flow rate.	152
7.2	Comparison of calculated steady state parameters for dialyzed chemostat cultures with varying dialysis flow rate.	154
9.1	Summary of parameter values used in the model development.	179

LIST OF FIGURES

Figure	Title	Page
2.1	Schematic representation of an IgG antibody molecule.	7
2.2	Schematic representation of an IgM antibody molecule.	9
2.3	Main pathways of the utilization of glucose and glutamine by mammalian cells.	13
2.4	An elementary representation of the mammalian cell cycle.	17
4.1	Schematic of the 100 mL spinner flasks (Corning, NY) used in this study.	33
4.2	Schematic of the CellLift™ Impeller.	35
4.3	Schematic diagram showing the reactor configuration for the dialyzed chemostat experiments.	36
5.1	Profiles of viable cell density during the batch growth of non-adapted cells in media with three different glutamine to glutamate ratios.	39
5.2	Profiles of cell viability during the batch growth of non-adapted cells in media with three different glutamine to glutamate ratios.	41
5.3	Profiles of glutamine concentration. Non-adapted cells were grown in media with three different glutamine to glutamate ratios.	42
5.4	Profiles of glucose concentration. Non-adapted cells were grown in media with three different glutamine to glutamate ratios.	43
5.5	Profiles of glutamate concentration. Non-adapted cells were grown in media with three different glutamine to glutamate ratios.	44

5.6	Ammonia production during the batch growth of non-adapted cells in media with three different glutamine to glutamate ratios.	45
5.7	Lactate production during batch growth of non-adapted cells in media with three different glutamine to glutamate ratios.	46
5.8	MAB production in batch spinner flask cultures of non-adapted cells. Media with three different glutamine to glutamate ratios were used.	47
5.9	Profiles of viable cell density during the batch growth of partially adapted cells in media with three different glutamine to glutamate ratios.	50
5.10	Profiles of cell viability during the batch growth of partially adapted cells in media with three different glutamine to glutamate ratios.	51
5.11	MAB production in batch spinner flask cultures of partially adapted cells in media with three different glutamine to glutamate ratios.	52
5.12	Profiles of glutamine concentration. Partially adapted cells were grown in media with three different glutamine to glutamate ratios.	54
5.13	Profiles of glutamate concentration. Partially adapted cells were grown in media with three different glutamine to glutamate ratios	55
5.14	Ammonia concentration profiles during the batch growth of partially adapted cells in media with three different glutamine to glutamate ratios.	56
5.15	Profiles of glucose concentration. Partially adapted cells were grown in media with three different glutamine to glutamate ratios.	57
5.16	Lactic acid concentration profiles during the batch growth of partially adapted cells in media with three different glutamine to glutamate ratios	58
5.17	Viable cell density during batch spinner flask cultures of hybridomas in media with three different glutamine to α -ketoglutarate ratios. Results from Experiment 1.	60

5.18	Profiles of cell viability during the batch growth of hybridoma cells in media with three different glutamine to α -ketoglutarate ratios. Results from Experiment 1.	61
5.19	MAB production by hybridoma cells in batch spinner flask cultures with three different glutamine to α -ketoglutarate ratios. Results from Experiment 1.	62
5.20	Profiles of glutamine concentration in batch cultures of hybridomas in media with three different glutamine to α -ketoglutarate ratios. Results from Experiment 1.	63
5.21	Profiles of glutamate concentration in batch spinner flask cultures using media with three different glutamine to α -ketoglutarate ratios. Results from Experiment 1.	64
5.22	Effect of varying glutamine to α -ketoglutarate ratios on ammonia production in batch spinner flask cultures. Results from Experiment 1.	65
5.23	Glucose concentration profiles in batch cultures of hybridomas using media with varying glutamine to α -ketoglutarate ratios. Results from Experiment 1.	66
5.24	Lactic acid concentration profiles in batch cultures of hybridomas using media with varying glutamine to α -ketoglutarate ratios. Results from Experiment 1.	67
5.25	Effect of α -ketoglutaric acid on the viable cell density of hybridomas during batch culture in spinner flasks. Results from Experiment 2.	70
5.26	Effect of α -ketoglutaric acid on the viability of batch hybridoma cultures. Results from Experiment 2.	71
5.27	MAB production in batch spinner flask cultures with varying ratio of glutamine to α -ketoglutaric acid. Results from Experiment 2.	72
5.28	Profiles of glutamine concentration during batch experiments with	73

	varying ratio of glutamine to α -ketoglutaric acid. Results from Experiment 2.	
5.29	Profiles of glutamate concentration during batch experiments with varying ratio of glutamine to α -ketoglutaric acid. Results from Experiment 2.	74
5.30	Ammonia production during the batch growth of hybridoma cells in media with three different glutamine to α -ketoglutaric acid ratios. Results from Experiment 2.	76
5.31	Glucose concentration profiles during batch cultures with varying ratio of glutamine to α -ketoglutaric acid in the medium. Results from Experiment 2.	77
5.32	Lactic acid concentration profiles during the batch growth of hybridomas in media with varying ratio of glutamine to α -ketoglutaric acid in the medium. Results from Experiment 2.	78
5.33	Viable cell density profiles for batch cultures in media containing four different glucose to glutamine ratios.	81
5.34	Cell viability profiles for batch cultures in media containing four different glucose to glutamine ratios.	82
5.35	MAB production in media containing four different glucose to glutamine ratios.	83
5.36	The effect of stirring speed on viable cell density in 100 mL batch spinner flask cultures without methylcellulose. Results from Experiment 1.	86
5.37	The effect of stirring speed on cell viability in 100 mL batch spinner flask cultures without methylcellulose. Results from Experiment 1.	87
5.38	The effect of stirring speed on MAB production in 100 mL batch spinner flask cultures without methylcellulose. Results from Experiment 1.	89
5.39	The effect of stirring speed on viable cell density in 100 mL batch	90

	spinner flask cultures with 0.3% <i>w/v</i> methylcellulose. Results from Experiment 1.	
5.40	The effect of stirring speed on cell viability in 100 <i>mL</i> batch spinner flask cultures with 0.3% <i>w/v</i> methylcellulose. Results from Experiment 1.	91
5.41	MAB production in 100 <i>mL</i> batch spinner flask cultures agitated at various rates. 0.3% <i>w/v</i> methylcellulose was added. Results from Experiment 1.	92
5.42	Viable cell density profiles in 100 <i>mL</i> batch spinner flask cultures stirred at 430 <i>RPM</i> and supplemented with varying MCL concentrations.	94
5.43	Cell viability profiles in 100 <i>mL</i> batch spinner flask cultures stirred at 430 <i>RPM</i> and supplemented with varying MCL concentrations.	95
5.44	MAB production in 100 <i>mL</i> batch spinner flask cultures stirred at 430 <i>RPM</i> and supplemented with varying MCL concentrations.	96
5.45	Viable cell density profiles in 100 <i>mL</i> batch spinner flask cultures stirred at 560 <i>RPM</i> and supplemented with varying MCL concentrations. Results from Experiment 2.	100
5.46	Cell viability profiles in 100 <i>mL</i> batch spinner flask cultures stirred at 560 <i>RPM</i> and supplemented with varying MCL concentrations. Results from Experiment 2.	101
5.47	MAB production in 100 <i>mL</i> batch spinner flask cultures stirred at 560 <i>RPM</i> and supplemented with varying MCL concentrations. Results from Experiment 2.	102
6.1	Chemostat experiments: Viable cell density and viability transients during a step change in dilution rate from 0.5 d^{-1} to 0.4 d^{-1} .	104
6.2	Steady state viable cell density and viability in the chemostat with	106

	respect to the dilution rate.	
6.3	Specific growth rate and death rate in the chemostat as a function of the dilution rate.	108
6.4	Residual nutrient and waste product concentrations at steady states using four different dilution rates.	109
6.5	Steady state MAb concentration in the chemostat as a function of dilution rate.	111
6.6	Steady state values of the specific MAb production rate (q_m) at four different growth rates. Data by Miller et al. (1988) are also shown here.	112
6.7	Steady state specific uptake rates of glucose (q_c) and glutamine (q_n) as functions of the specific growth rate.	115
6.8	Steady state specific production rate of lactate (q_l) and maximum yield of lactate from glucose ($Y_{l/c}$) as functions of the specific growth rate.	116
6.9	Specific production rate of ammonia (q_a) and maximum yield of ammonia from glutamine ($Y_{a/n}$), as functions of the growth rate.	118
6.10	Viable cell density in a chemostat at four different pH values.	121
6.11	Profile of cell viability in a chemostat where pH was controlled at four different values.	122
6.12	Profile of MAb concentration in a chemostat where pH was controlled at four different values (as shown).	123
6.13	Glucose and lactate concentration profiles in a chemostat culture where pH was controlled at four different values.	124
6.14	Glutamine and glutamate concentration profiles in a chemostat culture where pH was controlled at four different values.	125
6.15	Ammonia concentration profiles in a chemostat where pH was controlled at four different values.	126
6.16	Effect of dissolved oxygen (DO) on viable cell density and viability	128

	in a chemostat culture.	
6.17	Profile of viable cell density and viability in a chemostat culture with a 5/1 glucose to glutamine ratio in the feed medium.	131
6.18	Profile of MAb concentration in a chemostat culture with a 5/1 glucose to glutamine ratio in the feed medium.	132
6.19	Profile of lactate and glucose concentration in a chemostat culture with a 5/1 glucose to glutamine ratio in the feed medium.	133
6.20	Profile of glutamine, glutamate and ammonia concentration in a chemostat culture with a 5/1 glucose to glutamine ratio in the feed medium.	134
6.21	Profile of viable cell density and viability in a chemostat culture with a 5/2 glucose to glutamine ratio in the feed medium.	135
6.22	Profile of MAb concentration in a chemostat culture with a 5/2 glucose to glutamine ratio in the feed medium.	136
6.23	Profile of lactate and glucose concentration in a chemostat culture with a 5/2 glucose to glutamine ratio in the feed medium.	138
6.24	Profile of glutamine, glutamate and ammonia concentration in a chemostat culture with a 5/2 glucose to glutamine ratio in the feed medium.	139
6.25	Profile of viable cell density and viability in a chemostat culture with a 5/3 glucose to glutamine ratio in the feed medium.	140
6.26	Profile of MAb concentration in a chemostat culture with a 5/3 glucose to glutamine ratio in the feed medium.	141
6.27	Profiles of lactate and glucose concentration in a chemostat culture with a 5/3 glucose to glutamine ratio in the feed medium.	142
6.28	Profiles of glutamine, glutamate and ammonia concentration in a chemostat culture with a 5/3 glucose to glutamine ratio in the feed medium.	143

7.1	Profiles of viable cell density and viability in the non-dialyzed control chemostat culture.	146
7.2	Profiles of viable cell density and viability in the dialyzed chemostat run with dialysis rate of 5 L/d. The dialyzing medium was standard DMEM with no FBS added. The dialysis tubing had a total length of 3 m and a 1000 molecular weight cut-off.	147
7.3	Profile of MAb concentration in the dialyzed chemostat run with dialysis rate of 5 L/d. The dialyzing medium was standard DMEM with no FBS added. The dialysis tubing had a total length of 3 m and a 1000 molecular weight cut-off.	149
7.4	Profiles of viable cell density and viability in the second dialyzed chemostat run with dialysis rate of 2 L/d.	151
8.1	The specific MAb production rate (q_m) as a function of the specific death rate in chemostat hybridoma cultures. The straight lines were determined using linear least squares regression on the experimental data.	158
8.2	Natural logarithms of steady state death rate values (k_d) versus the inverse of specific growth rate (μ) in chemostat hybridoma cultures. The straight lines were determined using linear least squares regression on the experimental data.	161
8.3	Steady state values of glucose uptake rate versus specific growth rate (data from Chapter 6 of this work). The straight line illustrates the deviation from the maintenance energy model by Pirt (1975) at lower growth rate values.	163
8.4	Experimental data of steady state specific glucose uptake rate (q_c) in chemostat cultures. Data from this work and from Miller et al. (1988) are shown. The curves represent the GME model	164

	predictions for growth rates from $0.5 d^{-1}$ to $1.4 d^{-1}$.	
8.5	Experimental data of steady state specific glutamine uptake rate (q_n) as a function of growth rate, compared with the values calculated using the proposed GME model.	166
8.6	Comparison of experimental data from this work with calculated specific growth and death rate values for dilution rates ranging from $0.5 d^{-1}$ to $1.1 d^{-1}$.	167
9.1	Cell cycle representation used in the development of the proposed model.	171
9.2	Experimental values of death rate in a steady state chemostat culture versus the fraction of cell f_0 arrested in the G_1 phase of the cell cycle.	180
9.3	The steady state cell age distribution in state A as a function of the dilution rate in a chemostat culture.	182
9.4	The profile of the fraction of G_1 arrested cells versus the specific growth rate in steady state chemostat cultures.	184
9.5	Comparison of the model predictions with experimental data of specific growth and death rates from this work.	185
9.6	Comparison of the model predictions with experimental data of specific growth and death rates reported by Miller et al. (1988).	186
9.7	Comparison of the model predictions with experimental data of cell viability in steady state chemostat cultures.	187
9.8	Comparison of the model predictions with experimental data of cell viability reported by Miller et al. (1988).	188
9.9	Model predictions of cell fractions in the division cycle for a range of dilution rates. The parameters used were computed from the chemostat data reported in this work.	190

9.10	Model predictions of cell fractions in the division cycle for a range of dilution rates. The parameters used were computed from the chemostat reported by Miller et al. (1988).	191
9.11	Model predictions of the average cycle time as a function of the specific growth rate in a chemostat bioreactor.	192

LIST OF SYMBOLS

A	a cohort of cells with the same age
C	concentration, $mmol/L$ or $mg\ MAb/L$
d_o, d_1	parameters in Equation (8.3), d^{-1}
D	dilution rate, d^{-1}
e	nutrient economy coefficient, $\mu mol/10^6\ cells$.
f	cell fraction
k_d	overall specific death rate, d^{-1}
k_c, k_0	death rate in cycling and arrested fraction of state A cells respectively, d^{-1}
k_H	ammonia hydrolysis rate, d^{-1}
m	maintenance requirement, $\mu mol/(10^6\ cells \cdot d)$
q	specific uptake (or production) rate, $mmol/(10^9\ cells \cdot d)$
q_m	specific MAb production rate, $\mu g/(10^6\ viable\ cells \cdot d)$
Q_m	volumetric MAb Productivity, $mg/(L \cdot d)$
t	duration of a phase or cycle, d
T_C	critical time, d
v_x	viability
x	cell concentration, $10^6\ cells/mL$
X	cell population
Y	yield coefficient

Greek Letters

α	cell age, d
α	parameter in Equation (1), $\mu g/(10^6\ viable\ cells \cdot d)$
β	parameter in Equation (1), $\mu g/10^6\ viable\ cells$
λ	average culture age, d
λ	rate of cell transition from state A to phase B, d^{-1}

μ	specific growth rate, d^{-1}
τ	age of a cell entering phase B of the cell cycle, d
ϕ	probability density function, Equation (9.18)

Subscripts

a	ammonia
A	state A
B	phase B
c	glucose, cycling cells
C	critical
d	death, dead cells
n	glutamine
l	lactate
m	monoclonal antibody
max	maximum value
min	minimum value
t	total (live + dead) cells
v	viable cells
x	biomass
0	arrested state A cells
1	cycling state A cells

Superscripts

*	reduced value
---	---------------

Abbreviations

ADP	Adenosine diphosphate
ATCC	American Type Culture Collection
ATP	Adenosine triphosphate
AMM	Ammonia

CoA	Cofactor A
DMEM	Dulbecco's Modified Eagle's Medium
DO	Dissolved Oxygen
ELISA	Enzyme Linked Immuno-Sorbent Assay
ER	Endoplasmic Reticulum
FBS	Fetal Bovine Serum
GLC	Glucose
GLN	Glutamine
GLT	Glutamate
GME	Generalized Maintenance Energy (model)
Ig	Immunoglobulin
KGA	α -ketoglutaric acid
LAC	Lactate
MAB	Monoclonal Antibody
MCL	Methylcellulose
MW	Molecular weight
MWCO	Molecular Weight Cutoff
NAD	Nicotinamide Adenine Dinucleotide
NADH	Nicotinamide Adenine Dinucleotide, reduced form
NADP	Nicotinamide Adenine Dinucleotide Phosphate
NADPH	Nicotinamide Adenine Dinucleotide Phosphate, reduced form
TCA	Tricarboxylic acid

1. INTRODUCTION

When Köhler and Milstein (1975) developed the first hybridoma cell line, they cleared the way for the commercial *in vitro* production of monoclonal antibodies, protein molecules of the vertebrate immune system. The most valuable property of monoclonal antibodies is their capability to bind in a very specific fashion with large molecules (antigens), such as the proteins on the surface of invading microorganisms. Antibody-antigen binding results in labeling of the invader for destruction by the cells of the immune system. The extraordinary specificity of MAb makes them indispensable for a wide range of applications in diagnostic and therapeutic medicine, as well as in related research.

Monoclonal antibodies are used today largely for *in vitro* diagnostic tests applicable to both human medicine and animal care. To a certain extent MAb are also used in purification and research. In the area of flow cytometry dyes chemically bound to MAb are attached specifically to the cells of interest so that they can be studied independently. In the area of *in vivo* imaging the principle is basically the same; radioactive labels are bound to MAb which in turn bind to specific sites (e.g. neoplasias etc.) when injected into a patient's body. If powerful toxins are substituted for the radioactive labels, MAb can also guide the toxic agent precisely to the targeted abnormal cells with minimal toxic effect on the surrounding healthy tissue.

With a widening array of applications the demand of monoclonal antibody is expected to increase dramatically in the next few years. Monoclonal antibody-based products used to treat bacterial sepsis or septic shock with an estimated market of more than 400,00 patients are awaiting FDA approval (Thayer, 1991). Monoclonal antibodies used to treat various cancers are also on the horizon as some of the next big biotechnology drugs (Thayer, 1990). Moreover, biotechnology industry revenues in the area of diagnostics are expected to increase by a factor of 10 in the next ten years (Burill and Lee, 1990). The development of the antibody diagnostic market will require a capacity for the economical manufacturing of kilogram quantities of antibody.

Monoclonal antibodies were initially produced by hybridomas grown *in vivo*, in the peritoneal cavities of mice. Scaling up of MAb production in "rodent reactors" is limited by both moral and logistical problems. Tens of thousands of mice would have to be sacrificed to produce a kilogram of MAb. This method is also labor intensive, and hence very costly. In addition, other major drawbacks are inherent in the method, such as recovering and purifying the MAb from the protein rich ascites fluid. Finally, *in vivo* cultures for the production of human-human derived MAb are very hard to imagine.

Hybridoma cells can be propagated indefinitely in culture, i.e. the hybridoma cell lines are "immortal". Furthermore, since they are transformed cells, hybridomas do not need surface attachment to survive and hence can be grown in suspension. Hybridomas in suspension usually grow relatively fast, producing high yields of antibody. Results from *in vitro* hybridoma cultures, however, show that they produce MAb titers almost ten times lower than those achieved in the ascites fluid of mice (Birch et al. 1984). Therefore, large scale cultures will be required for commercial production of antibodies in high quantities. When it comes to scale-up from the 1 L bench scale reactors to the production reactors with hundreds of liters of capacity, the key element for success will be the understanding of the kinetics of hybridoma growth and MAb production.

Unlike bacterial cell fermentations, hybridoma cell cultures are very complicated to study, due to the cell sensitivity to many nutritional and environmental factors. Also mammalian cells in general are extremely sensitive to shear stress and can only survive within very narrow ranges of pH and temperature. They require a complex medium with two basic carbon and energy sources (i.e. glucose and glutamine). Furthermore, they require growth factors that are supplemented by adding serum to the medium. Finally, the culture kinetics are complicated by the often significant toxic effect of the cell metabolism by-products ammonia and lactate.

Due to their increased sensitivity, hybridoma cells exhibit a death rate that in many cases cannot be neglected as is usually the case in microbial cultures. Furthermore, the cell death rate increases sharply at lower growth rates. As a result, a homo-

geneous, well controlled physiological environment and a reliable growth rate control mechanism is a desirable feature of a hybridoma culture. Chemostat cultures are very well suited to fill such a requirement. Efficient mixing ensures homogeneity and a desired growth rate can be easily maintained by setting a constant, predetermined flow rate. For research purposes, the kinetics of cell growth and MAb production can be studied at well defined steady states in a chemostat, thus eliminating the effect of transient phenomena, although long terms of over one month are required for each steady state.

In the present study the effects of media composition and culture conditions on hybridoma growth and MAb production were experimentally studied in both batch and chemostat cultures. Experimental results from the chemostat cultures were used in developing models of hybridoma growth, death and MAb production. This thesis documents both the experimental and the modeling efforts with considerable effort devoted to ensuring that the basic concepts will be understood by readers with a chemical engineering rather than a biotechnology background.

After this short introduction, Chapter 2 provides the necessary background information so that a non-expert reader will be able to follow the experimental as well as the modeling work presented. Chapter 3 reviews previous experimental and modeling work on the elucidation of the hybridoma growth and MAb kinetics in culture. The objectives of our work are also presented in the closing part of Chapter 3.

The experimental part of this thesis commences with Chapter 4 where brief descriptions of the experimental methods and equipment are presented. Chapter 5 contains the experimental results from batch cultures that were used to examine the effect of medium composition and shear stress on hybridoma cells. The results from continuous (chemostat) cultures are presented in Chapter 6. Chapter 7 describes the performance of a dialyzed chemostat culture with respect to the production of monoclonal antibody.

Chapters 8 and 9 present two different steady state models. An empirical model is presented in Chapter 8 that can describe steady state MAb production, cell death and

uptake of glucose and glutamine. A cell cycle model of hybridoma growth and death in chemostat cultures is presented in chapter 9.

Finally, the conclusions from the entire thesis are summarized in Chapter 10. In the same chapter recommendations are given for further work in the area of hybridoma cell culture.

2. BACKGROUND INFORMATION

2.1. ANTIBODIES

The immune system, unique to vertebrates, is a set of mechanisms that serves a double purpose: firstly it fights threatening microorganisms such as bacteria and viruses when they invade an animal's body and secondly it "remembers" an invader long after the initial encounter and efficiently fights it off when it challenges again. If the various types of blood cells are the soldiers of the war machine (immune system), then the antibodies are certainly the "smart bombs" each type aimed at a very specific target.

Antibodies are protein macromolecules that effectively neutralize the invading organisms by binding directly on their surfaces. Additionally, antibodies precipitate chemical reactions with end result the destruction of the infected cells (complement-mediated cell lysis). The production of antibodies by the immune system is the last step in a sequence of events taking place immediately after the invasion of a microorganism.

2.1.1. The immune response

The reaction of the immune system, called immune response, starts with the recognition of an invading microorganism as "non self". Immediately some of the invaders are engulfed and destroyed by a class of white blood cells, the macrophages. Characteristic molecules on the invader surface membrane, called antigens, are displayed by the macrophages and they signal the invasion to another class of immune system cells, called helper T cells.

The helper T cells bind to the macrophages stimulating them to secrete the lymphokine interleukin 1 (IL-1) at elevated rates. IL-1 stimulates the brain to raise the body temperature, causing fever, which enhances the activity of immune cells. IL-1 further stimulates the helper T cell population to multiply and secrete two more lymphokines: interleukin-2 that stimulates growth and proliferation of killer T cells and B-cell growth factor that causes B-cells to multiply.

Killer T cells sacrifice the body cells that have been infected by a virus by punc-

turing their membranes and disrupting in this manner the proliferation cycle of the invader. B cells, on the other hand, multiply until another lymphokine secreted by helper T cells, the B-cell differentiation factor, instructs them to stop replicating and to start producing antibodies.

2.1.2. Antibody structure and function

Antibody molecules are "Y" shaped and symmetric (Figure 2.1). They are constructed of two "heavy" amino acid chains with molecular weight (MW) from 50,000 to 75,000 and two "light" chains (MW approximately 25,000). The heavy (H) chains are joined by disulfide bonds to each other and each light (L) chain is joined by a disulfide bond to one heavy chain (Figure 2.1). Attached to heavy chains are asparagine-linked carbohydrate sequences.

Within each chain, homology units of approximately 110 amino acids fold up to form domains. Each domain has a single internal disulfide bond which holds it together. An L chain has two domains while an H chain has four or five domains. In most heavy chains a hinge region consisting of a small number of amino acids is found after the first two domains. At the hinge region the cysteine residues are located whose SH groups are linked to form the -S-S (disulfide) bridges between the two monomer units of the antibody dimer.

Antibodies are grouped into five main classes, according to the type of heavy chains; IgM, IgD, IgG, IgE and IgA antibodies possess μ , δ , γ , ϵ and α heavy chains respectively. Individual antibody classes have distinctive structural and biological properties. All classes of immunoglobulin (i.e. antibodies with no known antigen) have one of two types of an L chain protein, called the kappa (κ) and lambda (λ) chains. In mice, 95% of the antibodies have κ light chains whereas in humans it is close to 50%. An individual antibody molecule can have only one type of L chain and one type of H chain.

The first two N-terminal domains of the H chains interact with the two L-chain domains, producing a compact unit, known as the variable (V) region, because it varies greatly between antibody molecules. The variable region acts as the antigen binding

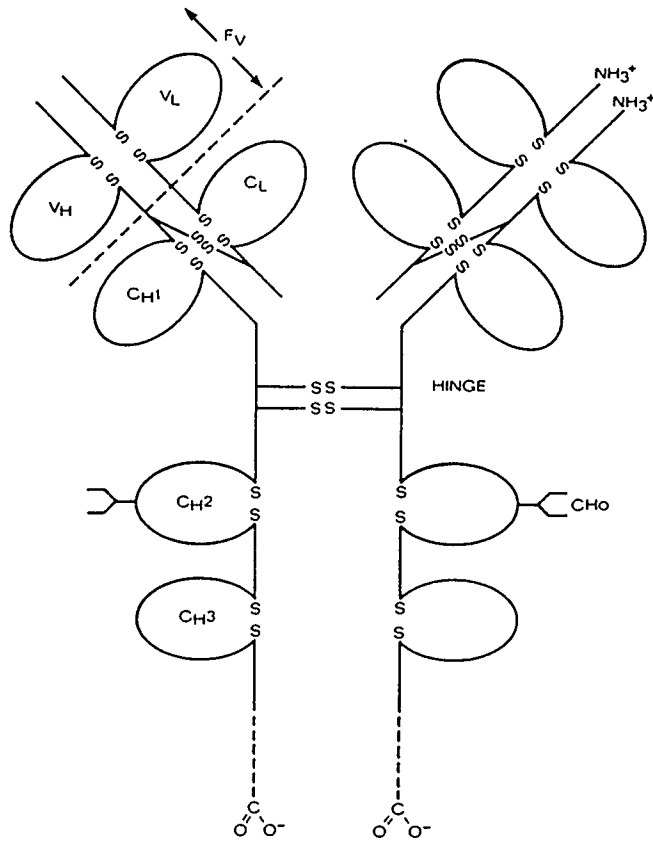


Figure 2.1 Schematic representation of an IgG antibody molecule.

end of the antibody molecule. Each antibody molecule has two identical antigen combining sites except for polymeric IgM which has ten.

In mammals, the secreted form of IgM consists of a pentamer (approximately 900 *kd*). The pentameric IgM formation also contains a single J chain (Figure 2.2), a very acidic polypeptide (≈ 15 *kd*), which is very rich in carbohydrate and cysteine residues. The J chain is involved in the polymerization of IgM, and is probably added in the endoplasmic reticulum. IgM is the first antibody to appear in most immune responses. In some cases, particularly for autoantibodies, it may be the only class represented. IgM antibodies are usually of relatively low affinity, and their affinity does not seem to rise (i.e. "mature") with time. The relatively low affinity of IgM antibodies is compensated for by multivalency. Because pentameric IgM has ten binding sites its functional affinity may be extremely large, and it may thus perform well in an initial response to infection (Goding, 1983). Furthermore, IgM antibody is very effective in complement-mediated cell lysis.

2.1.3. Biosynthesis of antibodies

The biosynthesis of antibodies follows the same general pathway as other secretory and membrane proteins containing carbohydrate molecules (glycoproteins). Nascent chains are formed on polyribosomes bound to the cytoplasmic surface of the endoplasmic reticulum. The N-terminal hydrophobic "leader sequence" of the nascent forms guides them through the membrane and into the lumen. As the nascent chain appears on the luminal side, its leader sequence is proteolytically removed and the carbohydrate groups are added (glycosylation). Secretory forms of heavy chains pass into the lumen, while membrane forms remain embedded in the membrane via their hydrophobic C-terminus. Membrane and secretory forms are assembled in the same intracellular compartment.

Shortly after synthesis, pairing of heavy and light chain commences. In some cases the order of assembly is H- HH- HHL- LHHL, while in others it is H - HL - LHHL. Assembly appears to depend on random collision and follows the law of mass action.

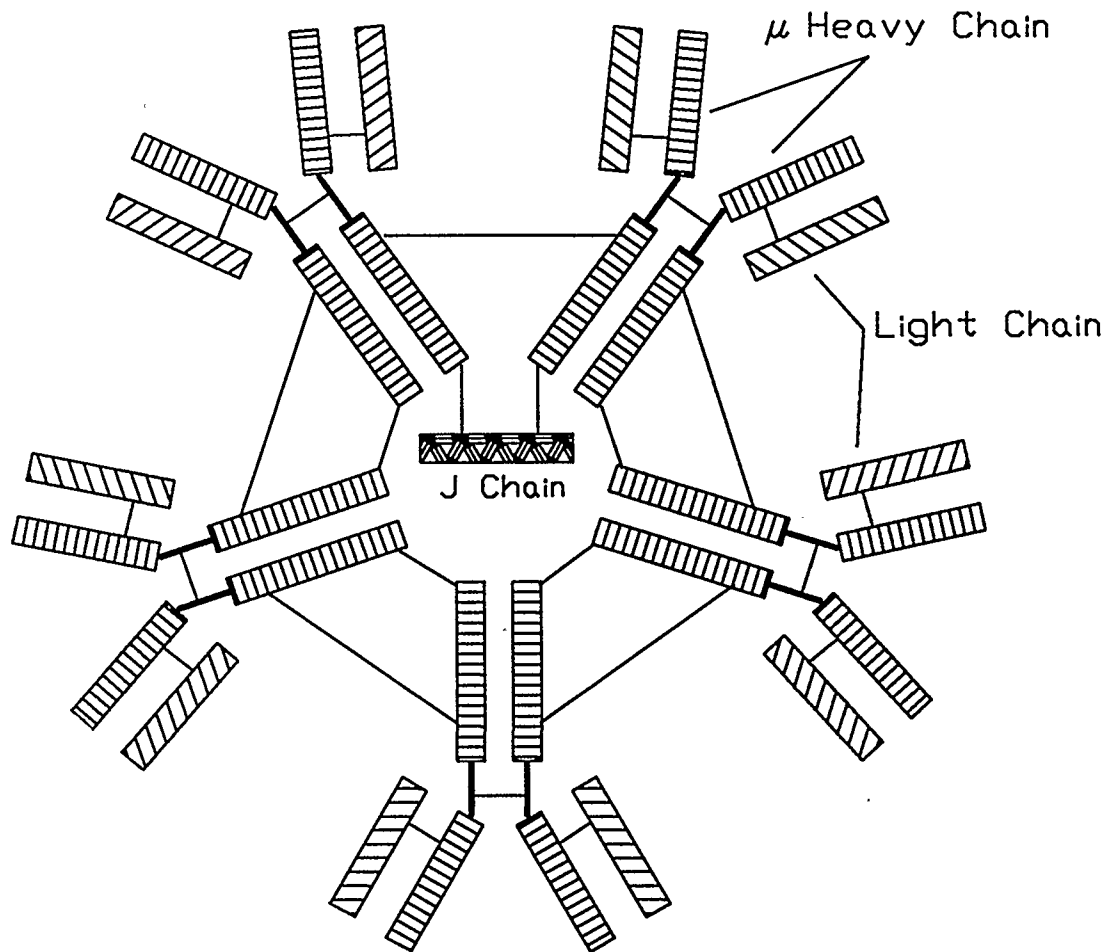


Figure 2.2 Schematic representation of an IgM antibody molecule.

Most immunoglobulin-secreting cells make an excess of light chains, and these are usually secreted. Isolated heavy chains without light chains are thought to be toxic to the cell. Following initial glycosylation and assembly, immunoglobulins are transported to the Golgi apparatus where the carbohydrate chains are trimmed and galactose and sialic acid added. Polymerization of IgM to the pentameric form and addition of the J chain occur in the endoplasmic reticulum.

2.1.4. Monoclonal antibodies

In a normal organism there exists a large variety of antibodies of a given class, each recognizing a specific antigen. To explain the capability of the immune system to respond to a practically unlimited variety of antigenic structures, the "clonal selection theory" is generally accepted today. According to this theory all antibody producing cells are identical but occur in the form of clones. Each cell clone produces only one specific antibody (however, several cell clones, producing different antibodies against the same antigen, can coexist in any normal organism). The clones can be stimulated into proliferation and antibody production by the antigen the antibody is directed against.

The capability of isolating and selectively culturing an isolated clone of B lymphocyte cells producing "monoclonal antibody" is of great importance to clinical research. The monoclonal antibodies are beginning to find commercial applications, especially in the field of diagnostic assays. In the case of diagnostic applications, although the amount of antibody used in each test may be trivial, kilogram quantities may be required per year, if the test is widely used (Birch et al., 1984).

The first large scale use of monoclonal antibodies was for ABO blood typing. In Alberta, Chembiomed Ltd. (Edmonton) is currently producing an array of blood typing reagents. Its neighbor Biomira is specializing in antibodies for *in vivo* imaging and therapeutic applications. In the case of *in vivo* imaging, if one assumes that a few hundred micrograms are used per patient, then for each 10,000 patients one will require several grams of antibody. Veterinarian applications may also require large quantities of monoclonal antibody. Molecular Genetics Inc. has developed a monoclonal-antibody based

therapy for Scours disease in newborn calves. In the case of immunopurification, applications are still at a relatively small scale, but as antibodies become available in larger quantities and more cheaply we are likely to see an increasing interest in large scale applications, using perhaps kilograms of antibody.

2.2. HYBRIDOMAS

Köhler and Milstein (1975) were credited with the "invention" of hybridomas, produced by the fusion of tumor cells, called myelomas, and antibody producing spleen cells. The hybridoma cell lines were designed to propagate indefinitely in culture and produce antibody of the desired specificity.

2.2.1 Formation and properties of hybridoma cells

Each normal B lymphocyte from a mouse spleen is capable of producing a single antibody. If a mouse is injected with an antigen, a B lymphocyte cell that makes an antibody against the specific antigen is stimulated to grow and form a clone of cells in the spleen or in the bone marrow. Normal lymphocyte lines, however, have a limited lifespan in culture. The difficulty is resolved by fusing normal B lymphocytes, with cancerous lymphocytes called myeloma cells. Unlike normal lymphocytes myeloma cell lines are "immortal", i.e. they are capable of proliferating indefinitely in culture.

Many different cultured cell lines of myeloma cells from mice and rats have been established. From these, mutant cell lines have been selected that are unable to grow in a special (HAT) medium containing hypoxanthine, aminopterin and thymidine. When these mutant myeloma cells are fused with normal antibody-producing cells from a rat or mouse spleen, hybridoma cells result. Like myeloma cells, hybridoma cells can proliferate indefinitely on culture; like normal spleen cells, the fused cells have enzymes enabling them to grow in HAT medium. If a mixture of fused and unfused cells is placed in HAT medium, the unfused mutant myeloma cells will not be able to survive and the unfused spleen cells die due to their limited life span in culture. Therefore, what remains is a culture of immortal hybridoma cells each producing a single antibody.

The next step is screening of the hybridomas for the isolation of the clone producing the desired antibody. Typically the technique of limiting dilution combined with Enzyme Linked Immunosorbent Assays (ELISA's) are used for this purpose.

2.2.2. Metabolism of hybridomas cells in culture.

Hybridoma cells are mammalian cells with their origin in an environment (mammalian organism) where all necessary growth factors and nutrients were made available by the host organism. When cultured *in vitro*, hybridoma cells require a complex growth medium containing two basic carbon sources, glutamine and glucose, other amino acids, vitamins and salts. Furthermore, the medium has to be supplemented with serum (usually between 1.0% to 10% v/v). The serum contains all the growth factors necessary for the cell proliferation.

As mentioned above, glucose and glutamine are the major carbon and energy sources used by mammalian cells in culture. Both nutrients have essential anabolic roles but are complementary for the production of other metabolites and energy (Miller et al., 1989a). Figure 2.3 shows the main pathways of utilization of glucose and glutamine in mammalian cells. The proportion of nutrient usage in each pathway depends mainly on the cell type and the metabolic state of the culture.

Glucose mainly proceeds through the anaerobic glycolysis cycle with lactic acid as the end product. A smaller amount of glucose is channeled through the pentose phosphate biosynthetic pathway. Reitzer et al. (1979) showed that 80% of the glucose utilized by a HeLa cell culture was converted to lactate via glycolysis, while only 4-5% entered the tricarboxylic acid (TCA) cycle through pyruvate. Low and Harbor (1985) examined the metabolism of two murine hybridoma lines in four different commercial media. The metabolic quotient of lactate showed a 100% conversion of glucose to lactate. The above authors, however, did not account for the production of lactate from other sources, mainly glutamine.

Glutamine is in most part oxidized to CO₂ in the tricarboxylic acid (TCA) cycle. A glutamine molecule has the α -amino group enzymatically removed to give ammonia and

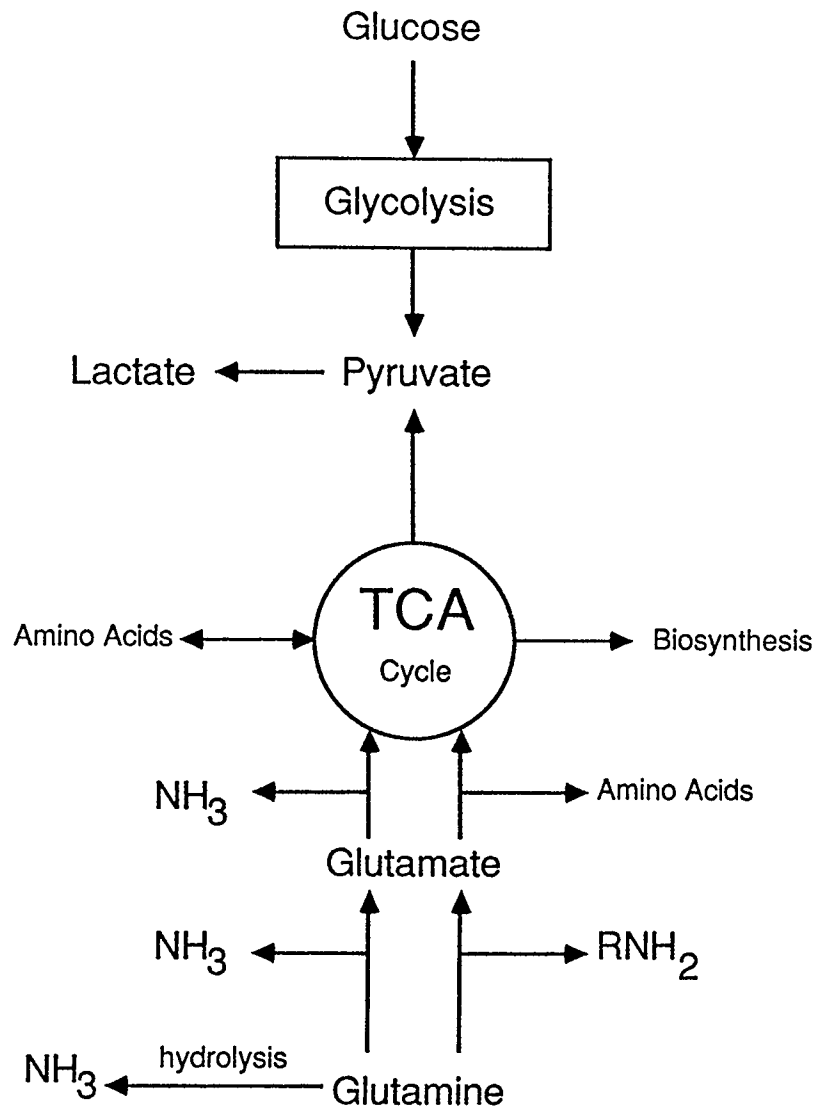


Figure 2.3 Main pathways of glucose and glutamine utilization by mammalian cells.

glutamate. Glutamate is then enzymatically converted into α -ketoglutaric acid, an intermediate in the TCA cycle. Up to two molecules of ammonia can be produced for each molecule of glutamine used. Glutamine metabolism typically provides 30% - 65% of the energy for mammalian cell growth (Reitzer et al., 1979; Zielke et al., 1980). Glutamine carbon is also partially converted to lactate through acetyl-CoA and pyruvic acid. Zielke et al. (1980) concluded from isotope studies that human fibroblasts in culture metabolize up to 13% of glutamine to lactate. In the same study it was also shown that 15% of the glutamine consumed by the cells was converted to glutamate.

Glutamine and other amino acids also serve as building blocks of proteins and other important biomolecules, such as hormones and vitamins. Furthermore, glutamine spontaneously decomposes in the culture medium to form pyrrolidone carboxylic acid and ammonia (Ozturk and Pallson, 1990; Glacken et al., 1986; Tritsch and Moore, 1962).

2.2.3. Reproduction cycle of hybridoma cells

The existence of a cell depends totally on its ability to proliferate. Indeed, the main characteristic of a living cell is its ability to reproduce. Some specialized forms of cells (e.g. spores, cysts etc.) can survive for longer periods of time without reproducing. However, when a cell loses its capability to proliferate then it is destined for death.

The cell reproduction cycle consists of three components: growth, DNA reproduction and cell division. The hybridoma cell cycle is considered to begin with the completion of one cell division and to end with the completion of the next division. The time taken for one cell cycle is the generation time, while the period between two divisions is called interphase. Cell division is a convenient marker because it can be readily observed or measured. In a strict sense, however, the beginning and the end of the cell cycle is a point in early interphase, at which the decision is made to stop proliferation (resulting in "cell arrest") or to proceed to the next cell division.

There are two discrete steps in the cycle, DNA duplication and division or mitosis. These two steps allow the cycle to be divided into four successive intervals, G_1 ,

S, G_2 , and M. G_1 is the time gap between the completion of cell division and the beginning of DNA replication that occurs in the S phase; G_2 is the time gap between the end of DNA replication and the onset of cell division or mitosis; and M is the time taken for mitosis (Figure 2.4). The pre-synthetic G_1 phase represents the most variable period of the cycle. The duration of G_1 in a cell population increases considerably at slower growth rates. Moreover, cells in the same population exhibit widely varying G_1 durations. In contrast, experimental results indicate that the lengths of S, G_2 and M phases in mammalian cells are practically constant, with typical durations of 6-10 h, 3-5 h and 1 h respectively (Prescott, 1976).

The transition probability model of cell growth, proposed by Smith and Martin (1973; 1974) has been very successful in explaining the observed variability in the cell cycle and it has been in direct agreement with a large volume of experimental results (Brooks, 1979; Brooks 1977; Shields, 1979; Shields, 1978; Shields et al. 1978). According to the transition probability model all daughter cells, following mitosis, enter state A which is of indeterminate duration. In state A the cellular activity is not directed towards replication. However, each state A cell has a constant probability per unit time to exit to phase B and to move on towards mitosis. On leaving state A, cells enter phase B in which their activities are "deterministic" and directed towards replication. In addition to the S, G_2 and M phases, phase B also includes the terminal part of the G_1 phase, considered to be of constant duration Alberghina and Mariani, 1978; Burns and Tannock, 1970).

In general, regulation of cell growth in culture could occur by altering either the duration of phase B or the probability of transition from state A to phase B or the fraction of non-cycling (arrested) cells (Shields and Smith, 1977). The duration of phase B is practically constant and does not affect the growth rate significantly. Both the arrested cell fraction and the transition probability, however, have been shown to affect the kinetics of human diploid fibroblasts in culture (Rabinovitch, 1983). Therefore, the arrested cell fraction should be an important variable in a cell cycle model of mammalian cell

THE CELL CYCLE

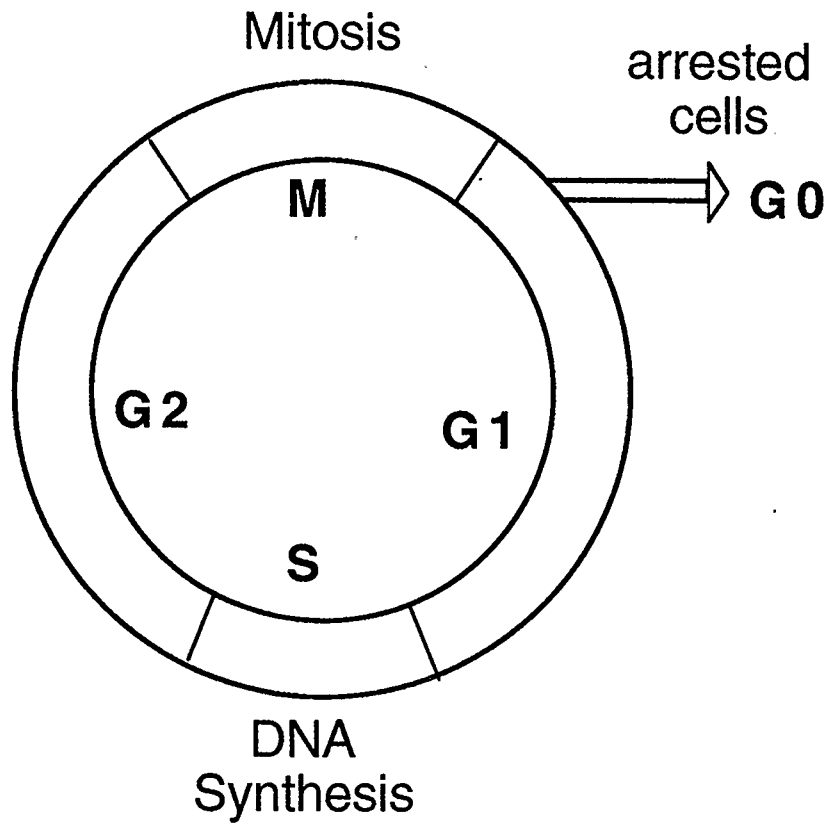


Figure 2.4 An elementary representation of the mammalian cell cycle.

growth and death.

There is experimental evidence suggesting that in mammalian tissues only late G_1 cells leave the germinative population. It was shown specifically, that cell loss does not occur in the S and M phases, and that cells spend a minimum amount of time in G_1 phase before leaving the cycling fraction of the population (deMaerteler, 1978; Quastler and Sherman, 1959). This observation suggests that cell loss must be considerably increased after cells reach a certain age in the G_1 phase. The above observations are in agreement with the existence of a restriction point in late G_1 phase. Cells reaching this restriction point stop dividing and become "arrested", unless signaled to continue through another whole cycle (Alberts et al., 1983; Suzuki and Ollis, 1989a). Arrested cells lose their capability to synthesize DNA and replicate and hence, they eventually disintegrate (Pardee, 1989).

Recently popularized flow cytometric methods enable researchers to distinguish among subpopulations in various cell cycle phases (Darzynkiewicz et al., 1980). Cell cycle models of MAb growth and MAb production are expected to become popular as a result. MAb production was modeled as a cell cycle dependent event by Suzuki and Ollis (1989a) and a cell cycle model of cell growth and death was developed as part of this work. It is expected that even more sophisticated cell cycle models will appear in the near future. However, heuristic models were the first to appear and will remain popular due to their simplicity. The following chapter contains a brief review of experimental and modeling studies that appeared in the literature in the recent years.

3. KINETICS OF HYBRIDOMA GROWTH AND MAb PRODUCTION

3.1. EXPERIMENTAL STUDIES - LITERATURE REVIEW

Many researchers have studied the effects of various parameters on suspension hybridoma cultures. The main findings are summarized in the following paragraphs. Results from cultures of other mammalian cells have also been included.

3.1.1. Effect of nutrient levels on cell metabolism.

A challenging aspect of modeling a hybridoma cell culture is the limitation of the growth rate by two complementary nutrients, glucose and glutamine. Both of these nutrients are necessary for the cell growth but they can be partially substituted by each other. Baltzis and Fredrickson (1988) emphasized the fact that in a system with two potential limiting substrates, the cell yield on each of the nutrients depends on which nutrient is the limiting. The example of a microbial system was presented, where the yield of biomass on ammonia when ammonia limited the growth rate was roughly twice as great as that when glucose was limiting.

A phenomenon that can be attributed to variable yields has been observed in mammalian cell cultures. More specifically, Hu et al. (1987) observed that the glutamine oxidation rate increased with decreasing glucose concentration, while at the same time glucose consumption decreased. The above authors proposed a mixed type inhibition equation to describe the effects of glucose concentration on glutamine oxidation. Miller et al. (1989b) showed that an increase in glutamine concentration in a chemostat culture resulted in increased glutamine and oxygen uptake rates and a reduced glucose uptake rate. Zielke et al. (1978) also observed a reciprocal regulation of glucose and glutamine consumption in a human diploid fibroblast culture. Luan et al. (1987c) tested the effect of various glucose/glutamine ratios on hybridoma batch culture. The results showed that maximum cell growth was obtained in a broad range of ratios from 0.6 to 6.0.

An increased level of glucose has been shown to shift the glucose metabolism from the pentose phosphate pathway to the anaerobic glycolysis cycle producing lactate

(Glacken et al., 1986). Luan et al. (1987a) showed that in batch cultures high glucose concentration leads to extensive lactate formation during the growth phase. It was also observed that oxygen uptake rate was higher when the glucose was depleted. Addition of glucose to a swine testicular cell culture resulted in an immediate decrease in the oxygen uptake. Removal of the glucose resulted in an immediate return to the original rate (Frame and Hu, 1985). Glacken et al. (1986) achieved a significant reduction in the lactate produced in a controlled culture by maintaining a low glucose level at all times. Hu et al. (1987) showed that in batch cultivation the specific consumption rate of glucose and the fraction of glucose converted to lactate can be reduced by programmed feeding designed to keep the glucose concentration low. Finally, high levels of glucose have also been shown to be toxic to certain transformed cell lines; Truskey et al. (1990) showed that glucose levels above 5.5 *mmol/L* inhibited the growth of a human lymphoma cell line.

Wohlpert et al. (1990) investigated the effects of glucose and glutamine levels on the respiration rate of hybridoma cells. It was found that in cells suspended in Hanks balanced salt solution levels of glucose in excess of 1 *g/L* reduced the uptake rate, while addition of glutamine at 0.30 *g/L* increased the respiration rate by 13% when the salt solution contained 0 or 1 *g/L* of glucose. Flickinger et al. (1987), using a cell recycling bioreactor, showed that a significantly greater fraction of cellular maintenance energy is required to maintain hybridoma cells capable of continued MAb secretion at very slow growth rates than during rapid growth.

3.1.2. Toxic effect of waste products

Two main toxic by-products are produced by mammalian cells: lactic acid and ammonia. It has been shown by certain researchers that growth inhibition by lactic acid is very mild or non-existent at the levels measured at the end of a typical batch run, namely 2.0 to 2.5 *g/L*. (Reuveny et al., 1986; Dodge et al., 1987). On the other hand, Glacken et al. (1988) showed that lactate significantly inhibited monoclonal antibody production in initial rate batch experiments. It is suggested that lactic acid toxicity be

examined for the individual cell line and the culture conditions of interest.

Ammonia has been shown to inhibit the growth of many mammalian cell lines including hybridomas (Truskey et al., 1990; Glacken et al., 1986; Reuveny et al., 1986; Reuveny et al., 1987; McQueen and Bailey, 1990). Ammonia toxicity may appear at levels as low as 2 *mmol/L* (Reuveny et al., 1986). In contrast to the findings of most researchers, Jo et al. (1990) concluded that concentrations as high as 8-10 *mmol/L* did not have any apparent toxic effect in dense batch hybridoma cultures growing in a balanced fortified medium. Doyle and Butler (1990) showed that ammonia toxicity varied with the pH of the medium and suggested that ammonia and not ammonium ion may be the toxic species in spent culture medium.

Dodge et al. (1987) found that other inhibitory factors besides ammonia and lactic acid may be formed in the culture medium at the end of a batch culture. These factors were found to be dialyzable, i.e. of a small molecular weight.

3.1.3. Effect of pH, dissolved oxygen and temperature

Operating a reactor as a controlled environment for cell growth requires *a priori* knowledge of the suitable growth conditions. Unfortunately, the responses of different mammalian cells to the same environmental conditions have been found to vary widely (Birch and Edwards, 1980). Therefore, the effects of pH and DO on cell growth and viability have to be established experimentally for each cell line of interest.

The effect of extracellular pH was studied by McQueen and Bailey (1990) in batch hybridoma cultures concluding that pH changes in the range of 6.8 to 7.6 had only minor effects on cell growth. The specific production rate of MAb was not affected. Miller et al. (1988) studied the effect of pH in the range 6.8 to 7.7 on a chemostat hybridoma culture. The optimum pH for the maximum viable cell concentration was found between 7.1 and 7.4. Higher antibody production quotients were obtained at the extreme pH values indicating that stress induces increased MAb production. Higher specific nutrient consumption rates were also observed at the extreme pH values; however, glucose consumption was inhibited at low pH. Birch et al. (1980) studied the effect

of the pH on the growth of a mammalian cell line in batch culture. It was found that growth rate had a broad maximum between pH 7.0 and 7.6. However, the maximum cell density showed a very sharp maximum at the vicinity of pH 7.4. The glucose consumption was measured to be approximately constant between pH 6.8 and pH 7.6 but it dropped dramatically for pH values below 6.8. Lavery et al. (1985) found that pH control did not assist in the prolongation of the growth phase or the delay of death phase in batch hybridoma cultures.

The effect of oxygen on mammalian cell cultures has been studied by many researchers. Kilburn and Webb (1968) examined the growth of LS mouse cells in suspension batch cultures at controlled partial oxygen pressures (pO_2) from 1.6 *mm Hg* to 320 *mm Hg*. They found a well defined optimum range, from about 40 to 100 *mm Hg*, in which the maximum viable cell count was about 1.2×10^6 *cells/mL*. The highest pO_2 level of 320 *mm Hg* was found to be seriously inhibitory, to the extent of permitting only single-stage doubling of the inoculum. Balin et al. (1976) found that cells grown at a dissolved oxygen tension less than 6% of saturation had a significantly reduced growth rate as compared to cells grown at a DO around 30%. Boraston et al. (1984) performed batch runs with a mouse hybridoma cell line producing an IgM antibody, over a range of DO from 0 to 100%. The cell density had a maximum of 1.99×10^6 at a DO of 8% and a minimum of 1.31×10^6 at a DO of 60%. The specific growth rate did not appear to vary as much (0.055 h^{-1} to 0.047 h^{-1}).

Miller et al. (1987) reported that in a chemostat culture the steady state concentration of viable cells increased with a decreasing DO until a critical level of 0.5% of saturation was reached. At lower DO values the glutamine oxidation was incomplete and the glucose consumption and lactate production increased significantly. The oxygen uptake rate was essentially constant at DO values greater than 10% but dropped with DO decreasing below the 10% level. A very interesting point made in this paper was that the optimum for antibody production was 50% as compared to a 0.5% for growth.

Reuveny et al. (1986) showed that temperatures lower than 37°C increased the

time cells remained viable but decreased MAb production. Shureshkumar and Mutharasan (1991) in batch experimental studies found that cultivation temperature significantly affects the specific MAb production rate, the maximum specific growth rate, the specific rates of glucose uptake and lactate production. Within the range of examined temperatures (from 33° to 39° C) the specific MAb production rate increased with temperature. The specific production rate at 33° C was 43% of that observed at 39° C. Maximum specific growth rate at 33° C was about 76% of the value found at other temperatures. These findings indicate that the level of cellular metabolism increases with temperature.

3.1.4. Effect of shear stress

Hybridomas, like other mammalian cells, are extremely sensitive to shear stress due to lack of a protective cell wall. When grown in suspension, hybridomas may be subject to extreme shear forces produced by agitation and by bubble action when direct sparging is employed.

The shear sensitivity of various hybridoma lines has been determined in a reproducible way by using well defined shear conditions in laminar flow viscometers. Abu-Reesh and Kargi (1989) showed that, for the same shear level and exposure time, turbulent shear causes more damage than laminar shear. They formulated a model to predict loss of biological functions at different stress levels and exposure times. In an excellent study Petersen et al. (1988) showed that the shear sensitivity of hybridomas grown in suspension depends on the growth conditions and the age of the culture. Cells from the lag or stationary phases were more sensitive than exponentially growing cells. Lee et al. (1988) reached a similar conclusion using different agitation speed in spinner flask cultures. Schürch et al. (1988), McQueen et al. (1987), Dodge and Hu (1986) and Augenstein et al., (1971) also studied the effects of shear on mammalian cells with similar findings.

In bioreactor cultures the ratio of surface area to cell suspension volume decreases with increasing height. Therefore, Surface aeration may not be adequate to

replenish the oxygen consumed by cells. Air can then be sparged in order to improve oxygen transfer into the medium. The combined effect of agitation and bubble action has attracted attention in recent years. Kunas and Papoutsakis (1989) showed that agitation rates up to 700 *RPM* can be tolerated by cells if there is no vortex formation with bubble entrainment and break-up. Yang et al. (1989) postulated that cells are rendered non-viable by the break-up of large bubbles into smaller bubbles in the impeller stream region. They constructed a model and showed that cell death rate at low cell concentrations is proportional to the total bubble surface area per unit volume of media.

Jöbses et al. (1991) examined the lethal effects of sparging in a bubble column. Their results indicated that bubble break-up was the main cause of cell death. They also found that the protective activity of the surfactant Pluronic F68 against sparging resulted from a direct interaction with cells rather than influencing bubble-liquid interface properties. Kilburn and Webb (1968) showed that cell damage from breaking bubbles can be prevented by increasing the serum concentration or by adding 0.02% Pluronic F68. Ramirez and Mutharasan (1989) suggested that the protective effect of Pluronic F68 is due to the decrease of the plasma membrane fluidity resulting in decreased cell sensitivity. Carboxymethyl-cellulose (methylcellulose, MCL) has been shown to protect melanoma cells and hybridomas against shear damage (Leist et al., 1990, Backer et al., 1988). The increase in medium viscosity has been proposed by Leist et al. (1990) as the main protective mechanism of MCL. The same authors observed a possible toxicity of MCL on human melanoma cells at concentrations in excess of 0.3% (w/v).

Al-Rubeai et al. (1990) studied the effects of hydrodynamic stress on hybridoma metabolism. They found that DNA synthesis is inhibited under conditions of intense hydrodynamic stress. However, cellular metabolic activity is increased, perhaps due to repair mechanisms. The same researchers also found that the sensitivity to stress was increased under conditions of suboptimal culture temperature and nutrient deprivation, possibly due to the inhibition of repair mechanisms.

3.1.5. Effect of growth rate on MAb production

The most important issue in modeling hybridoma cultures is the dependence of MAb production on the state of the culture. In microbial systems the rate of formation of a secondary metabolite is generally proportional to the specific growth rate. One would expect a similar behavior for the formation of MAb.

Results from batch cultures of hybridoma cells do not support the above postulation. Birch et al. (1984) reported that 50% of the antibody in a batch experiment was produced after the stationary phase. Similarly, Reuveny et al. (1985) reported that most of the antibody was produced after the exponential phase of growth. Luan et al. (1987c) concluded from batch experiments that if essential precursors for MAb synthesis are present, MAb formation occurs at a constant rate, in proportionality to the viable cell count. When improved viability was achieved in batch cultures of hybridomas by supplemental feeding of amino acids and vitamins, the MAb titers were four times that found in their typical batch culture (Luan et al., 1987b).

Birch et al. (1984) found in large scale chemostat cultures that the growth rate was not affecting the MAb production rate under glutamine or oxygen limitation. Miller et al. (1988) in a chemostat culture limited by both glucose and glutamine found that the MAb production rate was higher for lower growth rates. Glacken et al. (1988) reported that a positively growth associated specific MAb production rate for growth rates below $0.4 d^{-1}$ becomes constant at growth rates over $0.5 d^{-1}$. Suzuki and Ollis (1989b) studied the effect of various growth and protein synthesis inhibitors on the production of MAb. Their results strongly indicated the existence of intrinsic negatively growth associated MAb production.

The uncertainty about the MAb production kinetics is hampering the effective scale up of MAb producing reactors. Not only the operating conditions but also the reactor type and the mode of operation (batch, fed batch, cell retention etc.) depend on the relationship between growth rate and MAb production. It becomes apparent that the elucidation of the question of MAb production kinetics may result in tremendous time and

cost savings in the hybridoma culture scale up process. Moreover, the large scale production economics will be very attractive, due to increased antibody outputs.

3.2 BRIEF REVIEW OF MODELING EFFORTS IN THE LITERATURE

Due to the complexity of mammalian cell cultures relatively few modeling efforts have appeared in the literature. The majority of models have been empirical but recently structured models of MAb biosynthesis and secretion have appeared. Furthermore, with the popularity that flow cytometry is enjoying recently, cell cycle models of cell growth and MAb production are also becoming popular. The following section is a brief overview of the main modeling efforts in the literature.

3.2.1 MAb production

In the early efforts to elucidate the MAb production kinetics researchers were puzzled by the fact that in batch cultures a very high amount of antibody seemed to be produced in the death phase of the culture. As we have shown in previous paragraphs, even today there is conflicting evidence with respect to the dependence of MAb on growth rate. In steady state chemostat cultures, however, it has become rather clear that a higher specific MAb production rate should be expected at lower growth rates (Miller et al., 1988; Linardos et al. 1991c).

Miller et al. (1988) first showed that in chemostat hybridoma cultures the specific MAb production rate is not a linear function of the specific growth rate. Bree et al. (1988) modeled the MAb production in large scale batch hybridoma cultures using a Monod type equation in biomass with an inhibition term in glutamine, the only limiting nutrient. Dalili et al. (1990) described the behavior of the MAb production rate in glutamine limited batch cultures as a Monod equation in glutamine with a serum dependent coefficient. Suzuki and Ollis (1989a) suggested that monoclonal antibody production is proportional to the fraction of cells arrested in the G_1 phase of the cell cycle. This model simply expressed in mathematical terms experimental evidence already existent in literature (Garatun et al., 1976; Golding et al., 1988; Ramirez and Mutharasan, 1990) and it

was successful in predicting the steady state MAb production rate in chemostat cultures.

Savinell et al. (1989) proposed an equation for estimating the maximum possible MAb specific production rate, based on the availability of mRNA in the cells. Bibila and Flickinger (1991) proposed a structured model for monoclonal antibody synthesis in exponentially growing and stationary phase hybridoma cells. The model was successful in predicting the intracellular heavy and light chain mRNA levels and the extracellular accumulation of antibody during a batch culture. Suzuki and Ollis (1989b) proposed a structured model of MAb synthesis that was based on the principle of mRNA molecule availability during the different cell cycle phases. In their equation, which was similar to that of Savinell et al. (1989), the specific MAb production rate was inversely proportional to the specific growth rate.

3.2.2 Specific growth and death rate

The specific growth rate in batch and continuous hybridoma cultures has been modeled using a Monod equation with glucose and/or glutamine as the limiting nutrient. The proposed equation included inhibition terms for lactic acid and ammonia (Bree et al., 1988; Miller et al. 1988). Frame and Hu (1991) modeled the specific growth rate in continuous culture of non-producing hybridomas. They proposed a Monod-type model in glucose concentration with a threshold glucose concentration and a minimum specific growth rate; the model is meaningful only at glucose concentrations and specific growth rate above these levels. Glacken et al. (1988) proposed a growth rate equation for initial growth rates, that superimposed Monod equations in serum and glutamine with "noncompetitive-type" inhibition relations in ammonium and lactate.

A death rate equation is included, consisting of an inverted Monod-type function of glucose concentration. Bree et al. (1988) modeled death rate as a Monod function of lactate and ammonia containing a death inhibition term for glutamine. A similar death rate relationship was proposed by Dalili et al. (1990) for glutamine limited batch cultures. The proposed equation was based on the postulation that cell death was exclusively a result of the depletion of the limiting nutrient, glutamine.

3.2.3 Uptake of nutrients and waste production

The uptake rate of glutamine was modeled by Miller et al. (1988) using the maintenance energy model (Pirt, 1975). In their chemostat experiments Miller et al. found that the specific uptake rate of glucose deviates from linearity at low growth rates. To account for this observation they added a lactate production term to the maintenance energy model. Bree et al. (1988) and Dalili et al. (1990) also used modified maintenance energy relationships to model the glutamine uptake in glutamine limited batch cultures of hybridomas. Frame and Hu (1991) again proposed a modified maintenance energy equation to describe the glucose uptake in chemostat hybridoma cultures. Glacken et al. (1986) modeled glutamine uptake in batch fibroblast cultures using a Monod type equation in glutamine concentration. All the above models could satisfactorily describe the experimental results they were based upon.

Truskey et al. (1990) used the concept of variable yields in order to model the uptake of glutamine and the production of ammonia in fed batch cultures of a hybridoma and a lymphoma cell line. Batt and Kompala (1987) presented a structured model based on the division of the cell mass in four constituent pools: amino acids and their TCA cycle precursors, nucleotides including RNA and DNA, protein and lipids. The model was successful in describing steady state chemostat data as well as the culture response to step changes in the dilution rate.

3.3 SCOPE OF THE STUDY

The present study has focused on the kinetics of MAb production by suspension cultures of hybridomas. The experiments performed served the purpose of collecting data that were used for the development of an empirical and a cell cycle model. In addition, part of the experimental work was devoted to investigating methods for improving the MAb productivity of suspension cultures by medium manipulation and by employing a new reactor design. The following objectives were identified:

1. Determination of the effect of partial substitution of glutamine by an alter-

nate nutrient on ammonia production, cell growth and MAb production in batch cultures.

2. Determination of the protective effect of methylcellulose against shear stress in batch spinner flask cultures.
3. Study of the effect of glucose to glutamine ratio on cell growth and MAb production in batch and chemostat suspension cultures.
4. Study of the effect of dilution rate on hybridoma growth and MAb production on chemostat cultures at steady state. Elucidation of the effect of growth rate on MAb production. Determination of optimum pH and dissolved oxygen values (ranges) for chemostat hybridoma cultures.
5. Development of a high productivity modified chemostat bioreactor for continuous MAb production using the principle of selective removal of toxic waste by-products and/or nutrient replenishment.
6. Development of an empirical model describing the steady state operation of a chemostat.
7. Application of the cell cycle principles in the development of a model for hybridoma cell growth and death in culture.

4. EXPERIMENTAL APPARATUS AND PROCEDURES

This chapter describes briefly the main materials, equipment and techniques that were used in the experimental part of this work.

4.1. MATERIALS AND METHODS

4.1.1. Cell line

The cell line used throughout this experimental study was the mouse-mouse hybridoma 96.FR2.10, property of Chembiomed Ltd. (Edmonton, Alberta). For the development of this line, spleen cells from mice immunized with OLe^b human red blood cells and the Le^b natural blood group substance were fused with SP 2/0 Ag14 myeloma cells (ATCC) in the presence of polyethylene glycol (PEG). For the immunization both Freud's complete and incomplete adjuvant was used (consisting of 850 mL/L paraffin oil and 150 mL/L Arlachel A, with or without 500 mg/L killed *Mycobacterium smegmatis*).

The fused cells were selected in HAT medium and subcloned by the method of limiting dilution. The anti-Lewis^b producers were finally selected on the basis of OLe^b agglomeration test and by ELISA screening. The 96.FR2.10 hybridoma line isolated secretes an IgM immunoglobulin against the Lewis^b carbohydrate structure. The purified antibody is used in blood typing kits sold worldwide by Chembiomed Ltd.

The cell cultures were regularly screened for mycoplasma infection using the Mycotest method (Gibco). This method is based on the detection of higher than normal concentrations of adenosine phosphorylase, produced by the mycoplasmas. Furthermore, routine tests for bacterial and fungal growth were performed, by culturing the cells in antibiotic free medium typically for a period of 2 weeks.

4.1.2. Culture medium

Dulbecco's Modified Eagle's medium (DMEM; Sigma) was used throughout the present study. The DMEM basal medium composition is given in Appendix A. The concentration of certain components, most commonly glucose and glutamine, were varied in

some experiments, in order to study the effects.

For medium preparation the powdered mixture supplied by Sigma was dissolved in 9.5 L of high quality water. The water used had been deionized by reverse osmosis and subsequently purified in a Mega-Pure water purification system (Corning). The medium was supplemented with 3.5 g/L of D-glucose (Sigma) to a final concentration of 4.5 g/L. The buffering effect was provided by 3.7 g/L sodium bicarbonate also added at this stage (Sigma). In addition, 0.016 g/L of phenol red was added as a pH indicating dye. The pH of the final solution was adjusted to 7.0 with the addition of 4 mol/L hydrochloric acid and the final volume was brought to 10 L with water. The medium was sterilized by filtering through a 0.2 μm Millipack 40 filter (Millipore Corp.).

Before use DMEM was supplemented with 1.5% Fetal Bovine serum (FBS ; Gibco) and 0.033% of a 10 g/L solution of gentamicin sulfate, an antibiotic routinely used at Chembiomed Ltd. Both components were added aseptically.

4.1.3. Sampling and sample storage

Samples were aseptically removed from the cultures. The sample size varied depending on the culture volume. The reactor sample volume was approximately 5 mL, while 2 mL samples were removed from the 100 mL spinner flask cultures. The cell count was performed on a haemocytometer, using trypan blue exclusion for dead cell discrimination. Typically eight cell counts were averaged for the determination of viable cell density and viability. Fresh cell suspension samples were typically centrifuged at 300 g for 10 min and the supernatant was stored at -20° C for further analysis. A small quantity (0.01 % v/v) of 0.01 mol/L thimerosalTM solution was added as a preservative.

4.1.4. Enzymatic methods of analysis

The concentrations of glucose, glutamine, lactic acid and ammonia in the sample supernatant were determined using enzymatic assays (SIGMA). A brief description of the assay principles will be given here.

The glucose assay was based on the enzymatic conversion of glucose to

glucose-6-phosphate. This reaction is coupled with the subsequent reduction of NADP to NADPH by the action of glucose-6-phosphate dehydrogenase. In the presence of NADPH, phenazine methosulfate is reduced. The reduction product is then responsible for the reduction of iodinitrotetrazolium chloride to a product absorbing light at 520 *nm*. The colorimetric response was proportional to the glucose concentration.

Lactic acid was also determined enzymatically. Lactate in the sample was completely reacted with NAD in the presence of the enzyme lactate dehydrogenase, producing pyruvic acid and NADH. The increase of absorbance at 340 *nm* is proportional to the amount of NADH produced, i.e. proportional to the lactate concentration.

A similar enzymatic method was used for the ammonia assay. Ammonia was reacted with 2-oxoglutarate and excess NADH in the presence of glutamate dehydrogenase, to give NAD and glutamic acid. The decrease of absorbance at 340 *nm* was proportional to the ammonia concentration.

Glutamine and glutamate were determined enzymatically in most experiments. Briefly, two sets of supernatant aliquots were used. One was treated with glutaminase in the presence of ADP so that all glutamine was converted to glutamate. Subsequently, both sets were incubated with glutamate dehydrogenase in the presence of NAD. The change of absorbance at 340 *nm* was proportional to the glutamate concentration in the samples. In the first set the glutamate measured included the quantity produced from the glutamine conversion. The actual glutamate concentration was determined in the second set. A subtraction of the second reading from the first reading revealed the amount of glutamate produced by glutamine.

4.1.5. HPLC analysis

Glutamine in certain chemostat experiments was determined by high performance liquid chromatography (HPLC), using a Resolve 5 column (Waters Assoc.). The supernatant solution was appropriately diluted and then derivatized with o-phthalaldehyde (Seaver et al., 1987). The reacted mixture was passed through the column. A UV detector (Hewlett Packard) was used for detection of the derivatized

amino acids at the column outlet.

4.1.6. Monoclonal antibody assay

An Enzyme Linked Immuno-Sorbent Assay (ELISA) was used for the specific determination of MAb. Briefly, a number of ninety six-well plates (Maxisorp, Nunk, Denmark) were coated with antigen, produced synthetically by Chembiomed Ltd. The antigen absorbed on the surface of the polystyrene plate wells. Standards and samples when then added. Antibody in the samples chemically bound to the absorbed antigen. A goat anti-mouse antibody conjugated with the enzyme horseradish peroxidase was coupled to the initial antigen enzyme complex. Excess was removed by a washing step. Subsequently, a color buffer containing o-phenylenediamine was added. In the presence of the enzyme horseradish peroxidase and hydrogen peroxide a yellow colored product of o-phenylenediamine was produced. The absorbance at 490 μm was proportional to the antibody concentration, as it was confirmed by using known standards. A set of standards was included in each plate and a separate calibration line was prepared. Readings from four duplicate determinations per sample were routinely averaged for the MAb titer.

4.2. CELL CULTURE EQUIPMENT

4.2.1 Spinner flasks

In the batch experiments 100 *mL* spinner flasks (Corning) were used (Figure 4.1). The diameter of the cylindrical body of the flasks was approximately 60 *mm*. A 9 *mm* Teflon coated magnetic stirring bar was located approximately 10 *mm* above the flask bottom. The spinner flasks were placed on Bellco multistirrer units located inside incubators at 37° C. 7% *v/v* CO₂ was used in the incubators in order to maintain the pH of the bicarbonate buffered medium in an acceptable area (between 6.80 and 7.20). A strobe light was used to precisely adjust the stirring speed in the beginning of each batch growth experiment. The standard stirring speed was 150 *RPM* but speeds up to 560 *RPM* were used in the shear sensitivity experiments.

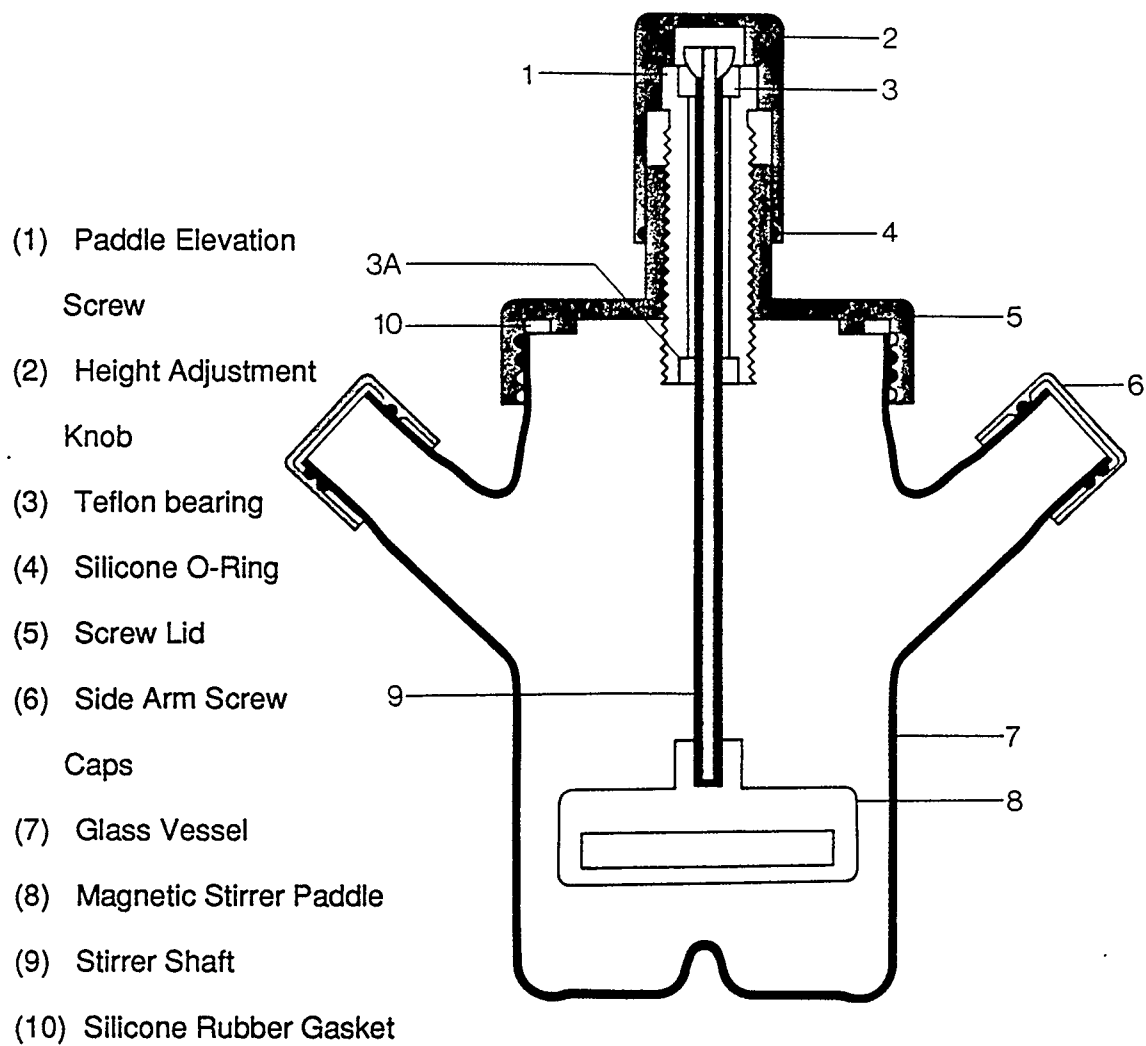


Figure 4.1 Schematic of the 100 mL spinner flasks (Corning, NY) used in this study.

4.2.2 Celligen bioreactor

A 1.5 L Celligen bioreactor was used in all chemostat experiments. The working volume was 1.3 L. The main reactor vessel is made of glass and has a round bottom. The head plate is stainless steel with ports accommodating pH and dissolved oxygen probes, feed and harvest lines, a thermometer well and other auxiliary ports. Heating is provided by an electric heating mat lining the holding clamp of the vessel.

Low shear-mixing is achieved through the CellLift™ impeller, shown schematically in Figure 4.2. The three ports in the upper part of the rotating impeller face in the direction opposite to that of rotation. As a result, a suction effect is produced, which causes the cell suspension to lift gently through the hollow center tube and exit through the ports producing a recirculation pattern. Culture aeration and oxygenation was also provided by the Cel-Lift impeller. A gas mixture consisting of nitrogen, oxygen, carbon dioxide and air was sterilized by passing through a 0.2 μm hydrophobic filter and then entering the sparger embodied in the impeller. The sterile gas stream comes out of the ring sparger at the bottom of the aeration chamber. This chamber is enclosed by a 200-mesh stainless steel screen, which does not allow cells to enter and air bubbles to spread into the bulk medium. Exhaust gas exits through the hollow walls into the upper chamber, above the medium surface and it leaves the impeller assembly through a second screen used for foam destruction in the reactor headspace.

The reactor assembly including the vessel, pH and DO probes and tubing was sterilized in an autoclave at 121° C and 20 psig for 35 min. The reactor vessel was half filled with water during sterilization and properly vented through 0.22 μm filters. Special miniature Luer plugs were used to connect the tubing to the feed and harvest vessels after sterilization. After sterilization, the vessel was pressurized to empty the water into the outlet vessel and the proper amount of medium was gravity fed into the reactor.

The temperature in the reactor was always maintained at 37°± 0.1° C. The pH was controlled at 7.00± 0.05 and the dissolved oxygen concentration (DO) at 30%± 2% of saturation at all times, except when the effect of pH or DO was studied. Feed and

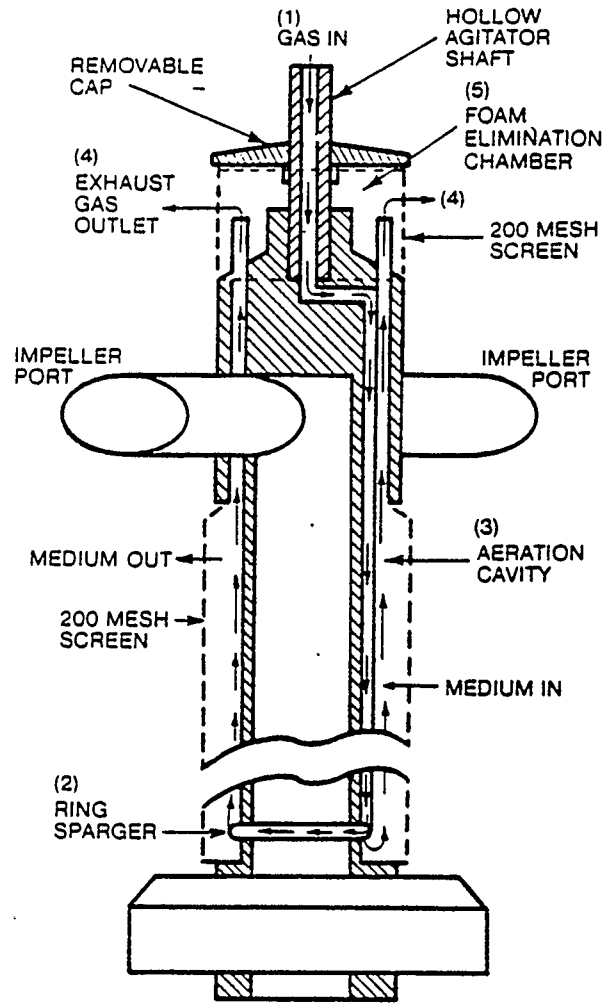


Figure 4.2 Schematic of the CellLift™ Impeller.

outlet flows were produced by a pair of 101U Watson Marlow peristaltic pumps. The outlet intake tube was fixed at the desired liquid level and the outlet pump was set at a slightly higher flow rate so that removal of the medium was ensured when the desired liquid level was exceeded. Silicon tubing was used for the feed and outlet lines.

4.2.3 Dialyzed chemostat

A modified 1.5 L Celligen bioreactor was used in this study. The working volume was 1.3 L. The temperature was maintained at $37^{\circ} \pm 0.1^{\circ} C$. The pH was controlled at 7.00 ± 0.05 and the dissolved oxygen concentration (DO) at $30\% \pm 2\%$ of saturation at all times.

The dialysis tubing (Spectra/Por) was made of cellulose and had a molecular weight cut-off (MWCO) of 1000. The inside diameter and length of the dialysis tubing were 6.2 mm and 3 m respectively. Prior to its use the tubing was boiled in a 0.1 mol/L EDTA solution to remove heavy metal contaminants (Sanbrook and Maniatis, 1989). Before use, the tubing was carefully washed in distilled water to remove any traces of potentially growth inhibiting substances.

Figure 4.3 is a schematic of the reactor configuration showing the dialysis tubing coiled inside the vessel. Each coil had a perimeter of approximately 30 cm. The tubing ends were connected to addition ports on the headplate. The surface area of tubing in contact with the cell suspension was calculated to be 1170 cm^2 and the dialysis surface area per unit reactor volume was approximately $0.9 \text{ cm}^2/\text{cm}^3$. The maximum reactor volume occupied by the tubing was 90 mL corresponding to 7% of the working bioreactor volume. The CellLift Impeller was also used in the dialyzed runs. For sterilization, the reactor and the tubing were filled with distilled water and the whole assembly was autoclaved at $121^{\circ} C$ and 20 psig for 30 min.

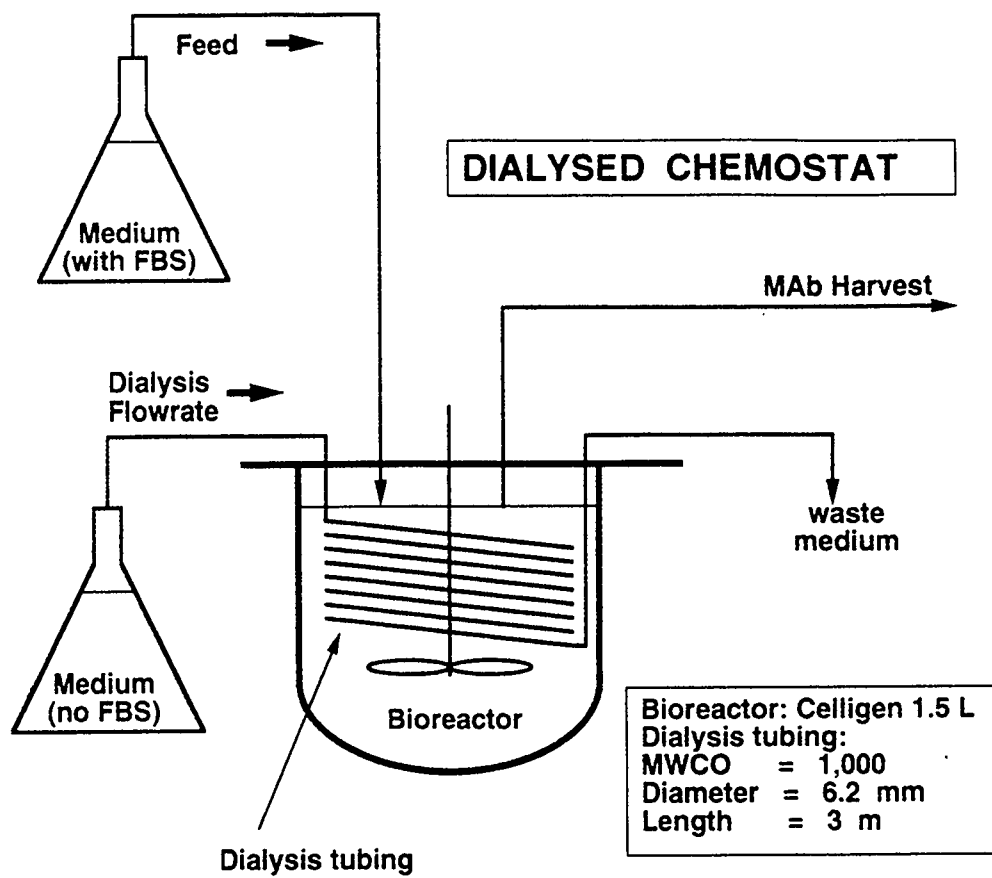


Figure 4.3 Schematic diagram showing the reactor configuration for the dialyzed chemostat experiments.

5. EXPERIMENTAL RESULTS - BATCH CULTURES

In this chapter a series of batch experiments is described. These experiments were performed in order to acquire a working knowledge with the cell line used and, furthermore, to establish media composition to be used in the chemostat mode of operation. There were two main themes in the experimental work. In the first group of experiments (described in sections 5.1, 5.2, and 5.3) glutamine (GLN) was partially substituted by glutamate (GLT), α -ketoglutaric acid (KGA) or glucose (GLC) by varying the ratio of glutamine to the alternative nutrient. The objective was to examine the potential reduction of ammonia production and its effect on hybridoma growth and MAb production. In the second series of experiments (described in section 5.4) methylcellulose was tested as an agent that can alleviate shear stress effects in stirred bioreactors. Batch spinner flask cultures with varying stirrer speeds and methylcellulose content were used for this purpose.

5.1. EFFECT OF GLUTAMINE TO GLUTAMATE RATIO

Two experiments were performed to study this effect; non-adapted cells were used in the first experiment while partially adapted cells were used in the second experiment. The partial adaptation was achieved by culturing the cells for four weeks (approximately 40 generations) in T-25 flasks, using the medium with the glutamine to glutamate ratio to be tested. The total amount of glutamine plus glutamate was kept constant at 4.8 *mmol/L*. Three media were compared: standard (containing no glutamate), 67/33 and 50/50. The glutamine and glutamate contents of the media are given in Table 5.1. Duplicate 100 *mL* spinner flasks were used for each medium type.

5.1.1. Non-adapted cells

Figure 5.1 shows the viable cell density profile during the batch growth of non-adapted cells in the three different media. The main observation is that glutamine content affects very strongly the growth of the cultures. It can be seen that the lower the glutamine content the lower the maximum cell density achieved and the faster the viabil-

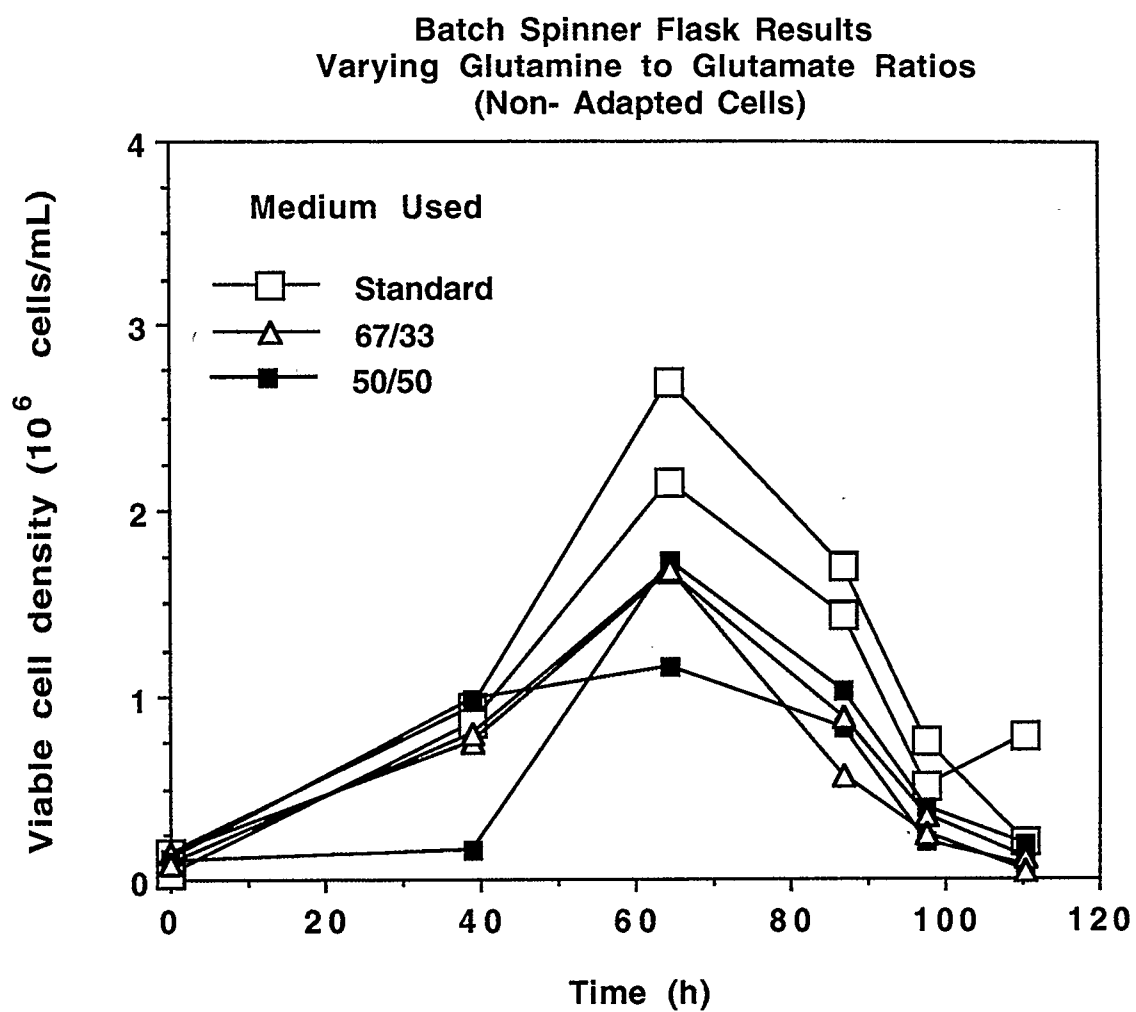


Figure 5.1 Profiles of viable cell density during the batch growth of non-adapted cells in media with three different glutamine to glutamate ratios.

ity drops off after the growth phase (Figure 5.2). It is important to notice that at time $t = 70$ h the viability is identical in the two media with lower initial glutamine content. This fact seems to indicate that the depletion of glutamine and not the presence of glutamate is mainly responsible for the difference in the three types of cultures.

Figure 5.3 shows the profile of glutamine concentration during the batch cultures. It can be seen that the higher the initial glutamine content the longer it takes for glutamine to become depleted. The glucose uptake appears to be much higher in the regular medium (Figure 5.4). However, the fact that glucose uptake is almost the same for the two alternative media, despite the large difference in cell number, seems to suggest that there exists a reciprocal regulation of glucose and glutamine catabolism, as suggested by Zielke et al. (1978) for fibroblast cultures.

The glutamate profiles, shown in Figure 5.5, indicate that there was no appreciable change in the glutamate concentration, although small quantities of glutamate are consumed in the two media with reduced initial glutamine content. This observation confirms that only a very small portion of glutamine can be replaced by glutamate in the medium. The profiles of ammonia in Figure 5.6 correspond to the glutamine profiles, i.e. the higher the initial glutamine content of the medium the more ammonia is produced. The same conclusion is true for lactate production (Figure 5.7).

Monoclonal antibody is the product of interest; therefore, the profiles of MAb production, shown in Figure 5.8, would be the most important indicator. It can be seen that MAb production is highest in the regular medium (also see Table 5.1). In that regard, the substitution of glutamine by glutamate did not have a positive effect of MAb production. The results of this experiment are summarized in Table 5.1 for quick reference.

5.1.2. Partially adapted cells

It was seen in the previous section that there was no positive effect in varying the glutamine to glutamate ratio in batch cultures of non-adapted cells. An experiment with partially adapted cells was undertaken next and the results are shown here.

Unlike with non-adapted cells, the maximum viable cell density in this experiment

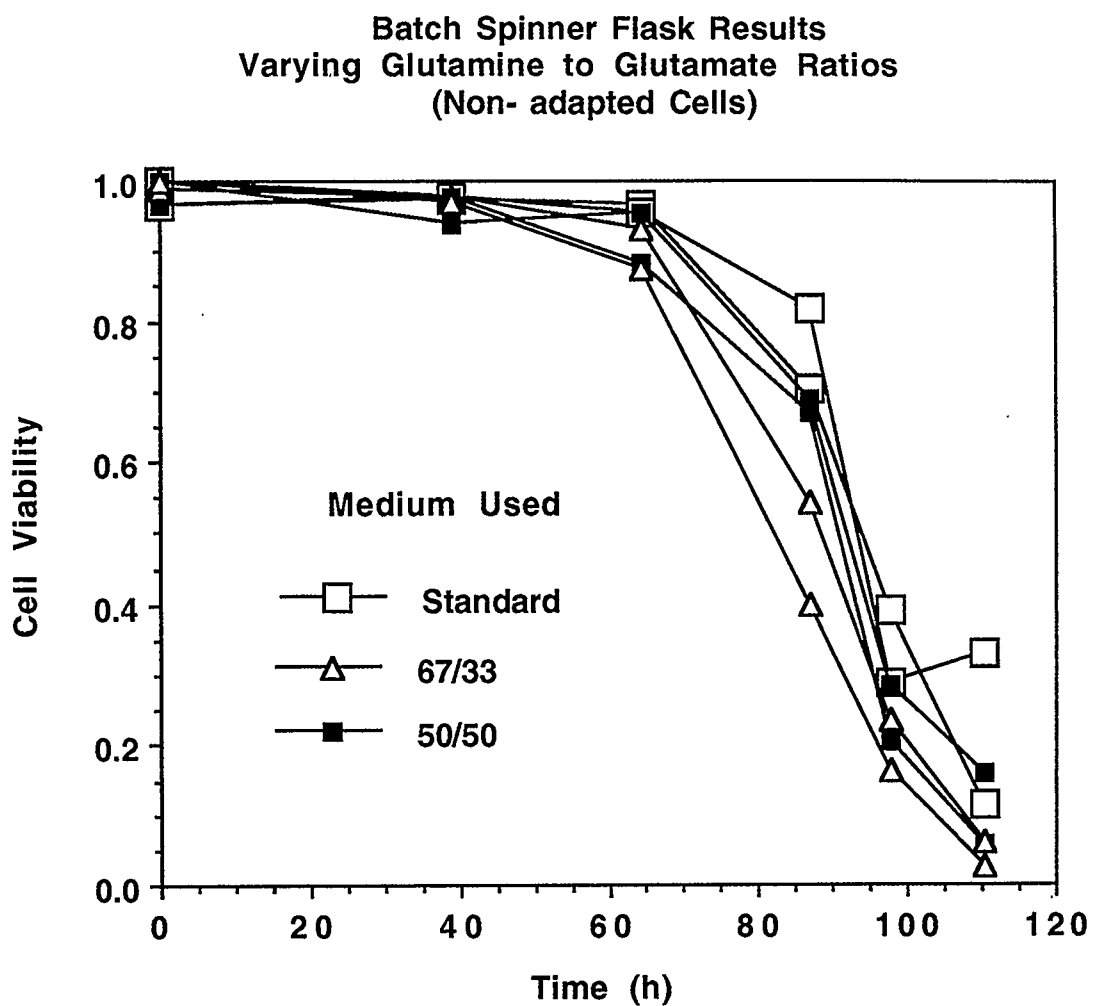


Figure 5.2 Profiles of cell viability during the batch growth of non-adapted cells in media with three different glutamine to glutamate ratios.

Batch Spinner Flask Results
Varying Glutamine to Glutamate Ratios
(Non-adapted Cells)

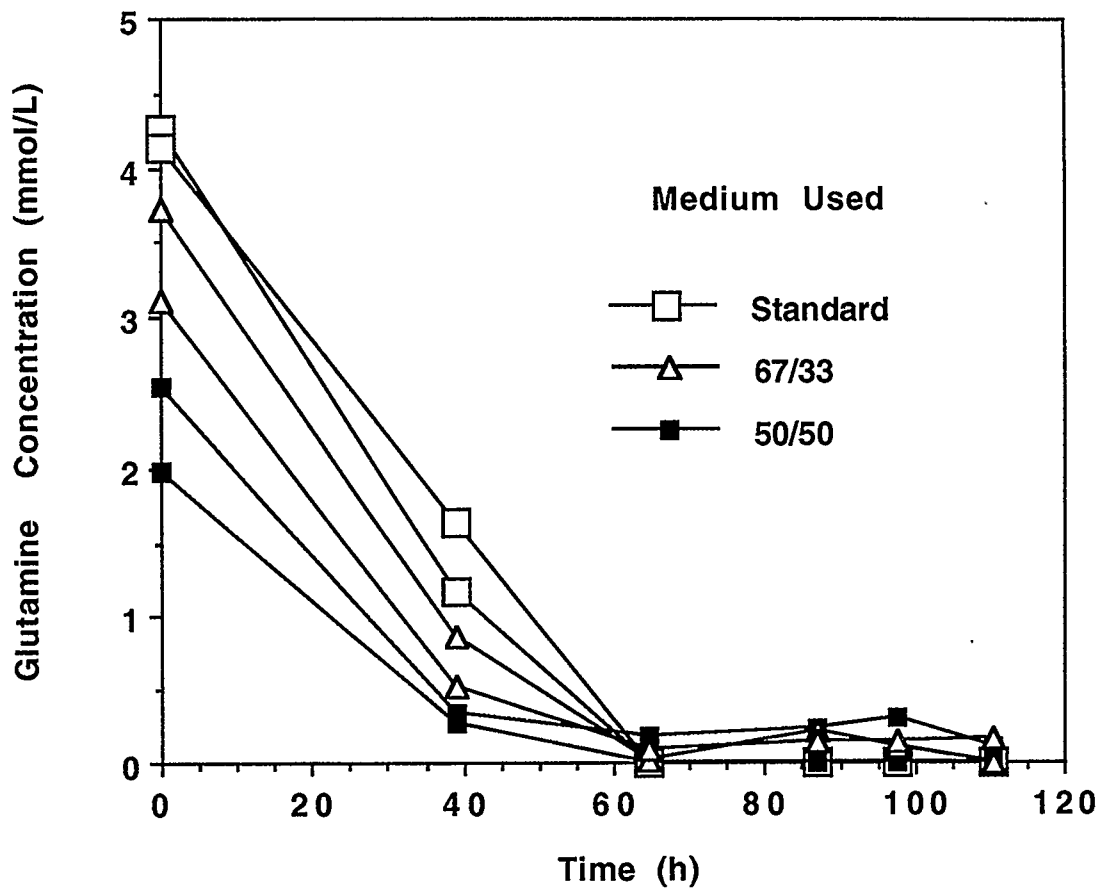


Figure 5.3 Profiles of glutamine concentration. Non-adapted cells cultured in media with three different glutamine to glutamate ratios.

Batch Spinner Flask Results
Varying Glutamine to Glutamate Ratios
(Non- adapted Cells)

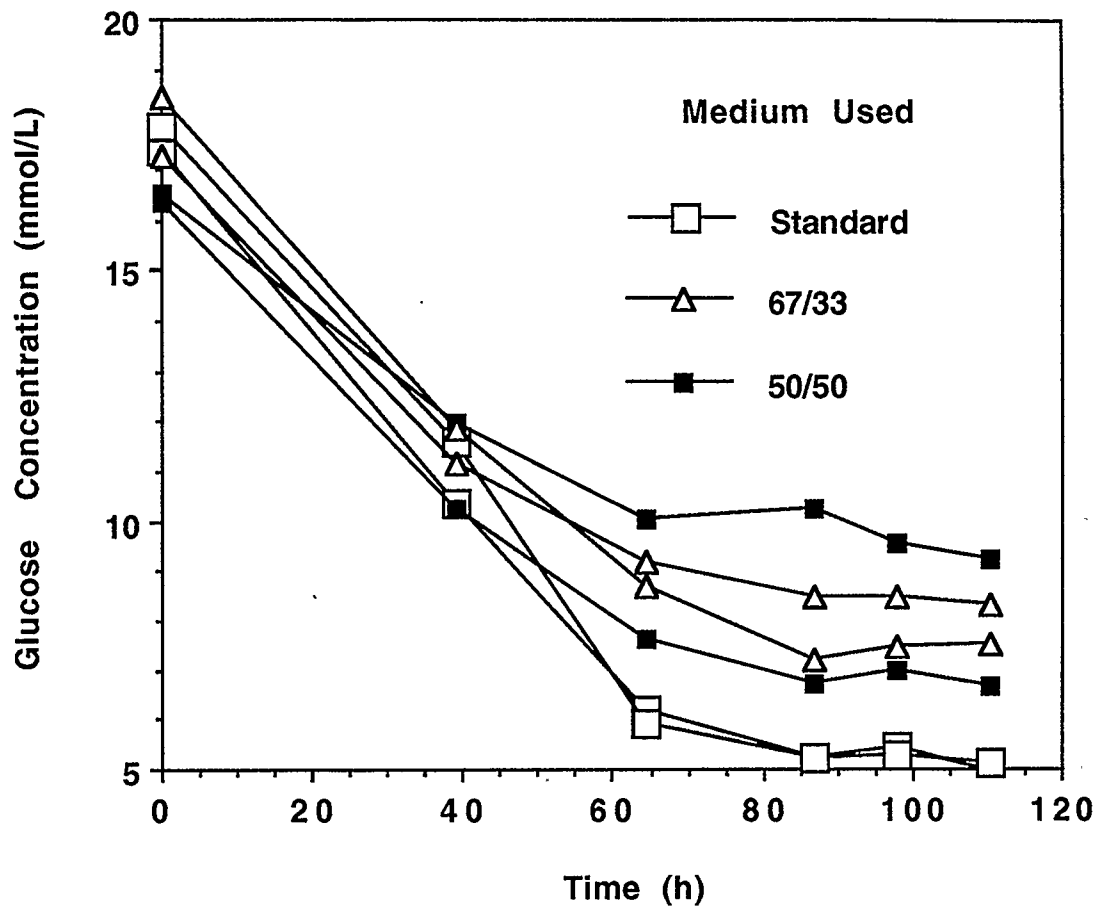


Figure 5.4 Profiles of glucose concentration. Non-adapted cells were cultured in media with three different glutamine to glutamate ratios.

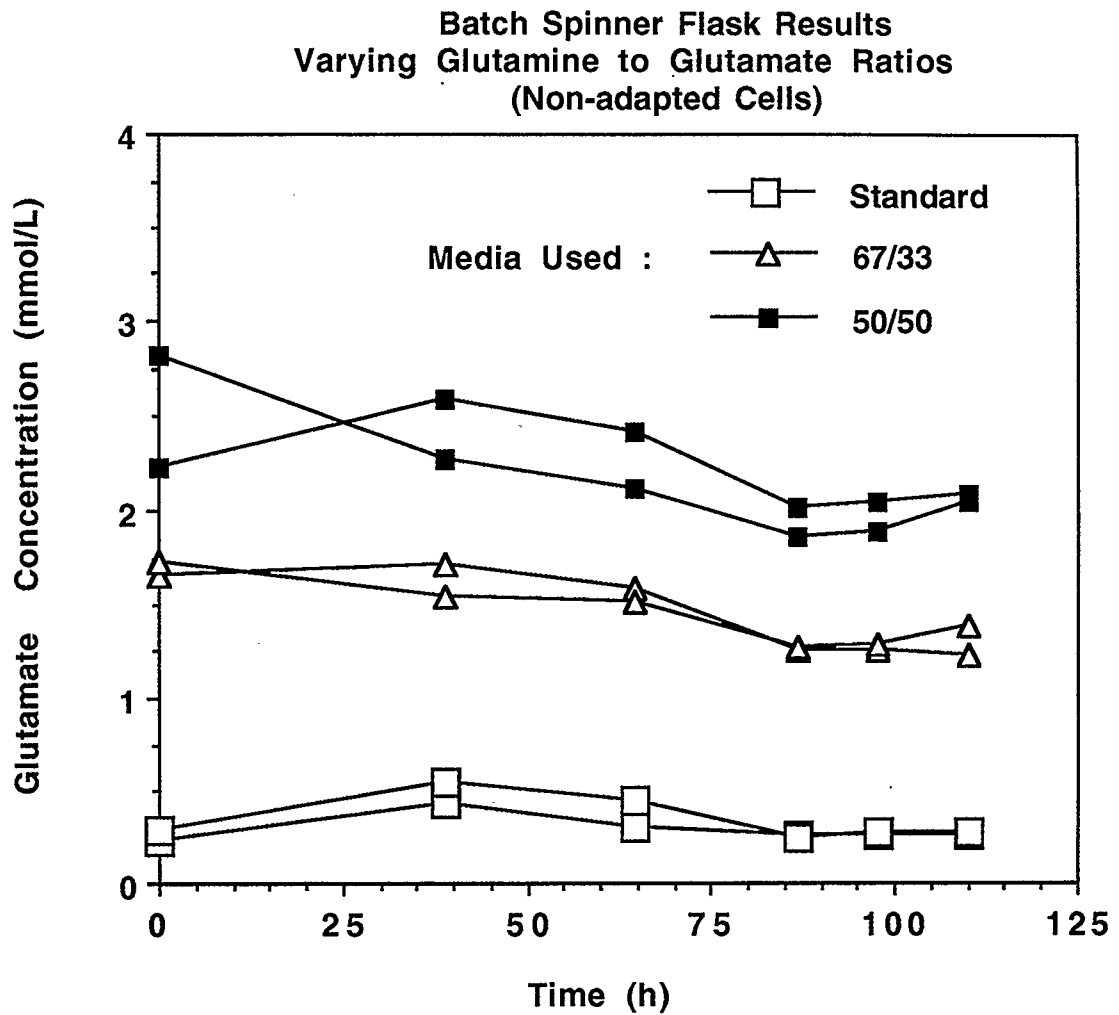


Figure 5.5 Profiles of glutamate concentration. Non-adapted cells were cultured in media with three different glutamine to glutamate ratios.

Batch Spinner Flask Results
Varying Glutamine to Glutamate Ratios
(Non-adapted Cells)

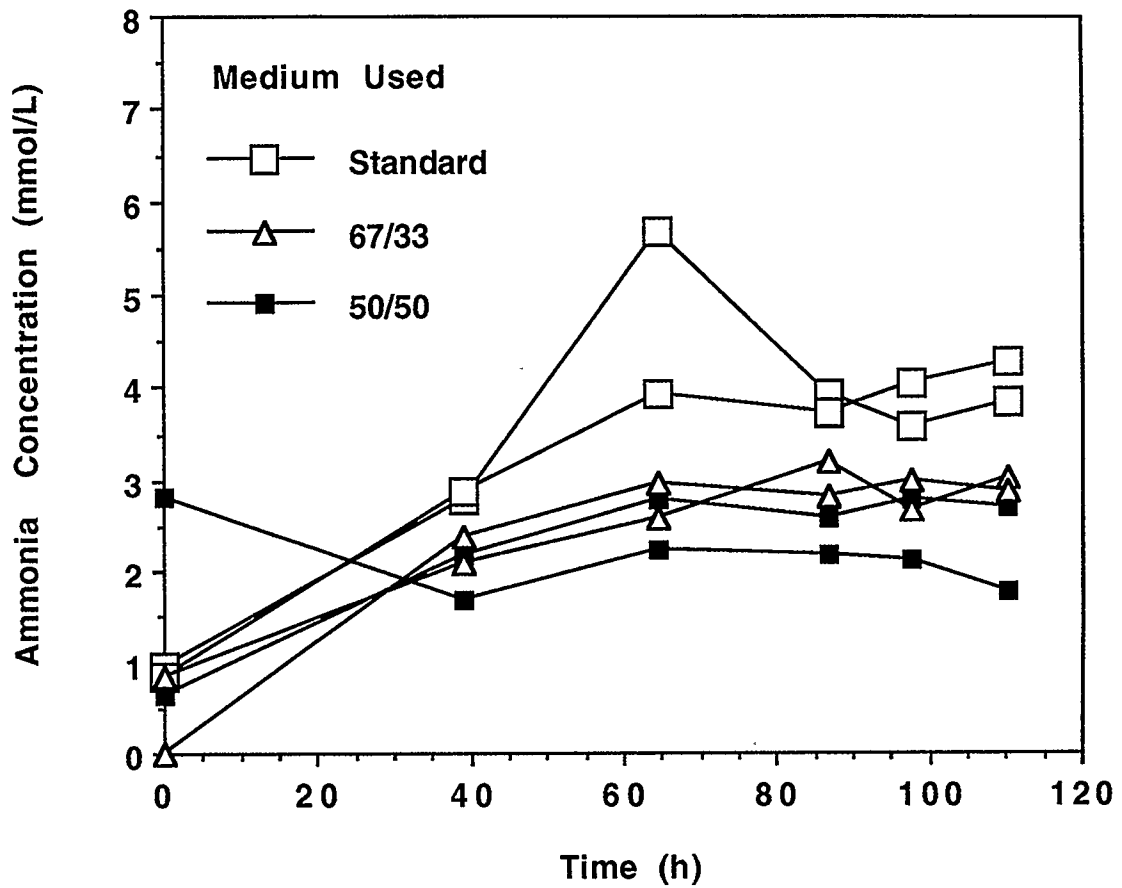


Figure 5.6 Ammonia production during the batch growth of non-adapted cells in media with three different glutamine to glutamate ratios.

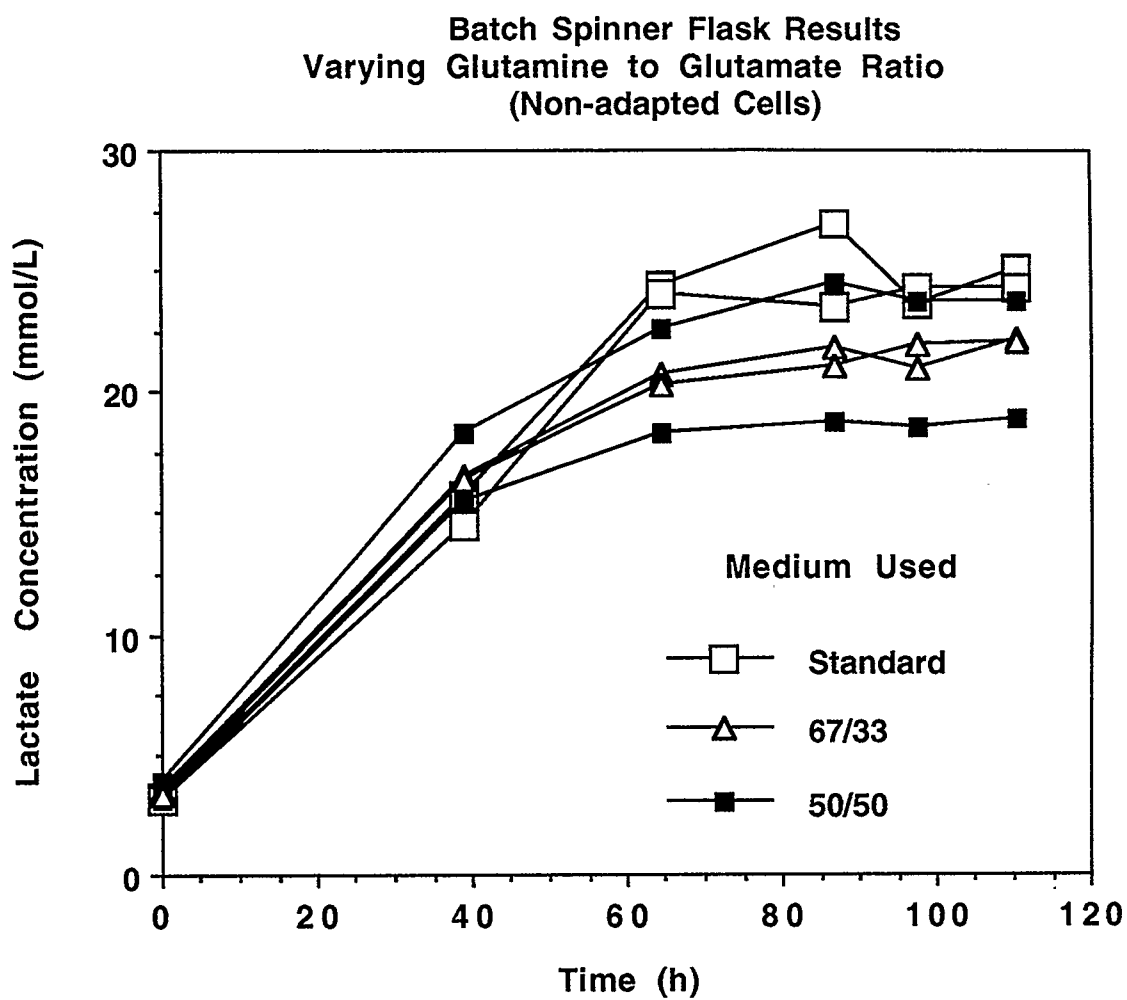


Figure 5.7 Lactate production during the batch growth of non-adapted cells in media with three different glutamine to glutamate ratios.

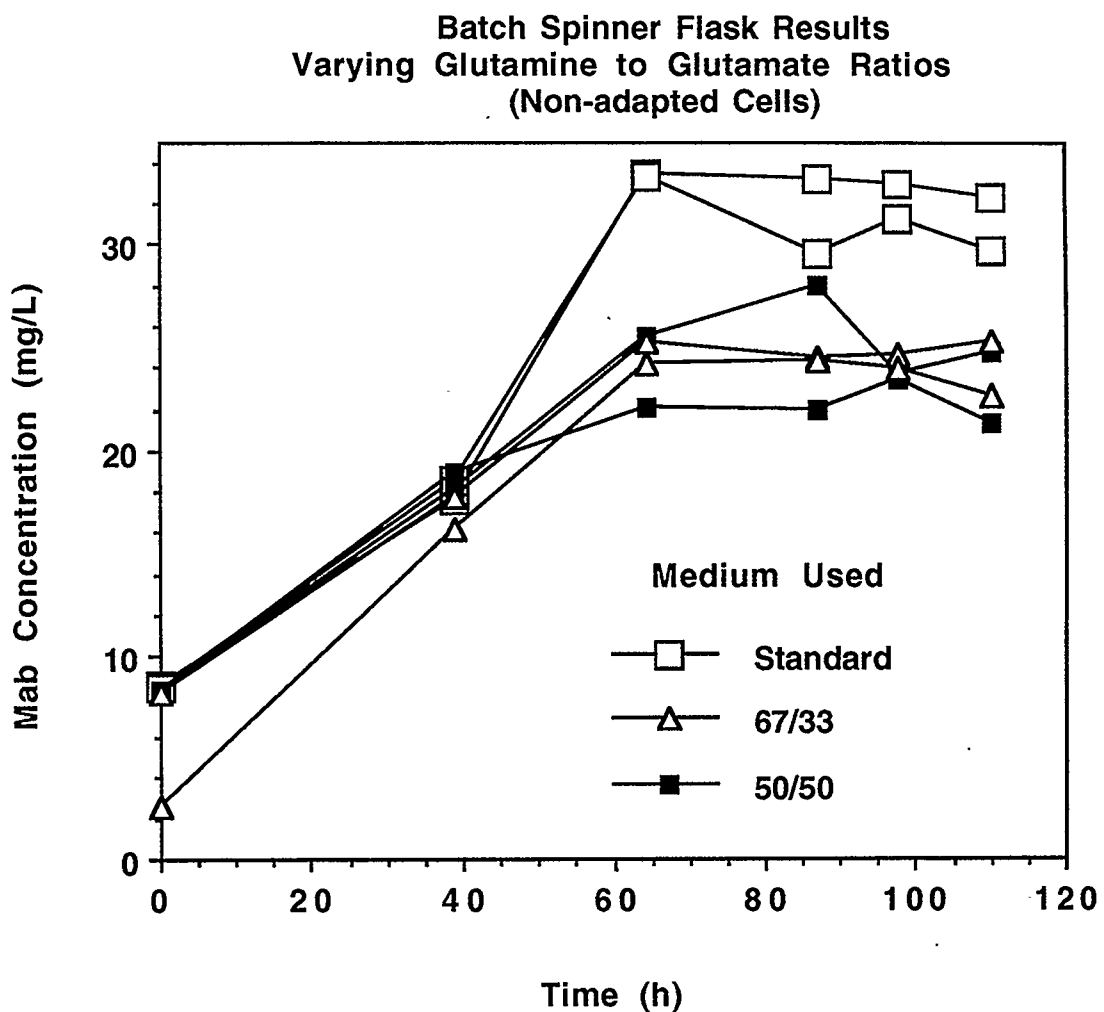


Figure 5.8 MAb production in batch spinner flask cultures of non-adapted cells. Media with three different glutamine to glutamate ratios were used.

Table 5.1. Effect of GLUTAMINE to GLUTAMATE Ratio (Non - Adapted Cells)							
Medium	Content		$x_{v,max}$	Net Production			
	Glutamine	Glutamate		MAb	Glutamate	Ammonia	Lactate
	<i>mmol/L</i>		$\times 10^6$ cells/mL	<i>mg/L</i>	<i>mmol/L</i>		
Regular	4.8	0.0	2.15	22	0	3.4	24
2/1	3.2	1.6	1.70	17	-0.45	2.9	22
1/1	2.4	2.4	1.20	19	-0.25	2.1	19

Table 5.1 Effect of varying glutamine to glutamate ratio on spinner flask cultures of non-adapted cells.

occurred in the 67/33 medium, while the 50/50 medium still yielded the lowest value (Figure 5.9). The profiles of viability (Figure 5.10), however, followed the same trend as with non-adapted cells (compare Figure 5.2). Due to the early decrease in viability, a sharp drop in viable cell density is observed after the maximum was reached in the 67/33 medium. The MAb profiles in this experiment are shown in Figure 5.11. Despite some scatter in the late stage measurements, it can be seen that even in partially adapted cells the higher glutamine concentration yields the highest amount of antibody (Table 5.2).

The glutamine, glutamate and ammonia profiles (Figures 5.12, 5.13 and 5.14 respectively) follow the same patterns as for non-adapted cells. A difference worth mentioning is that a more substantial amount of glutamate is consumed by the 50/50 culture (compare Tables 5.2 and 5.1). This may be a result of cell adaptation to medium containing a high glutamate concentration. It is interesting to observe in Figure 5.15 that the glucose consumption did not vary significantly in the three types of culture. However, if one accounts for the lower cell number in the 50/50 medium, it becomes apparent that the specific glucose consumption was increased in this medium. The profiles of lactate concentration (Figure 5.16) followed the same pattern as for non-adapted cells.

In conclusion, glutamine was shown to be an essential nutrient that cannot be substituted by glutamate in the medium. As a result, ammonia production was not affected significantly and it appeared to be proportional to the viable cell density. A slightly positive effect on cell growth was observed for partially adapted cells but on the other hand MAb production was always higher for higher initial glutamine content of the medium. There were indications of a reciprocal regulation of glucose and glutamine utilization, apparent in the cultures with reduced initial glutamine content in the medium.

5.2. EFFECT OF GLUTAMINE TO α -KETOGLUTARATE RATIO

To enter the TCA cycle a molecule of glutamine is first deaminated to glutamate producing one molecule of ammonia; glutamate is in turn converted to α -ketoglutaric acid (KGA) producing a second ammonia molecule. Therefore, if KGA can be

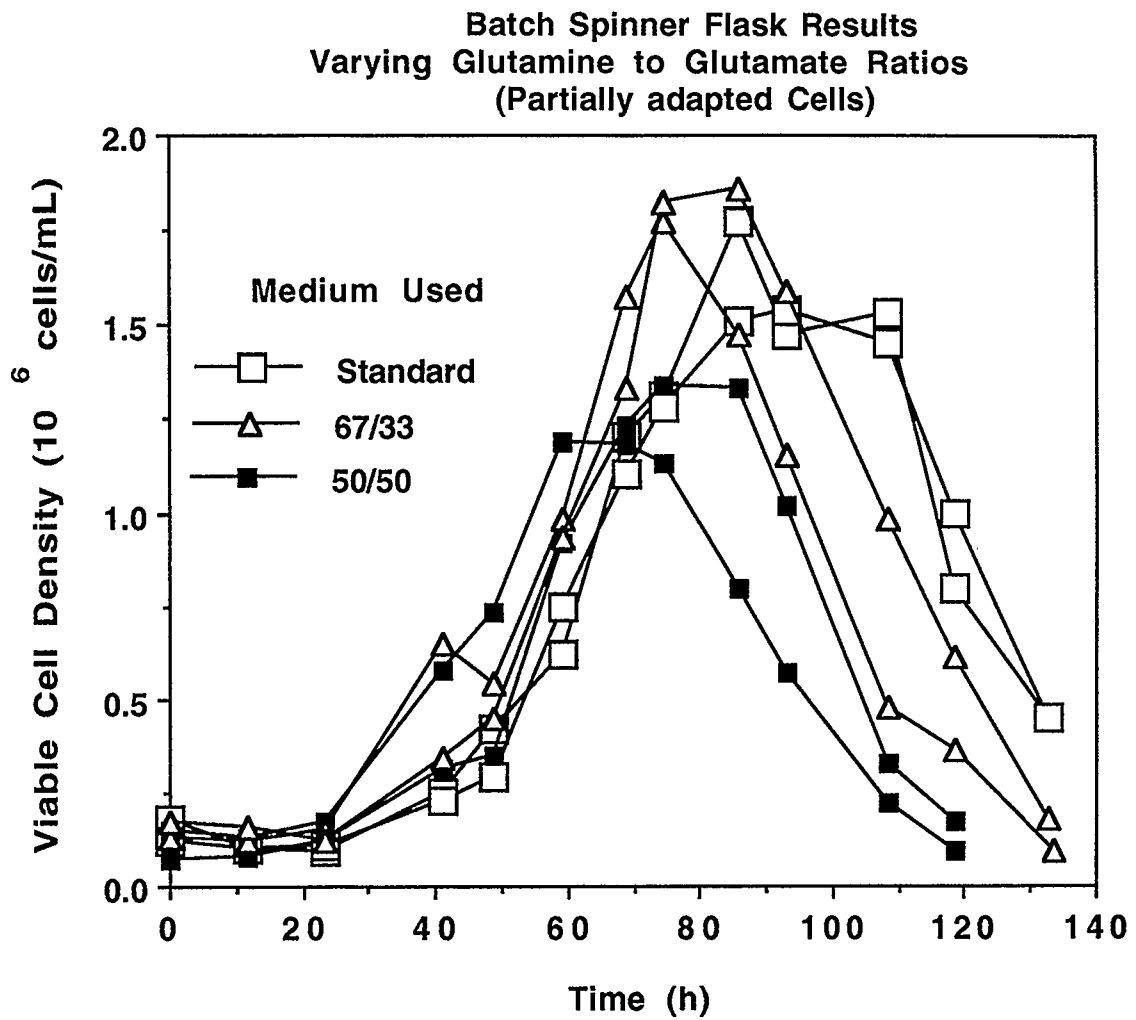


Figure 5.9 Profiles of viable cell density during the batch growth of partially adapted cells in media with three different glutamine to glutamate ratios.

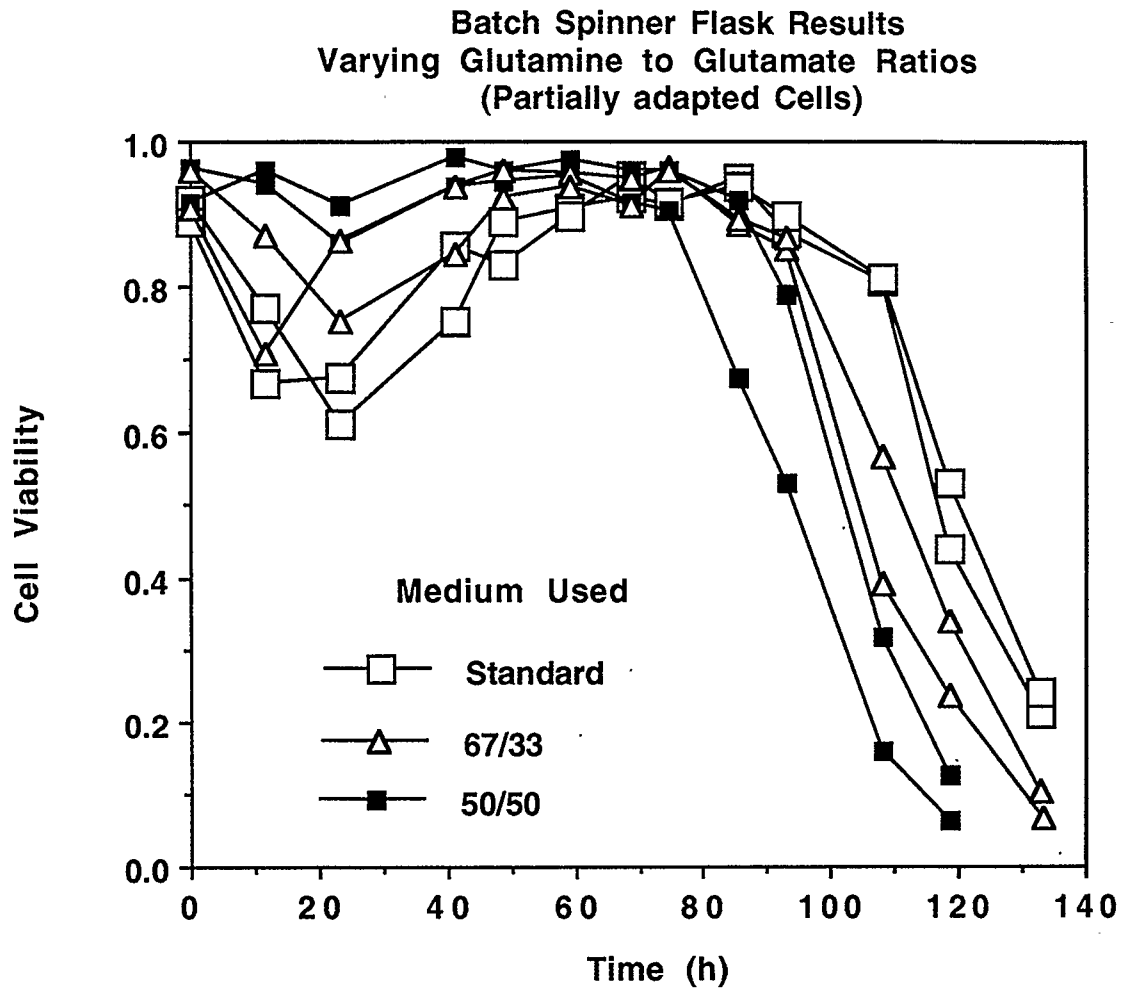


Figure 5.10 Profiles of cell viability during the batch growth of partially adapted cells in media with three different glutamine to glutamate ratios.

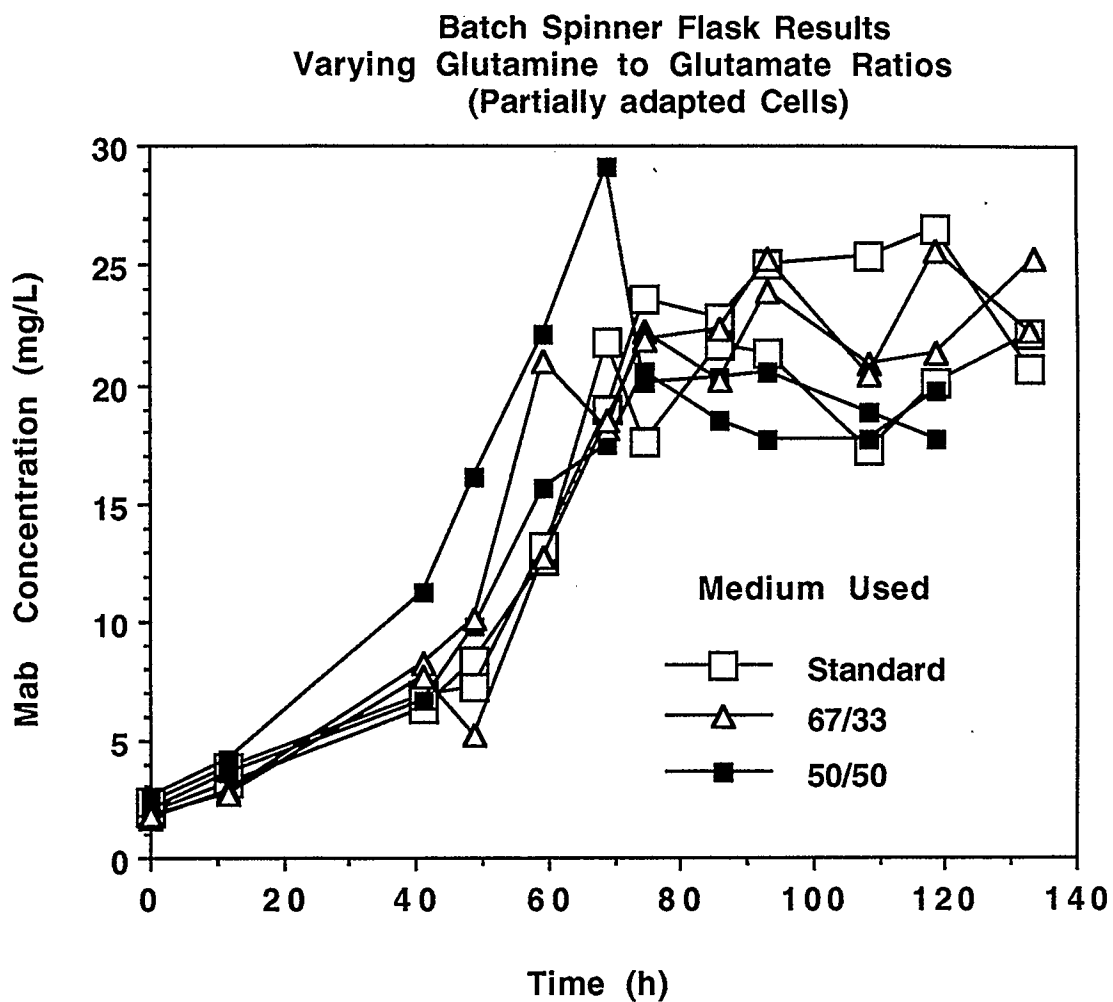


Figure 5.11 MAb production in batch spinner flask cultures of partially adapted cells in media with three different glutamine to glutamate ratios.

Table 5.2. Effect of GLUTAMINE to GLUTAMATE Ratio (Partially Adapted Cells)							
Medium	Content		$x_{v,max}$	Net Production			
	Glutamine	Glutamate		MAb	Glutamate	Ammonia	Lactate
	<i>mmol/L</i>		$\times 10^6$ cells/mL	<i>mg/L</i>	<i>mmol/L</i>		
Regular	4.8	0.0	1.55	25	0.15	1.7	19
2/1	3.2	1.6	1.70	23	-0.15	1.2	15.5
1/1	2.4	2.4	1.25	20	-1.0	0.95	13.5

Table 5.2 Effect of varying glutamine to glutamate ratio on spinner flask cultures of partially adapted cells.

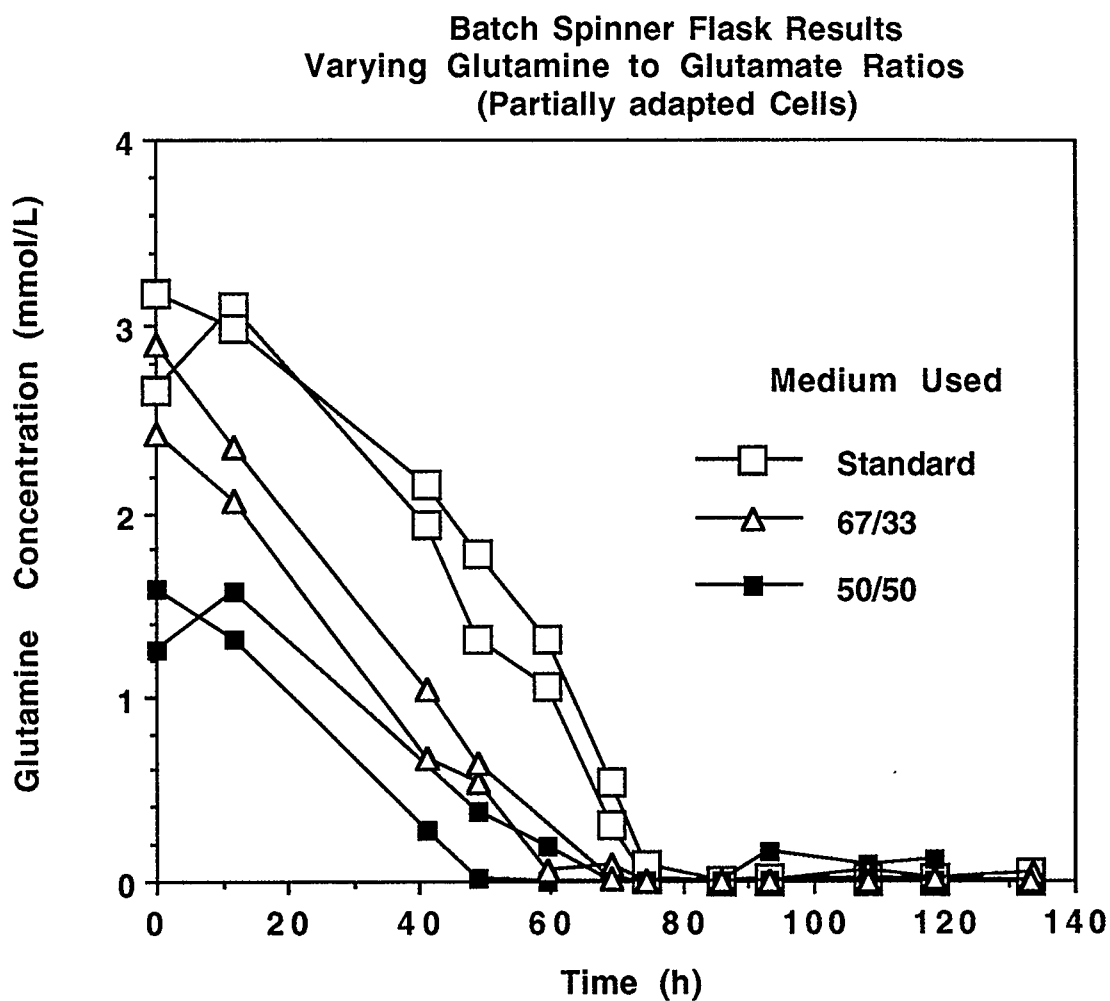


Figure 5.12 Profiles of glutamine concentration. Partially adapted cells were grown in media with three different glutamine to glutamate ratios.

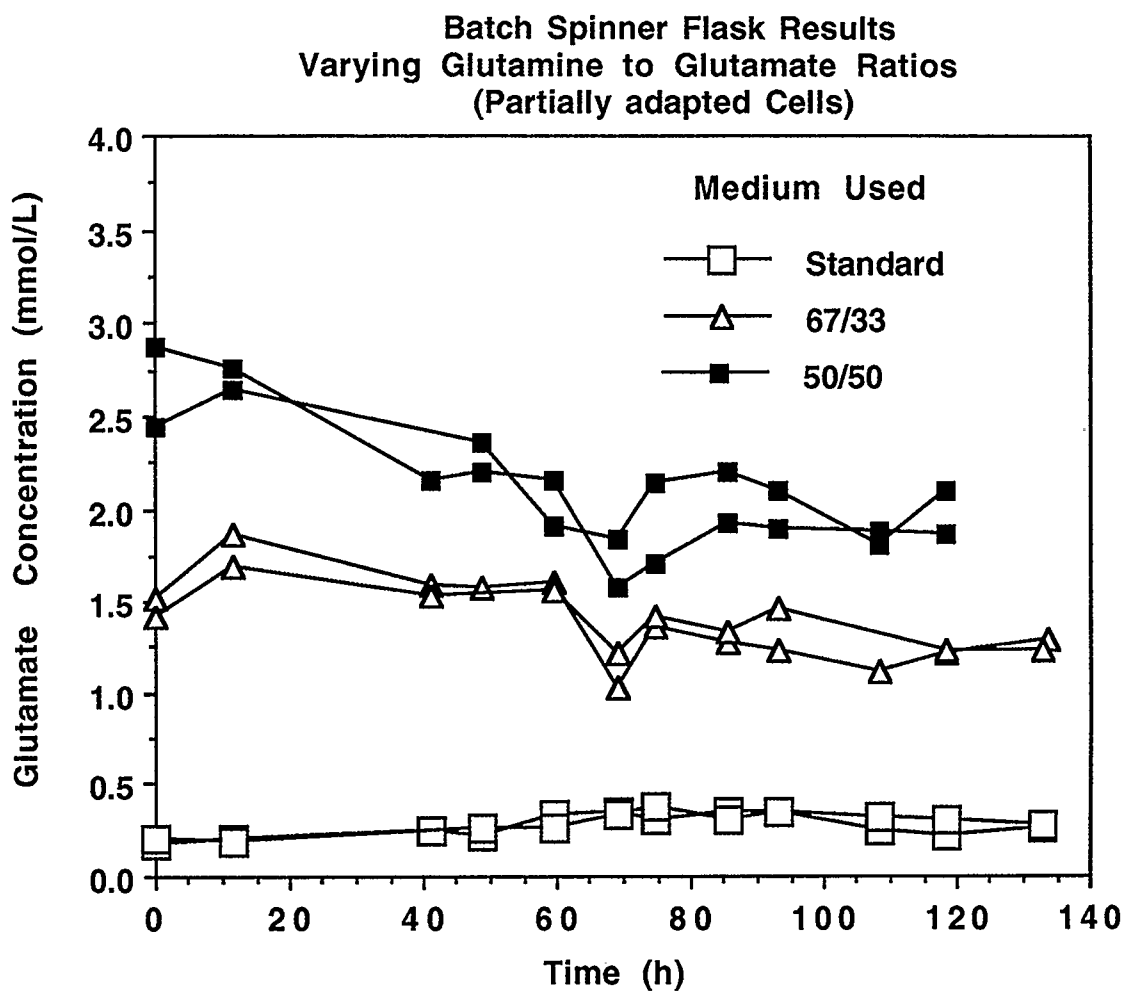


Figure 5.13 Profiles of glutamate concentration. Partially adapted cells were grown in media with three different glutamine to glutamate ratios

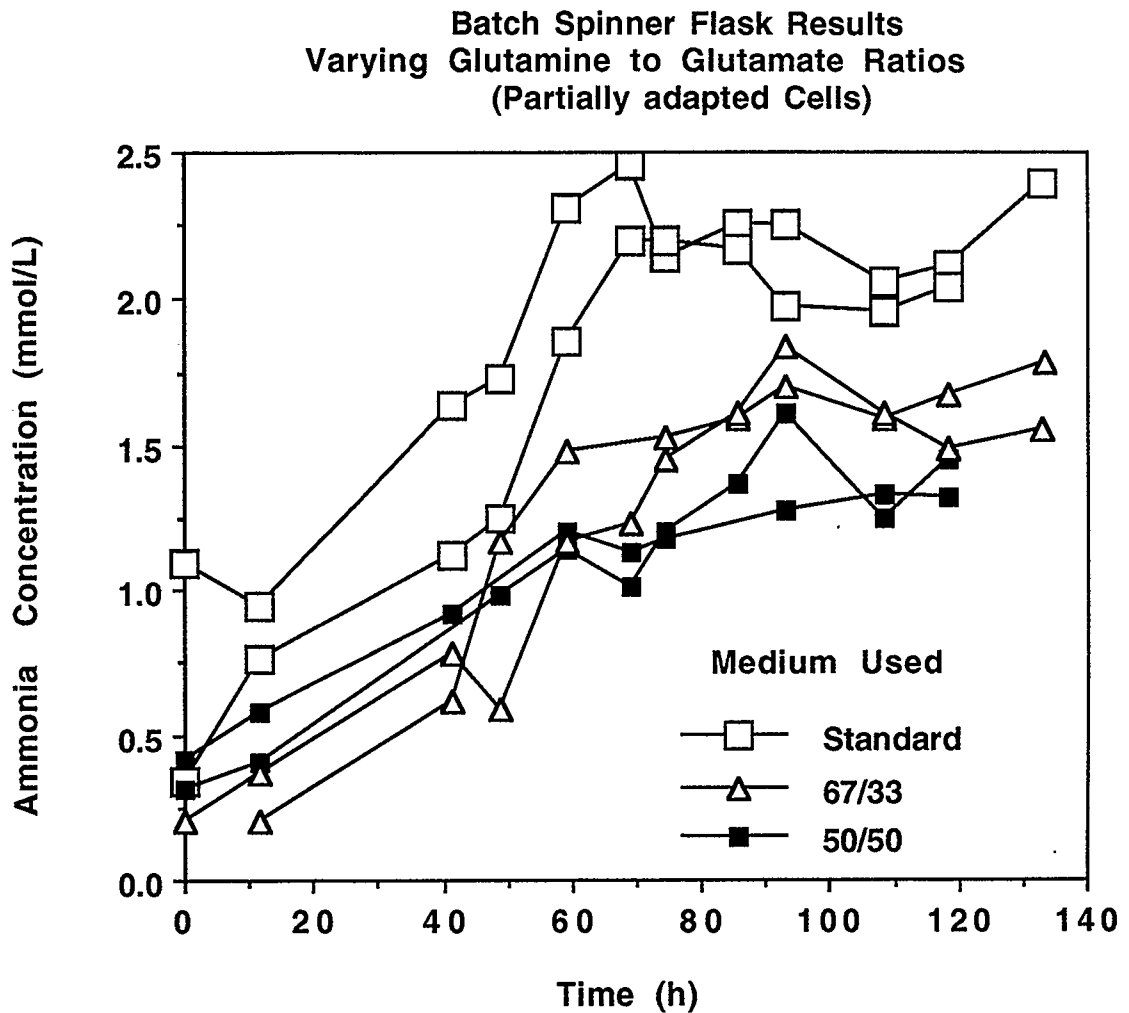


Figure 5.14 Ammonia concentration profiles during the batch growth of partially adapted cells in media with three different glutamine to glutamate ratios.

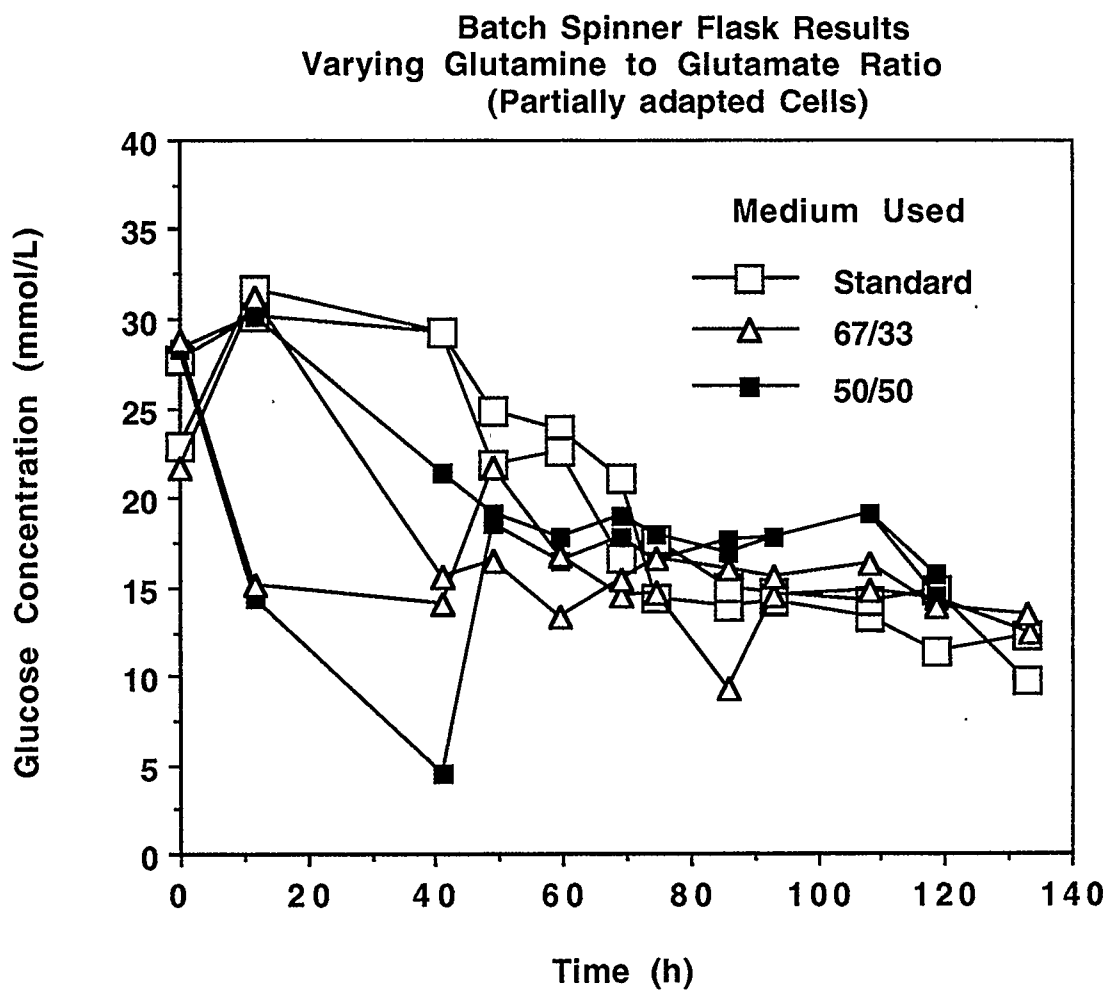


Figure 5.15 Profiles of glucose concentration. Partially adapted cells were grown in media with three different glutamine to glutamate ratios.

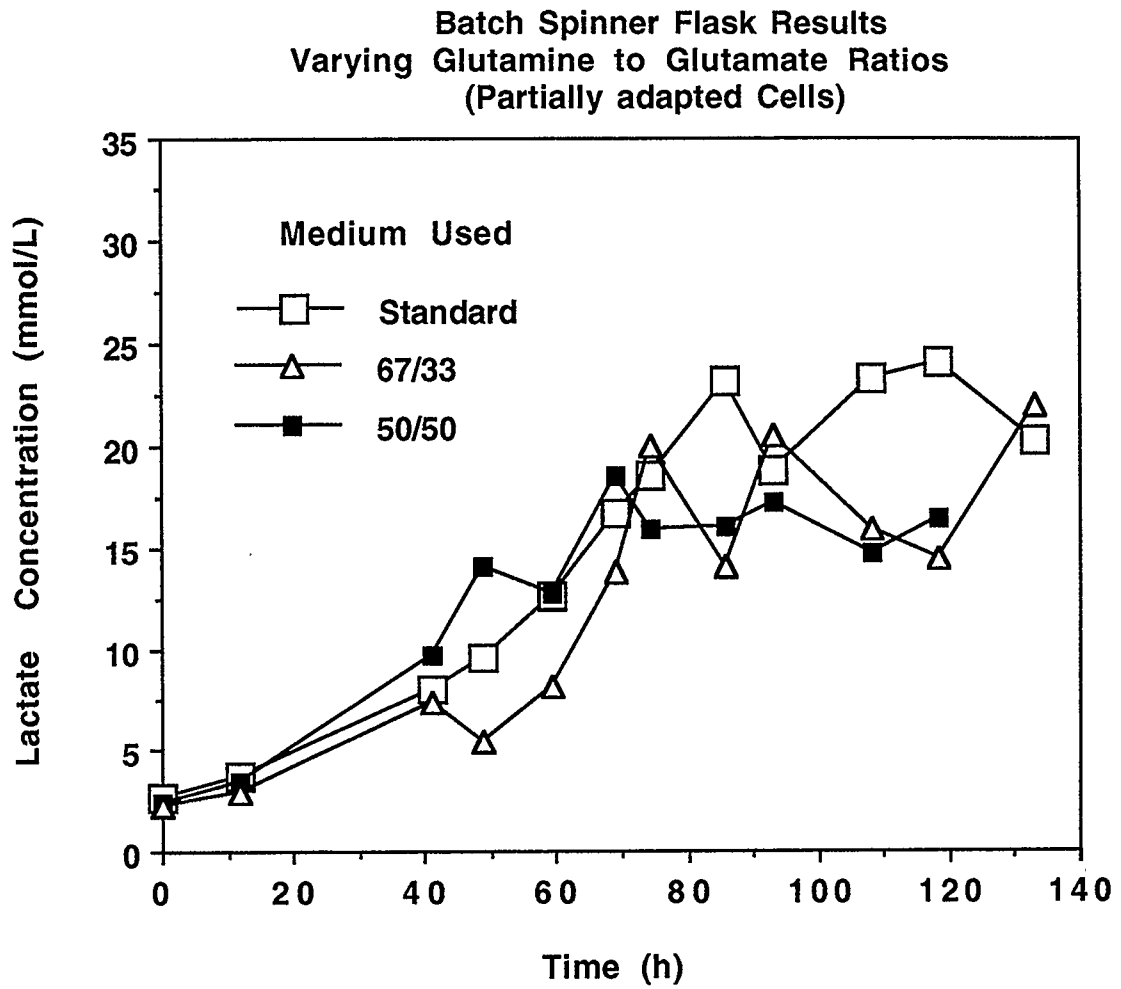


Figure 5.16 Lactic acid concentration profiles during the batch growth of partially adapted cells in media with three different glutamine to glutamate ratios

substituted for glutamine, two molecules of ammonia less are excreted per molecule of glutamine entering the TCA cycle. In this study we examined the effect of the partial substitution of glutamine with KGA. Two experiments were conducted; in the first experiment three different media were used, DMEM containing no KGA (standard), DMEM with 50% glutamine substituted by KGA (50/50) and finally DMEM with 75% of glutamine substituted by KGA (25/75). The total amount of glutamine and KGA was kept constant at 4.8 *mmol/L* (glutamine content of the standard medium). In this experiment the medium was also supplemented with 0.1% of methylcellulose.

Figures 5.17 and 5.18 show the viable cell density and viability profiles in the first experiment. It can be seen that substitution of glutamine by KGA clearly has a negative effect on the cell growth. Caution should be exercised in interpreting the results of this experiment, for the simple reason that the viability of the inoculum (Figure 5.18) was low and it may have affected the outcome. Nevertheless it is also pointed out that as Figures 5.17 and 5.18 indicate the cells grew normally after inoculation.

A negative effect on MAb production is apparent in Figure 5.19. As in the previous chapter, glutamine seems to be an absolutely necessary precursor for antibody synthesis and any glutamine shortfall has an immediate impact on the production of antibody. The profiles of glutamine concentration are shown in Figure 5.20 and as expected glutamine is first depleted in the low glutamine cultures. The glutamate profiles, shown in Figure 5.21, are very interesting. They reveal that while glutamate is consumed when regular medium is used, there is a net production of glutamate in the presence of KGA. Furthermore, glutamate production is higher in the 25/75 medium indicating that glutamate is produced from the KGA added in the medium.

In Figure 5.22 it can be seen that there was no positive effect (i.e. no significant decrease) on ammonia production. In contrast, if the maximum viable cell densities are taken into account, an increased specific ammonia production rate is apparent at least for the 25/75 medium. As expected, glucose consumption was higher in the regular medium and lactate production was also higher (see Figures 5.23 and 5.24). The

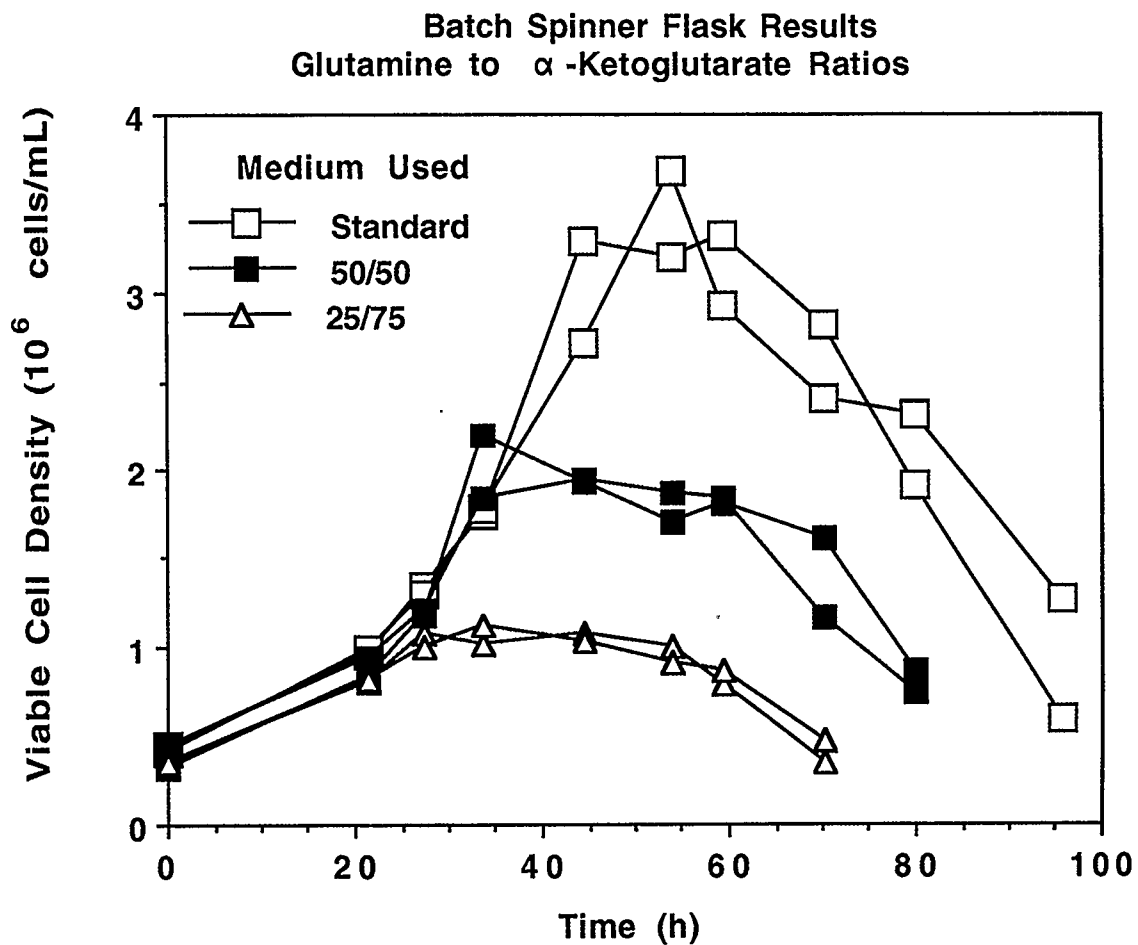


Figure 5.17 Viable cell density during batch spinner flask cultures of hybridomas in media with three different glutamine to α -ketoglutarate ratios. Results from Experiment 1.

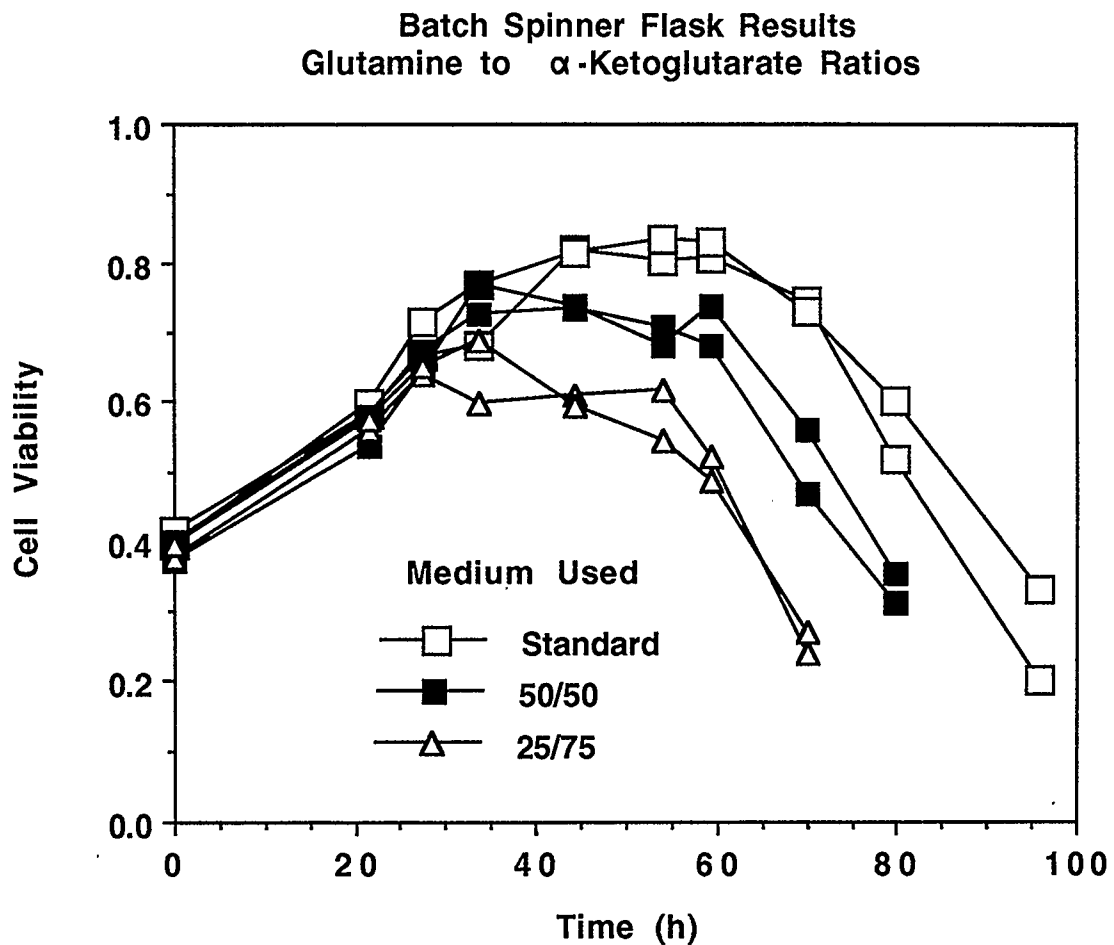


Figure 5.18 Profiles of cell viability during the batch growth of hybridoma cells in media with three different glutamine to α -ketoglutarate ratios. Results from Experiment 1.

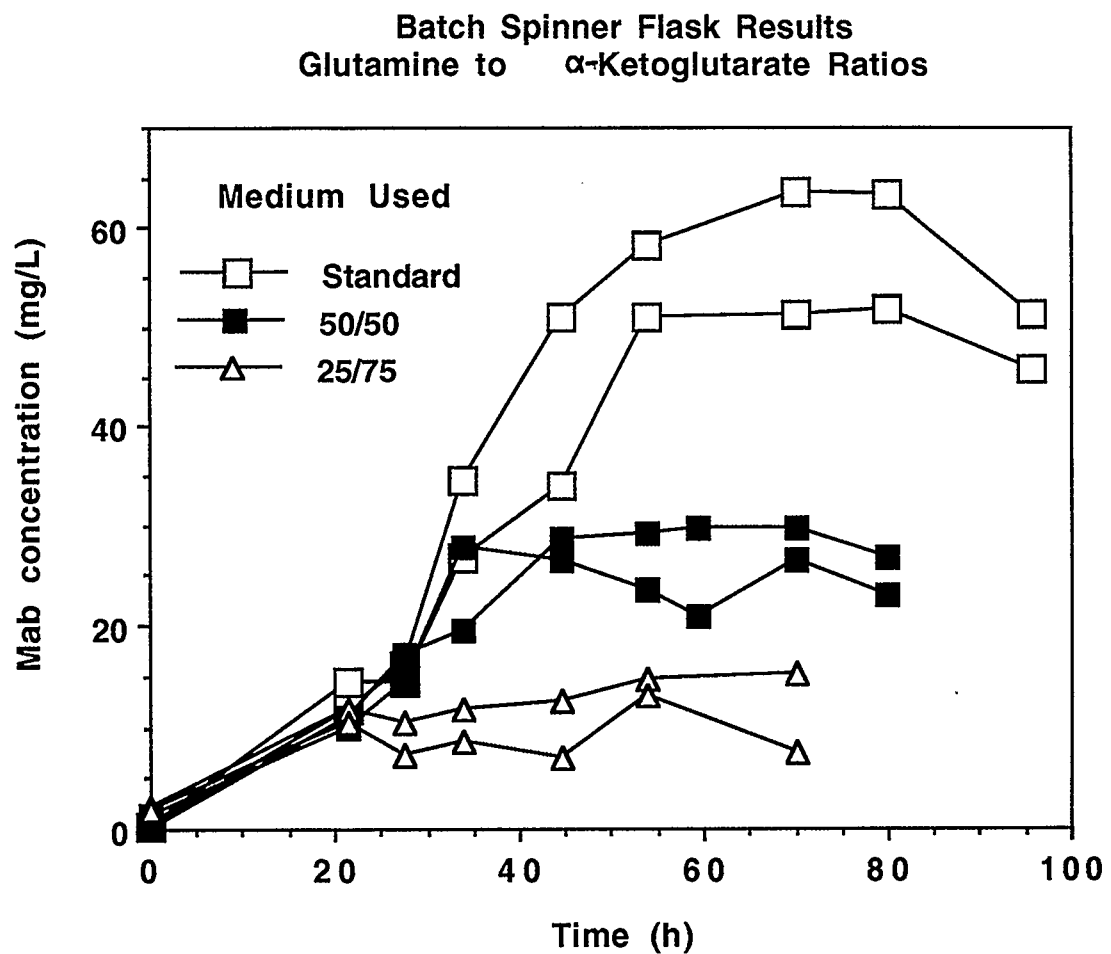


Figure 5.19 MAb production by hybridoma cells in batch spinner flask cultures with three different glutamine to α -ketoglutarate ratios. Results from Experiment 1.

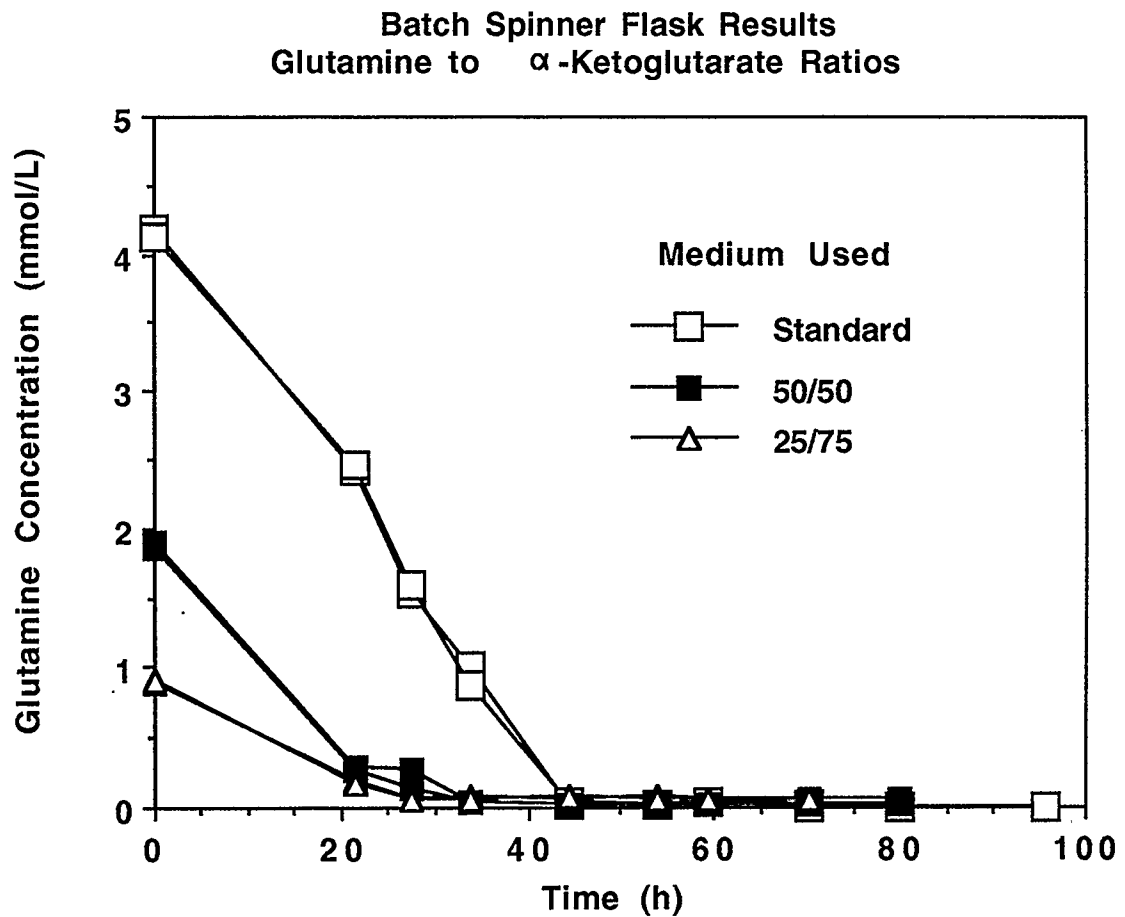


Figure 5.20 Profiles of glutamine concentration in batch cultures of hybridomas in media with three different glutamine to α -ketoglutarate ratios. Results from Experiment 1.

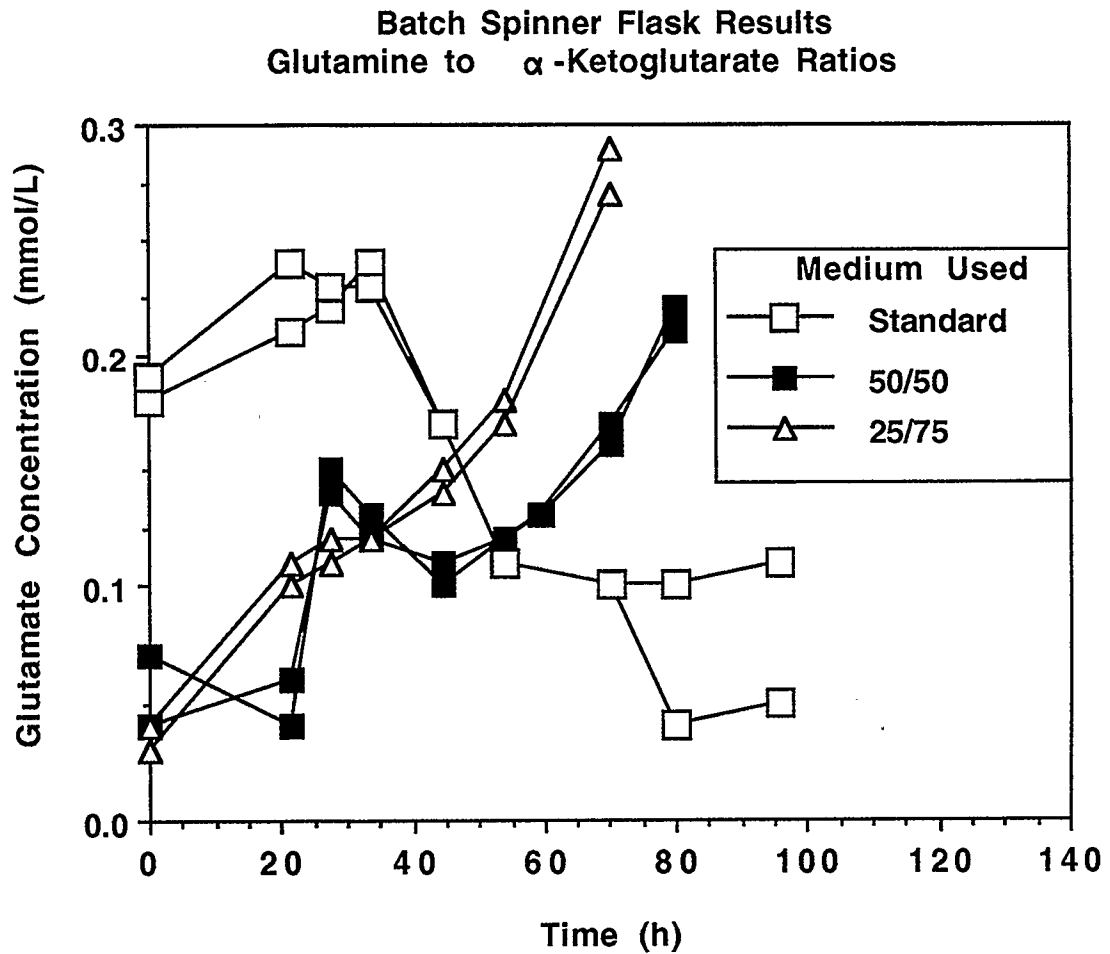


Figure 5.21 Profiles of glutamate concentration in batch spinner flask cultures using media with three different glutamine to α -ketoglutarate ratios. Results from Experiment 1.

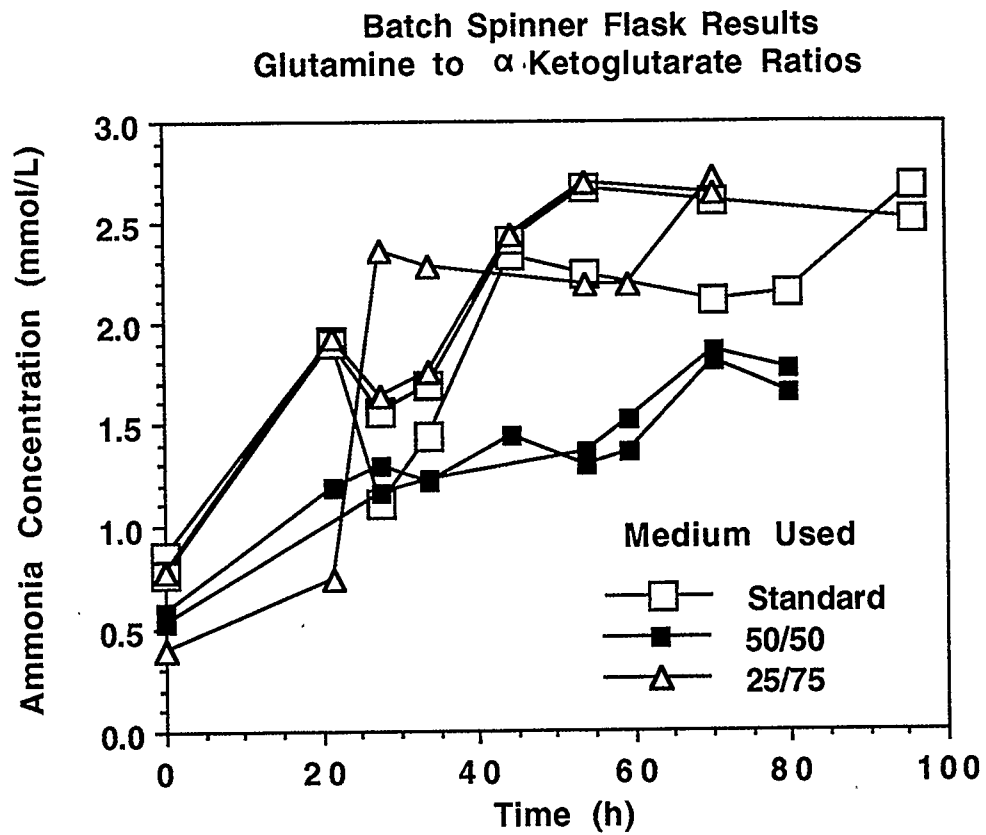


Figure 5.22 Effect of varying glutamine to α -ketoglutarate ratios on ammonia production in batch spinner flask cultures. Results from Experiment 1.

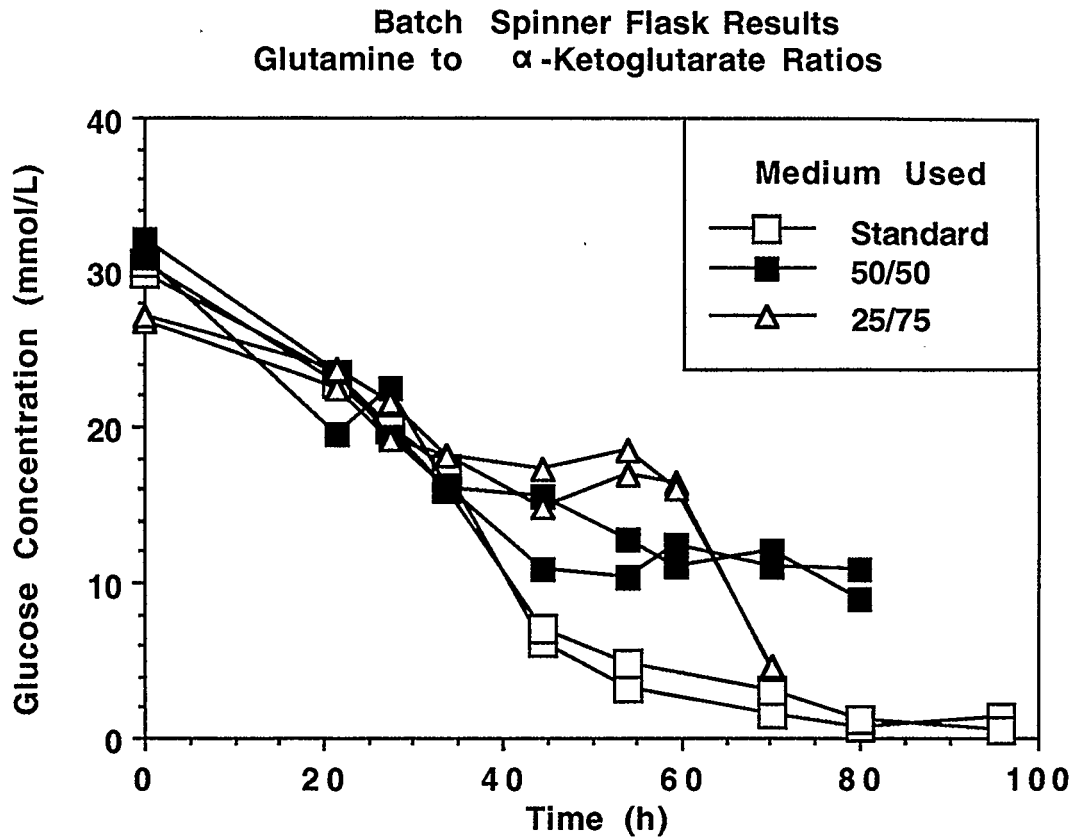


Figure 5.23 Glucose concentration profiles in batch cultures of hybridomas using media with varying glutamine to α -ketoglutarate ratios. Results from Experiment 1.

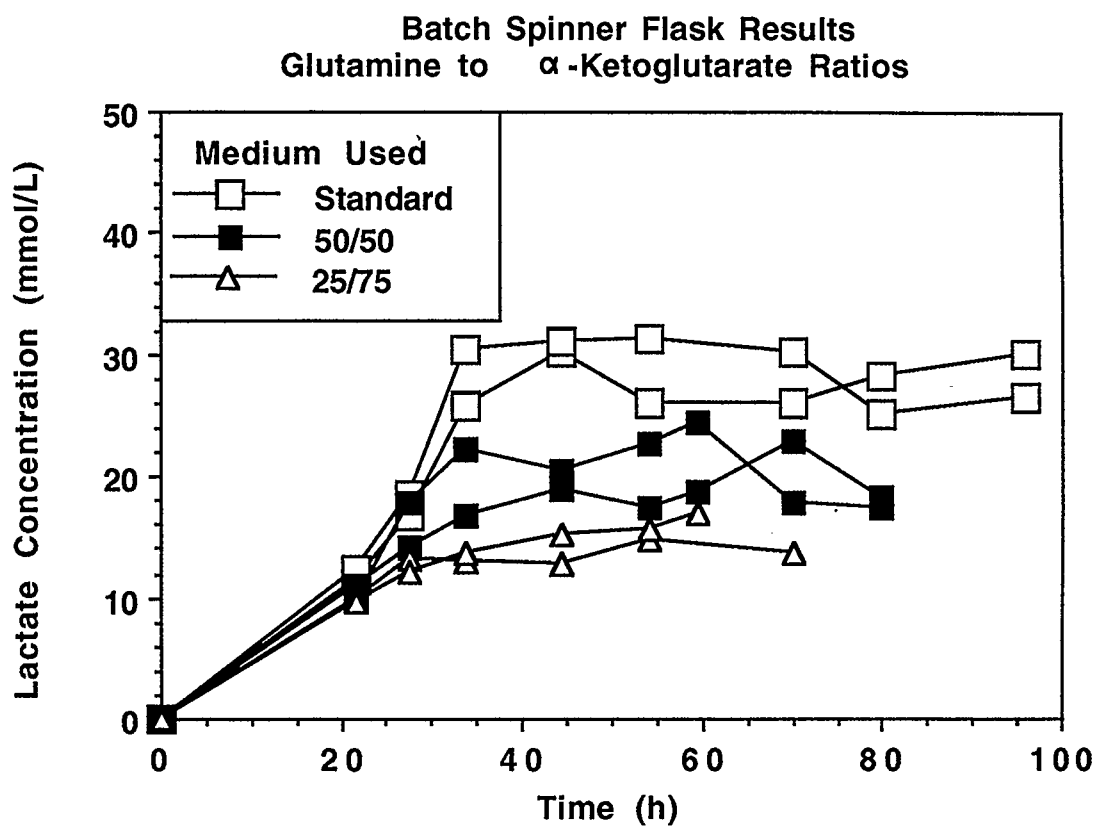


Figure 5.24 Lactic acid concentration profiles in batch cultures of hybridomas using media with varying glutamine to α -ketoglutarate ratios. Results from Experiment 1.

results from the first experiment are summarized in Table 5.3.

The previous experiment was repeated with a 70% cell viability at inoculation. In the second experiment duplicate flasks were again used for each of the three concentrations. Furthermore, a flask was included with a 70/30 ratio and one with regular medium supplemented with 4.8 *mmol/L* of KGA (100/100). Therefore 5 different media types were used in the second experiment. In addition a glutamine pulse and a KGA pulse were applied on each of the 25/75 cultures at the 55 *h* mark. The pulse corresponded to an increase of the substance concentration by 4.8 *mmol/L*. No methylcellulose was added in any of the media.

Figure 5.25 shows the viable cell densities for the five cases. It can be seen that in the medium supplemented with extra KGA the profile is shifted to the right, i.e. the cells remain viable longer. This can be also seen clearly in Figure 5.26 that shows the viability profiles. Otherwise, the results are very similar to that obtained in the first experiment. Both the viable cell density and viability increased sharply in the culture with the glutamine pulse but no effect was apparent from the KGA pulse. In Figure 5.27 we observe that the MAb production is not very different for the regular and the 100/100 media. Much lower titers of MAb were produced in media with partially substituted glutamine. However a remarkable amount of antibody was produced by the 25/75 culture when pulsed with glutamine, despite the relatively low viable cell density. This observation confirms the importance of glutamine in MAb production.

There are no surprises in the glutamine profiles shown in Figure 5.28. We can clearly see the increase in residual glutamine concentration after the glutamine pulse. The trends in the glutamate profiles, Figure 5.29, confirm the findings of the first experiment, i.e. higher amounts of glutamate are produced for higher initial KGA concentrations in the medium. After the pulse glutamate concentration increased in both cultures. The increase was much higher in the medium pulsed with glutamine but this can be probably explained by the fact that cells remained viable much longer in this culture. The ammonia production in this experiment appears to be higher for the regular and

Table 5.3. Effect of GLUTAMINE to α -KETOGLUTARATE (KGA) Ratio (Experiment 1)							
Medium	Content		$x_{v,max}$	Net Production			
	Glutamine	KGA		MAb	Glutamate	Ammonia	Lactate
	<i>mmol/L</i>		$\times 10^6$ cells/mL	<i>mg/L</i>	<i>mmol/L</i>		
Regular	4.8	0.0	3.5	55	-0.13	2.5	28
50/50	2.4	2.4	2.0	22	0.16	1.7	22
25/75	1.2	3.6	1.0	11	0.25	2.5	15

Table 5.3 Effect of varying glutamine to α -ketoglutarate ratio. Results from Experiment 1.

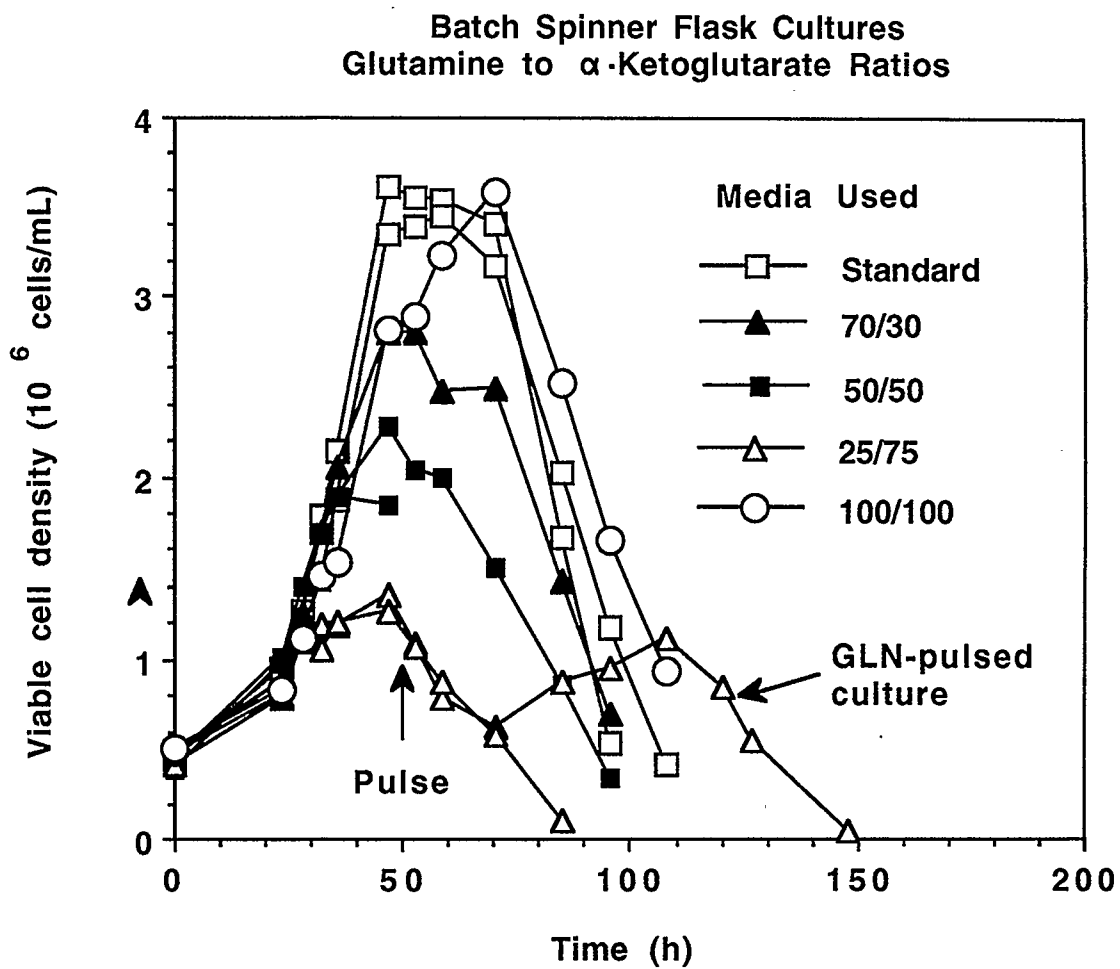


Figure 5.25 Effect of α -ketoglutaric acid on the viable cell density of hybridomas during batch culture in spinner flasks. Results from Experiment 2.

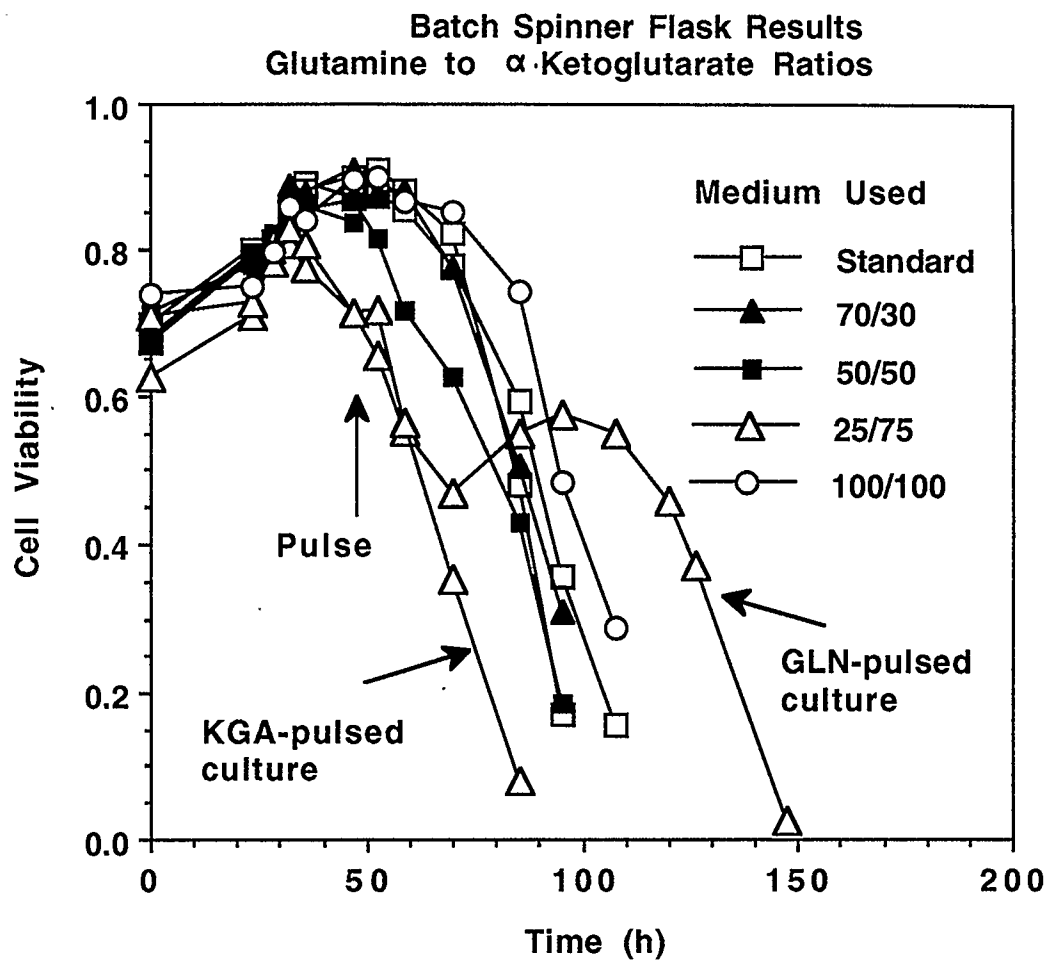


Figure 5.26 Effect of α -ketoglutaric acid on the viability of batch hybridoma cultures. Results from Experiment 2.

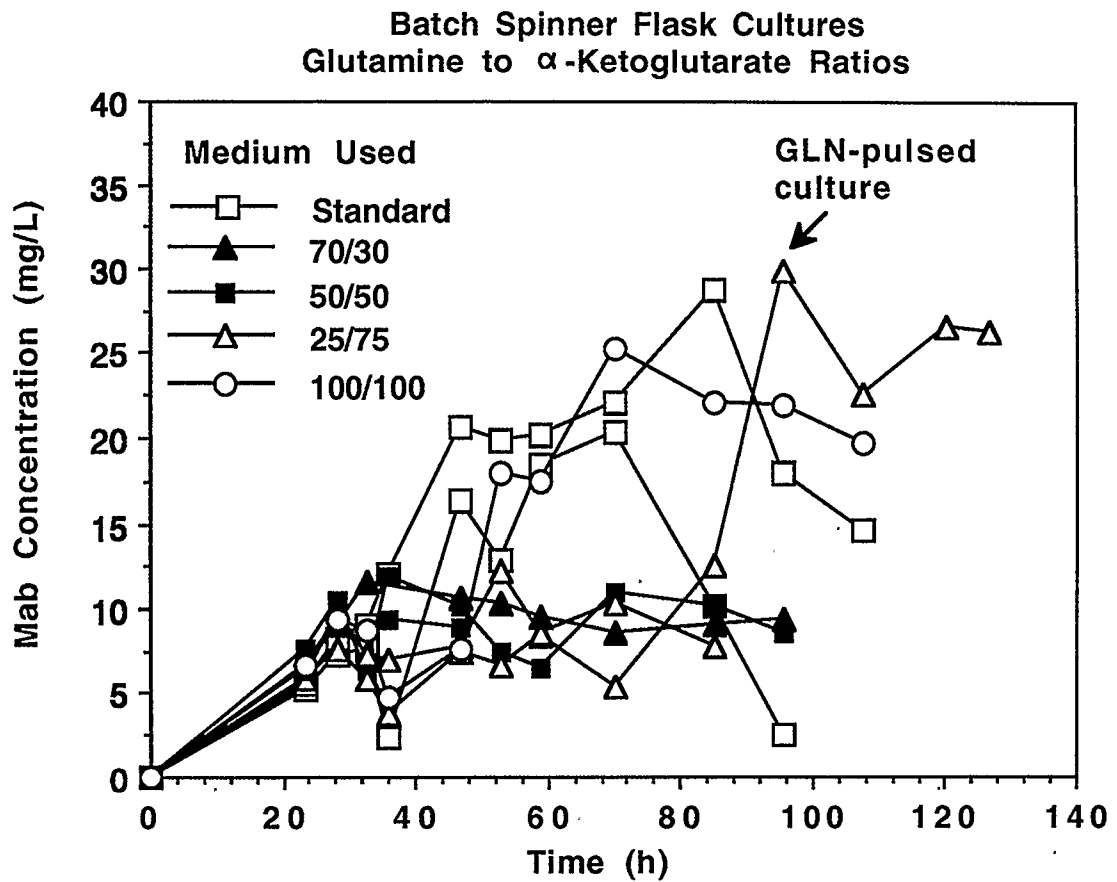


Figure 5.27 MAb production in batch spinner flask cultures with varying ratio of glutamine to α -ketoglutaric acid. Results from Experiment 2.

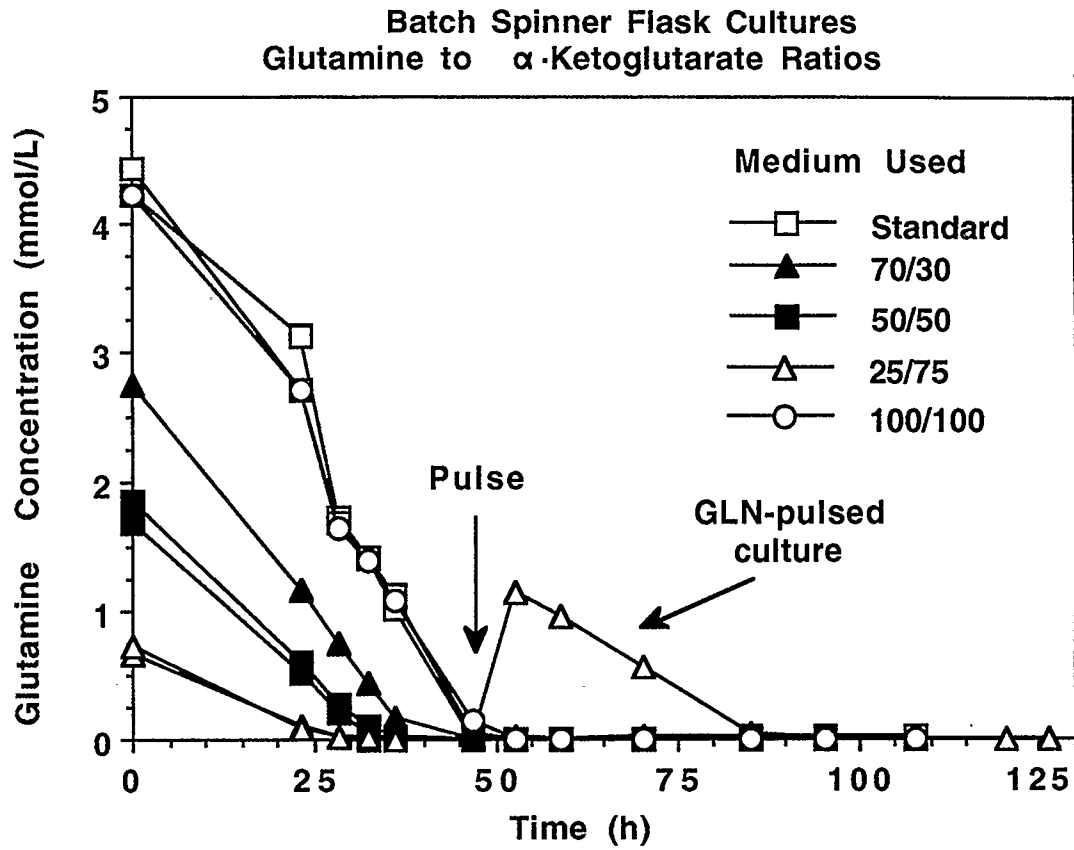


Figure 5.28 Profiles of glutamine concentration during batch experiments with varying ratio of glutamine to α -ketoglutaric acid. Results from Experiment 2.

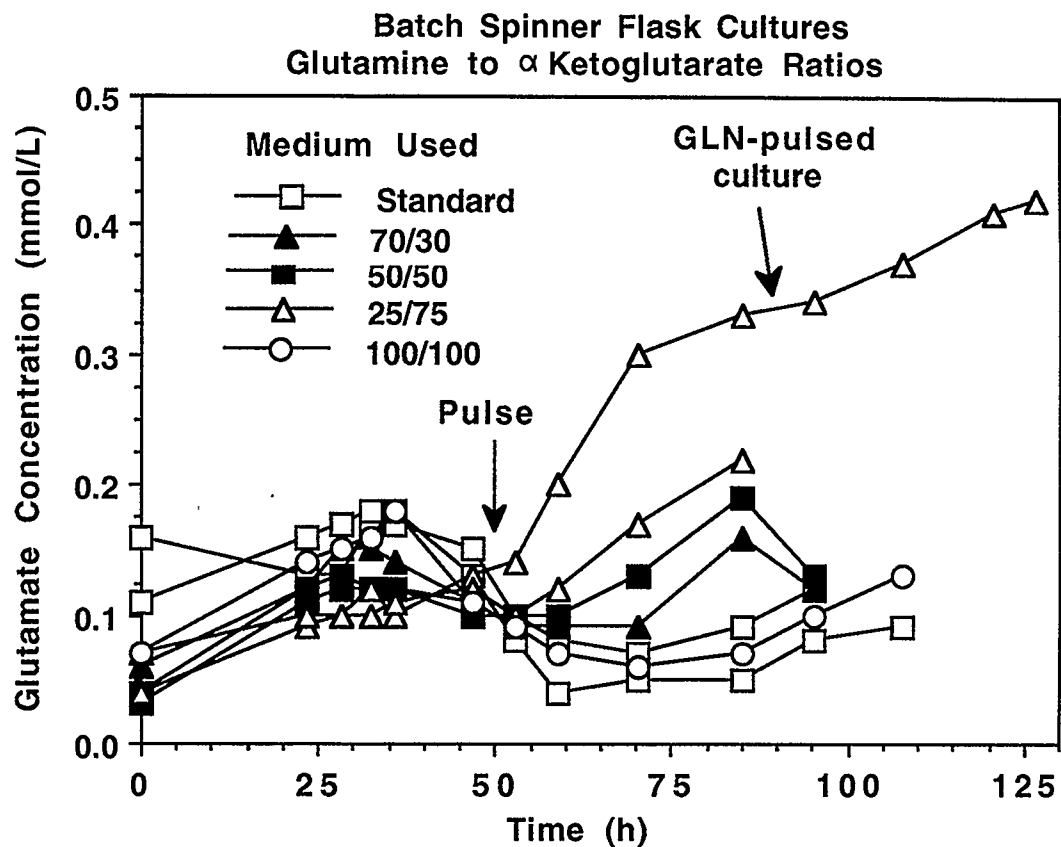


Figure 5.29 Profiles of glutamate concentration during batch experiments with varying ratio of glutamine to α -ketoglutaric acid. Results from Experiment 2.

100/100 media (Figure 5.30 and Table 5.4). Finally the glucose and lactate profiles shown in Figures 5.31 and 5.32 respectively exhibit the same trends as in the first experiment. The glucose profiles in regular and 100/100 media are almost identical. Therefore, there is no noticeable effect of KGA on glucose consumption. However, the pulse experiment revealed that production of lactate (Figure 5.32) may have been temporarily inhibited by glutamine until the 105 *h* point when glutamine was completely exhausted (compare Figure 5.28). The results of the second experiment are summarized in Table 5.4.

In conclusion, substitution of glutamine by KGA did not appear to have any positive effects in batch culture. Addition of extra amounts of KGA effectively retained the cells viable for longer periods, but no significant change was observed in either the maximum viable cell density or the MAb productivity. The glutamine pulse extended the life of the culture in the low glutamine medium and lead to a very significant increase in MAb production. The KGA pulse did not have any effect on the culture.

5.3. EFFECT OF GLUCOSE TO GLUTAMINE RATIO

In this experiment media with glucose to glutamine ratios 5/1 (standard), 5/2, 5/3 and 6/1 were used in spinner flask batch cultures. The concentrations were calculated so that the total energy (in the form of ATP) produced by glucose and glutamine remained the same as in the standard medium. The working assumption was that an average of 13 and 36 *mol* ATP were produced respectively for each *mol* of glutamine and glucose consumed. The actual initial concentrations of the media are given in Table 5.5 together with the summary of results for each medium used in this experiment.

Figure 5.33 compares the viable cell densities for the 4 different media while the corresponding viabilities are shown in Figure 5.34. The results indicate that the medium with a 5/2 ratio was the best for this type of culture. The final antibody concentration was also highest in this medium as it can be seen in Figure 5.35. In fact, the final MAb titer was much lower for the regular medium (5/1).

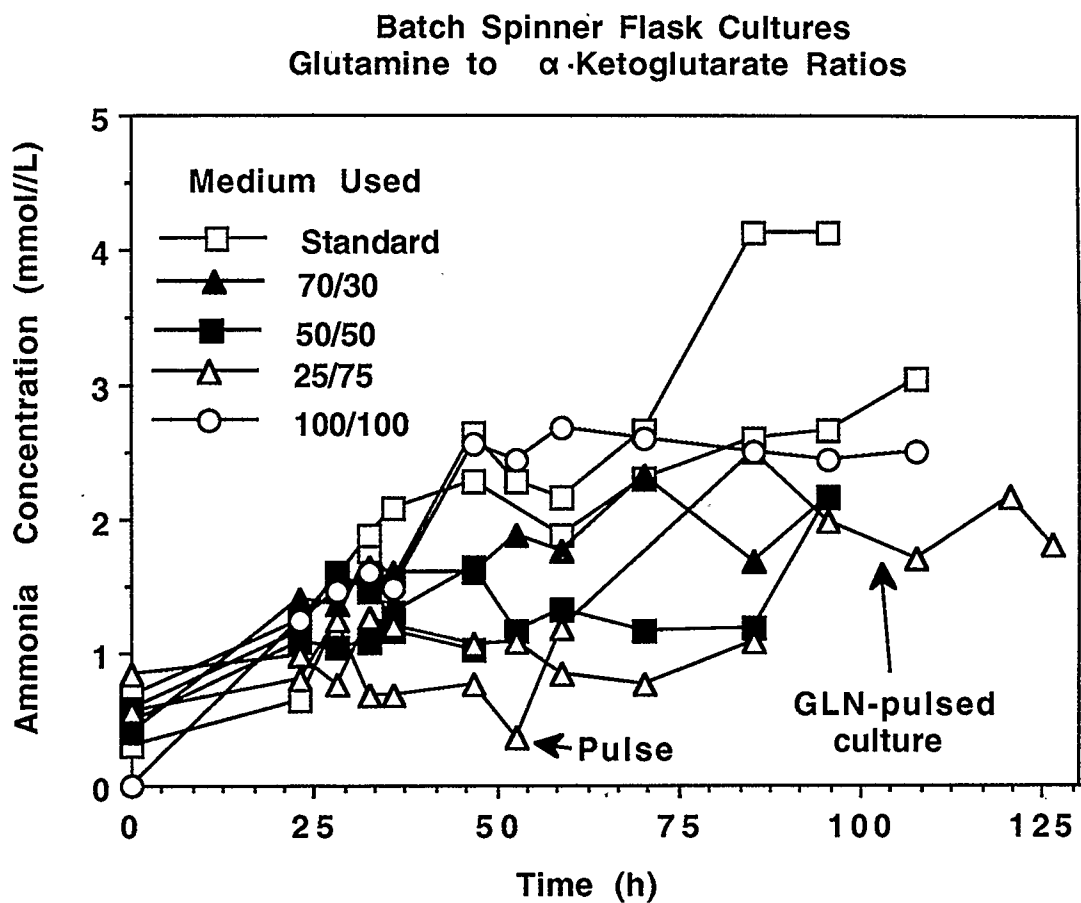


Figure 5.30 Ammonia production during the batch growth of hybridoma cells in media with three different glutamine to α -ketoglutaric acid ratios. Results from Experiment 2.

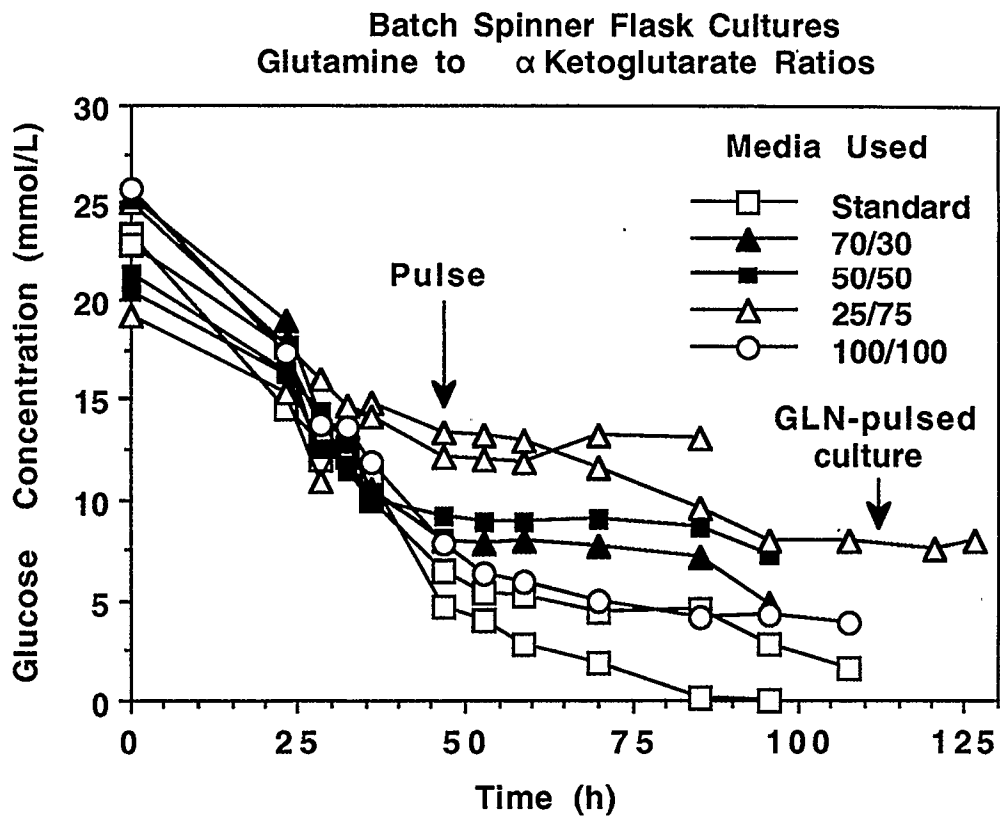


Figure 5.31 Glucose concentration profiles during batch cultures with varying ratio of glutamine to α -ketoglutaric acid in the medium. Results from Experiment 2.

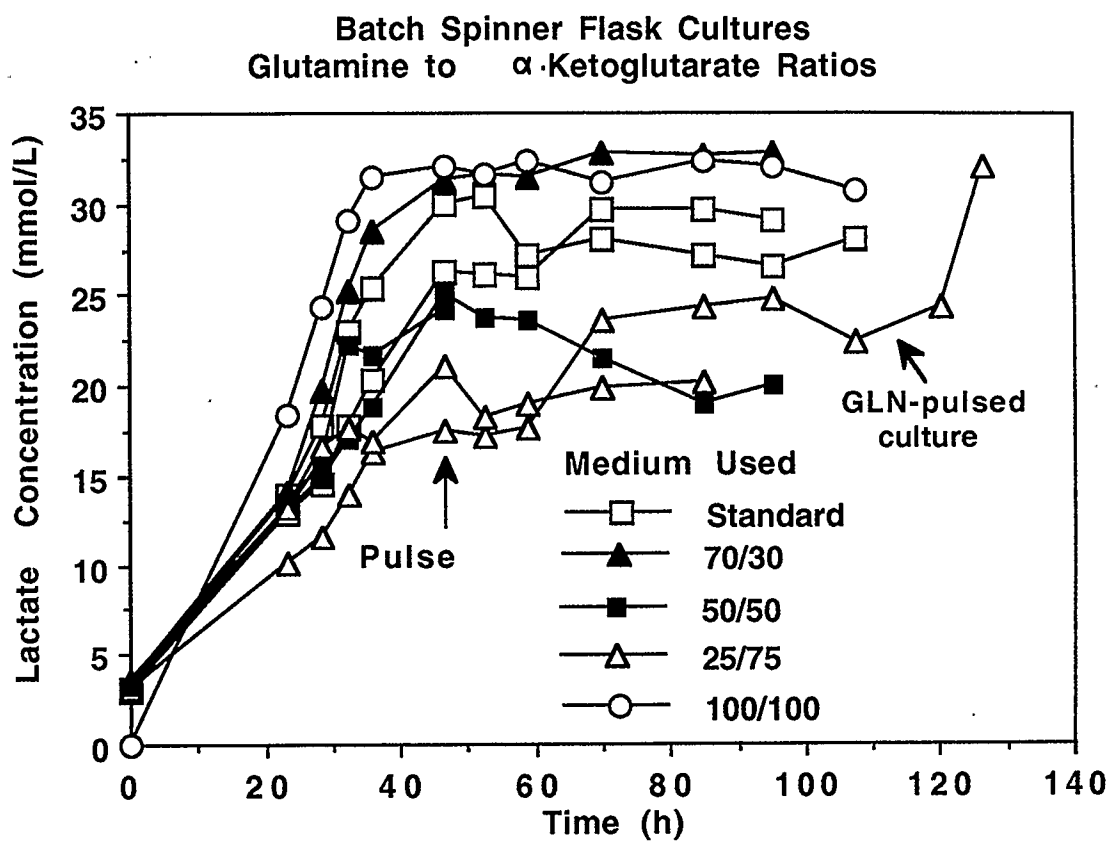


Figure 5.32 Lactic acid concentration profiles during the batch growth of hybridomas in media with varying ratio of glutamine to α -ketoglutaric acid in the medium. Results from Experiment 2.

Table 5.4. Effect of GLUTAMINE to α -KETOGLUTARATE (KGA) Ratio (Experiment 2)							
Medium	Content		$x_{v,max}$	Net Production			
	Glutamine	KGA		MAb	Glutamate	Ammonia	Lactate
	<i>mmol/L</i>		$\times 10^6$ cells/mL	<i>mg/L</i>	<i>mmol/L</i>		
Regular	4.8	0.0	3.5	29	0.0	1.3	24
70/30	3.4	1.4	2.8	22	0.04	1.6	29
50/50	2.4	2.4	2.1	11	0.10	0.5	18
25/75	1.2	3.6	1.2	11	0.15	0.25	17
100/100	4.8	4.8	3.7	26	0.04	2.55	32

Table 5.4 Effect of varying glutamine to α -ketoglutarate ratio. Results from Experiment 2.

Table 5.5. EFFECT OF GLUCOSE TO GLUTAMINE RATIO				
Medium	Content		$x_{v,max}$	Net Production of MAb at 94 h
	Glucose	Glutamine		
	<i>mmol/L</i>		$\times 10^6$ cells/mL	<i>mg/L</i>
Regular (5/1)	25.0	4.8	1.45	23
5/2	24.2	9.3	2.4	26
5/3	22.0	13.2	1.7	32
6/1	25.2	4.2	0.85	15

Table 5.5 Effect of varying glucose to glutamine ratio in batch spinner flask cultures.

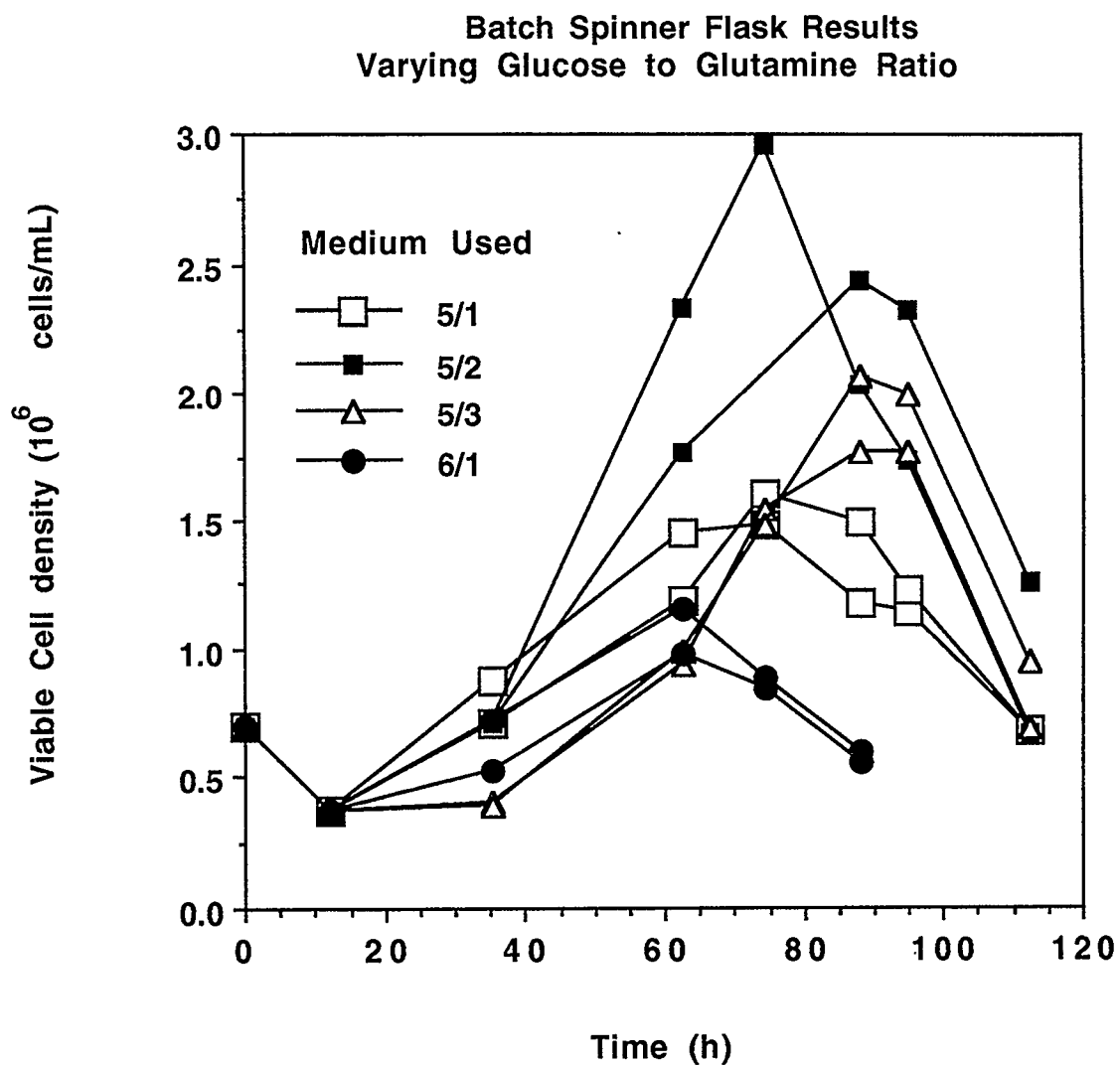


Figure 5.33 Viable cell density profiles for batch cultures in media containing four different glucose to glutamine ratios.

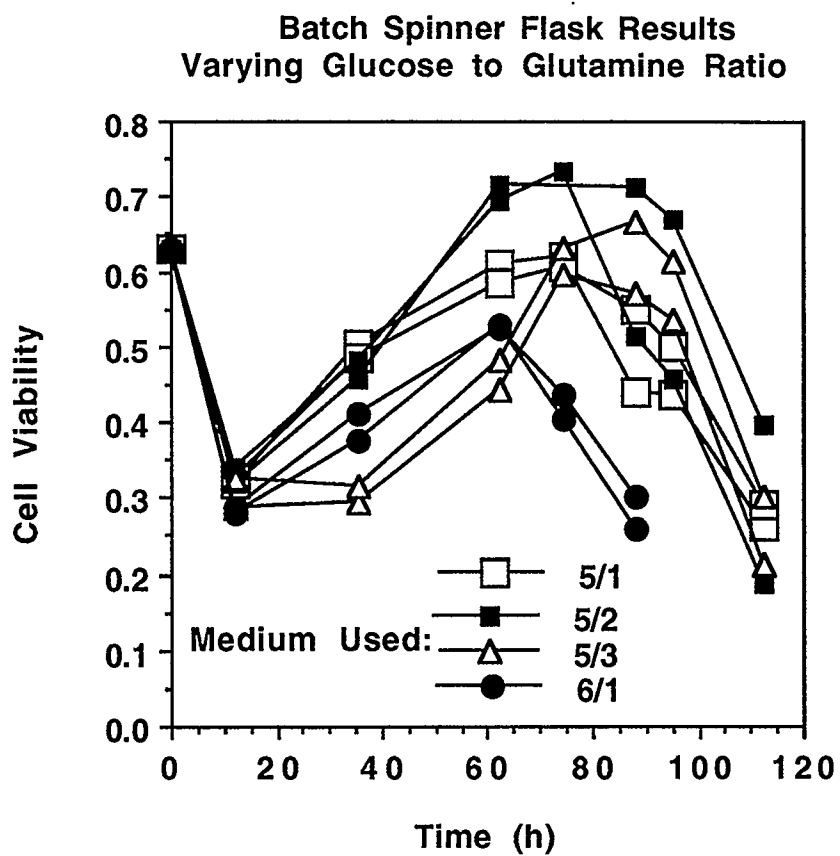


Figure 5.34 Cell viability profiles for batch cultures in media containing four different glucose to glutamine ratios.

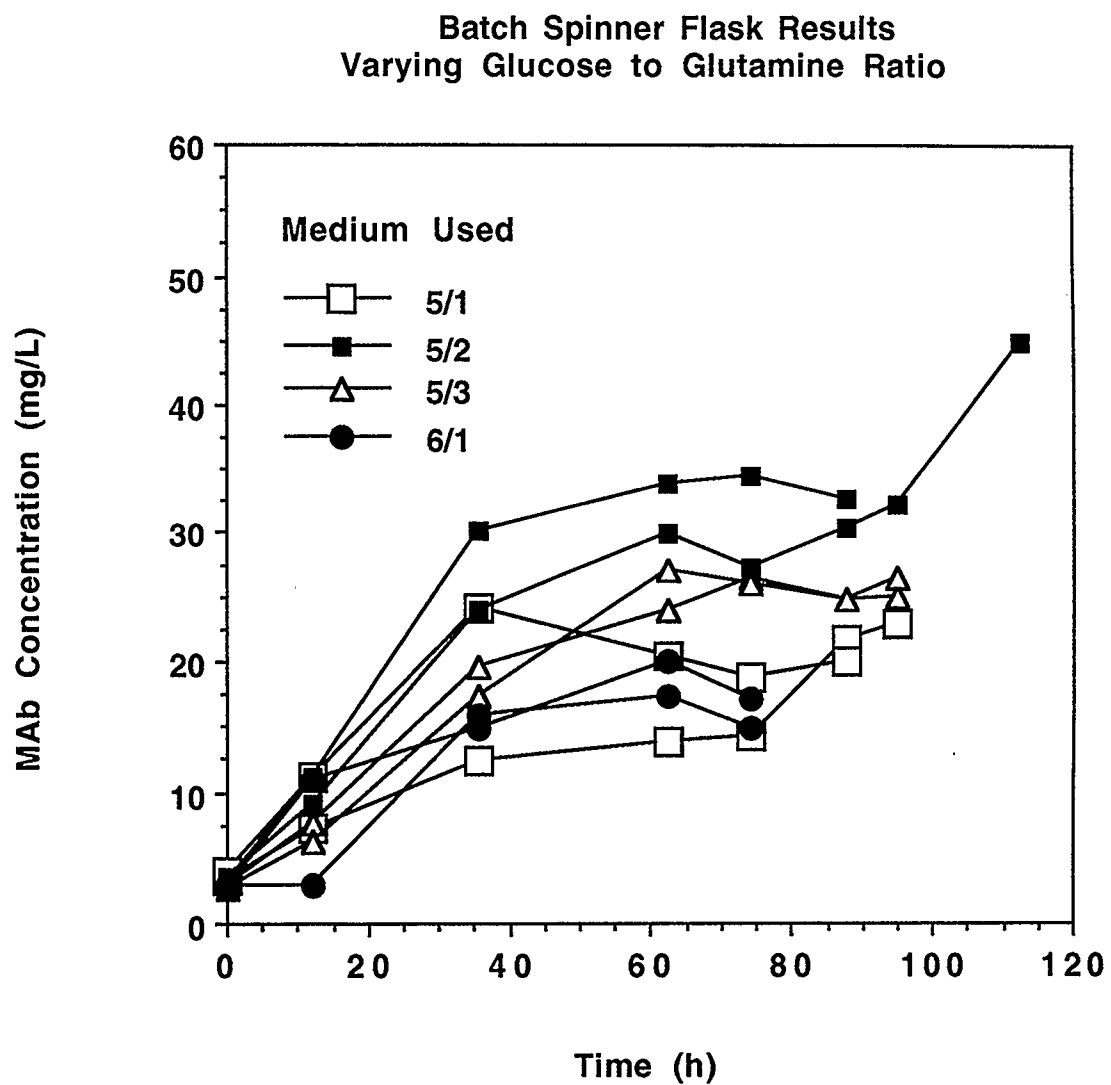


Figure 5.35 MAb production in media containing four different glucose to glutamine ratios.

In previous results from batch cultures in standard medium we have seen that glutamine is depleted quite early in the run, i.e. the batch cultures become glutamine limited very early. Therefore, it appears that doubling of the glutamine concentration (in the 5/2 medium) had a positive effect on growth and MAb production. The 5/3 medium was between the regular and the 5/2 and finally the 6/1 medium gave the poorest results.

5.4. SHEAR PROTECTION BY METHYLCELLULOSE

In this series of batch experiments we examined the protective effect of methylcellulose (MCL) against shear stress. The methylcellulose used was supplied by SIGMA (M- 6385). According to the specifications of the supplier a 2% solution at 25° C has a viscosity of 25 *cps*. The cells were grown in 100 *mL* spinner flasks (Figure 4.1). The stirring speeds and MCL concentration were varied in order to examine the MCL effect at different levels of shear stress. The stirring speed was measured accurately by using a strobe light. Viable cell density, viability and MAb titer were determined for each culture sample.

Two separate experiments were conducted. In the first experiment the effect of stirring speed on cells growing in medium with no MCL was studied. The stirring speeds used were 150, 320 and 430 *RPM*. The main results are summarized in Table 5.6. Figure 5.36 shows the profile of viable cell densities for the three different cases. It can be seen that at 150 and 320 *RPM* cultures attained the same maximum viable cell density with an important difference: the cell density in the 320 *RPM* culture remained high for approximately 30 *h* longer than the 150 *RPM* culture. The reason for the difference can be seen in the viability profile shown in Figure 5.37. The viability in the 150 *RPM* culture started to drop at 50 *h*, while the 320 *RPM* culture viability remained high until the 80 *h* mark. Finally it is clear that the shear stress at 430 *RPM* completely inhibited cell growth. In the viability profile we see that there was a plateau during the period that corresponded to the growth of cells and then the viability dropped very sharply. This observation indicates that the high nutrient level in the beginning of the run had a posi-

Table 5.6. EFFECT OF STIRRING SPEED - 0.0% METHYLCELLULOSE (Experiment 1)					
Stirring Speed	Inoculation		Results		
	x_v	V_x	$x_{v,max}$	V_x	MAb
<i>RPM</i>	$\times 10^6 \text{ cells/mL}$	%	$\times 10^6 \text{ cells/mL}$	%	<i>mg/L</i>
150	0.5	87	2.80	62	36
320	0.5	85	2.65	93	43
430	0.45	87	0.45	23	23

Table 5.6 Effect of stirring speed on 100 mL batch spinner flask cultures with no methylcellulose added. Results from Experiment 1.

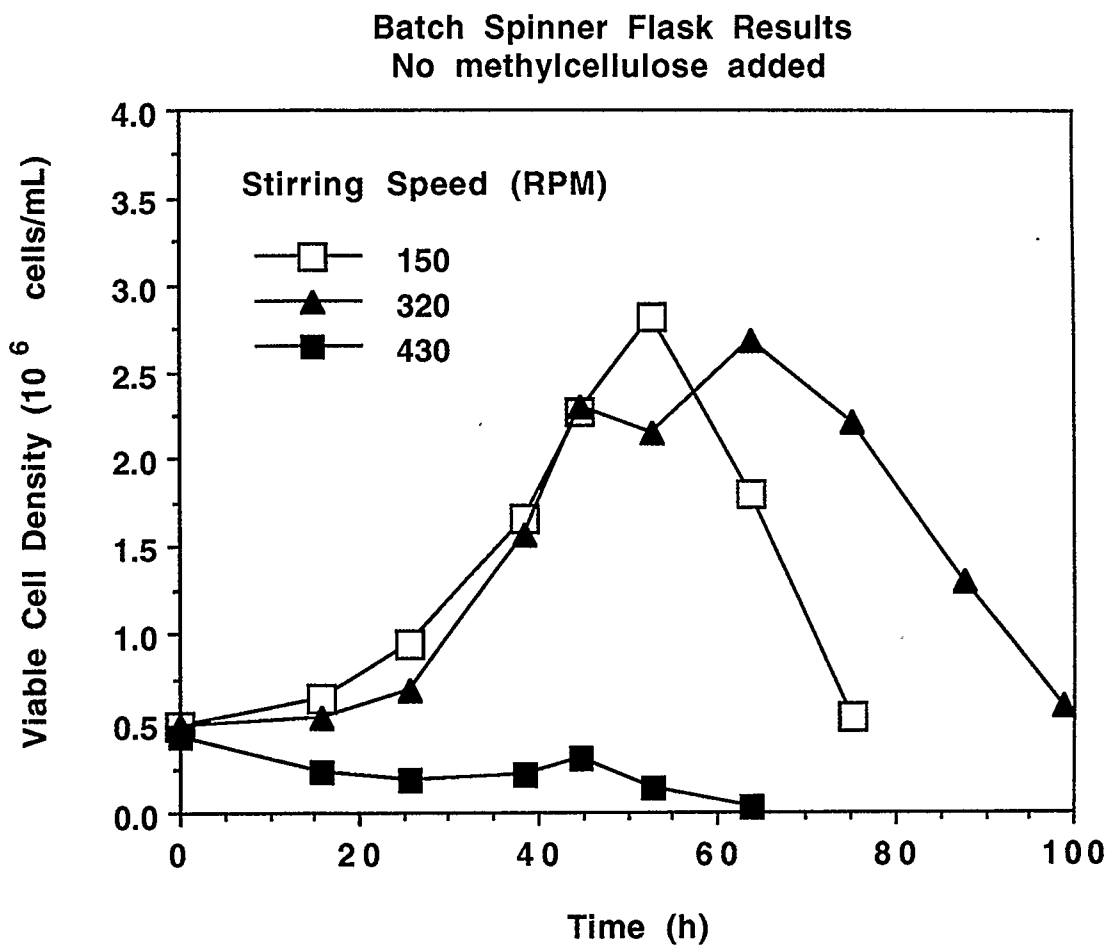


Figure 5.36 The effect of stirring speed on viable cell density in 100 mL batch spinner flask cultures without methylcellulose. Results from Experiment 1.

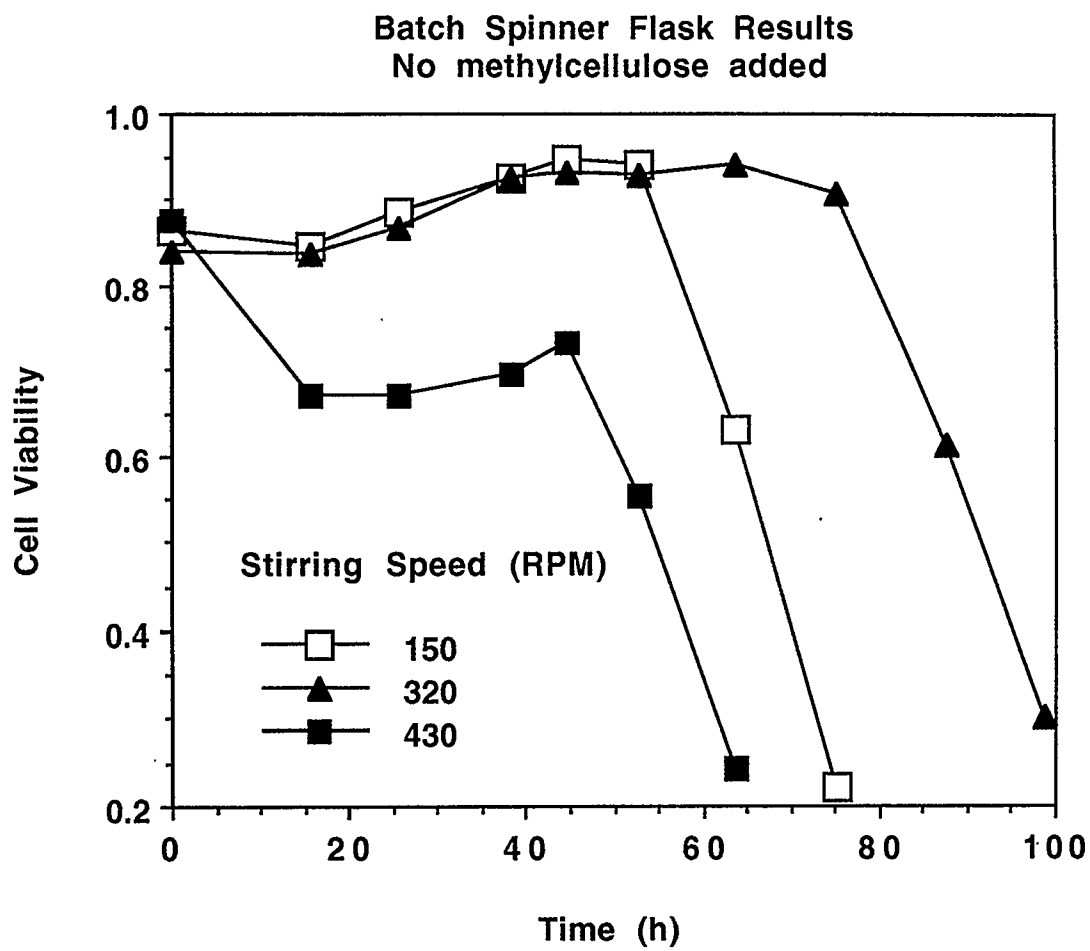


Figure 5.37 The effect of stirring speed on cell viability in 100 mL batch spinner flask cultures without methylcellulose. Results from Experiment 1.

tive effect on the resistance of cells to shear stress, which is in agreement with the observations of Petersen et al. (1988).

The MAb concentration profiles are shown in Figure 5.38. It can be seen that in the 320 *RPM* culture more antibody is produced because the cells were viable at a high density approximately 30 *h* longer than in the 150 *RPM* culture. The MAb production was limited in the 430 *RPM* culture. However, if one considers the very low viable cell density of the cells in that culture (approximately 0.3×10^6 *cells/mL*) it is easy to conclude that the specific MAb productivity in the 430 *RPM* culture was higher than in the low *RPM* cultures. Again this is an indication of increased MAb production under conditions of environmental stress.

The first experiment also included duplicate spinner flasks with cultures supplemented with 0.3% MCL. This concentration was found to be beneficial in insect cell cultures by Stavroulakis (1990). The stirring speeds tested were 150, 320 and 430 *RPM*. The profiles of viable cell density, viability and MAb titer are shown in Figures 5.39, 5.40 and 5.41 respectively. The main conclusion is that all three types of cultures exhibited the same growth and MAb production characteristics, i.e. MCL had a protective effect at the speeds examined. An interesting difference in MAb production can be observed in Figure 5.41 after the 65 *h* point. In the higher speed cultures the antibody seems to drop off more than in the low speed culture. The results are summarized in Table 5.7.

The second experiment examined the effect of MCL concentration at 430 and 350 *RPM*. The results for 430 *RPM* are compared in Figures 5.42, 5.43 and 5.44 (EXP 2). The corresponding results from the first experiment (EXP 1) are also plotted in the same figures for comparison. The main conclusion is that at 430 *RPM* the full protective effect of MCL is apparent at a 0.1% concentration. The results are also summarized in Table 5.8.

The viable cell density, viability and MAb profiles for a stirring speed of 560 *RPM* and varying MCL contents are shown in Figures 5.45, 5.46 and 5.47 respectively. These results were also collected in the second experiment. It can be seen that there

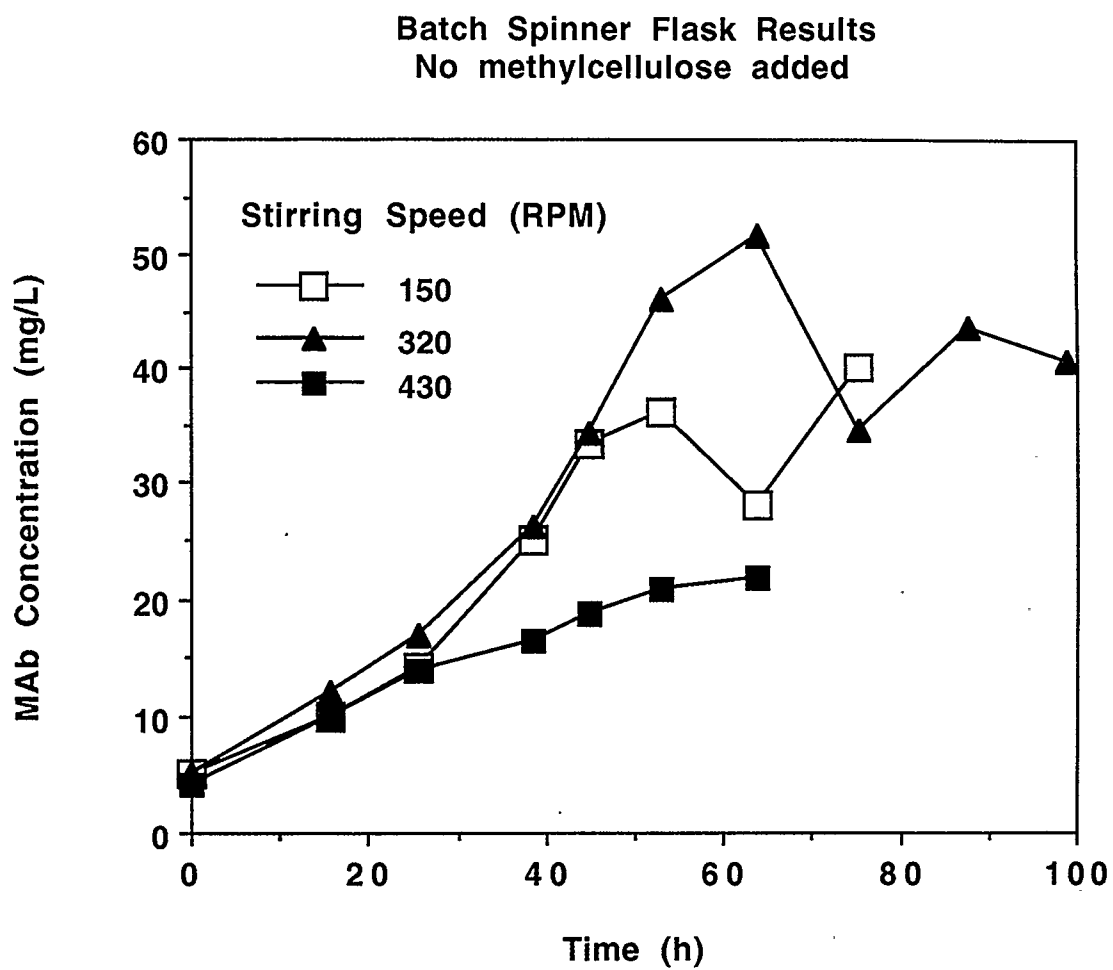


Figure 5.38 The effect of stirring speed on MAb production in 100 mL batch spinner flask cultures without methylcellulose. Results from Experiment 1.

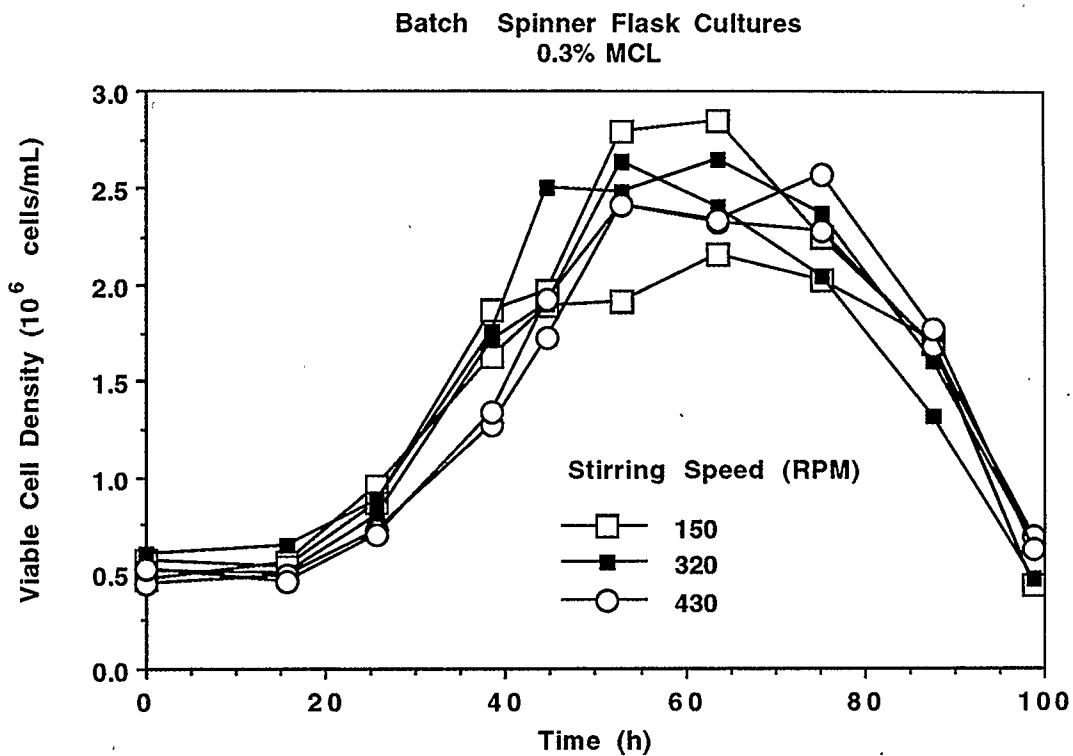


Figure 5.39 The effect of stirring speed on viable cell density in 100 mL batch spinner flask cultures with 0.3% *w/v* methylcellulose. Results from Experiment 1.

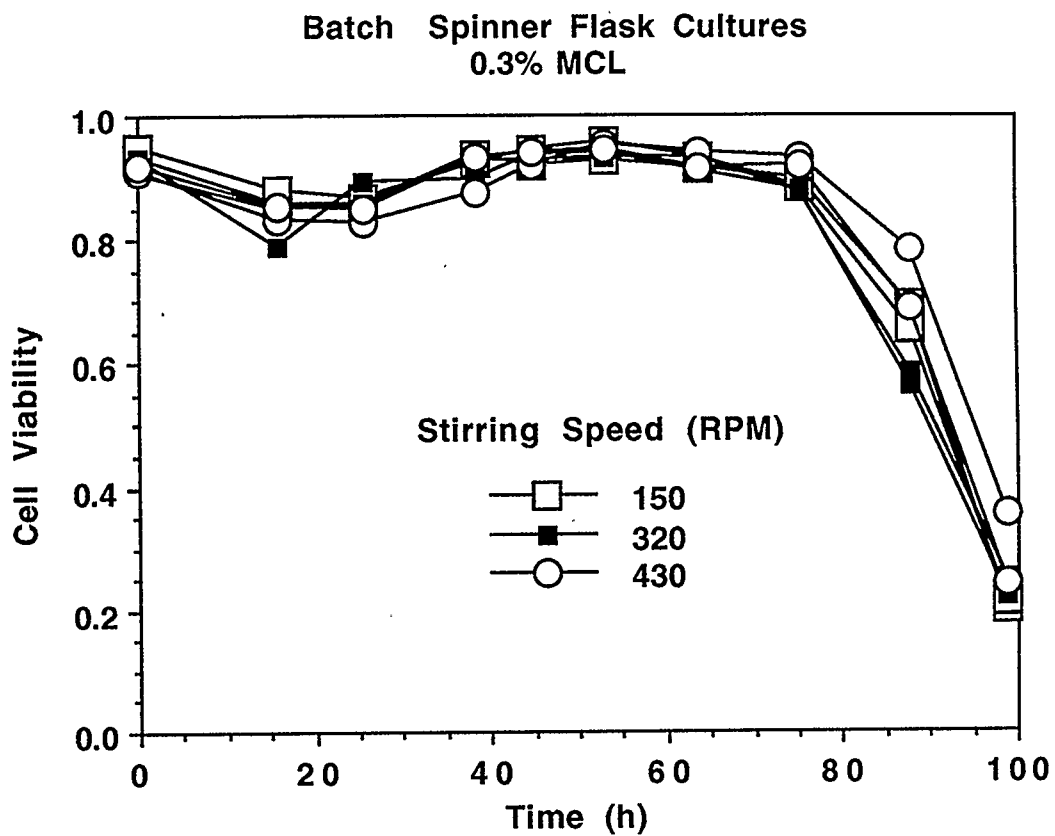


Figure 5.40 The effect of stirring speed on cell viability in 100 mL batch spinner flask cultures with 0.3% w/v methylcellulose. Results from Experiment 1.

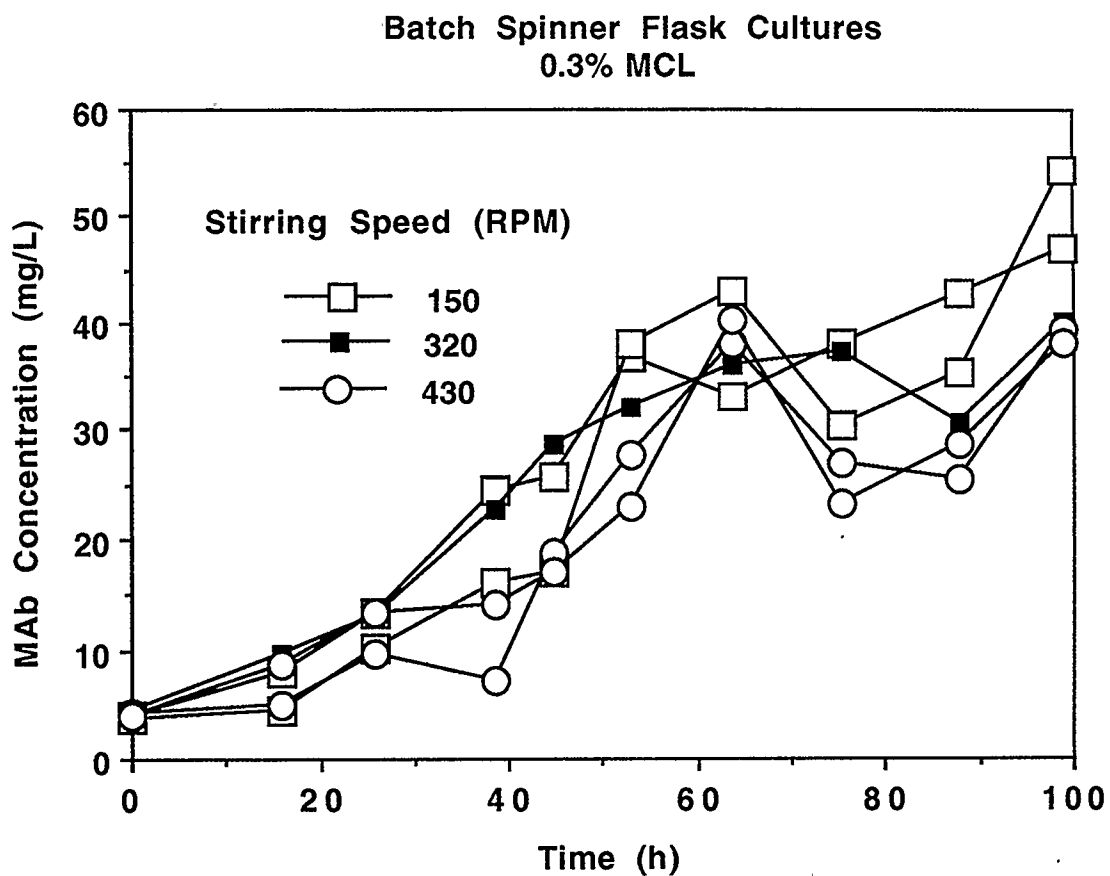


Figure 5.41 MAb production in 100 mL batch spinner flask cultures agitated at various rates. 0.3% w/v methylcellulose was added. Results from Experiment 1.

Table 5.7. EFFECT OF STIRRING SPEED - 0.3% METHYLCELLULOSE (Experiment 1 - * : Experiment 2)					
Stirring Speed	Inoculation		Results		
	x_v	V_x	$x_{v,max}$	V_x	MAb
<i>RPM</i>	$\times 10^6$ cells/mL	%	$\times 10^6$ cells/mL	%	mg/L
150	0.5	85	2.80	93	37
320	0.45	84	2.65	91	33
430	0.45	85	2.40	92	32
430*	0.45	80	2.25	88	33
560*	0.45	80	1.85	86	33

Table 5.7 Effect of stirring speed on 100 mL batch spinner flask cultures supplemented with 0.3% w/v methylcellulose.

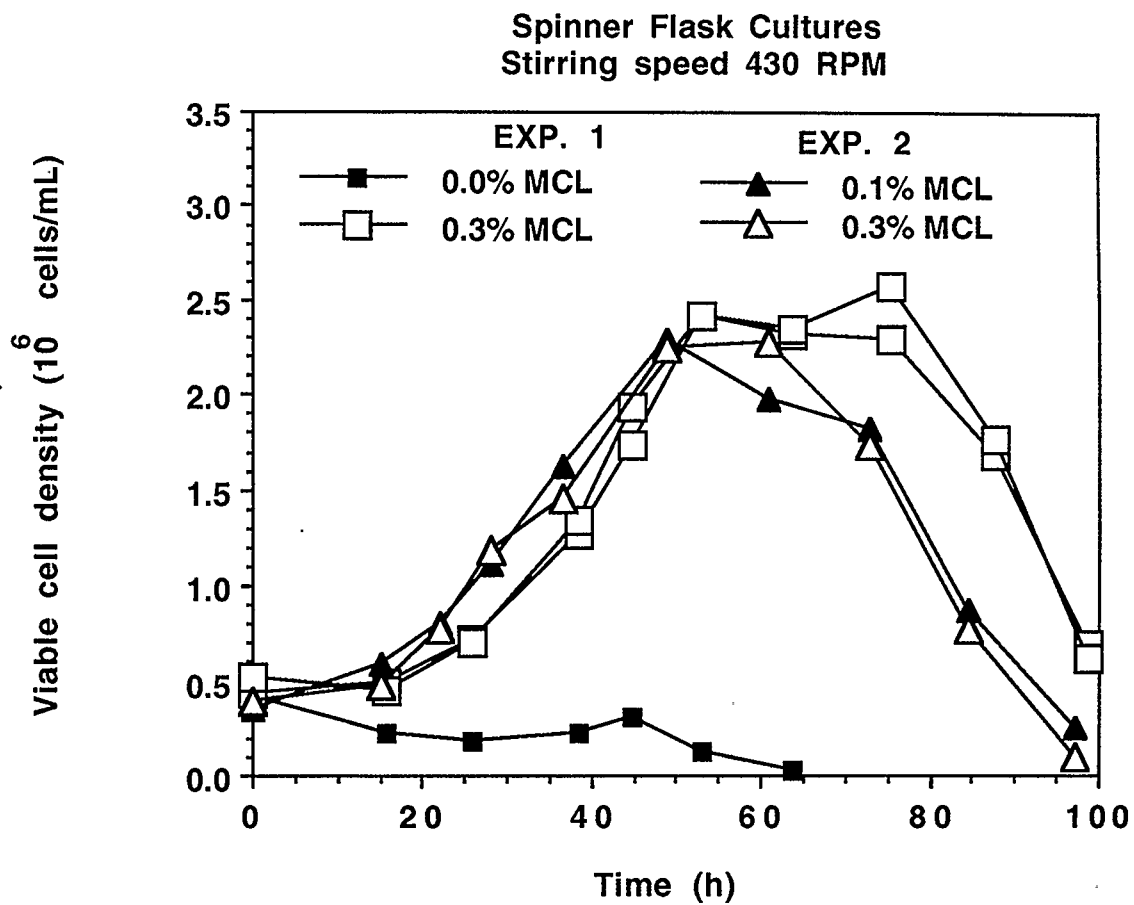


Figure 5.42 Viable cell density profiles in 100 mL batch spinner flask cultures stirred at 430 RPM and supplemented with varying MCL concentrations.

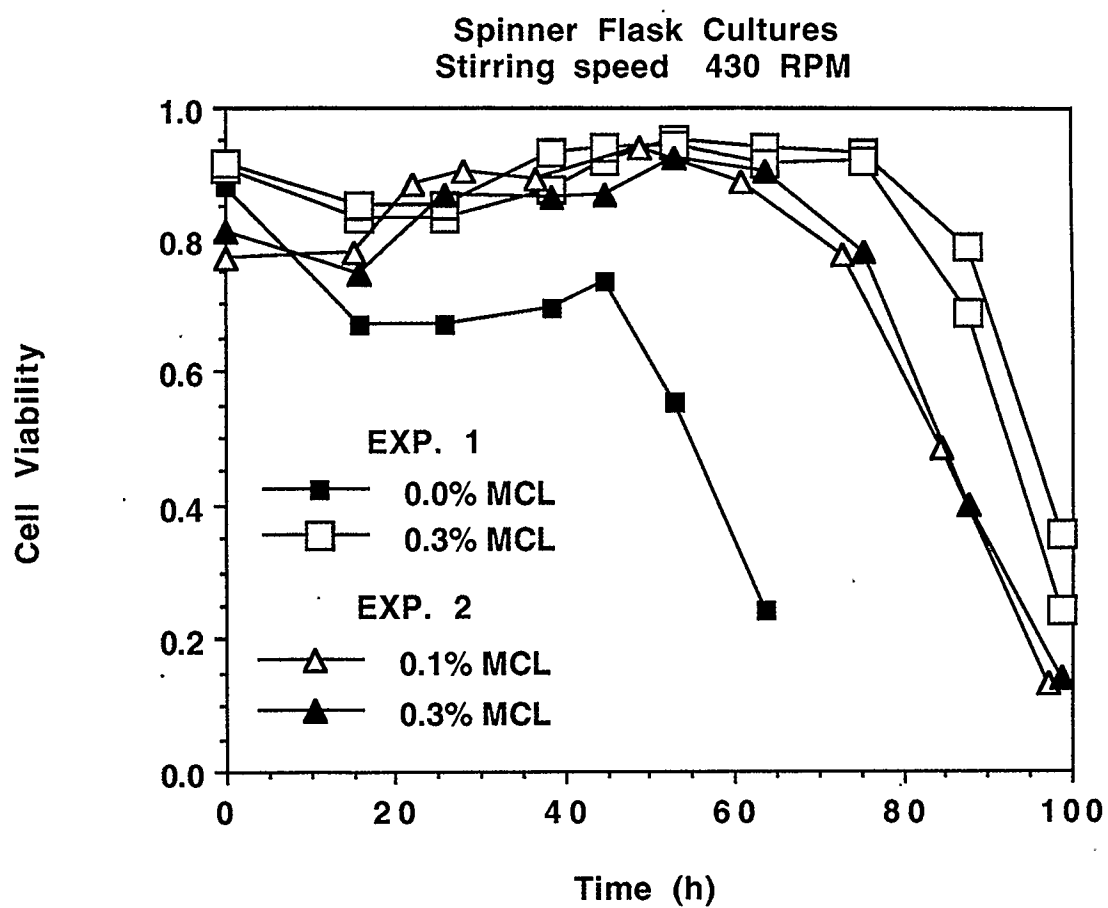


Figure 5.43 Cell viability profiles in 100 mL batch spinner flask cultures stirred at 430 RPM and supplemented with varying MCL concentrations.

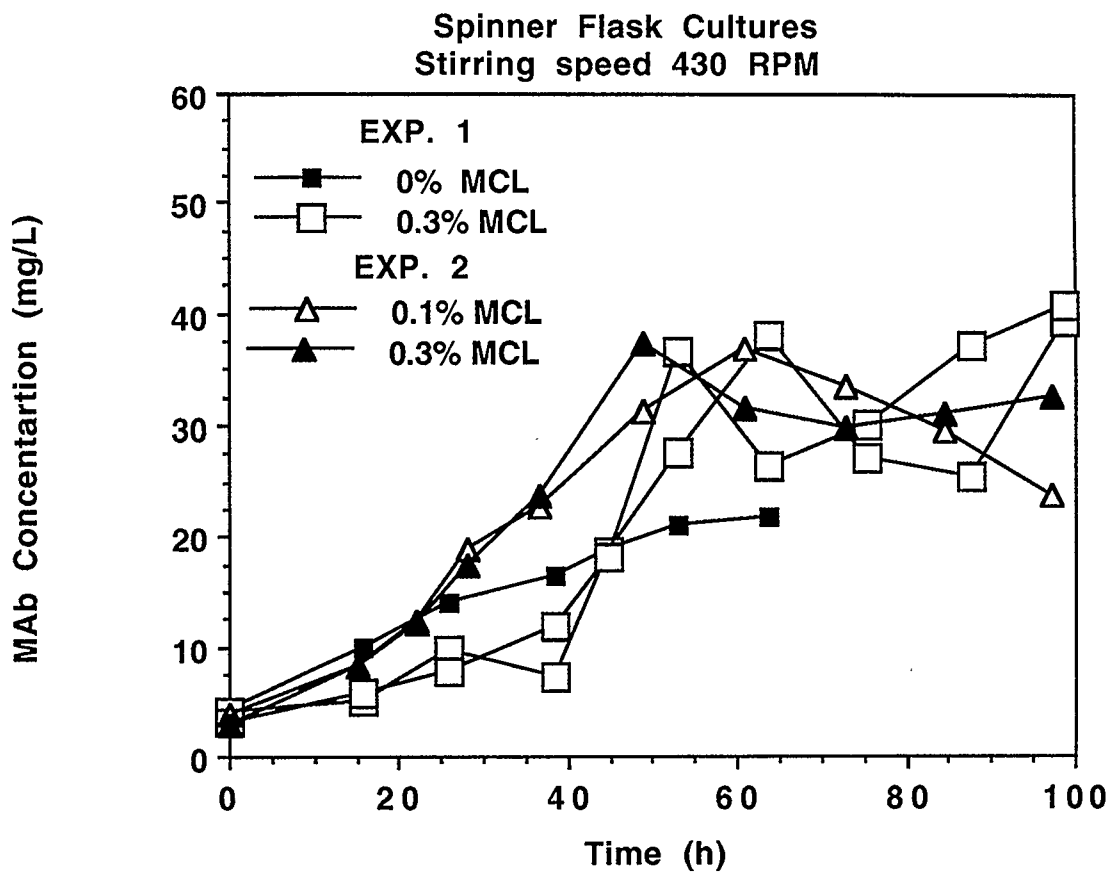


Figure 5.44 MAb production in 100 mL batch spinner flask cultures stirred at 430 RPM and supplemented with varying MCL concentrations.

was an increasing protective effect of MCL when its concentration increases from 0.1% to 0.3%; however, even at the lowest concentration of 0.1% the protective effect is remarkable. In Figure 5.47 we can see that the MAb titers are comparable for all three MCL concentrations. The results at 560 *RPM* are summarized in Table 5.9

In conclusion, MCL exhibited a remarkable protective effect against shear stress in spinner flask cultures. Methylcellulose concentrations as low as 0.1% were used without any loss in shear protection up to 560 *RPM*, as compared to cultures supplemented with 0.6% MCL.

Table 5.8 EFFECT OF METHYLCELLULOSE - 430 RPM (Experiments 1 and 2 [*])					
MCL Content	Inoculation		Results		
	x_v	V_x	$x_{v,max}$	V_x	MAb
%w/v	$\times 10^6$ cells/mL	%	$\times 10^6$ cells/mL	%	mg/L
0.0	0.45	87	0.45	23	23
0.1 [*]	0.4	78	2.30	88	32
0.3	0.45	85	2.40	92	32
0.3 [*]	0.4	82	2.25	88	33
0.6 [*]	0.45	72	2.20	82	31

Table 5.8 Effect of methylcellulose concentration on shear protection at a stirring speed of 430 RPM.

Table 5.9. EFFECT OF METHYLCELLULOSE - 560 RPM (Experiment 2)					
MCL Content	Inoculation		Results		
	x_v	V_x	$x_{v,max}$	V_x	MAb
%w/v	$\times 10^6$ cells/mL	%	$\times 10^6$ cells/mL	%	mg/L
0.1	0.5	79	1.75	83	35
0.3	0.45	80	1.85	86	33
0.6	0.45	72	2.20	82	31

Table 5.9 Effect of methylcellulose concentration on shear protection at a stirring speed of 560 RPM. Results from Experiment 2.

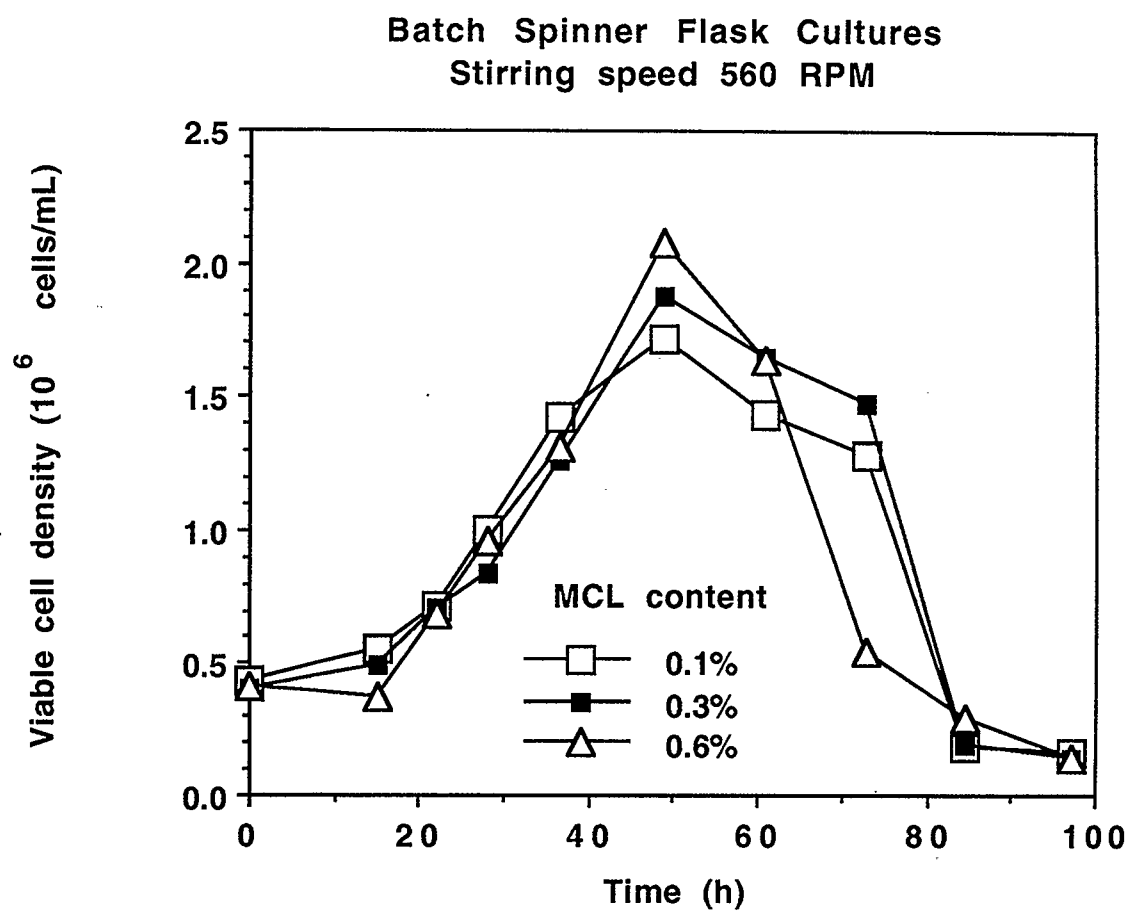


Figure 5.45 Viable cell density profiles in 100 mL batch spinner flask cultures stirred at 560 RPM and supplemented with varying MCL concentrations. Results from Experiment 2.

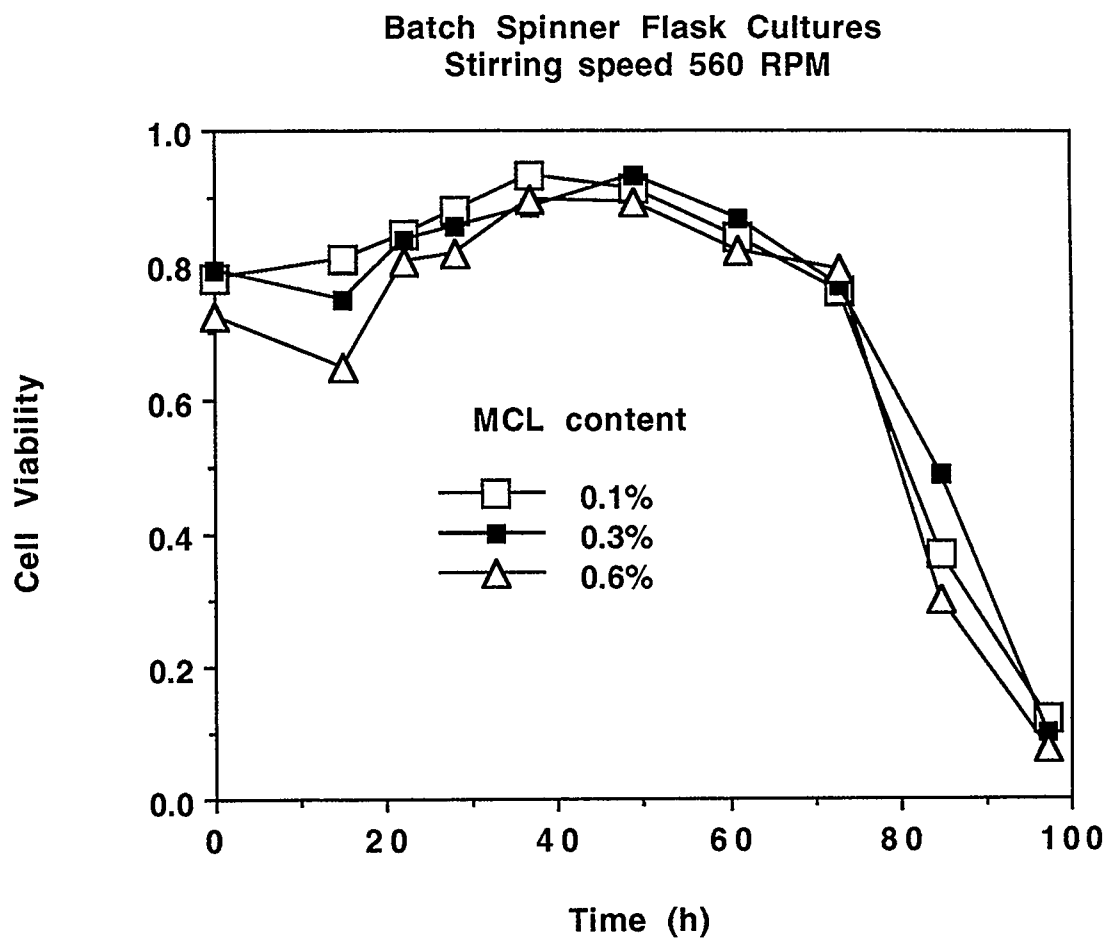


Figure 5.46 Cell viability profiles in 100 mL batch spinner flask cultures stirred at 560 RPM and supplemented with varying MCL concentrations. Results from Experiment 2.

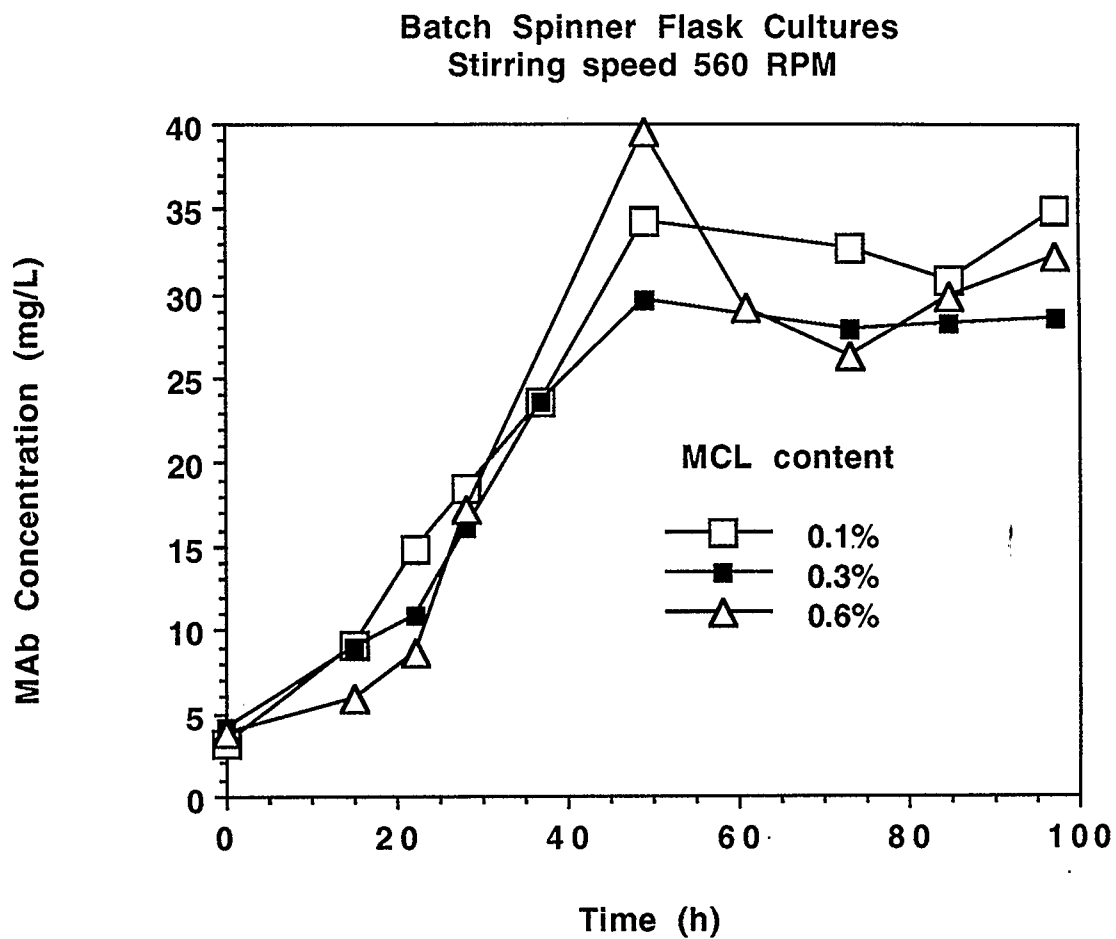


Figure 5.47 MAb production in 100 mL batch spinner flask cultures stirred at 560 RPM and supplemented with varying MCL concentrations. Results from Experiment 2.

6. EXPERIMENTAL RESULTS - CONTINUOUS CULTURES

It is well known that the steady state specific growth rate in chemostat cultures is determined by the the dilution rate (Pirt, 1975). In the experiments described in the first part of this chapter the dilution rate was maintained at four different values, giving rise to four different steady states. The medium used was regular DMEM (Appendix A) with 1.5% FBS. At all dilution rates pH was controlled at 7.00 ± 0.05 and the dissolved oxygen concentration (DO) at $30\% \pm 2\%$ of saturation. The steady state measurements were used to study the effect of growth rate on cell death, nutrient uptake and MAb production.

The dilution rate was kept constant at $0.45 d^{-1}$ in the chemostat experiments that followed. The effects of the environmental parameters pH and DO on cell growth and MAb production were studied in the chemostat runs described in section 6.2. In the section 6.3 the effect of glucose to glutamine ratio in the feed medium was examined in chemostat culture. This experiment was a continuation of the corresponding batch spinner flask experiments. Media with three different glucose to glutamine ratios were used, namely 5/1 (standard), 5/2 and 5/3. The pH and DO settings in this experiment were 7.00 and 30% respectively.

6.1. EFFECT OF DILUTION RATE

Typical profiles of the cell density and viability transients during step changes in the dilution rate in the chemostat are shown in Figure 6.1. The run shown started with a constant dilution rate $D = 0.5 d^{-1}$. After inoculation the cell density and the viability increased until a steady state was reached between 400 and 550 *h*. Subsequently the dilution rate was changed to $0.4 d^{-1}$. The viability started to drop after the change in the dilution rate. The cell density also exhibited a slight falling trend immediately after the step change. Both parameters reached their steady state values by 1000 *h*. The time needed for the reactor to reach steady-state in our experiments was comparable to 700 *h* reported by Tovey and Brouty-Boye (1976) for murine leukemia cells. Four different dilution rates were used in total. The steady state results are discussed in the

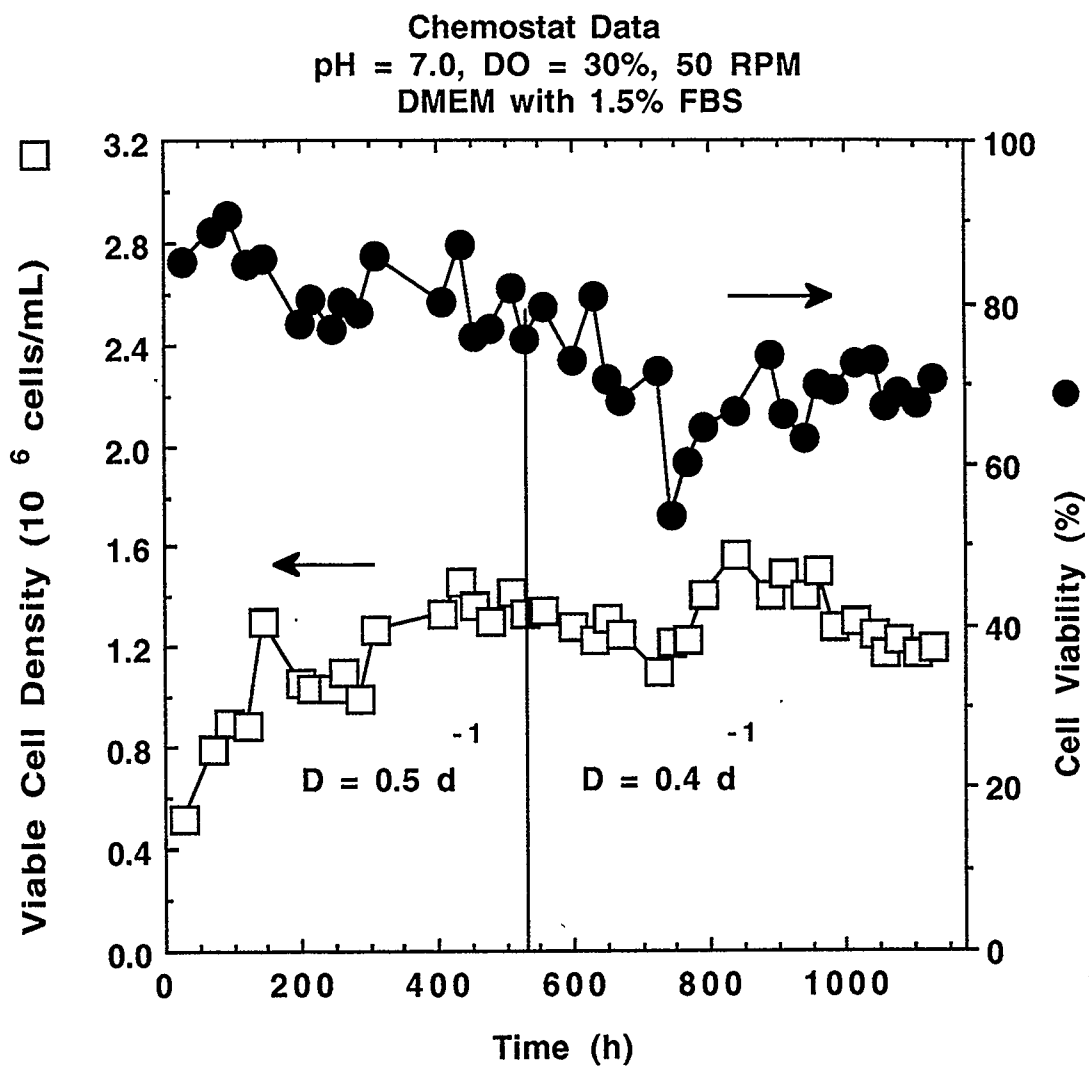


Figure 6.1 Chemostat experiments: Viable cell density and viability transients during a step change in dilution rate from 0.5 d^{-1} to 0.4 d^{-1} .

following paragraphs.

6.1.1 Viable cell density and viability

The profiles of viable cell density and cell viability are shown in Figure 6.2 with respect to the dilution rate. The viable cell concentration is clearly exhibiting a maximum in the vicinity of $D = 0.8 d^{-1}$. At higher dilution rates the viable cell count decreases due to increased medium throughput, while at lower dilution rates the viability drops sharply with a detrimental effect on viable cell density. The experimental data by Miller et al. (1988) in chemostat hybridoma cultures limited by both glucose and glutamine show a similar behavior. However, Tovey and Brouty-Boye (1976) observed a monotonically decreasing viable cell density with dilution rate in glucose-limited cultures of leukemia cells. Furthermore, in chemostat cultures of a non-producing hybridoma clone the viable cell concentration increased with decreasing dilution rate (Frame and Hu, 1991).

The culture viability, under well mixed conditions, is given by the equation

$$v_x = \frac{x_v}{x_t} \quad (6.1)$$

where x_v and x_t denote the viable and total (viable and dead) cell concentrations respectively. Figure 6.2 shows that the viability drops sharply with decreasing dilution rate, in agreement with the findings of Miller et al. (1988) and Boraston et al. (1984).

6.1.2 Growth rate and death rate

In a chemostat the viable cell density, x_v , is given as a function of time by the equation

$$\frac{dx_v}{dt} = (\mu - k_d - D)x_v \quad (6.2)$$

where μ is the specific growth rate, k_d is the specific death rate, and D is the dilution rate. At steady state the viable cell density is constant. Therefore, Equation (6.2) becomes

$$\mu = D + k_d \quad (6.3)$$

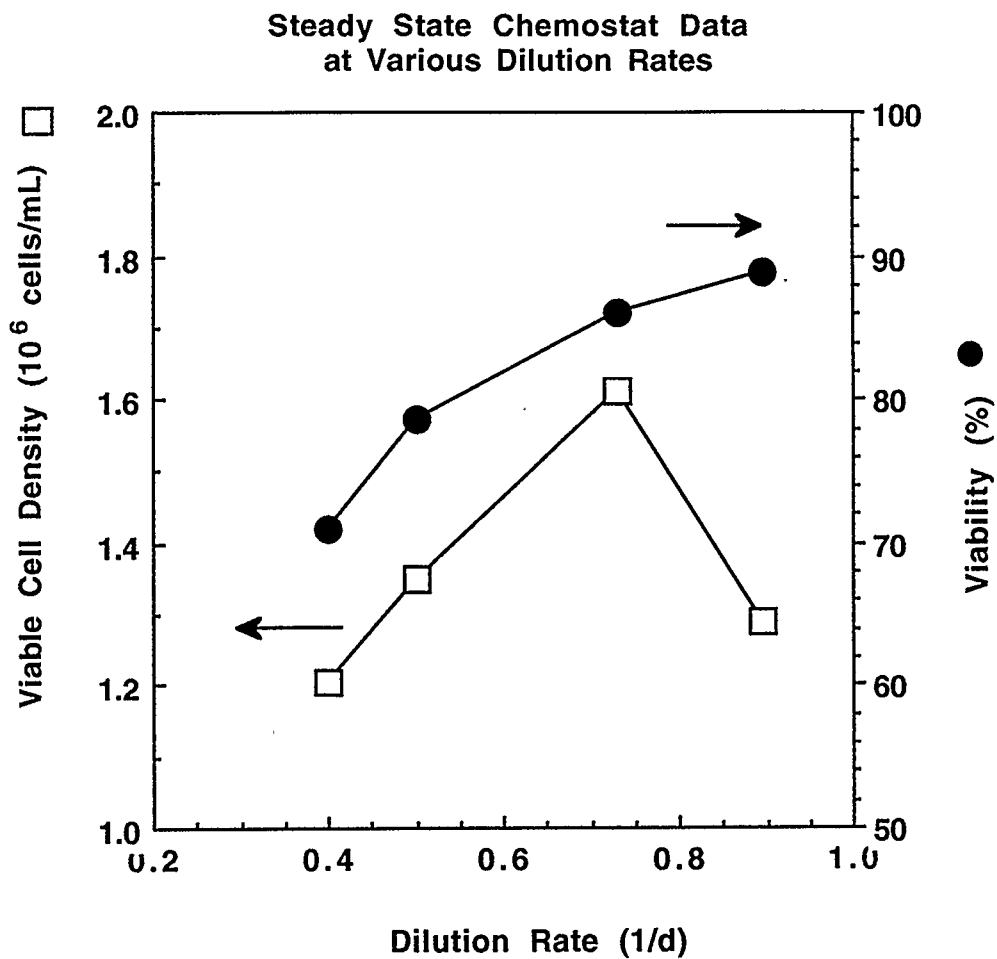


Figure 6.2 Steady state viable cell density and cell viability in the chemostat with respect to the dilution rate.

The dead cell density, x_d , is given by the equation

$$\frac{dx_d}{dt} = k_d x_v - D x_d \quad (6.4)$$

At steady state conditions Equation (6.4) yields

$$k_d x_v = D x_d = D (x_t - x_v) \quad (6.5)$$

Therefore, the steady state specific death rate, k_d , can be calculated by the relationship

$$k_d = D \left(\frac{1}{v_x} - 1 \right) \quad (6.6)$$

The steady state growth rate can then be calculated from Equation (6.3). The steady state growth and death rates for the four dilution rates used are given in Figure 6.3. The diagonal represents the case $\mu = D$, for all dilution rates, that is the case of negligible death rate.

6.1.3 Nutrient and waste concentrations

The steady state concentrations of four key components of the culture supernatant, namely the nutrients glucose and glutamine and, the toxic by-products of metabolism lactate and ammonia are shown in Figure 6.4. The profiles of residual nutrient concentrations show an increase at high dilution rates and a plateau at lower dilution rates. Miller et al. (1988) observed the same behavior with a slight increase of the residual concentrations of nutrients at lower dilution rates. Tovey and Brouty-Boye (1976) using a feed medium with only 1 g/L glucose, observed also a monotonic increase of the residual concentration of glucose with increasing dilution rate. Similar behavior was observed by Frame and Hu (1991).

The concentrations of the metabolites lactate and ammonia show a behavior closely corresponding to that of the nutrients glucose and glutamine. The major source of lactate and ammonia in mammalian cell cultures are glucose and glutamine respectively. The concentrations of the waste products exhibit a broad maximum, in the area

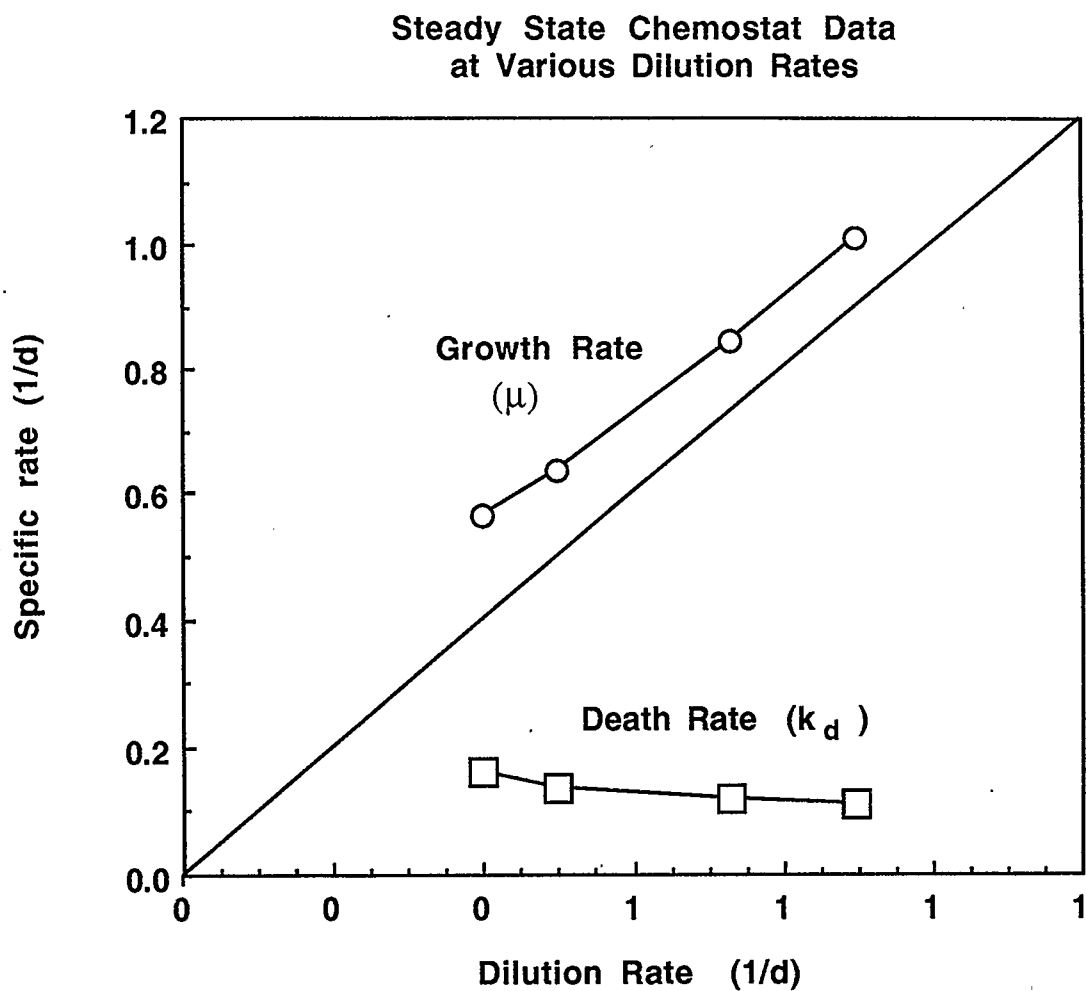


Figure 6.3 Specific growth rate and death rate in the chemostat as a function of the dilution rate.

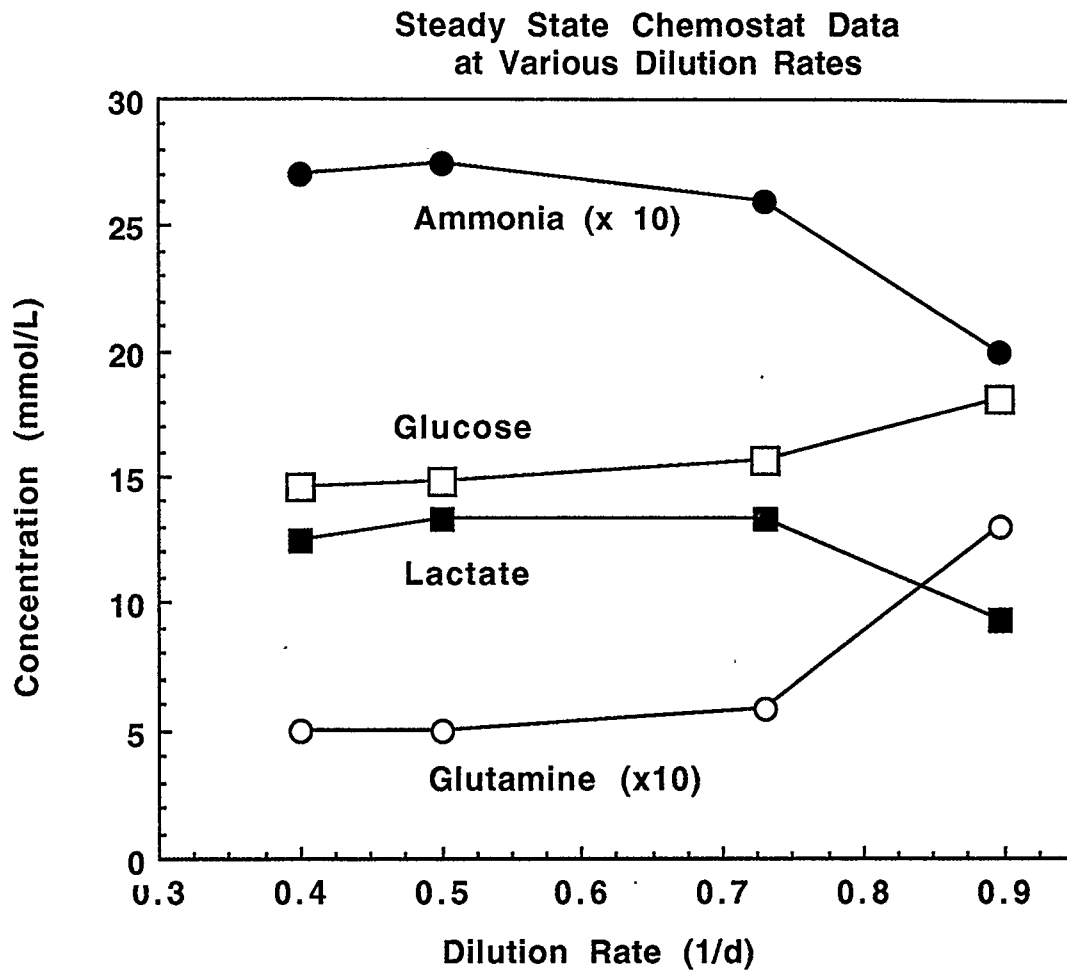


Figure 6.4 Residual nutrient and waste product concentrations at steady states using four different dilution rates.

of $D = 0.5 \text{ d}^{-1}$ for ammonia and 0.5 to 0.7 d^{-1} for lactic acid. With increasing growth rate (dilution rate) the concentrations drop sharply, due to the increasing dilution effect of the feed medium.

6.1.4 Monoclonal antibody production

Figure 6.5 shows the steady state MAb concentration for the four different dilution rates. It is clear that MAb titer increases sharply with decreasing dilution rate. The observed increase can be attributed to the reduced medium throughput and perhaps to increased production of MAb on a cell basis. In order to separate the effects we need to calculate the specific production rate of MAb.

The MAb concentration C_m in a chemostat satisfies the partial mass balance around the bioreactor, namely

$$dC_m/dt = q_m x_v - DC_m \quad (6.7)$$

where q_m is the specific MAb production rate. At steady state Equation (6.7) reduces to

$$q_m x_v = DC_m \quad (6.8)$$

The steady state specific MAb productivity, q_m , was calculated at the four dilution rates using Equation (6.8) and it is shown in Figure 6.6 as a function of the specific growth rate. As seen, q_m increases sharply at lower growth rates. In fact, there seems to exist an inverse relationship between q_m and the specific growth rate μ . This result is in excellent agreement with the findings of Miller et al. (1988) and Hagedorn and Kargi (1990). Furthermore, a similar behavior is predicted by the models of Suzuki and Ollis (1989a, 1989b). To explain the inverse relationship between growth and MAb production certain researchers postulate that "stress", i.e. conditions that lead to reduced cell growth and increased cell death rates have a positive effect on the MAb producing capability of hybridomas (Hagedorn and Kargi, 1990).

In support of the "stress" theory we note that the pattern of MAb production in our experiments bears some important similarities with the production of stress proteins

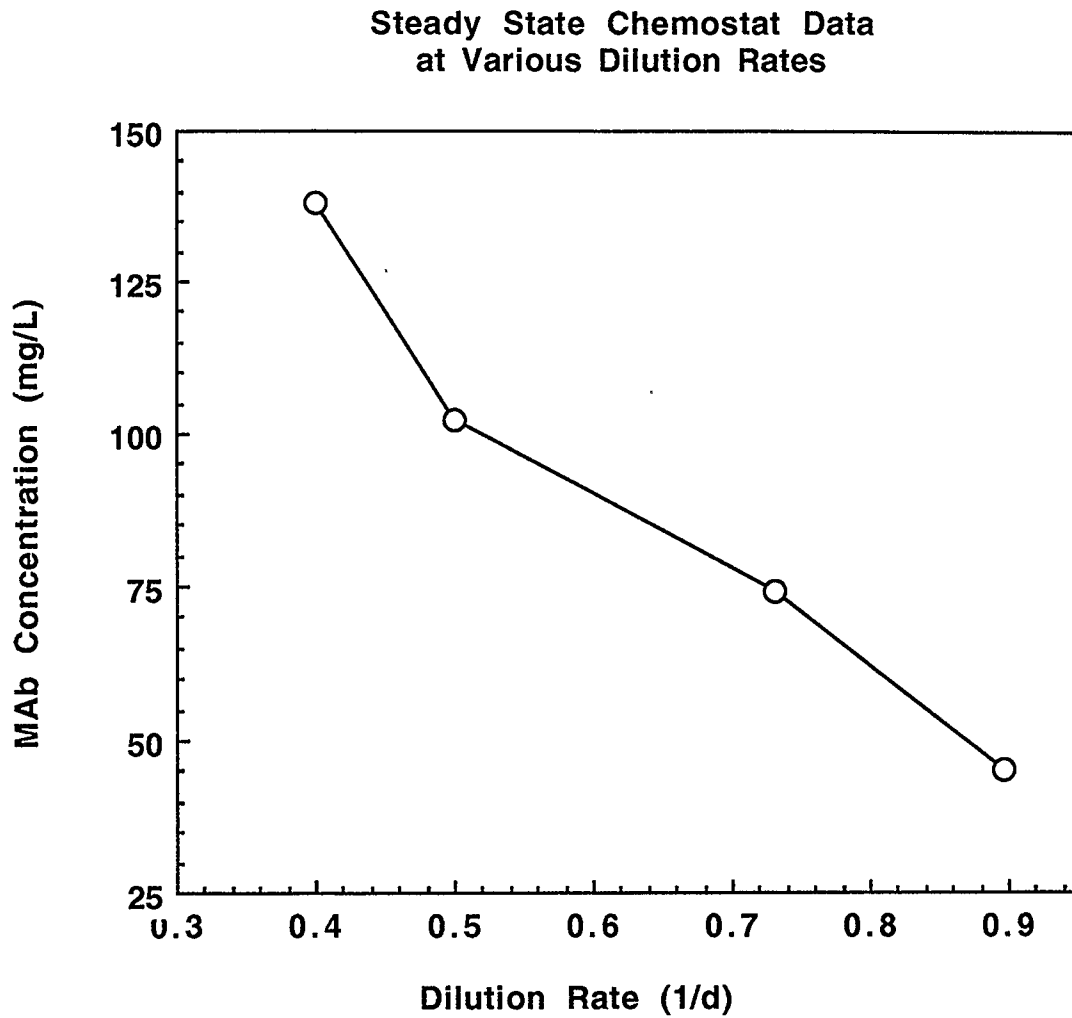


Figure 6.5 Steady state MAb concentration in the chemostat as a function of the dilution rate.

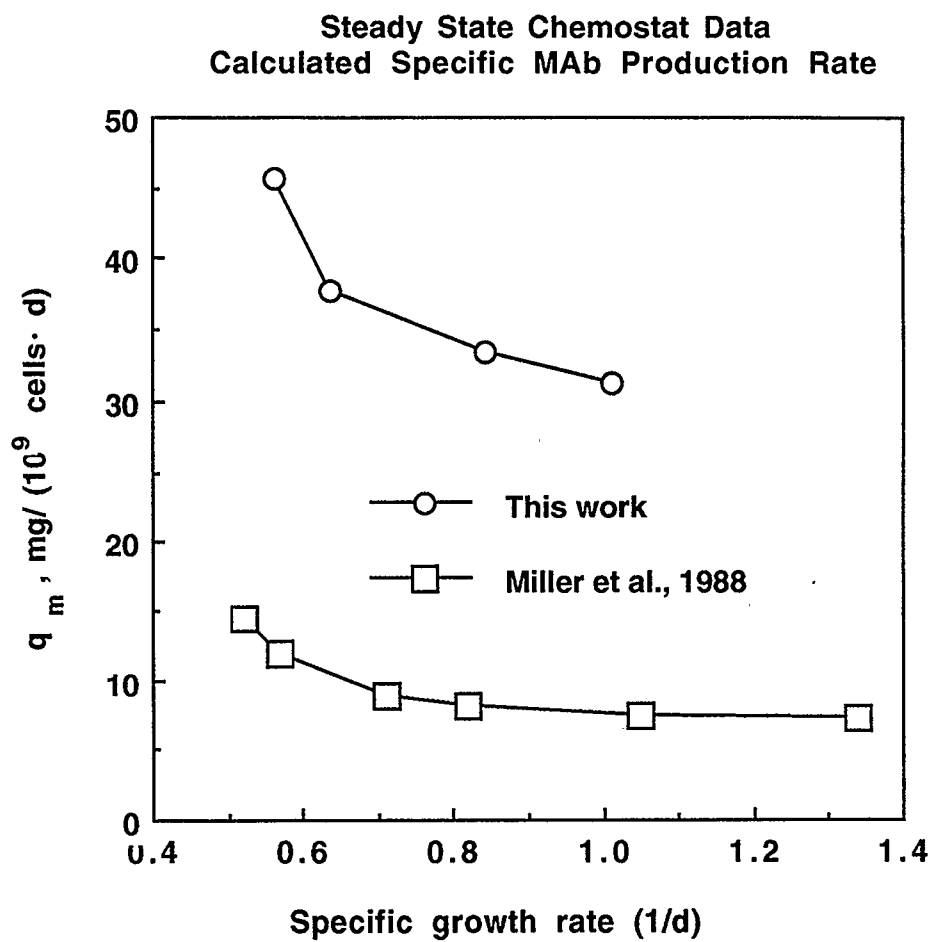


Figure 6.6 Steady state values of the specific MAb production rate (q_m) at four different growth rates. Data by Miller et al. (1988) are also shown here.

by mammalian cells. Most interesting is the analogy with the production of the group of glucose-regulated heat shock proteins GRP78 and GRP95. These proteins are produced at low basal levels in unstressed mammalian cells and at higher basal levels in unstressed secretory cells such as hybridomas and liver cells. The rate of synthesis of the above proteins increases as a result of glucose deprivation or heat shock. Increased synthesis can also be induced by a variety of other stress conditions and toxic agents (Goochee and Passini, 1988).

The glucose-regulated protein GRP78 has been proven to be identical to the immunoglobulin (Ig) heavy-chain binding phosphoprotein BiP which is found associated with immunoglobulin heavy chains in the endoplasmic reticulum (ER) of antibody secreting hybridomas. When no light chains are being assembled, heavy chains remain associated with BiP in the ER and are thus prevented from forming insoluble heavy-chain aggregates (Munro and Pelham, 1986; Bole et al., 1986). However, after assembly of the two light chains with the two heavy chains is complete, BiP dissociates from the Ig molecules. The Ig then proceeds to the Golgi apparatus and is eventually secreted. Therefore, BiP production and MAb production are two tightly interrelated processes.

Experimental work by Golding et al. (1988) has also linked cell stress to MAb production. The authors determined that a B-cell culture arrested in the G_1 phase contained a higher percentage of antibody producing cells. The same researchers determined experimentally that an inverse relationship existed between B-cell differentiation (or MAb production) and proliferation. A slowdown in growth rate caused an accumulation of cells in the G_1 phase and an elevated rate of MAb production. Suzuki et al. (1989a) suggested that cells arrested in the G_1 phase produce more antibody than cells in other phases of the cycle. Furthermore, the above researchers observed that the percentage of cells in the G_1 phase increased with a slowdown in growth rate. Conditions that can cause the growth rate to decrease include nutrient deprivation and adverse environmental conditions, such as pH and DO (Prescott, 1976). Therefore, high levels of environmental stress can lead to a higher percentage of cells in the G_1 phase, higher

death rates and higher MAb production rates.

6.1.5 Nutrient uptake and by-product formation.

Figure 6.7 shows the steady state glucose and glutamine specific uptake rates for the four different dilution rates used in this experiment. Miller et al. (1988) noticed that glucose uptake rates deviated from the straight line at lower growth rates. Such a trend is also apparent in the glucose uptake rate data shown in Figure 6.7. Miller et al. (1988) attributed the deviation to a lower lactate metabolic quotient at lower dilution rates, possibly reflecting a change in metabolic pathways. It is also possible that the deviation from the maintenance energy model is related to the cell physiology at the lower growth rates. Under such conditions the average cell age is increased and more cells are arrested in the G_1 compartment of the cycle (Suzuki and Ollis, 1989a).

The specific production rate of lactate as a function of the specific growth rate is shown in Figure 6.8. Lactate production is tightly interrelated to glucose consumption, in a hybridoma culture. It is known that transformed cells are capable of carrying out glycolysis, even under aerobic conditions (Lanks and Li, 1988). Reitzer et al. (1979) reported that in HeLa cell cultures up to 80% of the glucose carbon proceeded through the glycolysis pathway to lactate and only 4 to 5% entered the citric acid cycle, when the concentration of glucose was greater than 1 $mmol/L$.

In our experiments the residual glucose concentration was very high, up to 15 $mmol/L$, as shown in Figure 6.4. Therefore a high rate of glycolysis can be expected. The maximum yield of lactate from glucose, $Y_{l/c}$, is shown in Figure 6.8. For the calculation of $Y_{l/c}$ we have assumed that lactate is produced solely from glucose. It can be seen that up to almost 70% of glucose may have proceeded through the glycolytic pathway. Of course, a portion of lactate is produced from glutamine. Reitzer et al. (1979) showed, that in HeLa cell cultures 13% of the glutamine carbon was incorporated into lactic acid, independently of the glucose level. The behavior of $Y_{l/c}$ is in agreement with the observations of Luan et al. (1987a) who in an experimental study observed that during initial batch growth in a hybridoma culture, a large fraction of glucose was

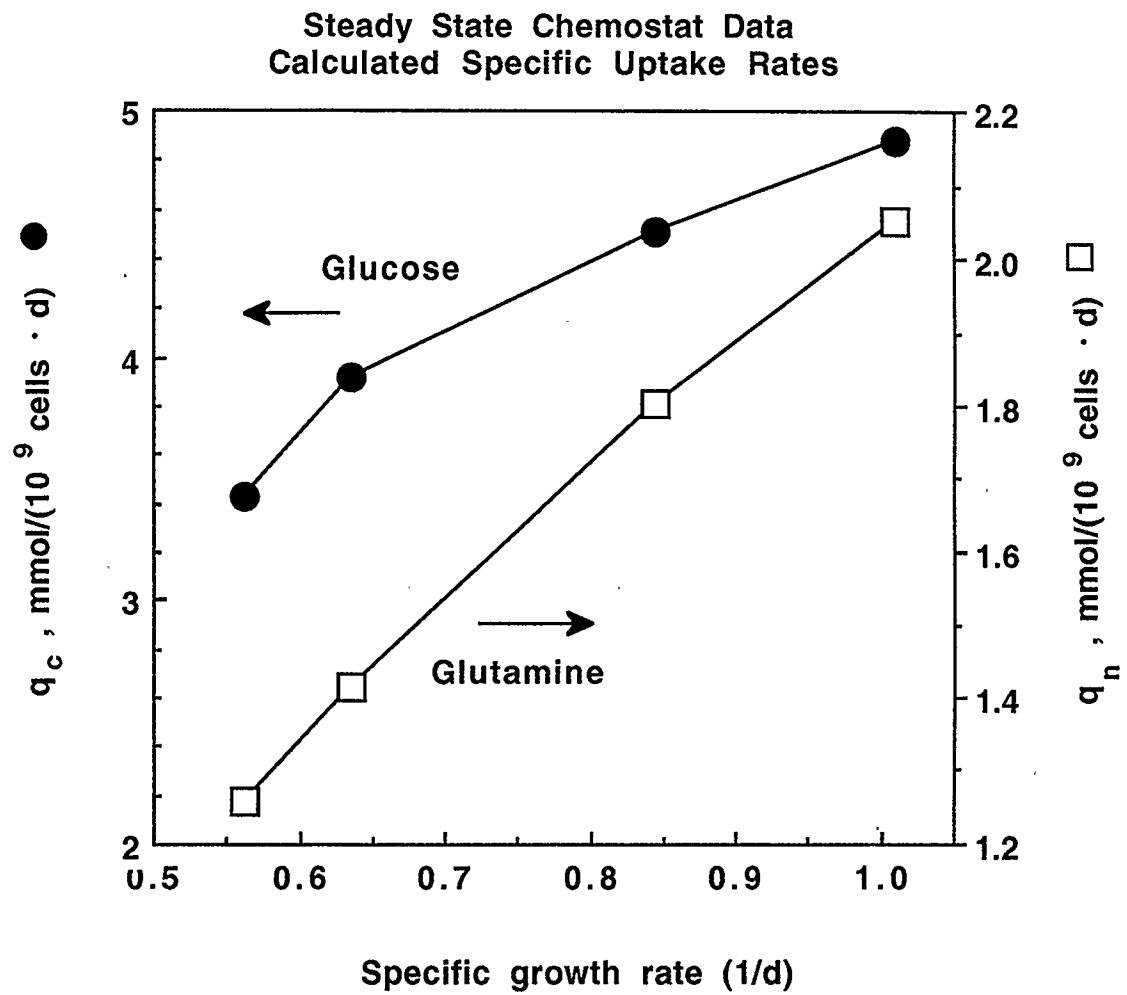


Figure 6.7 Steady state specific uptake rates of glucose (q_c) and glutamine (q_n) as functions of the specific growth rate.

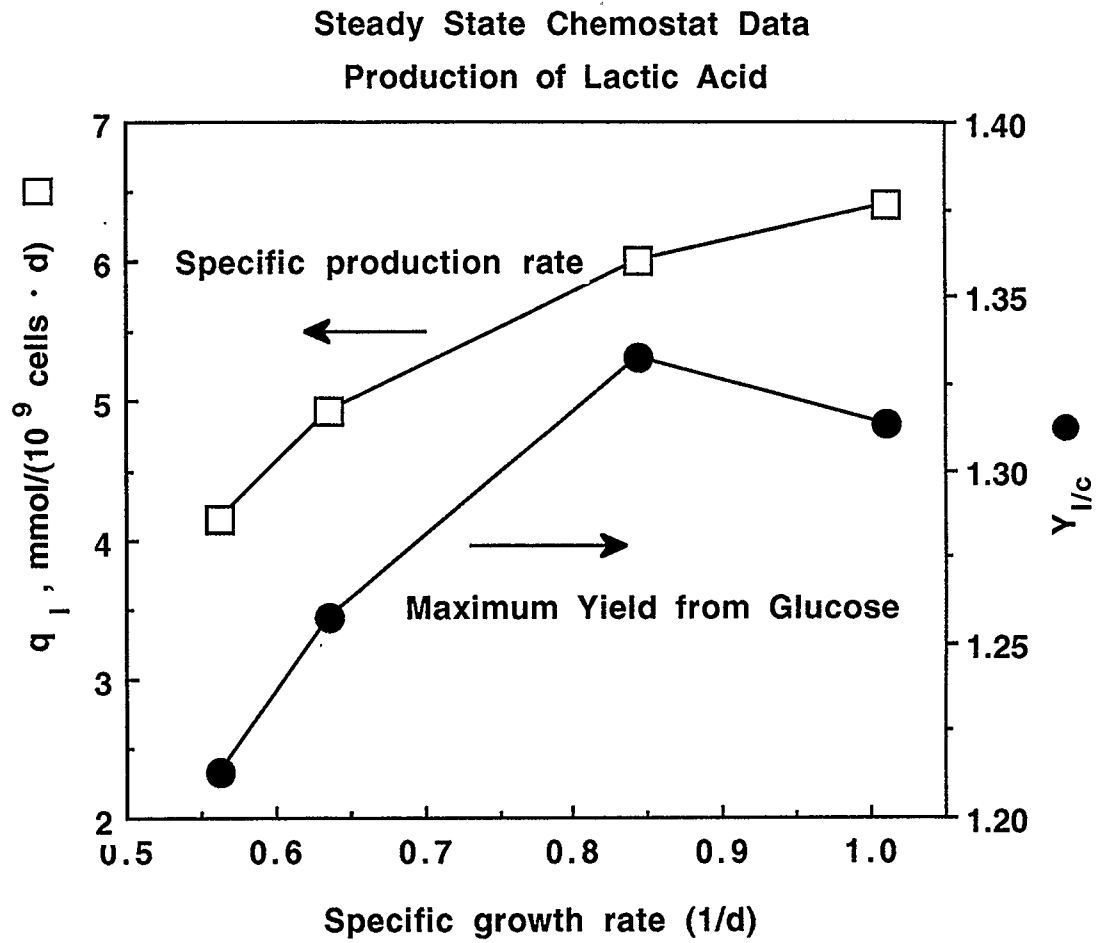


Figure 6.8 Steady state specific production rate of lactate (q_l) and maximum yield of lactate from glucose ($Y_{l/c}$) as functions of the specific growth rate.

metabolized to lactate, while in stationary phase, no net lactate was formed. The conversion rate of glucose to lactate as a function of growth rate in batch culture, in T-flasks and in a 500 mL bioreactor tended to indicate that lactate formation is primarily influenced by the growth rate, rather than the glucose concentration.

The major source of ammonia in a hybridoma culture is glutamine. As shown in Figure 2.3, glutamine can produce ammonia in two ways; through spontaneous hydrolysis and through its metabolic degradation. The hydrolysis of glutamine follows first order kinetics and the value of the rate constant, K_H , at 37 °C has been reported in the literature to be in the area of 0.115 to 0.118 d^{-1} (Tritsch and Moore, 1962; Glacken et al., 1988). When glutamine is metabolically degraded, it enters the TCA cycle in two steps, through two intermediates, glutamic acid and α -ketoglutaric acid. Up to two molecules of ammonia can be produced per molecule of glutamine utilized by the cells.

The specific production rate of ammonia by cells, excluding hydrolysis, is shown in Figure 6.9 as a function of the growth rate. The production of ammonia seems to level off at higher growth rates. The yield of ammonia from glutamine is also plotted in Figure 6.9. Although a theoretical maximum value of 2 is possible, the yield never exceeded the value of 0.6 in our runs. The residual glutamine concentration in our experiments was low, below 1.5 mmol/L, at all times and this may explain the low yield. Glacken et al. (1986) reported a yield of approximately 1.0 in a batch culture of human fibroblasts. However, a lower yield of approximately 0.86 was observed in a repeated fed batch culture where the glutamine level was kept below 1.8 mmol/L.

6.2. EFFECT OF pH AND DISSOLVED OXYGEN

The effect of pH on cell growth and MAb production in the chemostat mode of operation was studied in the 1.5 L Celligen bioreactor. Steady states were achieved at four different pH values. The steady state measurements are compared in Table 6.1. Figure 6.10 shows the profile of viable cell density during the entire run that lasted approximately 100 days. It is noted here that this run was interrupted twice at 40 d and at 62 d due to feed pump problems. The profiles of viability and MAb concentration are

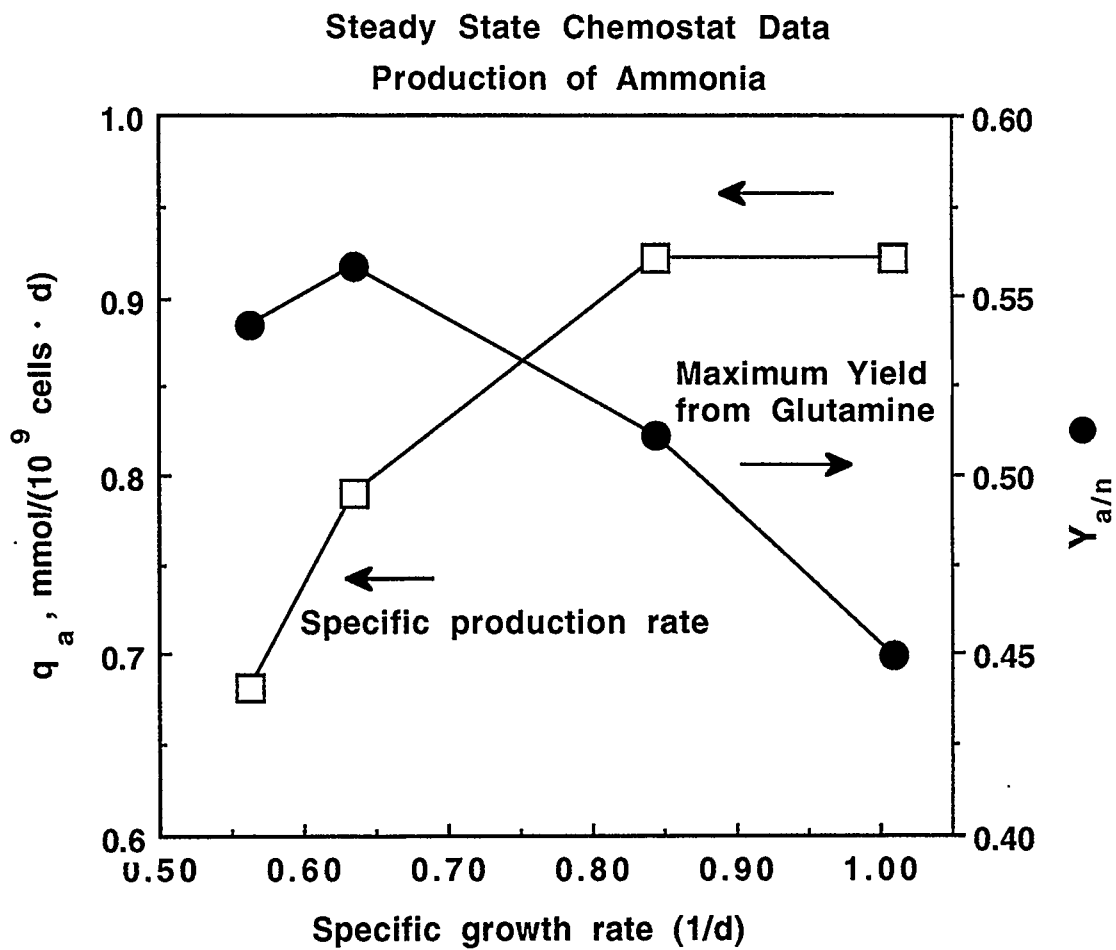


Figure 6.9 Specific production rate of ammonia (q_a) and maximum yield of ammonia from glutamine ($Y_{a/n}$), as functions of the growth rate.

shown in Figures 6.11 and 6.12.

In the above figures we can observe that the viable cell density was highest for pH values of 6.8 and 7.0, while it was significantly reduced for pH values of 7.1 and 7.2. The viability seemed to decrease for the highest pH value of 7.2 while the MAb concentration seemed to be highest at pH 6.80. In particular, it is emphasized that the MAb concentration at pH 6.8 was more than double than in any other pH value.

The glucose and lactate profiles are given in Figure 6.13, glutamine and glutamate profiles in Figure 6.14 and ammonia profiles in Figure 6.15. It can be seen that the glucose concentration dropped to practically zero values for pH 7.2. The residual glutamine concentration was highest for pH 7.1, while there was no significant effect of pH on the glutamate concentration. The concentration of ammonia was higher at pH 7.1-7.2 despite the lower cell density at these pH values.

The measurements summarized in Table 6.1 were used to calculate the specific uptake and production rates shown in Table 6.2. It appears that the specific MAb productivity is highest at the lower pH values. Miller et al. (1988) also obtained higher MAb production rates at lower pH values. Ammonia and glutamate production rates increased with increasing pH values, most probably a result of the increased glutamine consumption. Finally, both glucose consumption and lactate production increased considerably at higher growth rates. Miller et al. (1988) reported that glucose consumption was inhibited at low pH. Birch and Edwards (1980) measured a constant glucose consumption between pH 6.8 and 7.4, however they observed a dramatic drop for pH values below 6.8.

The effect of dissolved oxygen concentration (DO) was examined in another chemostat culture for DO levels of 60%, 30% and 15% of saturation. The viable cell density and viability results for the three DO levels are given in Figure 6.16. It is apparent that there is no significant effect of the DO concentration on either of the two parameters. This result is in agreement with the findings of Miller et al. (1987) in chemostat hybridoma cultures.

Table 6.1. EFFECT OF pH ON HYBRIDOMA CHEMOSTAT CULTURES (Steady state measurements at $D = 0.45 d^{-1}$)								
pH	x_v	V_x	MAB	GLC	LAC	GLN	GLT	AMM
	$\times 10^6$ cells/mL	%	mg/L	mmol/L				
6.8	2.25	83	115	14	19	0.2	0.18	1.45
7.0	2.40	87	70	8	20	0.2	0.20	1.60
7.1	1.50	87	45	6.5	33	0.5	0.22	2.20
7.2	1.60	80	55	≈ 0	33	0.15	0.25	2.25

Table 6.1 Effect of pH on chemostat hybridoma cultures. Steady state measurements.

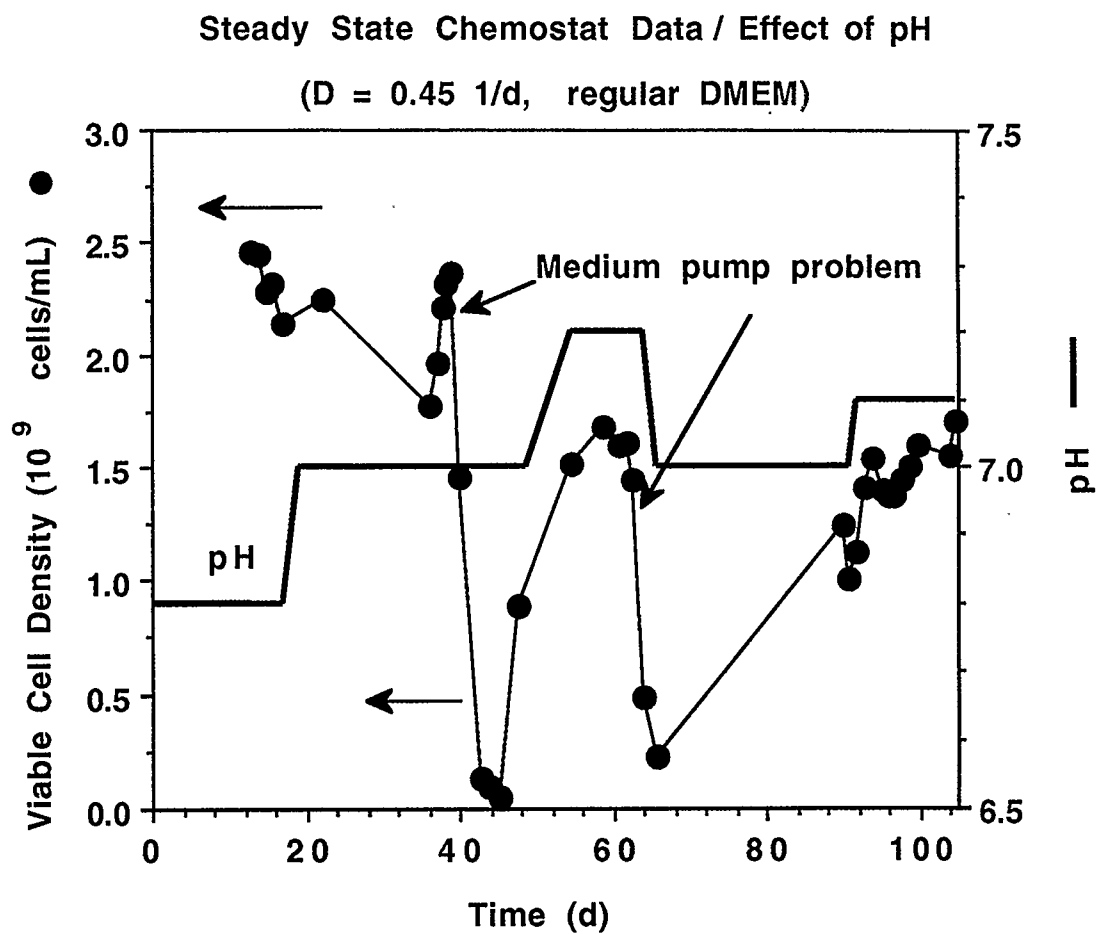


Figure 6.10 Viable cell density in a chemostat at four different pH values.

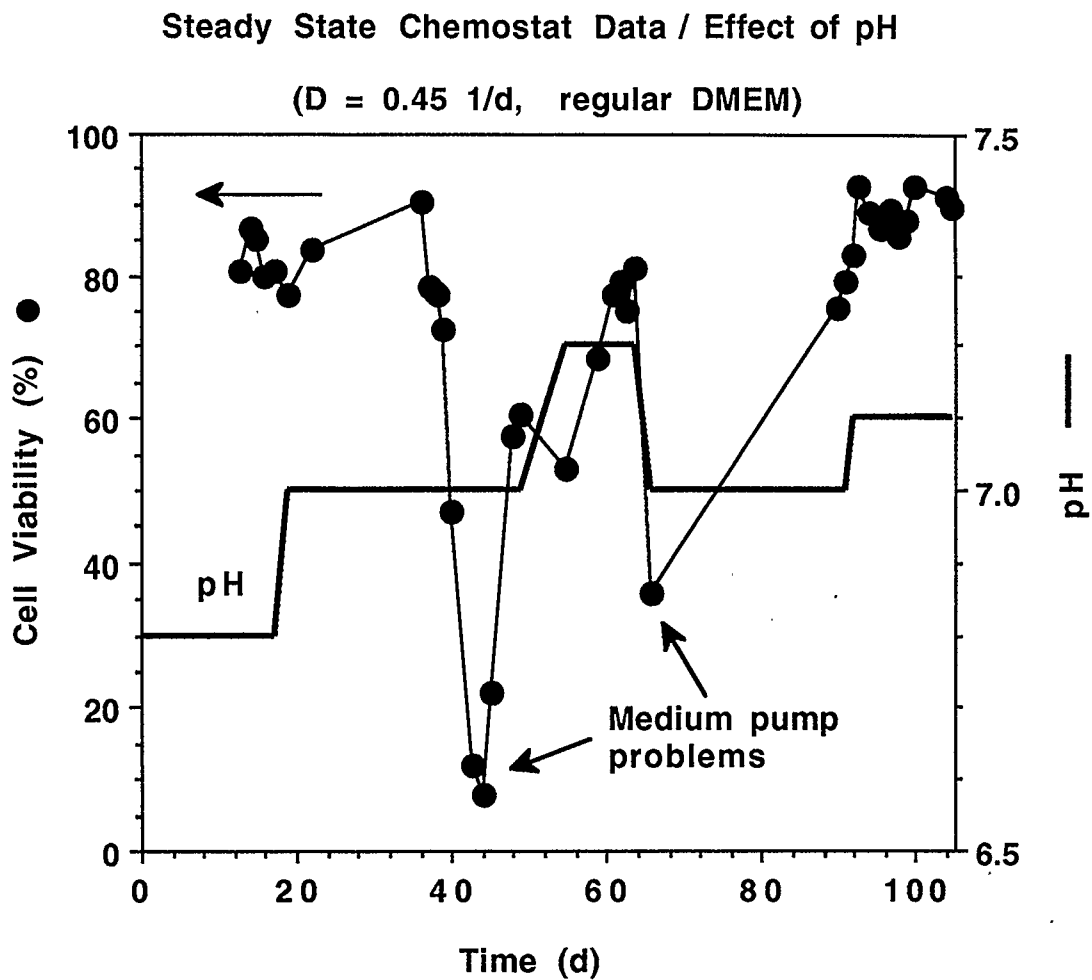


Figure 6.11 Profile of cell viability in a chemostat where pH was controlled at four different values.

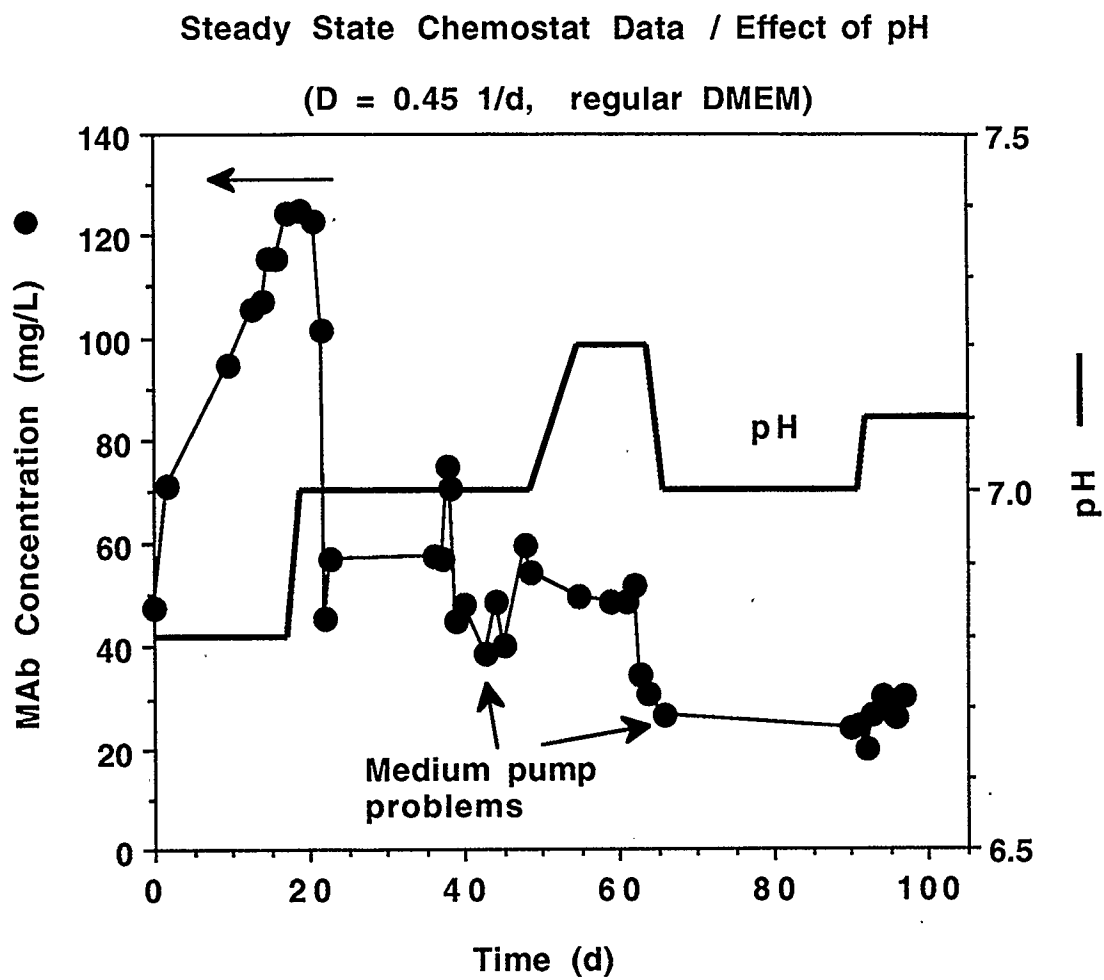


Figure 6.12 Profile of MAb concentration in a chemostat where pH was controlled at four different values (as shown).

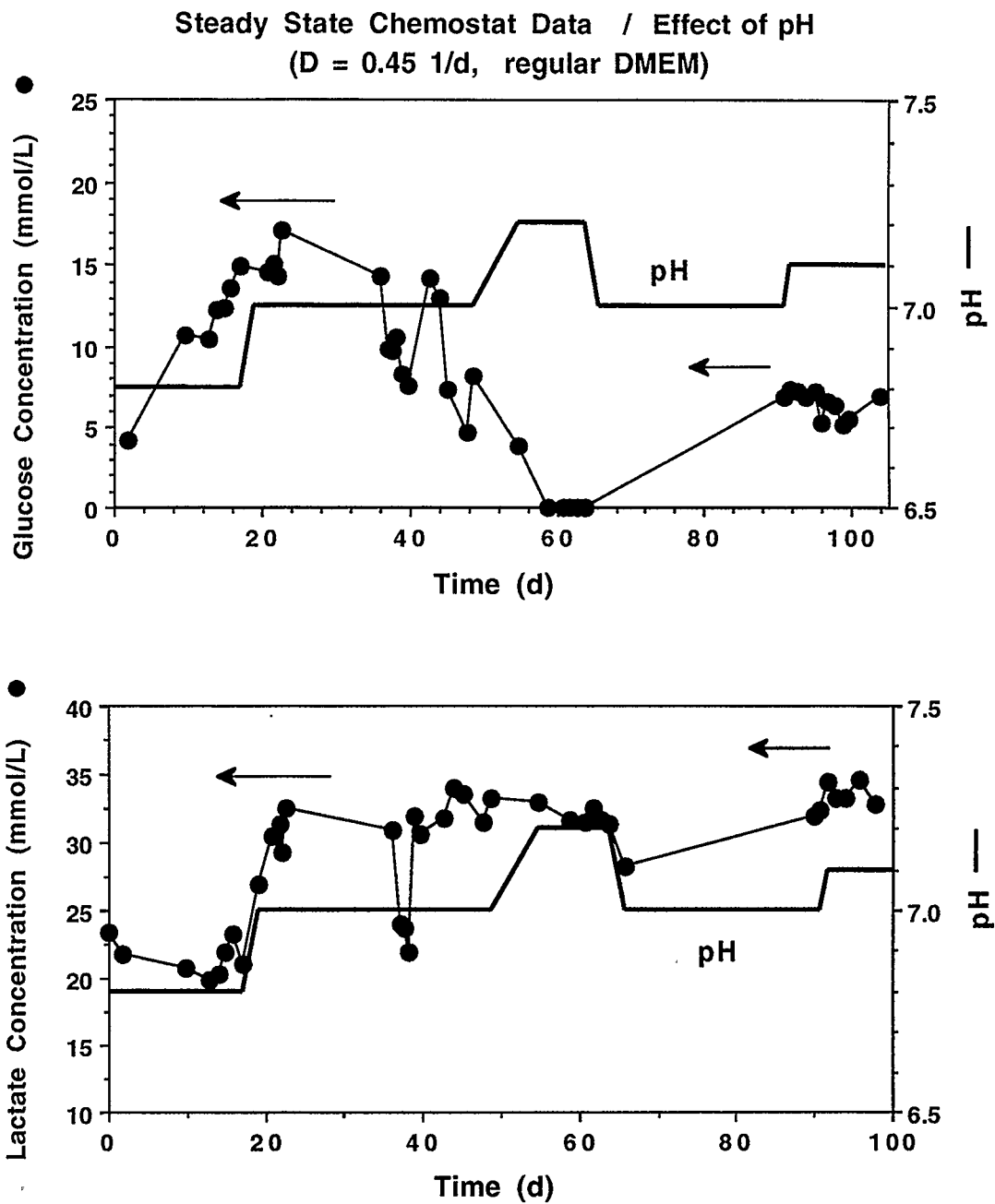


Figure 6.13 Glucose and lactate concentration profiles in a chemostat culture where pH was controlled at four different values.

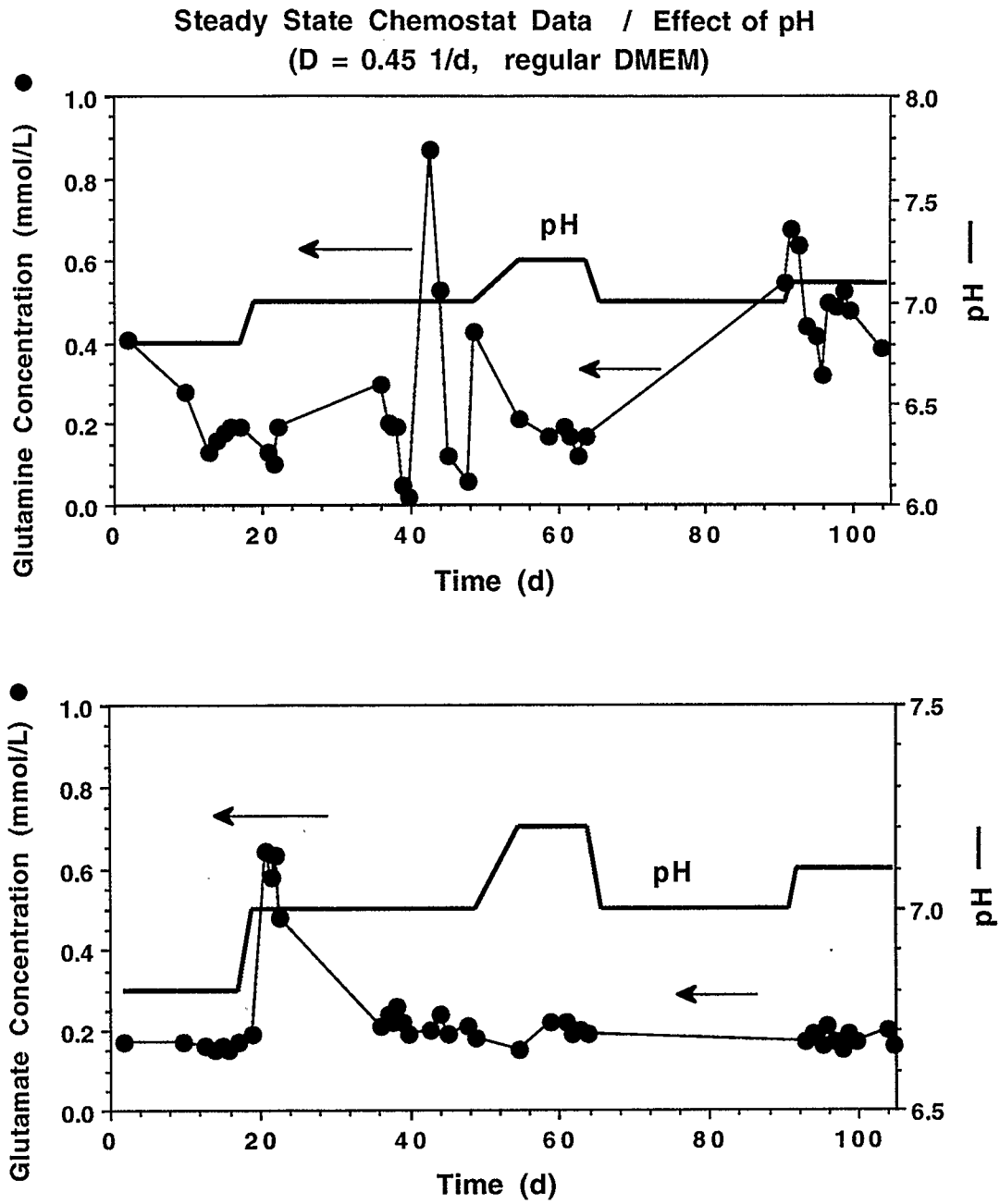


Figure 6.14 Glutamine and glutamate concentration profiles in a chemostat culture where pH was controlled at four different values.

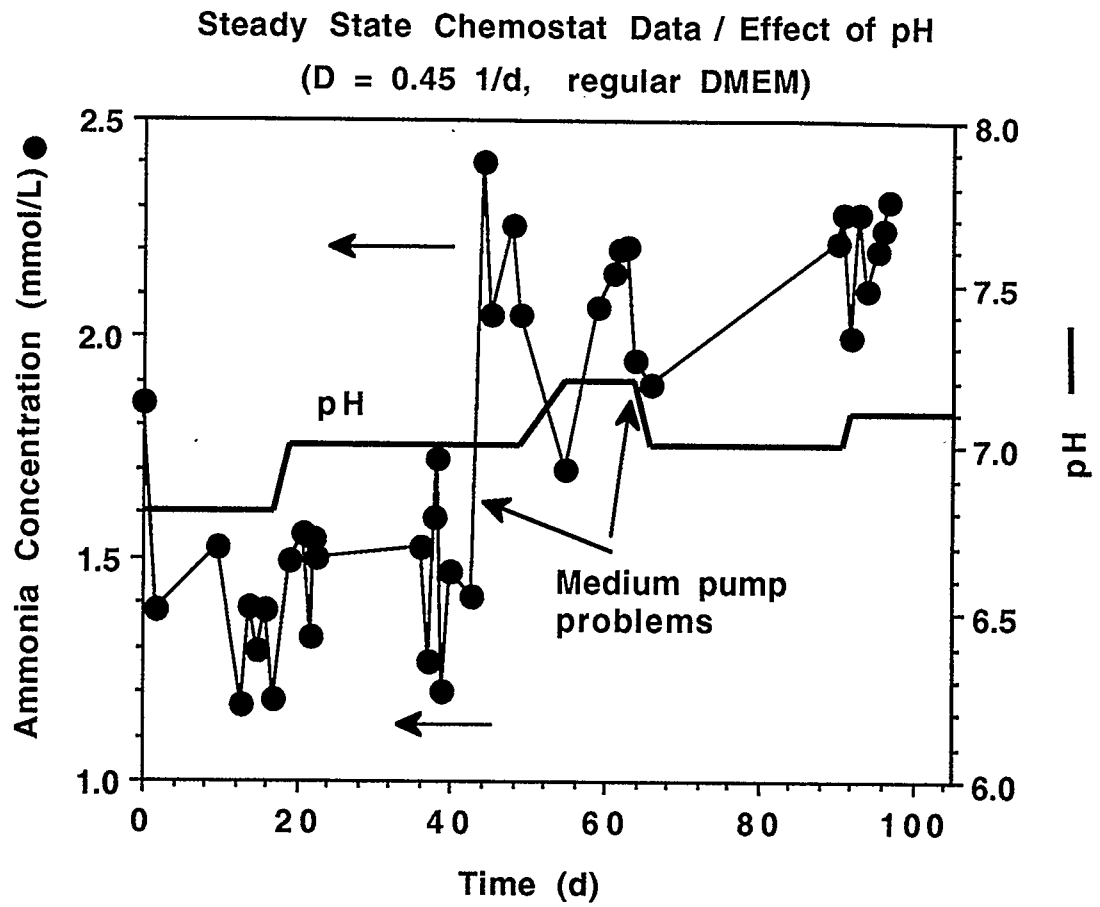


Figure 6.15 Ammonia concentration profiles in a chemostat where pH was controlled at four different values.

Table 6.2. EFFECT OF pH ON HYBRIDOMA CHEMOSTAT CULTURES						
(Calculations at steady state; $D = 0.45 d^{-1}$)						
pH	Specific production rate				Specific uptake rate	
	(per 10^6 viable cells)					
	MAb	LAC	GLT	AMM	GLC	GLN
	<i>mg/d</i>	<i>mmol/d</i>				
6.8	23	3.8	0.036	0.28	2.2	0.91
7.0	13.1	3.7	0.038	0.30	3.2	0.86
7.1	13.5	9.9	0.066	0.62	5.6	1.25
7.2	15.5	9.3	0.070	0.62	7.0	1.29

Table 6.2 Effect of pH on chemostat hybridoma cultures. Steady state measurements.

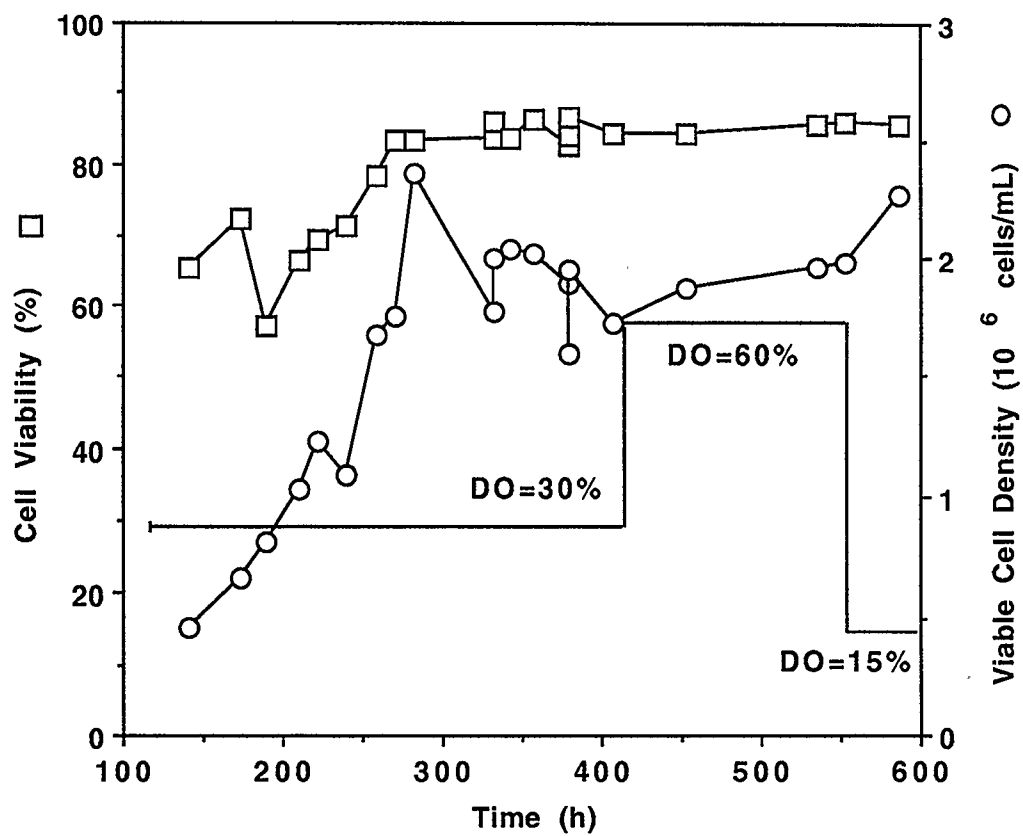


Figure 6.16 Effect of dissolved oxygen (DO) on viable cell density and viability in a chemostat culture.

6.3. EFFECT OF GLUCOSE TO GLUTAMINE RATIO

In the following experiment the glucose to glutamine ratio in the feed of a chemostat culture was varied in order to examine the effects on cell growth and MAb production. The dilution rate was kept constant at $0.45 d^{-1}$. The ratios used and the corresponding glucose and glutamine concentrations in the medium are shown in Table 6.3.

The first chemostat run was performed with standard DMEM medium containing glucose and glutamine in a ratio 5/1. The inoculation density was approximately 1.9×10^6 cells/mL at a viability of 83% (Figure 6.17). The steady state was achieved at approximately 300 h. Steady state results including viable cell densities and viability values are summarized in Table 6.3. Figure 6.18 presents the profile of MAb concentration during this run. Figure 6.19 shows the profiles of lactate and glucose, while Figure 6.20 shows the profiles of glutamine, glutamate and ammonia. Most of the concentrations did not change significantly during the run, except for the ammonia that showed a slight decrease at steady state compared to the initial values.

When the first steady state was achieved, the second medium with a glucose to glutamine ratio of 5/2 was used. After the medium change the cell density increased briefly but subsequently dropped to its new steady state value after 500 h and remained at steady state until the medium was changed again at 350 h (Figure 6.21). The MAb concentration shown in Figure 6.22 decreased significantly during this stage of the run. This observation is in disagreement with the results of the batch experiments described in Chapter 5. Higher MAb titers were produced with increasing glutamine in the batch mode of operation. Figure 6.23 shows the profiles of lactic acid and glucose, while Figure 6.24 the profiles of glutamine, glutamate and ammonia concentration. In the last figure we can observe the increasing residual concentration of glutamine in the bioreactor. Ammonia seemed to remain at the same levels. However, the specific production rate must have increased, since the viable cell density was lower for this ratio.

Medium with a glucose to glutamine ratio of 5/3 was used last. Pump problems that occurred after the 200 h mark disturbed the approach to steady state as it can be

Table 6.3. EFFECT OF GLUCOSE TO GLUTAMINE RATIO IN CHEMOSTAT FEED										
(Steady state chemostat measurements; $D = 0.45 d^{-1}$)										
Medium	Content		x_y	V_x	MAb	GLC	LAC	GLN	GLT	AMM
	GLC	GLN								
	<i>mmol/L</i>		$\times 10^6$ cells/mL	%	mg/L	<i>mmol/L</i>				
Standard (5/1)	25.0	4.80	2.3	82	68	5	36	0.07	0.12	1.2
5/2	24.2	9.3	1.9	81	34	6	39	1.85	0.15	1.7
5/3	22.0	13.2	1.3	79	40	7	20	7.9	0.7	6.2

Table 6.3 Effect of glucose to glutamine ratio in the feed medium of a chemostat culture.

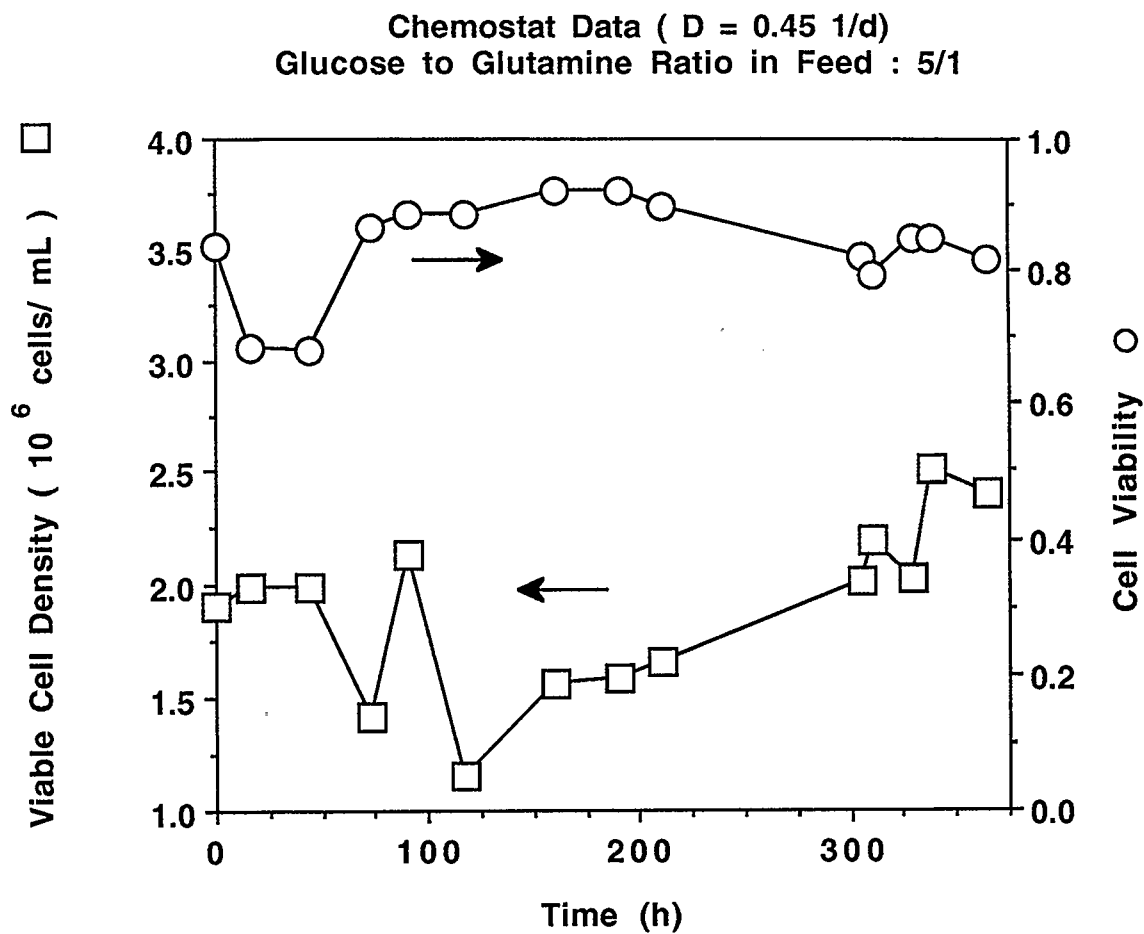


Figure 6.17 Profiles of viable cell density and viability in a chemostat culture with a 5/1 glucose to glutamine ratio in the feed medium.

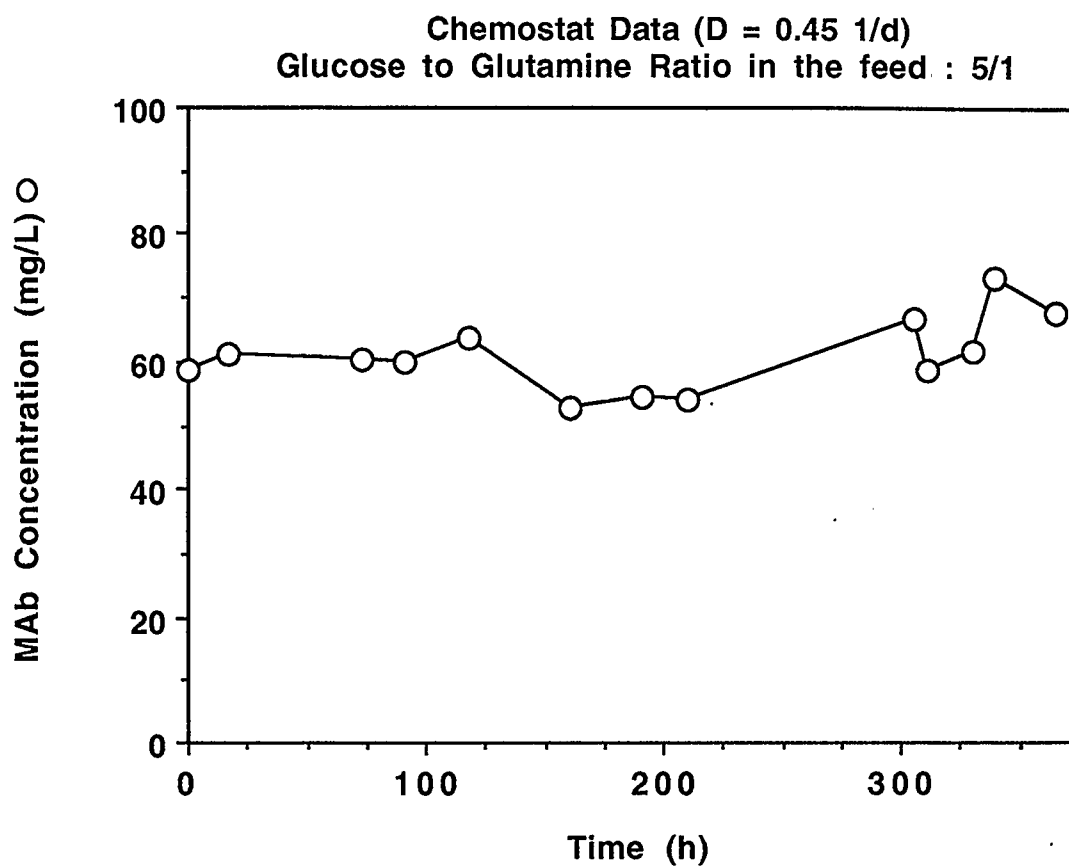


Figure 6.18 Profile of MAb concentration in a chemostat culture with a 5/1 glucose to glutamine ratio in the feed medium.

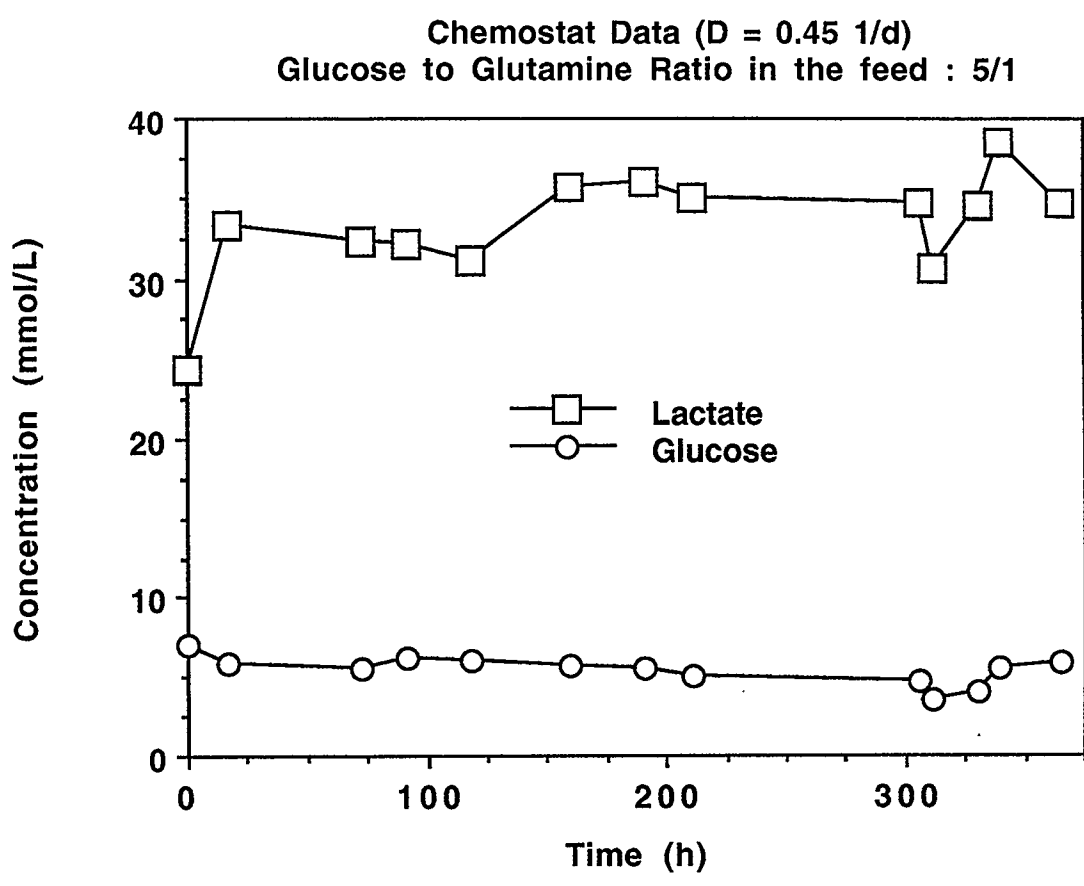


Figure 6.19 Profiles of lactate and glucose concentration in a chemostat culture with a 5/1 glucose to glutamine ratio in the feed medium.

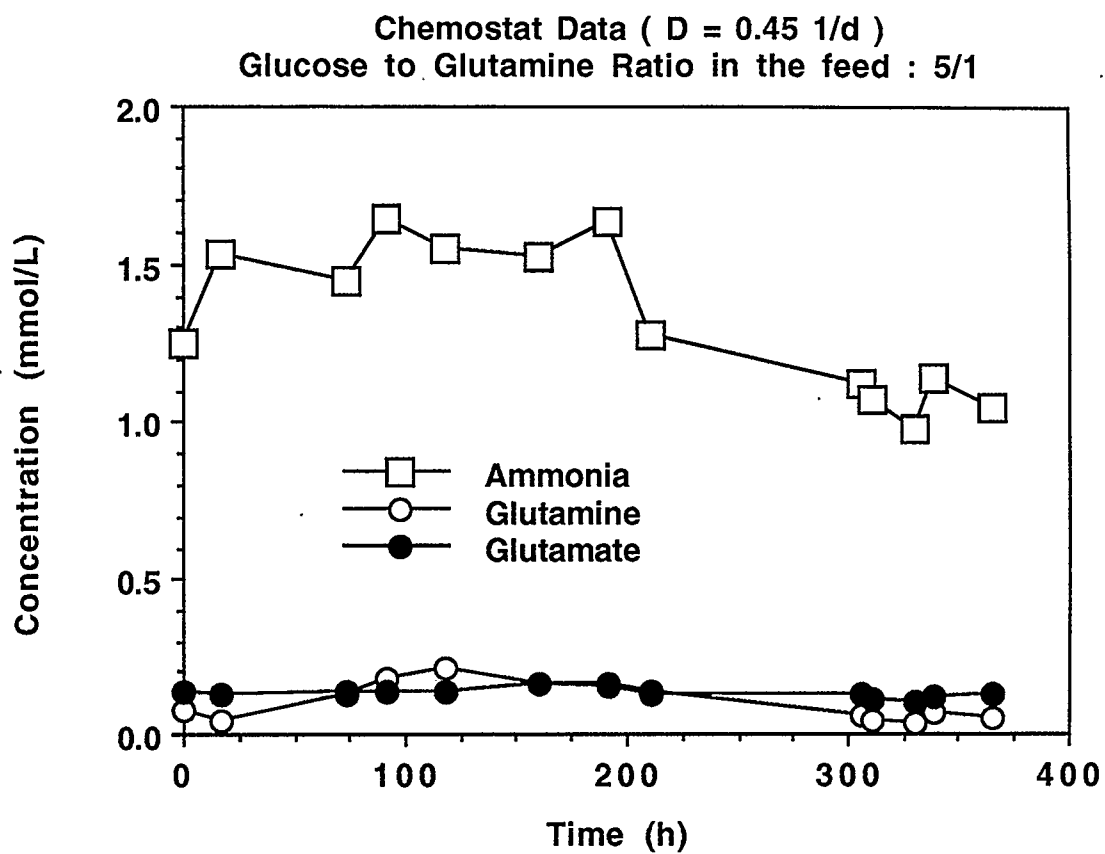


Figure 6.20 Profiles of glutamine, glutamate and ammonia concentration in a chemostat culture with a 5/1 glucose to glutamine ratio in the feed medium.

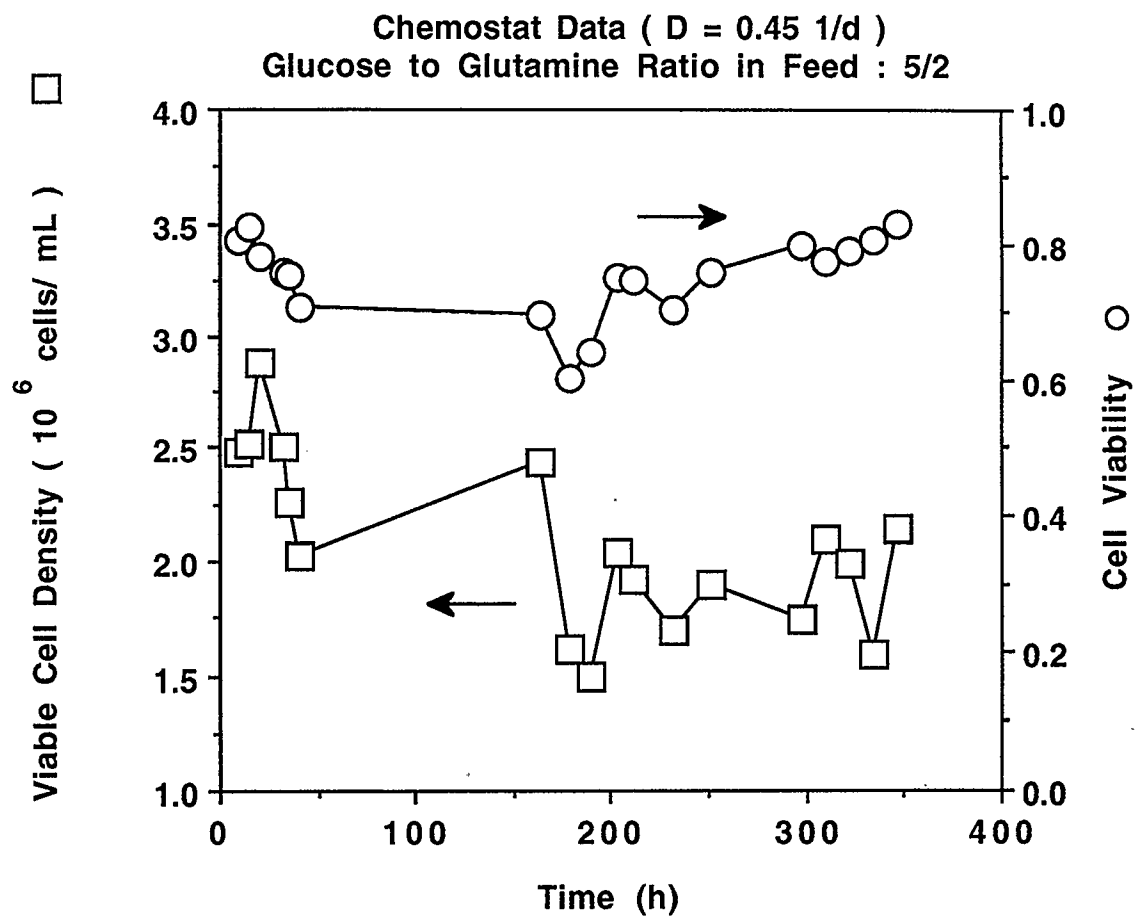


Figure 6.21 Profiles of viable cell density and viability in a chemostat culture with a 5/2 glucose to glutamine ratio in the feed medium.

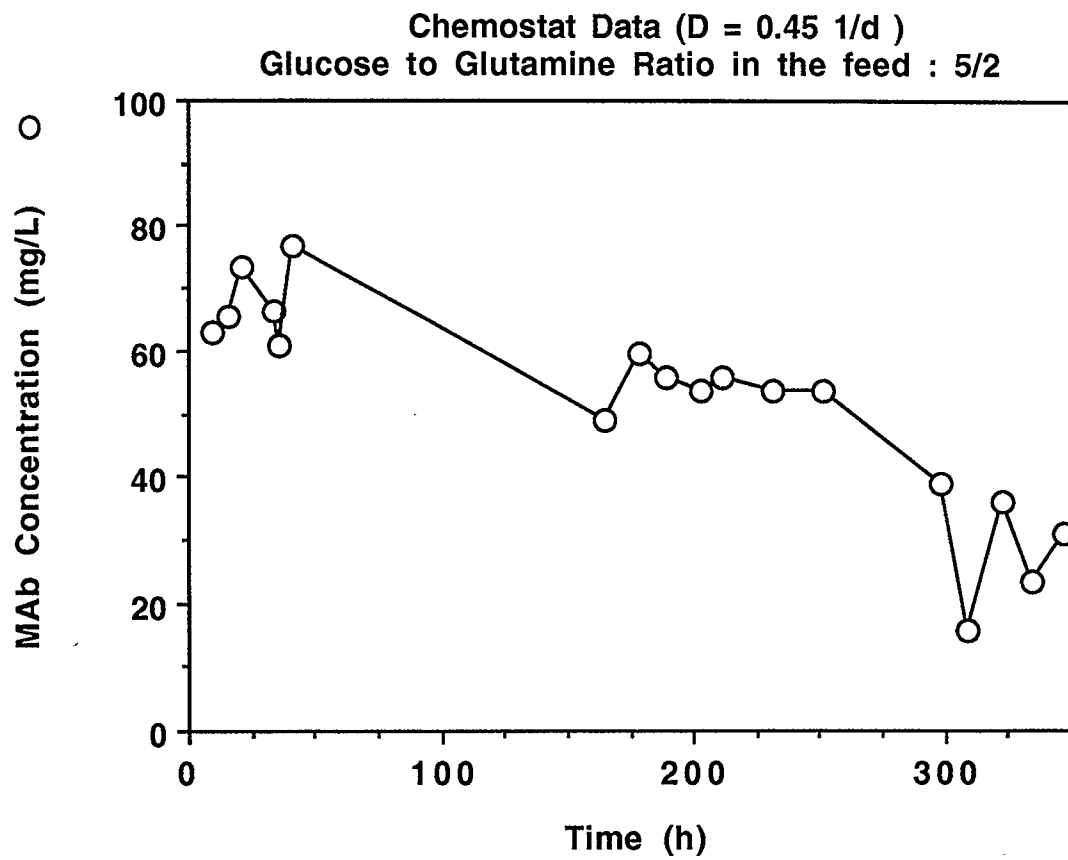


Figure 6.22 Profile of MAb concentration in a chemostat culture with a 5/2 glucose to glutamine ratio in the feed medium.

clearly seen in Figure 6.25. After the medium change the viability started to drop while the viable cell density did not exhibit any significant change. At the new steady state which was achieved after 400 *h* the viability had decreased slightly while the viable cell density had dropped substantially almost to half the previous steady state value (Table 6.3). The MAb concentration shown in Figure 6.26 seemed to remain at the same levels, despite the lower cell density. This fact denotes a higher specific MAb production rate for this glucose to glutamine ratio. The residual glucose concentration increased as shown in Figure 6.27 and the lactate concentration decreased as a result. Figure 6.28 shows the profiles of glutamine, glutamate and ammonia concentrations. The residual glutamine and the produced ammonia increased even further compared to the previous medium, while an increase in glutamate production was also observed.

In conclusion, a higher glutamine content in the feed medium has negative effects on cell growth and MAb production. The reason seems to be the increased production of ammonia. Although in batch culture (section 5.3) a 5/2 glucose to glutamine ratio was optimal, in continuous culture doubling of the glutamine had negative results. This contradiction can be explained by the different properties of batch and chemostat cultures. In batch cultures most of the ammonia is produced when the cell density is close to maximum. The resulting toxicity is not very significant because it mostly affects the death phase of the culture. In chemostat cultures at steady state an increased ammonia production results in an increased ammonia concentration that continuously affects the entire population. The dialyzed chemostat presented in the next chapter was designed for continuous removal of ammonia so that increased cell density and MAb production can be achieved in a chemostat.

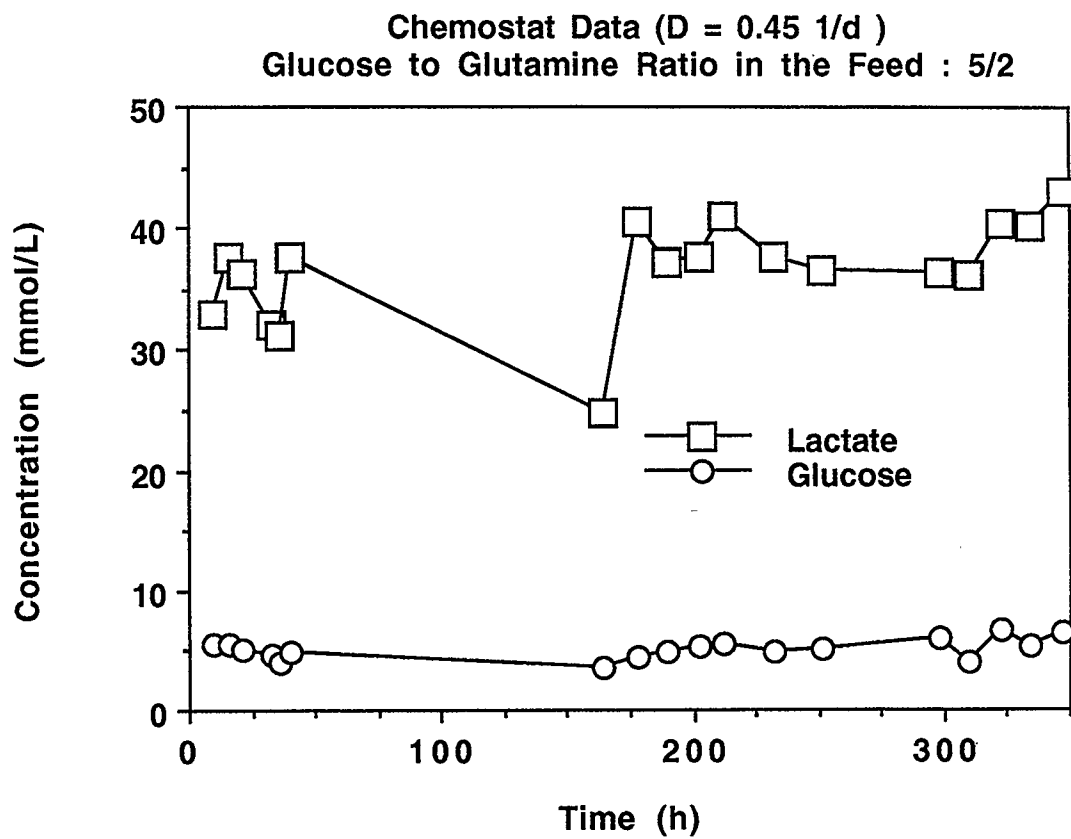


Figure 6.23 Profiles of lactate and glucose concentration in a chemostat culture with a 5/2 glucose to glutamine ratio in the feed medium.

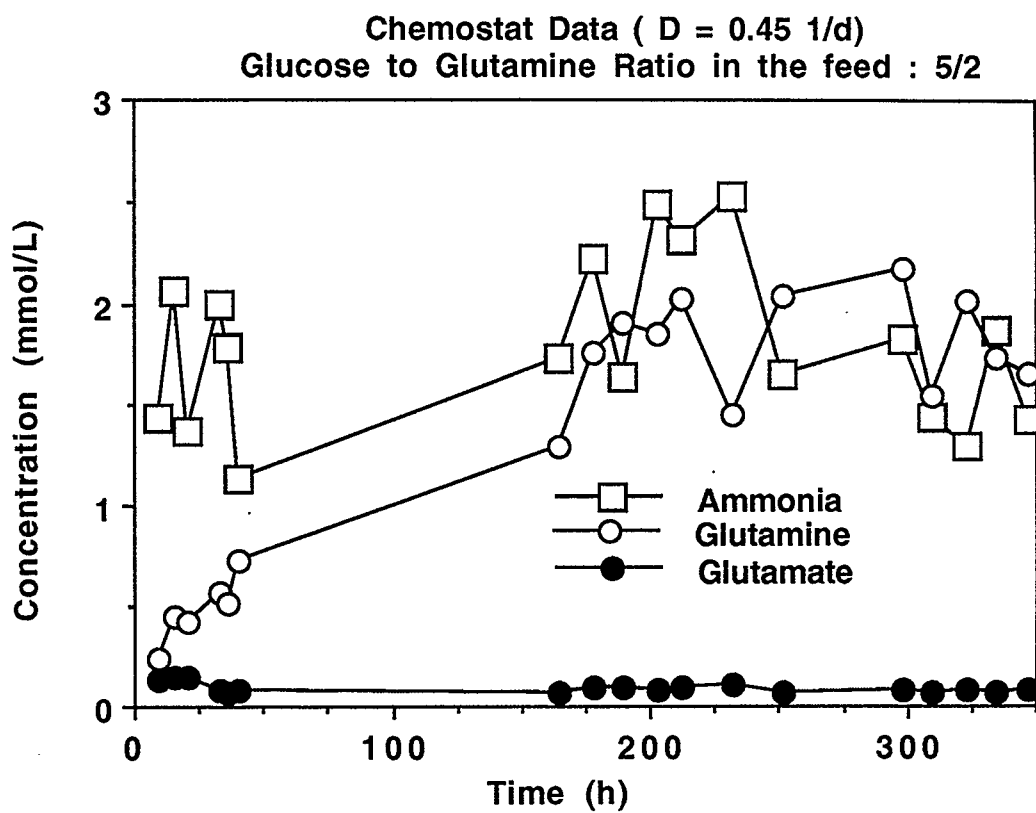


Figure 6.24 Profiles of glutamine, glutamate and ammonia concentration in a chemostat culture with a 5/2 glucose to glutamine ratio in the feed medium.

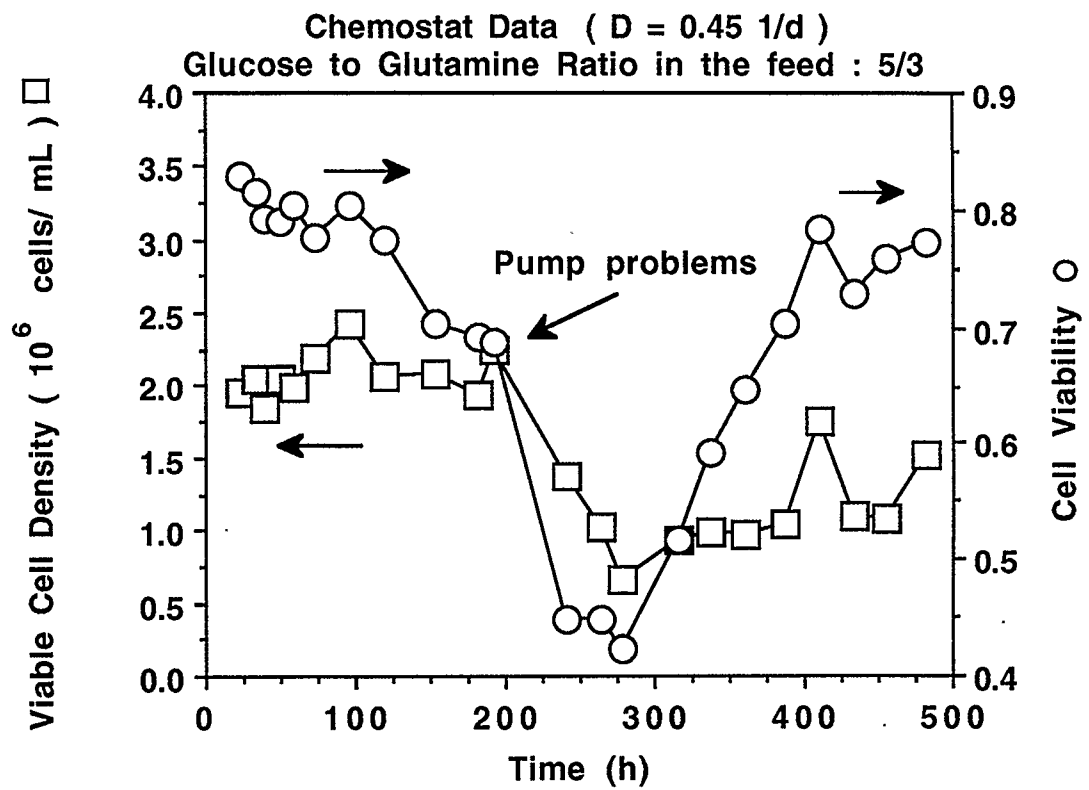


Figure 6.25 Profiles of viable cell density and viability in a chemostat culture with a 5/3 glucose to glutamine ratio in the feed medium.

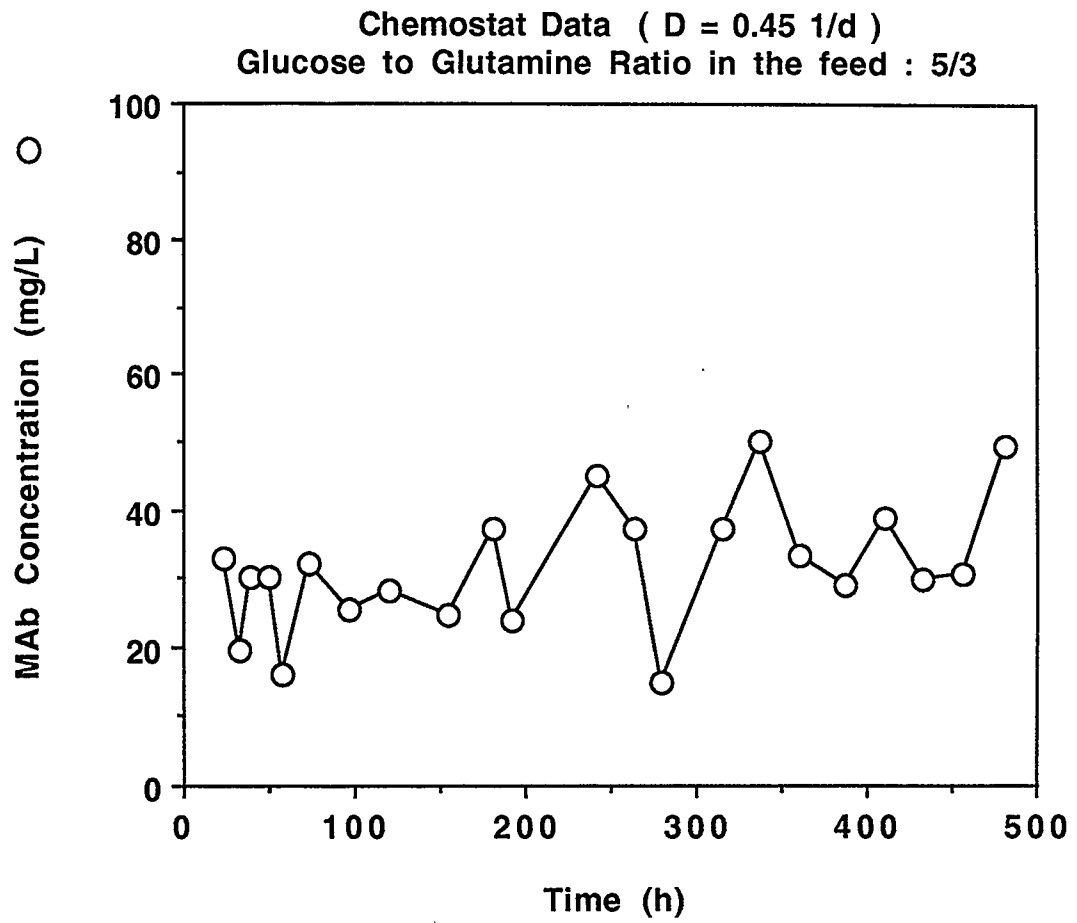


Figure 6.26 Profile of MAb concentration in a chemostat culture with a 5/3 glucose to glutamine ratio in the feed medium.

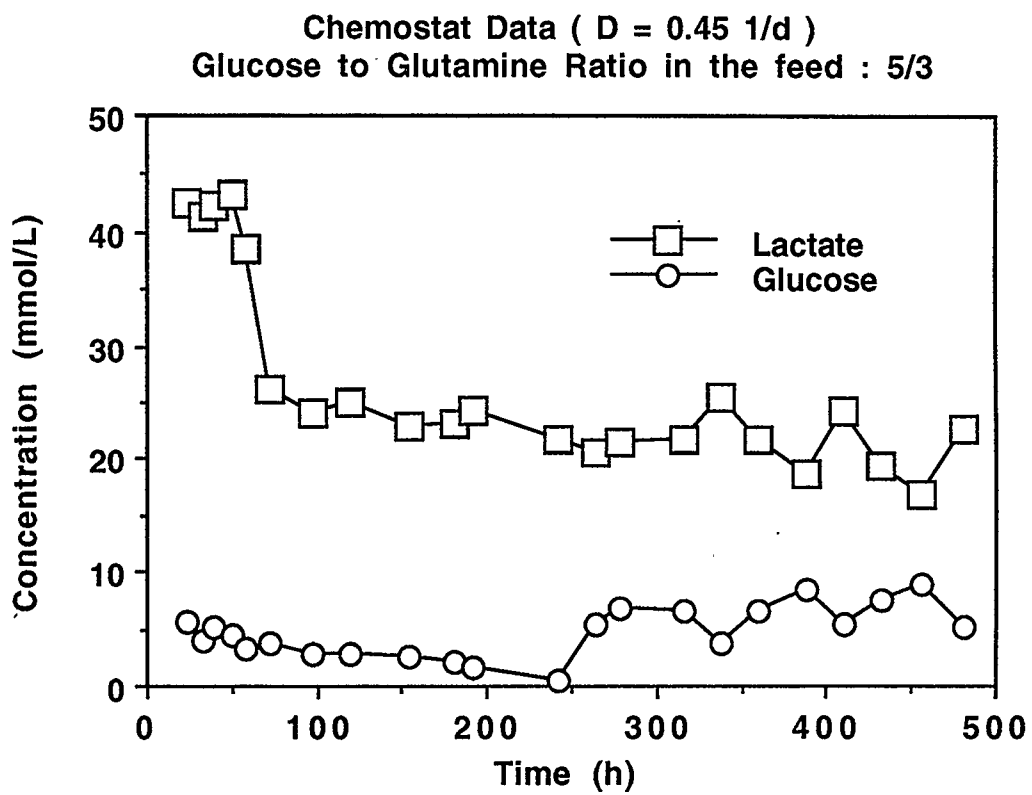


Figure 6.27 Profiles of lactate and glucose concentration in a chemostat culture with a 5/3 glucose to glutamine ratio in the feed medium.

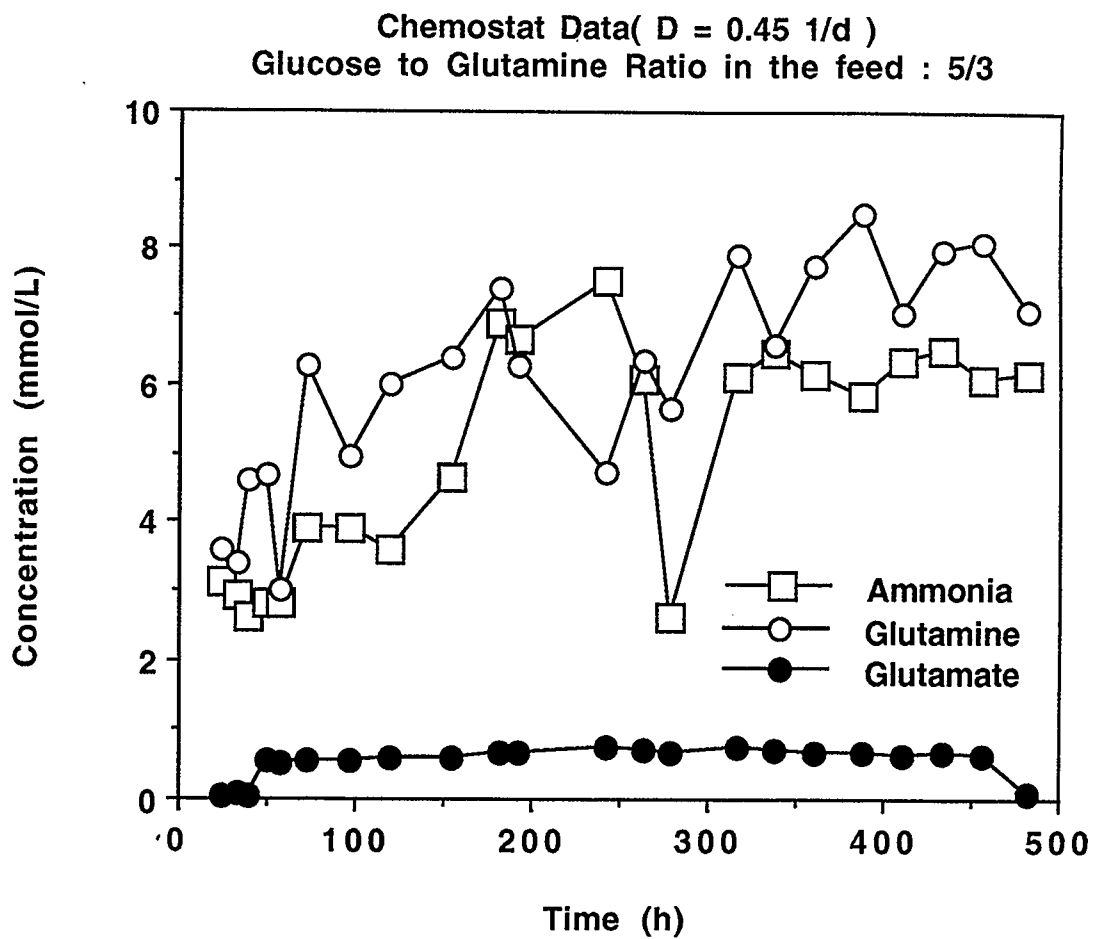


Figure 6.28 Profiles of glutamine, glutamate and ammonia concentration in a chemostat culture with a 5/3 glucose to glutamine ratio in the feed medium.

7. EXPERIMENTAL RESULTS - DIALYZED CHEMOSTAT

Various methods for limiting the levels of toxic byproducts in mammalian cell cultures have been reported in the literature. Initial efforts concentrated on the manipulation of the medium composition and feed rate since the rate of production of waste products depends strongly on the nutrient concentration in the reactor vessel (Hu et al., 1987; Lanks and Li, 1988; Luan et al., 1987a; Reitzer et al., 1979; Tritch and Moore, 1962). For example, Glacken et al. (1986) successfully employed controlled addition of glucose and glutamine in order to reduce the production of lactic acid and ammonia in a fibroblast microcarrier culture.

An alternative to the manipulation of the feeding medium is the removal of the waste products after their formation. Membranes facilitating mass transfer have been recently used for this purpose. Hecht et al. (1990) used hydrophobic silicon tubing to remove dissolved gaseous ammonia from an antibiotic fermentation. Exchange of medium constituents using hydrophilic membranes has recently found application in batch hybridoma cultures. Adamson et al. (1983) achieved a ten-fold increase in cell density and MAb productivity in batch cultures dialyzed against medium supplemented with serum. The use of a 6000 molecular weight cut-off (MWCO) hollow fiber bundle inside a well stirred and aerated vessel by Emery et al. (1987) reportedly resulted in more than two-fold increase in cell density and antibody titer. Recently, Kearns (1990) reported that in a stirred tank fermenter equipped with an unspecified internal dialysis device, MAb yields were almost twenty times higher than in a typical batch culture.

Dialysis tubing is readily available at many MWCO levels, easily and repeatedly sterilizable, and inexpensive as opposed to hollow fiber assemblies. Molecules much smaller than the nominal MWCO of the tubing can diffuse freely through its wall, driven by concentration and pressure gradients. The rate and the direction of mass transfer can be independently controlled for each component by manipulating its concentration in the tubing interior. Moreover, by selecting tubing with a low nominal MWCO important high molecular weight components (such as growth factors, antibody molecules etc.)

can be easily retained in the culture or even selectively removed on the basis of their molecular weight.

Dialyzed chemostat cultures are expected to become a powerful research tool because they combine the capability of independent control of the concentration of main culture components with ease in maintaining a desired growth rate. To emphasize this important fact, the performance of a dialyzed chemostat bioreactor was evaluated at two different dialysis flow rates and the effect of dialysis on cell growth and MAb production was determined. The experimental results are presented below.

7.1. CONTROL CHEMOSTAT RUN

A chemostat run with no dialysis flow was performed initially as a control experiment. The profiles of viability and viable cell density for this run are shown in Figure 7.1. At the time of inoculation the viable cell density was 2.6×10^6 cells/mL with a 77% viability. As seen by the viable cell density profile steady state conditions were reached approximately 200 h after the run started and it was maintained until the completion of the run at 310 h. The steady state values were calculated as the average over the steady state period of four days or longer. The steady state cell density was estimated at 2.2×10^6 cells/mL and the steady state viability was approximately 75%.

7.2. DIALYZED RUNS - BATCH START-UP

After the control run was completed the first dialyzed run was performed. The cells were initially grown in the batch mode until it was ensured that the equipment and the tubing were functioning properly with the dialysis flow on. Furthermore, a high cell concentration was desired before starting the continuous operation so that a faster approach to the steady state conditions could be achieved.

The profiles of viable cell density and viability during the batch start-up period are shown in Figure 7.2. In the first day of batch growth the dialysis flow rate was maintained at 1.0 L/d. At time $t = 22$ h, the flow rate was changed to 2 L/d. The dialysis flow was then kept constant up to time $t = 91.5$ h. The sample taken at $t = 91.5$ h revealed a

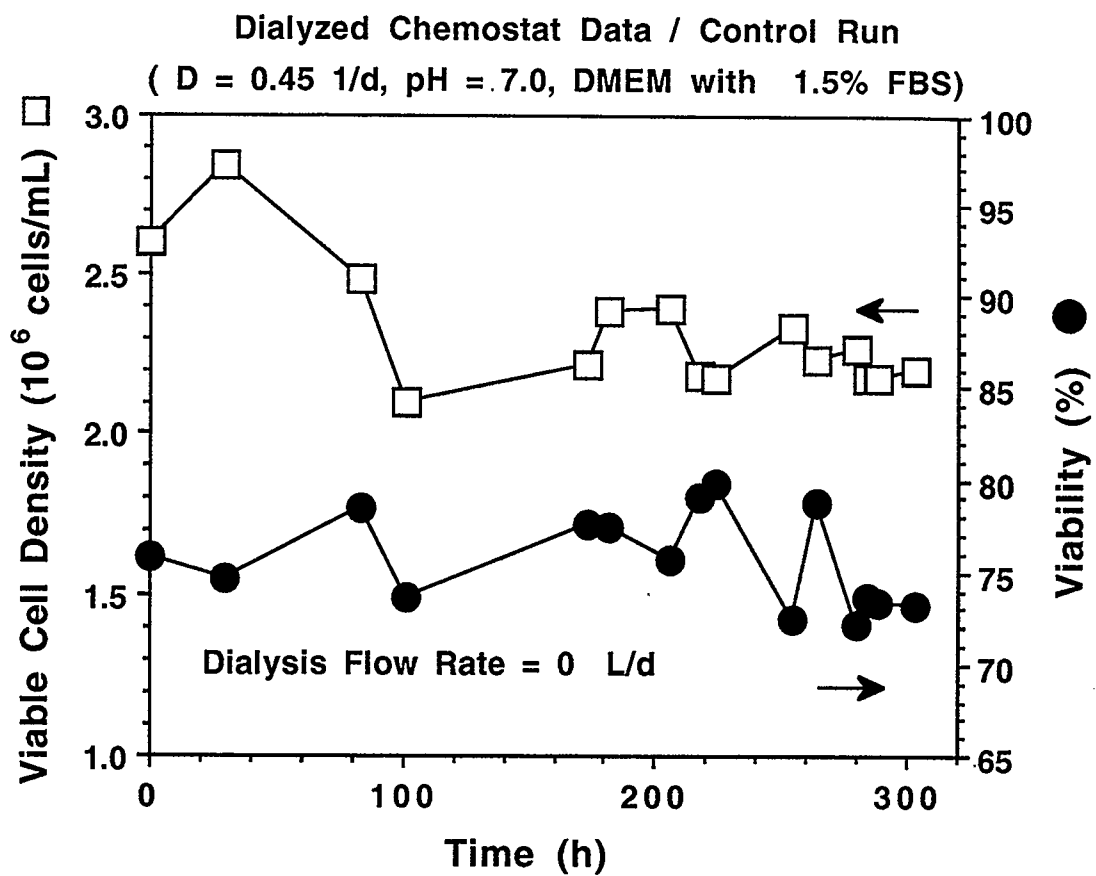


Figure 7.1 Profiles of viable cell density and viability in the non-dialyzed control chemostat culture.

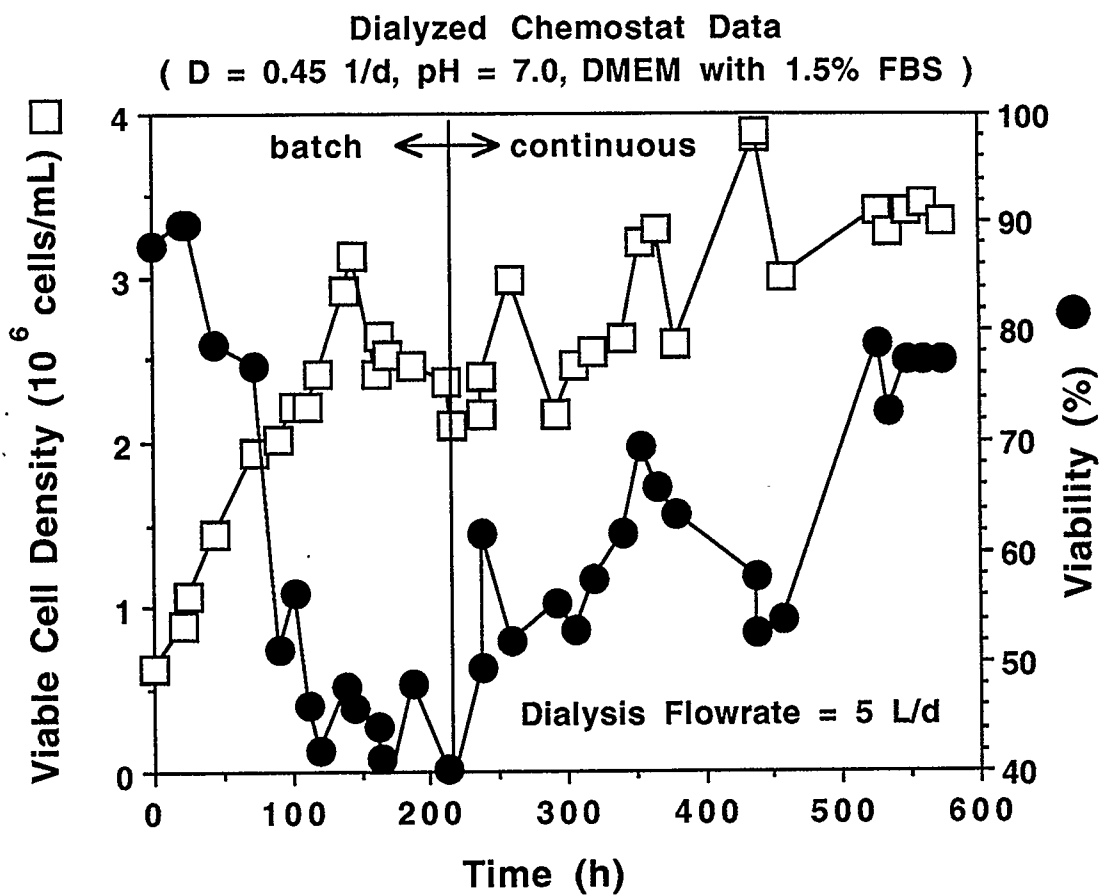


Figure 7.2 Profiles of viable cell density and viability in the dialyzed chemostat run with dialysis rate of 5 L/d. The dialyzing medium was standard DMEM with no FBS added. The dialysis tubing had a total length of 3 m and a 1000 molecular weight cut-off.

sharp drop in viability and a slowdown in the increase of the viable cell density, as seen in Figure 7.2. In order to examine the possibility of achieving an even higher viable cell density, the dialysis flow rate was increased to 4 *L/d*. As a result, the cell growth resumed as the brief increase in viability indicates. The culture reached a maximum viable cell density of 3.1×10^6 *cells/mL* and subsequently entered the death phase. Within 17 *h* after the maximum was achieved, the viable cell density dropped from 3.1 to 2.4×10^6 *cells/mL*. The dialysis flow was subsequently increased to 5 *L/d* at 180 *h* and at time $t = 212$ *h* the continuous feed was turned on.

It is interesting to observe the behavior of the viability during the batch dialyzed run, shown in Figure 7.2. The viability increased only during the first day and subsequently dropped to very low values (40% to 50%) due to the continuous accumulation of dead cells in the bioreactor. Despite the low viability, the viable cell density remained at high levels even after the maximum had been reached. When continuous operation started at $t = 212$ *h* the viability was only 40% while the viable cell density was 2.5×10^6 *cells/mL*.

The MAb concentrations during the batch start-up period are shown in Figure 7.3. From about 170 *h* until continuous operation commenced the MAb concentration stabilized at an average value of 170 *mg/L*. Typical batch runs in the Celligen bioreactor produce a final MAb titer of only 50-60 *mg/L* from a maximum viable cell density of 1.5 - 2.0×10^6 *cells/mL* (Linardos et al., 1988). Therefore, in the batch mode dialysis resulted in a roughly 2-fold increase in maximum cell density and 3-fold increase in MAb production.

7.3. DIALYZED RUNS - CONTINUOUS OPERATION

Two different dialysis flow rates, namely 2 *L/d* and 5 *L/d*, were used in the next two chemostat runs. The volumetric feed flow rate was maintained at 600 *mL/d* corresponding to a dilution rate of 0.45 d^{-1} . In each chemostat run the reactor was allowed to reach a steady state judged by the stability of the viable cell density and viability measurements for a period of four days or longer.

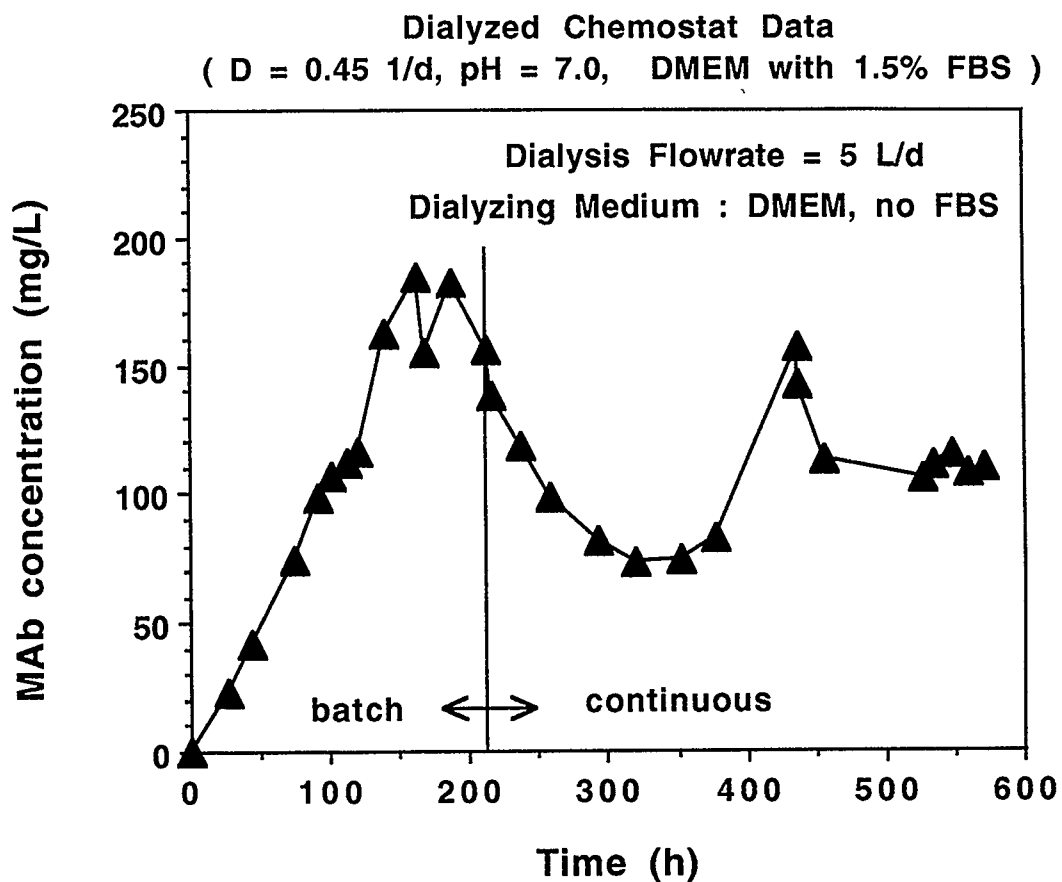


Figure 7.3 Profile of MAb concentration in the dialyzed chemostat run with dialysis rate of 5 L/d. The dialyzing medium was standard DMEM with no FBS added. The dialysis tubing had a total length of 3 m and a 1000 molecular weight cut-off.

The first chemostat run was a continuation of the batch growth phase described above. The dialysis flow rate was maintained at 5 *L/d*. The profiles of viable cell density and viability are shown in Figure 7.2. Soon after continuous feeding started, a sharp increase in the viability was observed as a result of physically removing dead cells that had been accumulating in the reactor. In addition to the increase in viability, the viable cell density also increased as a result of the initiation of direct feeding. An oscillatory behavior can be observed during the chemostat operation of the bioreactor. At time $t = 600$ a steady state appeared to have been reached. The steady state cell density was 3.4×10^6 *cells/mL* and the average viability reached approximately 76%.

The profile of MAb concentration during the batch start-up and the first dialyzed run is shown in Figure 7.3. When direct feeding was initiated the MAb concentration dropped due to the dilution effect and reached a minimum value of 70 *mg/L* at 320 *h*. Subsequently, the MAb concentration increased again reaching a maximum value of 155 *mg/L* at 440 *h*. Finally, the MAb concentration stabilized at 110 *mg/L* at the steady state period from 440 to 550 *h*.

In the second dialyzed chemostat run a dialysis flow rate of 2 *L/d* was used. The inoculum concentration was 1.8×10^6 *cells/mL* with an 80% viability. This dialyzed run lasted for about 45 days. The dialysis tubing withstood the continuous operation without any problems. Figure 7.4 shows the profiles of viable cell density and viability during this run. The steady state was achieved after 300 *h* and it was maintained until the end of the run at 1050 *h*. The steady state values of viable cell density and viability were 2.6×10^6 *cells/mL* and 73% respectively.

7.4. DISCUSSION

7.4.1. Comparison of Steady state Measurements

The steady state concentrations of glucose (C_c), lactate (C_l) and ammonia (C_a) are given in Table 7.1 for the three chemostat runs. The main observation is that in the dialyzed runs a high concentration of glucose is available to the cells. This fact indicates that dialysis has been successful in replenishing the nutrients in the reactor. Moreover,

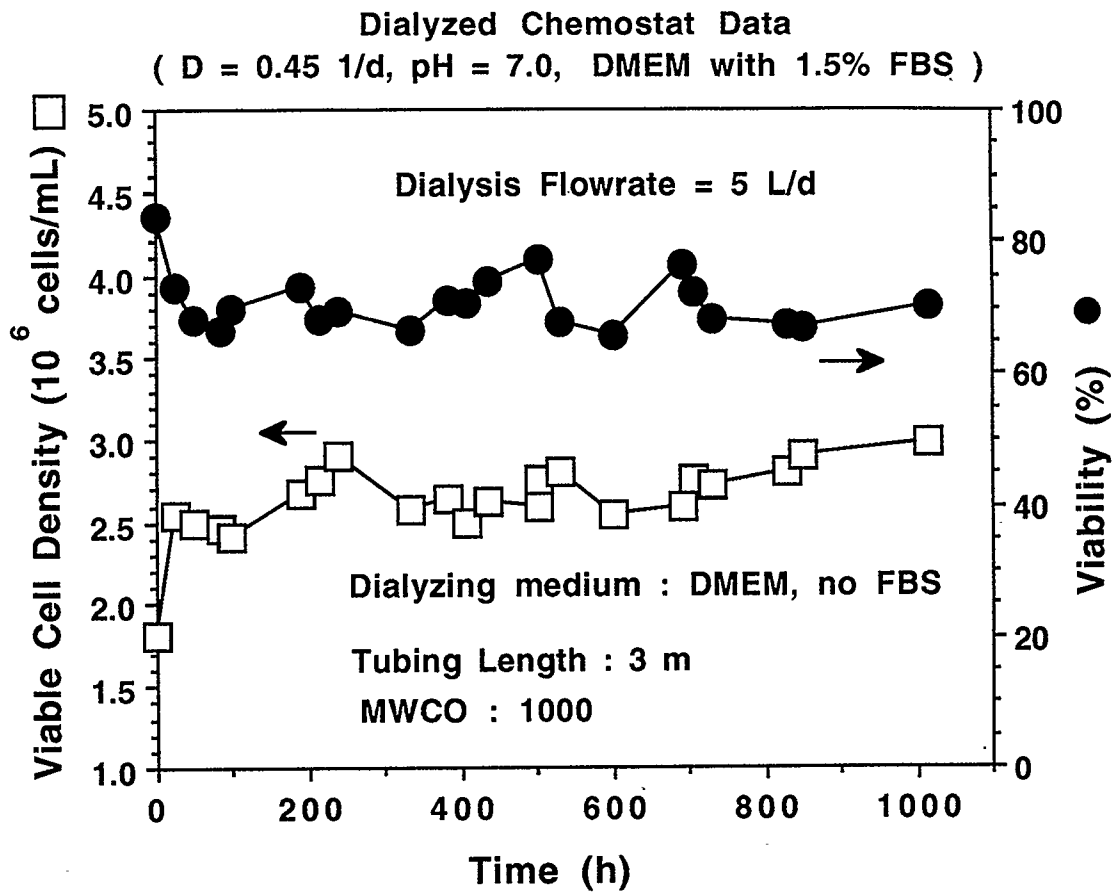


Figure 7.4 Profiles of viable cell density and viability in the second dialyzed chemostat run with dialysis rate of 2 L/d.

Table 7.1 Comparison of steady state measurements				
Steady State Measurements	Dialysis Flow rate (L/d)			Units
	0	2.0	5.0	
x_v	2.2	2.6	3.2	10^6 cells/mL
v_x	75	73	76	%
C_c	4.5	17.3	13.5	mmol/L
C_a	1.85	2.40	1.50	mmol/L
C_l	31	15	10	mmol/L
C_m	80	88	110	mg/L

Table 7.1 Comparison of steady state measurements in dialyzed chemostat cultures with varying dialysis flow rate.

the high residual glucose levels indicate that the culture cannot make full use of the available glucose. It is possible that the culture is limited either by the existence of an inhibitor or by the lack of another important nutrient. Most likely the inhibitor or the "missing" nutrient are of a high molecular weight so that they cannot be easily exchanged through the dialysis tubing.

On the other hand, the higher glucose concentration in the chemostat run with 2 L/d dialysis flow rate can be partially explained by the presence of a high ammonia concentration that may be growth limiting. It has been shown in mammalian cell cultures that ammonia becomes toxic when present in culture at levels higher than about 2 $mmol/L$ (Reuveny et al., 1986). It is important to note that in the chemostat run with a dialysis flow rate of 5 L/d the ammonia and especially the lactate concentration are significantly lower than the control case, despite the substantial increase in the viable cell density.

The steady state antibody concentration, C_m , is also given in Table 7.1 for the three chemostat runs. An increase of 11% and 39% is observed for dialysis rates of 2 L/d and 5 L/d respectively. The reason for the observed increase will become apparent in the following section where some important culture parameters are calculated from the raw data of Table 7.1.

7.4.2. Effects of Dialysis Rate on Cell Growth

The calculated values for μ and k_d are shown in Table 7.2. The steady state was achieved after 300 h . It can be readily observed that both the specific growth rate and the specific death rate remain practically constant as a function of the dialysis rate. This observation is consistent with the models presented in Chapters 8 and 9, according to which the steady state death rate in chemostat cultures does not depend on the individual concentrations of the inhibiting waste products or the concentrations of the nutrients.

Table 7.2 Calculated steady state parameters				
Steady State Values	Dialysis Flow rate (L/d)			Units
	0	2.0	5.0	
μ	0.60	0.62	0.59	d^{-1}
k_d	0.150	0.166	0.142	d^{-1}
q_m	16.4	15.3	15.5	$\mu g/(10^6 \text{ cells} \cdot d)$
Q_m	36	40	50	$mg/(L \cdot d)$

Table 7.2 Comparison of calculated steady state parameters for dialyzed chemostat cultures with varying dialysis flow rate.

7.4.3. Effect of Dialysis on the MAb Production

The volumetric MAb reactor productivity at steady state was calculated using the following equation

$$Q_m = D \cdot C_m \quad (7.1)$$

The results of the calculations are shown in Table 7.2. It can be seen that the overall reactor volumetric productivity increased by 11% and 39% for dialysis flow rates of 2 L/d and 5 L/d respectively. Since the dilution rate was constant this increase is exactly the same as for the antibody concentration. Furthermore, roughly the same increase was observed for the viable cell density. This indicates that the specific MAb productivity q_m remained practically constant.

The specific MAb productivity was calculated using Equation (6.8). The calculated values are shown in Table 7.2, where it can be seen that, indeed, q_m remained practically unchanged for the three different dialysis rates. This result is consistent with the predictions of the empirical model of MAb production in a chemostat bioreactor, presented in Chapter 8 of this thesis. Furthermore, since the growth parameters have not changed as a result of the dialysis, the constant value of q_m is also consistent with the predictions of the Suzuki and Ollis (1989a) model for antibody production.

It should be noted here that the increased MAb production was achieved using the basal unsupplemented and serum free dialysis medium. Since the price of basal unsupplemented medium is much lower than of regular medium containing serum, an efficient dialyzed chemostat may also prove more economical to operate than a conventional chemostat.

7.4.4. Concluding remarks

In conclusion, the main effect of dialysis was a 40% increase in viable cell density and monoclonal antibody production for the highest used dialysis flow rate of 5 L/d, as compared to a regular chemostat run at the same dilution rate (0.45 d^{-1}). In the batch mode, the maximum viable cell density and the MAb production were more than

double compared to those observed in a typical batch run.

Dialysis had no significant effect on the steady state viability, the specific growth and death rates and on the specific MAb productivity of the culture. This result is consistent with the predictions of the proposed hybridoma growth and MAb production models in this thesis (Chapters 8 and 9).

8. DEVELOPMENT OF A STEADY-STATE MODEL

In this chapter the development of a steady state model for cell growth, death and MAb production in a chemostat hybridoma culture is described. Steady state relationships for the specific MAb productivity, specific death rate and the specific uptake rates of glucose and glutamine are proposed. The model predictions agree very well with our chemostat data as well as with chemostat hybridoma culture data in the literature.

8.1. MAb PRODUCTION

As discussed earlier, batch experiments showed that increased antibody production should be expected during the stationary and early death phase rather than the exponential growth phase. This observation is in agreement with Miller et al. (1987, 1988) who showed that the MAb production was enhanced when the cells were under environmental stress such as pH and dissolved oxygen (DO) levels far from the experimentally determined optimum for cell proliferation. Passini and Goochee (1989) also showed that in a culture partially protected from sparging by a low concentration of Pluronic F-68[®], the values of maximum cell density and maximum growth rate were lower than in the control experiment, however the MAb titer was comparable or slightly higher. Therefore, it appears that MAb production is more directly related to cell death, which is an indirect measure of cell stress, than cell growth in a hybridoma culture.

To illustrate the relationship between antibody production and cell death, the MAb productivity q_m is plotted against the specific death rate, k_d in Figure 8.1. The experimental data clearly show a linear dependence of the MAb on the death rate. Data from Miller et al. (1988) also support this hypothesis as shown in Figure 8.1. These independent observations suggest that the MAb productivity can be modeled by the following linear relationship

$$q_m = \alpha + \beta k_d \quad (8.1)$$

where α and β are constants for a given cell line, under a given set of culture conditions.

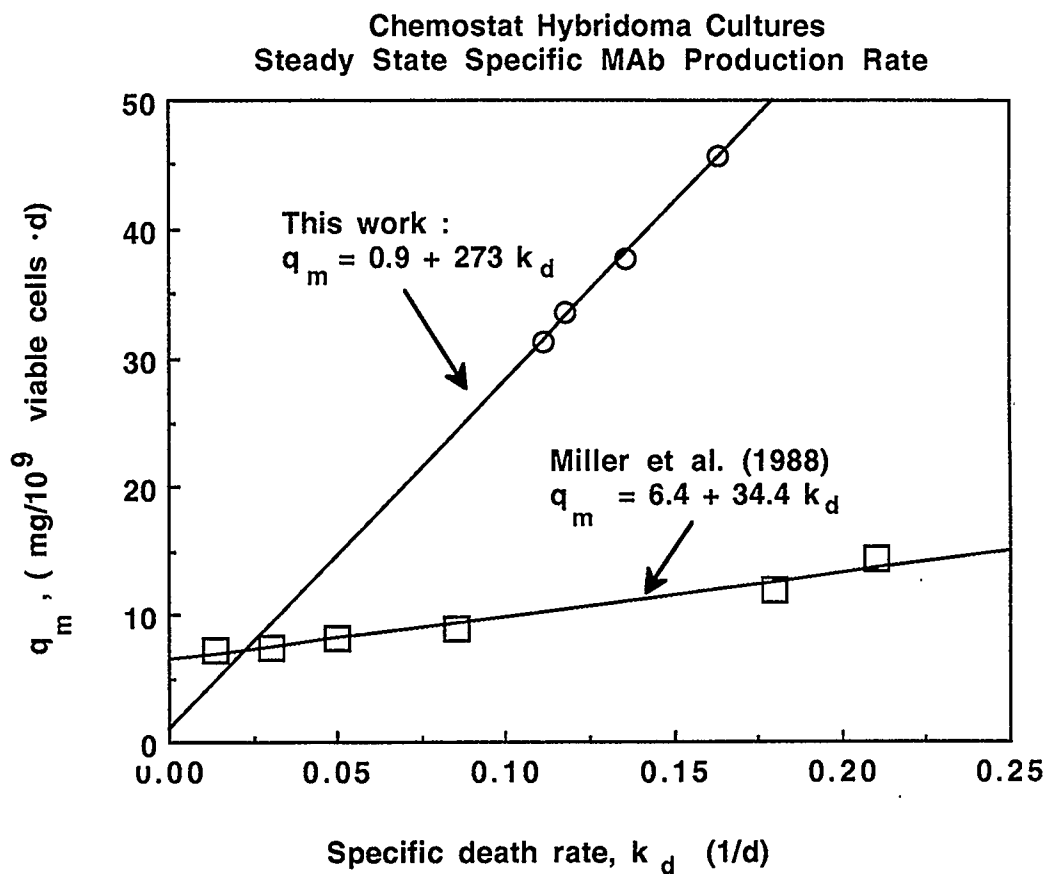


Figure 8.1 The specific MAb production rate (q_m) as a function of the specific death rate in chemostat hybridoma cultures. The straight lines were determined using linear least squares regression on the experimental data.

In our chemostat experiments, as well as Miller's runs, pH, DO and FBS concentration were kept constant. Therefore in a more generalized model, the values of α and β are expected, in principle, to be functions of these parameters. It should be pointed out, however, that for MAb production purposes, only one set of parameters, near the optimum operating conditions, is necessary.

The straight line in Figure 8.1 was produced by least squares fitting of the experimental points. The intercept is $0.9 \mu\text{g}/(10^6 \text{ viable cells}\cdot\text{d})$ and the slope is $273 \mu\text{g}/10^6 \text{ viable cells}$. For Miller's data the intercept is $6.4 \mu\text{g}/(10^6 \text{ viable cells}\cdot\text{d})$ and the slope is $34.38 \mu\text{g}/10^6 \text{ viable cells}$. The form of Equation (8.1) suggests that when no stress is exerted on the cells and the death rate approaches zero, the cells produce a small amount of MAb (corresponding to the value of α). For our system the contribution of α is very small, almost negligible, as compared to the effect of the parameter β on the value of the specific MAb productivity.

In interpreting Equation (8.1), one should not hastily conclude that MAb is leaking from dead cells. Birch et al. (1987) and Passini and Goochee (1989) suggested that cell associated antibody was negligible compared to the total MAb produced in a batch culture. Reddy and Miller (1989) using flow cytometry showed that dead hybridoma cells contain the same or higher levels of antibody than the average live cell and no antibody leakage was apparent. Therefore, the elevated production of MAb at high death rates is viewed as a result of increased MAb synthesis by live cells due to environmental stress factors, which can be "quantified" indirectly by the specific death rate.

8.2. CELL DEATH

The next step in our modeling efforts was to relate the death rate to culture parameters that can be readily computed so that predictions of the MAb productivity could be made.

Experimental data from mammalian cell cultures tend to agree that environmental stress delays the passage of the cells through the G_1 phase of the division cycle resulting in a reduced proliferation rate. The length of the G_2 , M and S phases is only

slightly affected. Therefore, the length of the cycle is primarily dictated by the length of the G_1 phase. The time that cells spend in the G_1 phase increases with the severity of the environmental stress and so does average culture age and the proportion of cells in the G_1 phase. (Prescott, 1976 and Lloyd et al., 1982). Under suboptimal conditions cells are known to move from G_1 to a non-proliferative state call G_0 . Some types of cells can remain healthy in G_0 for long periods of time (Pardee, 1989). However, cells in G_0 have lost their ability to synthesize DNA and to reproduce and they eventually disintegrate without dividing. In a steady state chemostat culture, the rate of cells entering the G_0 phase eventually determines to a great extent the death rate.

We can conclude from the above discussion that cell death due to external stress conditions is correlated to the length of G_1 phase and therefore to the average cell age of the culture. At steady state the average cell age in exponentially growing cultures of mammalian cells has been shown to be proportional to the inverse of the growth rate (Cook and James, 1964; Wiedemann and Moser, 1988).

$$\lambda \propto 1/\mu \quad (8.2)$$

The natural logarithms of steady state death rates versus the inverse of measured specific growth rates are shown in Figure 8.2. Our data suggest a linear relationship between $\ln(k_d)$ and the inverse of the specific growth rate. Data from Miller et al. (1988) also to support this hypothesis as shown in Figure 8.2. Therefore, it appears that an exponential relationship exists between k_d and λ , or equivalently between k_d and μ ,

$$k_d = d_o \exp(d_1/\mu) \quad (8.3)$$

In general, the values of the parameters d_o and d_1 depend on the particular cell line, as well as on environmental conditions such as pH, DO and FBS concentration. By applying linear regression on our experimental data, the values of $0.069 d^{-1}$ and $0.467 d^{-1}$ were estimated for the parameters d_o and d_1 respectively.

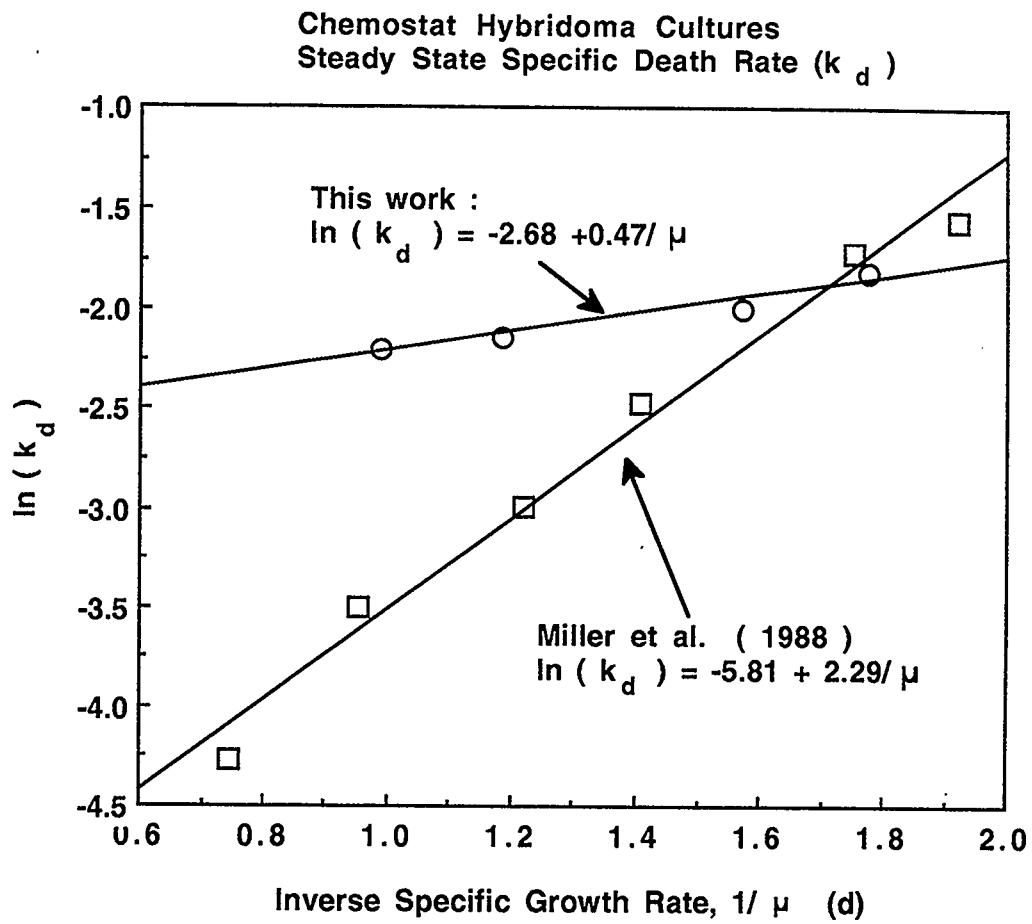


Figure 8.2 Natural logarithms of steady state death rate values (k_d) versus the inverse of specific growth rate (μ) in chemostat hybridoma cultures. The straight lines were determined using linear least squares regression on the experimental data.

8.3. GLUCOSE AND GLUTAMINE UPTAKE

In microbial systems the specific uptake rate of glucose is traditionally modeled according to the maintenance energy model, (Pirt, 1975)

$$q_c = m_c + \mu/Y_{x/c} \quad (8.4)$$

where q_c is the specific uptake rate of glucose, m_c is the amount of glucose used for cell maintenance and $Y_{x/c}$ is the yield of biomass from glucose. The glucose uptake rates calculated in this work are shown in Figure 8.3 as a function of the specific growth rate. It can be seen that a linear relationship cannot sufficiently describe the suppressed nutrient uptake rate at lower growth rates. Miller et al. (1988) also arrived at the same conclusion, regarding their experimental data from chemostat hybridoma cultures.

It appears that a different approach is needed in modeling glucose uptake by hybridomas. In contrast to microbial cells, animal cells are highly specialized and need a very well defined environment to function properly. It is reasonable to assume that nutrient limitations, toxic effects or other types of stress will modify the metabolic efficiency of the cells. If this assumption is true, the uptake rate of nutrients in a hybridoma culture is expected to be a function of the environmental stress and consequently of the specific death rate.

In this work, a generalized model for nutrient uptake by hybridomas is proposed. A third term has been added to the maintenance energy model to account for the effect of the cell death, as given by

$$q_c = m_c + \mu/Y_{x/c} - e_c k_d \quad (8.5)$$

where e_c is a parameter we name "Nutrient Economy Coefficient". This parameter is used to quantify the apparent increase in nutrient utilization efficiency with increasing death rate or, equivalently, with increasing cell stress. The above equation can describe the experimental data for glucose uptake with great success, as shown in Figure 8.4. By linear regression, the value of the maintenance requirement has been found to be $4.7 \mu\text{mol of glucose}/(10^6 \text{ cells} \cdot \text{d})$ the yield $0.593 \times 10^6 \text{ cells}/\mu\text{mol of glucose}$ and the

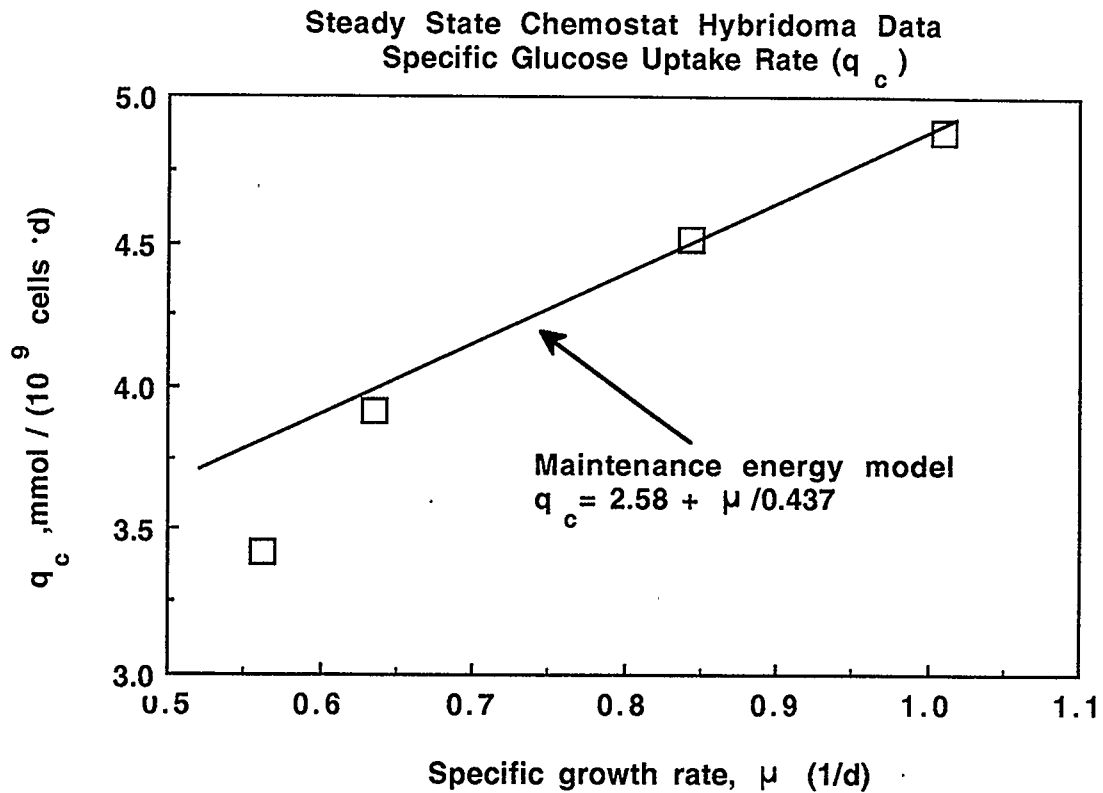


Figure 8.3 Steady state values of glucose uptake rate versus specific growth rate (data from Chapter 6 of this work). The straight line illustrates the deviation from the maintenance energy model by Pirt (1975) at lower growth rate values.

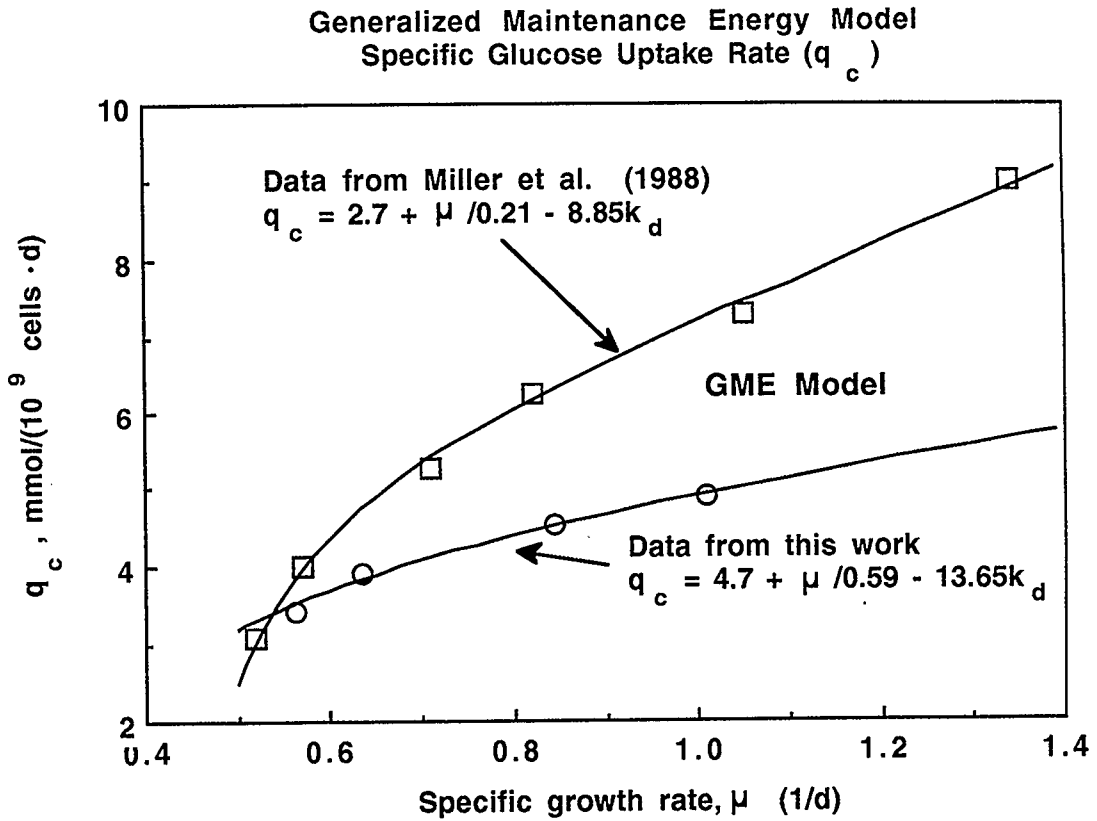


Figure 8.4 Experimental data of steady state specific glucose uptake rate (q_c) in chemostat cultures. Data from this work and from Miller et al. (1988) are shown. The curves represent the GME model predictions for growth rates from 0.5 d^{-1} to 1.4 d^{-1} .

nutrient economy constant was equal to $13.65 \mu\text{mol of glucose}/10^6 \text{ dying cells}$. It has been shown that the data by Miller et al. (1988) can also be satisfactorily described by the proposed generalized maintenance energy equation. The corresponding parameter values are also shown in Figure 8.4.

The proposed Generalized Maintenance Energy (GME) Model can also describe glutamine uptake rate data as shown in Figure 8.5. The maintenance requirement was found, by linear regression, to be $0.7 \mu\text{mol of glucose}/(10^6 \text{ cells}\cdot\text{d})$ the yield coefficient had a value of $0.63 \times 10^6 \text{ cells}/\mu\text{mol of glutamine}$ and the glutamine economy factor was $2.0 \mu\text{mol of glutamine}/10^6 \text{ dying cells}$. It is apparent however, since the line is almost straight, that the effect of stress on the glutamine uptake is very small for our system under the reported operating conditions and it can be neglected for practical purposes. Nevertheless, the value of the GME model lies in the fact that it offers a generalized relationship for modeling the uptake of a nutrient by hybridoma cells. Moreover, it is conceivable that the effect is significant for different hybridoma lines or for operating conditions inducing a high rate of cell death.

8.4. STEADY-STATE BEHAVIOR OF THE CHEMOSTAT

At a steady state, the following equation applies for a chemostat bioreactor

$$\mu - k_d = D \quad (8.6)$$

According to Equation (8.3) the steady state value of death rate, k_d , is only a function of μ . As a result, the left hand side of Equation (8.6) becomes a function of the steady state growth rate only. Therefore, under a given set of operating conditions the dilution rate which is set by the experimentalist determines the steady state growth rate and, consequently, the corresponding death rate. In Figure 8.6 the calculated growth rates at various dilution rates are shown. These calculations were made by substituting Equation (8.3) into Equation (8.6) and then solving the resulting nonlinear equation for μ in a range of dilution rates from 0 to 1.2 d^{-1} . The experimental data are compared with the calculated line and a very good agreement can be observed. The diagonal in Figure 8.6

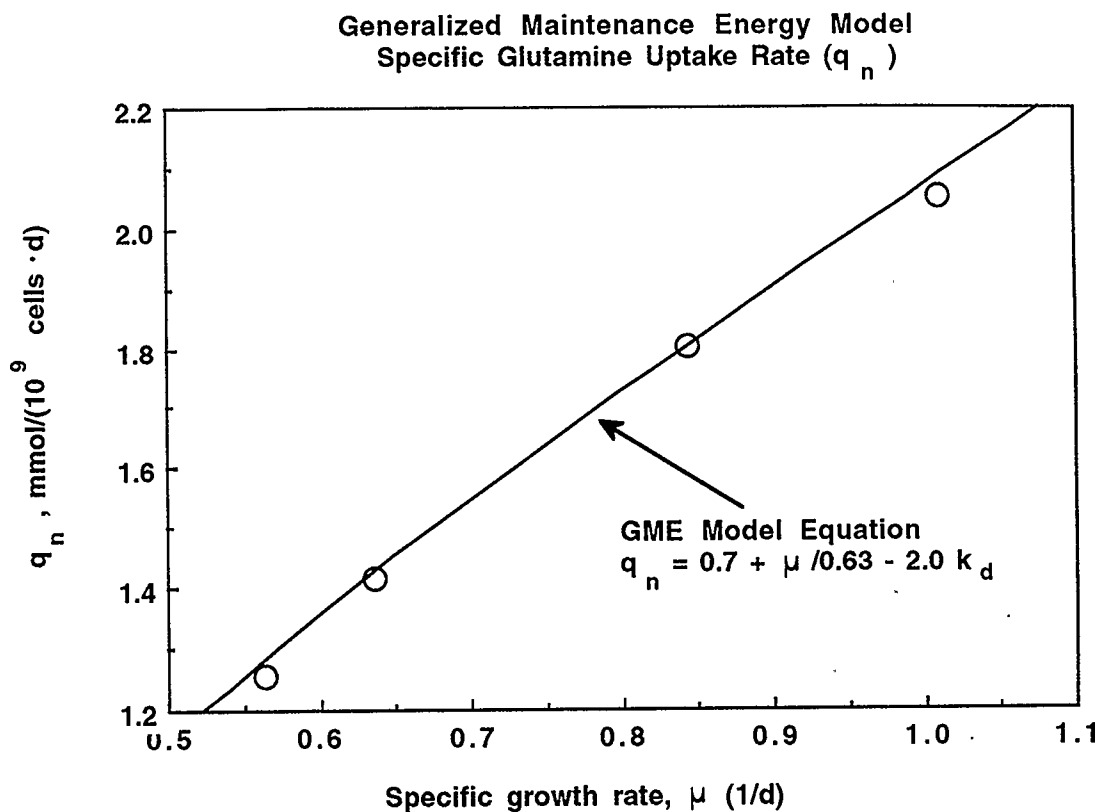


Figure 8.5 Experimental data of steady state specific glutamine uptake rate (q_n) as a function of growth rate, compared with the values calculated using the proposed GME model.

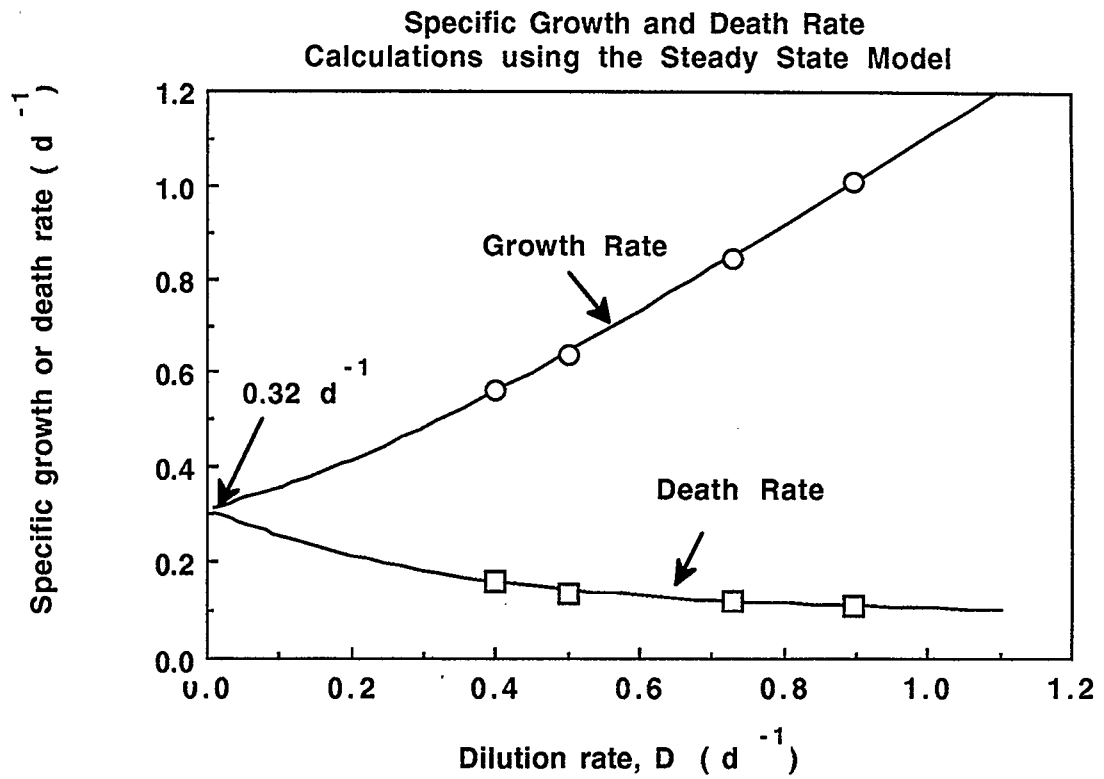


Figure 8.6 Comparison of experimental data from this work with calculated specific growth and death rate values for dilution rates ranging from $0.5 d^{-1}$ to $1.1 d^{-1}$.

represents the case of negligible death rate. It is well known from microbial systems that in this case, the steady-state growth rate is equal to the dilution rate (Pirt, 1975).

An important implication of Equation (8.6) is that as D tends to zero, the growth rate tends to become equal to the death rate. At the limit, where the dilution rate becomes practically zero, the steady state growth rate is only marginally higher than the death rate and its approximate value is $0.32 d^{-1}$. The corresponding steady state conditions are very difficult to reach and maintain, since the viable cell density is very small and any fluctuation can cause a rapid death of the culture. The minimum steady-state growth rate can also be calculated from the equation

$$\mu - k_d(\mu) = 0 \quad (8.7)$$

when the death rate equation is known. Our observations regarding the behavior of the steady state growth rates are also supported by the independent findings of Miller et al. (1988) and Reuveny et al. (1985) from chemostat cultures of hybridoma cells.

8.5. CONCLUDING REMARKS

A steady state model was developed to describe chemostat data presented in this work. The model was also successful in describing data from chemostat hybridoma cultures, that appeared in the literature recently.

The proposed model expresses the specific monoclonal antibody production rate as a linear function of the death rate in hybridoma cell chemostat cultures. The value of the death rate is viewed as a measure of the nutritional and environmental stress exerted on the cells. Furthermore, the death rate of the cells was related to the growth rate in the culture. The implication is that under constant environmental conditions the steady state growth rate and death rate in a chemostat are determined by the dilution rate.

A Generalized Maintenance Energy model was proposed to describe the specific uptake rate of glucose in chemostat hybridoma cultures. According to the proposed equation the uptake rate is proportional not only to the growth rate but also to the death

rate of the culture. The proposed model was also applied to the modeling of the glutamine uptake, although the contribution of the cell death was found to be rather small under the conditions of the conducted experiments.

9. DEVELOPMENT OF A CELL CYCLE MODEL

9.1. CELL CYCLE REPRESENTATION

In the present work the cell cycle representation shown in Figure 9.1 has been followed. After mitosis (M) all daughter cells enter the indeterminate state A which comprises the initial, variable part of the G_1 phase (Smith and Martin, 1973; Darzynkiewicz et al., 1980). Cells entering phase B have spent varying lengths of time in state A. We advocate that the portion f_0 of G_1 phase cells that have remained in state A longer than a critical time T_C are to be considered arrested in the G_1 phase. Arrested cells comprise the non cycling fraction, f_0 , of the viable cell population, while f_1 denotes the fraction of the cycling cell population that are cycling in state A. In fibroblast cultures, serum-sensitive events which direct cells either towards replication or arrest, are completed short time (approximately 2 h) before cell entrance into the S phase (Yen and Pardee, 1978; Schneiderman et al., 1971). This indicates that the terminal part of the G_1 phase indeed belongs to the "deterministic" phase B. Cells entering phase B require a constant length of time to reach mitosis and divide. Upon cell division, two daughter cells are produced which reenter the indeterminate state A to complete the cycle.

9.2. PROPOSED MODEL

In the proposed model the death rate has been modeled as a linear function of f_0 , the arrested cell fraction in the G_1 phase. The cell age distributions have been determined for the cycling and non-cycling cells in state A and the corresponding cell fractions have been calculated. Important chemostat culture parameters such as growth rate, death rate and viability were calculated as functions of the dilution rate and compared successfully to recently published experimental data.

SCHEMATIC REPRESENTATION OF CELL CYCLE

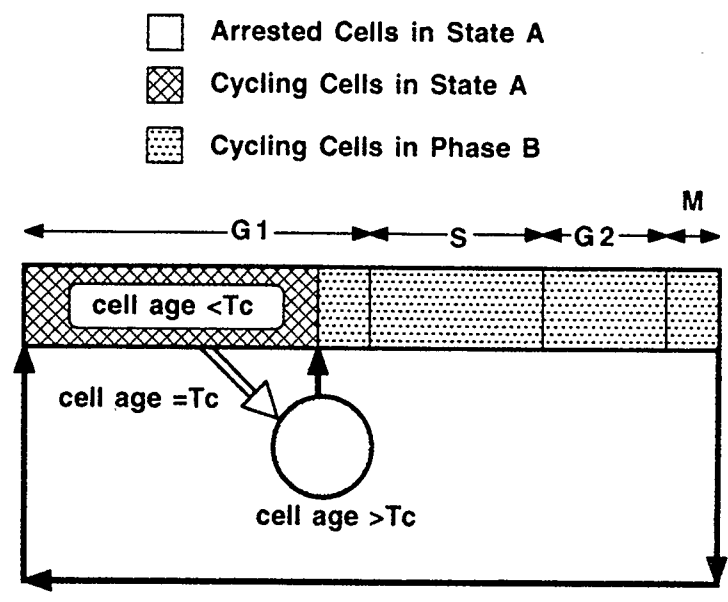


Figure 9.1 Cell cycle representation used in the development of the proposed model.

9.2.1. Steady-state death rate

In rapidly proliferating hybridoma cultures, the measured death rate is normally low (Miller et al., 1988). Cell death in optimized culture environments can be mainly attributed to the small effect of external factors, such as direct cell injuries due to agitation or combined action of agitation and sparging (Kunas and Papoutsakis, 1990; Yang et al., 1991). The death rate in hybridoma cultures increases continuously with decreasing growth rate. It has been postulated that the arrested fraction of the cell population is exposed to an increased death incidence as a result of aging and loss of capability to effect repairs (Pardee, 1989; Bowen, 1981).

In the proposed model the overall specific death rate k_d is described by the relationship

$$k_d = k_c(1 - f_0) + k_0f_0 \quad (9.1)$$

where k_c is the specific death rate of the cycling cell fraction, and k_0 is the specific death rate of the arrested cell fraction, f_0 .

Cell loss in some mammalian tissues is uniformly distributed over the entire cycle (Marques-Pereira and Leblond, 1965). To model this case the value of k_0 can be set equal to the value of k_c . For bone marrow stem cells it has been shown that cell death mainly occurs in the arrested phase (Burns and Tannock, 1970). The proposed death rate equation is capable of describing this case by giving a very small (or zero) value to k_c . The death rate in hybridoma chemostat cultures seems to follow the latter pattern, as will become evident in the following paragraphs.

9.2.2. Cell age distributions in state A.

The fractions of cells in the cycling and arrested populations are determined by the cell distribution in the corresponding compartments of state A. Since we postulate that cells which have been in state A longer than a critical time T_C are considered

arrested, the age distributions of state A cells can be determined as follows.

Let us consider the cell balance around a chemostat bioreactor for cycling state A cells (fraction f_1) with cell age α strictly greater than zero. Cells are removed randomly from the considered population due to (i) transition to phase B, (ii) physical exit from the reactor, or (iii) cell death. Thus, the cell balance can be written as

$$f_1 x_v \left[\frac{\partial w_1}{\partial \alpha} + \frac{\partial w_1}{\partial t} \right] = \left[-\lambda - D - k_c \right] w_1 f_1 x_v \quad 0 < \alpha \leq T_C \quad (9.2)$$

where $w_1 = w_1(\alpha, t)$ is the age distribution of cycling state A cells and λ is the constant rate of cell transition from state A to phase B. The above equation simplifies to

$$\frac{\partial w_1}{\partial \alpha} + \frac{\partial w_1}{\partial t} = \left[-\lambda - D - k_c \right] w_1 \quad 0 < \alpha \leq T_C \quad (9.2.a)$$

At steady state $\frac{\partial w_1}{\partial t} = 0$ and Equation (9.2.a) becomes

$$\frac{dw_1}{d\alpha} = - \left[\lambda + D + k_c \right] w_1 \quad 0 < \alpha \leq T_C \quad (9.3)$$

According to the transition probability theory (Smith and Martin, 1973) the rate of transition λ is independent of cell age. Furthermore, we assume that in the cycling state A cell population, the specific death rate takes a constant value k_c . Therefore, Equation (9.3) can be integrated analytically to yield

$$w_1(\alpha) = w_1(0) \exp \left[- (\lambda + D + k_c) \alpha \right] \quad 0 < \alpha \leq T_C \quad (9.4)$$

The value of $w_1(0)$ can be obtained by a cell balance at age zero. In particular, the rate of cells entering the cycle with age zero should satisfy is given by the equation

$$f_1 x_v w_1(0) = 2\mu x_v \quad (9.5)$$

The factor 2 denotes the fact that for every cell that divides (increasing thus the total cell number by one) two cells re-enter the cycle with age zero. Equation (9.5) can be

simplified to

$$w_1(0) = \frac{2\mu}{f_1} \quad (9.5.a)$$

Therefore, Equation 9.4 can be written as

$$w_1(\alpha) = \frac{2\mu}{f_1} \exp(-\lambda_c \cdot \alpha) \quad 0 < \alpha \leq T_C \quad (9.6)$$

where $\lambda_c = \lambda + D + k_c$.

The cell age distribution function, $w_0(a)$, for cells arrested in state A can also be obtained in a similar fashion. At time T_C the rate of cells exiting the cycling fraction f_1 is equal to the rate of cell becoming arrested, namely

$$w_1(T_C) \cdot f_1 = w_0(T_C) \cdot f_0 \quad (9.7)$$

The cell age distribution w_0 is defined for cell ages higher than or equal to the critical age T_C ; Equation (9.7) can be used to calculate the initial value of w_0

$$w_0(T_C) = w_1(T_C) \frac{f_1}{f_0} = \frac{2\mu}{f_0} \exp(-\lambda_c \cdot T_C) \quad (9.7.a)$$

Following the same development as for Equation (9.3), the cell balance for the arrested state A cells is expressed as

$$\frac{dw_0}{d\alpha} = -[\lambda + D + k_0]w_0 \quad T_C \leq \alpha < \infty \quad (9.8)$$

Equation (9.8) can also be integrated analytically since a constant (i.e. cell age independent) specific death rate value, k_0 , was assumed for the cells arrested in state A

$$w_0(\alpha) = \frac{2\mu}{f_0} \exp(-\lambda_c T_C) \exp(-\lambda_0 \alpha) \quad T_C \leq \alpha < \infty \quad (9.9)$$

where $\lambda_0 = \lambda + D + k_0$.

If we consider cell age as a random variable whose domain is $0 < \alpha < \infty$, its pro-

bability density function $w(\alpha)$ is given by

$$w(\alpha) = \begin{cases} \frac{w_1(\alpha)f_1}{f_0 + f_1} & \text{for } 0 < \alpha < T_C \\ \frac{w_0(\alpha)f_0}{f_0 + f_1} & \text{for } T_C \leq \alpha < \infty \end{cases} \quad (9.10)$$

9.2.3. Calculation of cell fractions

The fraction of cycling state A cells, f_1 , can be calculated by applying the constraint

$$\int_0^{T_C} w_1(\alpha) d\alpha = 1 \quad (9.11)$$

since $w_1(\alpha)$ is a probability density function. Equation (9.11) can be integrated analytically and solved for f_1 to yield

$$f_1 = \frac{2\mu}{\lambda_c} (1 - e^{-\lambda_c T_C}) \quad (9.12)$$

The above relationship allows the calculation of f_1 as a function of the specific growth rate and the dilution rate in a chemostat culture. The fraction of arrested cells, f_0 , can be calculated from the constraint on $w_0(\alpha)$, i.e.,

$$\int_{T_C}^{\infty} w_0(\alpha) d\alpha = 1 \quad (9.13)$$

Similarly, Equation (9.13) can be solved for f_0 to yield

$$f_0 = \frac{2\mu}{\lambda_0} e^{-\lambda_c T_C} \quad (9.14)$$

The fraction of cells in phase B, f_B , is simply given by

$$f_B = 1 - f_1 - f_0 \quad (9.15)$$

9.2.4 Steady state growth rate and cycle time

In a chemostat bioreactor, under steady state conditions the specific growth rate and death rate are related through the equation (Miller et al., 1988)

$$\mu = D + k_d \quad (9.16)$$

where D is the dilution rate. The above equation is useful in introducing the effect of dilution rate into the steady state calculations.

The average time, t_A , a cycling cell spends in state A until its successful transition to phase B can be calculated from the transition probability theory (Smith and Martin, 1973). According to this theory, the length of time τ a cell spends in state A is exponentially distributed with density function

$$\phi(\tau) = \lambda \exp(-\lambda\tau) \quad (9.17)$$

where λ is the rate of cell transition from state A to phase B. The mean value is then given by the relationship (Blank, 1980)

$$t_A = E(\tau) = \frac{1}{\lambda} \quad (9.18)$$

The duration of phase B, t_B , is considered to be practically constant (Shields, 1978; Shields et al., 1978). The specific growth rate is related to t_A , t_B and the average cycle time t_c through the following equation

$$\frac{(1 - f_0) \ln 2}{\mu} = t_A + t_B = t_c \quad (9.19)$$

The term $(1 - f_0)$ takes into account the fact that only the cycling cell fraction contributes to the experimentally measured growth rate.

9.3. MODEL PARAMETERS

Model parameters were used for the chemostat data reported in Section 6.1 of this thesis and for data by Miller et al. (1988). The two sets of data come from

chemostat cultures of two different SP2/0 derived hybridoma lines and they consist mainly of growth rate, viability and monoclonal antibody (MAb) productivity profiles for a range of dilution rates.

9.3.1. Calculation of f_0

The profile of the arrested cell fraction f_0 was generated from the experimental MAb productivity values using the model of Suzuki and Ollis (1989a) since no experimental values of f_0 in chemostat hybridoma culture were available. According to this model, the specific MAb productivity q_m is directly proportional to the fraction of cells arrested in the G_1 phase, namely

$$q_m = q_c(1 - f_0) + q_0 f_0 \quad (9.20.a)$$

This equation can be solved for f_0 to yield

$$f_0 = \frac{q_m - q_c}{q_0 - q_c} \quad (9.20.b)$$

The parameters q_c and q_0 represent the specific MAb productivities of cycling and arrested cells respectively. Under rapid growing conditions the arrested cell fraction is very small and can be neglected (Suzuki and Ollis, 1989a). Therefore, at this limit q_c becomes approximately equal to q_m . The experimental data were extrapolated to high growth rate regions using the model of growth and antibody production developed in this work (Chapter 8). According to this model

$$q_m = \alpha + \beta d_o e^{d_1/\mu} \quad (9.21)$$

The values of the parameters α , β , d_o and d_1 are given in Table 9.1, along with the calculated values of q_c . The maximum growth rate is $1.5 d^{-1}$ for both sets of data (Miller et al., 1988; Linardos et al., 1988). The value of q_0 for the data by Miller et al. (1988) was estimated to be between 30 and 40 $\mu g/(10^6 \text{ cells} \cdot d)$ by Suzuki and Ollis (1989a). A

value of $45 \mu\text{g}/(10^6 \text{ cells}\cdot\text{d})$ was used in this work instead, as it provided for a better fit of the experimental data.

To estimate the value of q_0 for the chemostat data in this work it was assumed that the ratio of the q_0 values for the two sets of data is equal to the ratio of the q_c values ($26.6/7.0 = 3.8$; see Table 9.1). Expressed in other words this assumption implies that the cell line used in our experiments produced 3.8 times more antibody than the one used by Miller et al. (1988) and that the proportionality holds in both the arrested and cycling cell populations. Based on this reasoning, a q_0 value of $170 \mu\text{g}/(10^6 \text{ cells}\cdot\text{d})$ was estimated for the experimental data in this work (Table 9.1).

9.3.2. Calculation of k_c and k_0

The model parameters k_c and k_0 represent the death rate in the cycling and the arrested cell fractions respectively. The parameters values were estimated using linear least squares estimation from the experimentally measured death rate versus the estimated values of f_0 . Figure 9.2 shows the linear correlation between the parameters k_d and f_0 for both data sets. The estimated parameter values are shown in Table 9.1. The parameter k_c can be alternatively estimated using the expression for the death rate we have proposed, namely

$$k_c \approx d_0 e^{d_1/\mu_{max}} \quad (9.22)$$

Using Equation (9.19), k_c was found to be 0.094 d^{-1} and 0.014 d^{-1} for the data of this work and the Miller et al. (1988) data respectively. The above values are in reasonable agreement with the values estimated using linear least squares estimation (Table 9.1.) It can be seen that the basal death rate is much higher in our data. The difference is attributed to the different culture conditions and mainly to the reduced serum concentration (1.5%) we have used.

Summary of Parameter Values				
Model employed	Parameter	Data		Units
		This work	Miller et al., 1988	
Empirical	α	0.9	6.4	$\mu\text{g}/(10^6 \text{ cells}\cdot\text{d})$
	β	273.0	34.4	$\mu\text{g}/(10^6 \text{ cells})$
This work	d_o	0.069	0.003	d^{-1}
	d_1	0.467	2.290	
Suzuki and Ollis, 1989a	q_c	26.6	7.0	$\mu\text{g}/(10^6 \text{ cells}\cdot\text{d})$
	q_0	171	45	
Cell cycle model	k_c	0.094	0.012	d^{-1}
	k_0	0.62	1.13	
This work	t_B	0.46	0.46	d
	T_C	0.60	0.48	

Table 9.1 Summary of parameter values used in the model development.

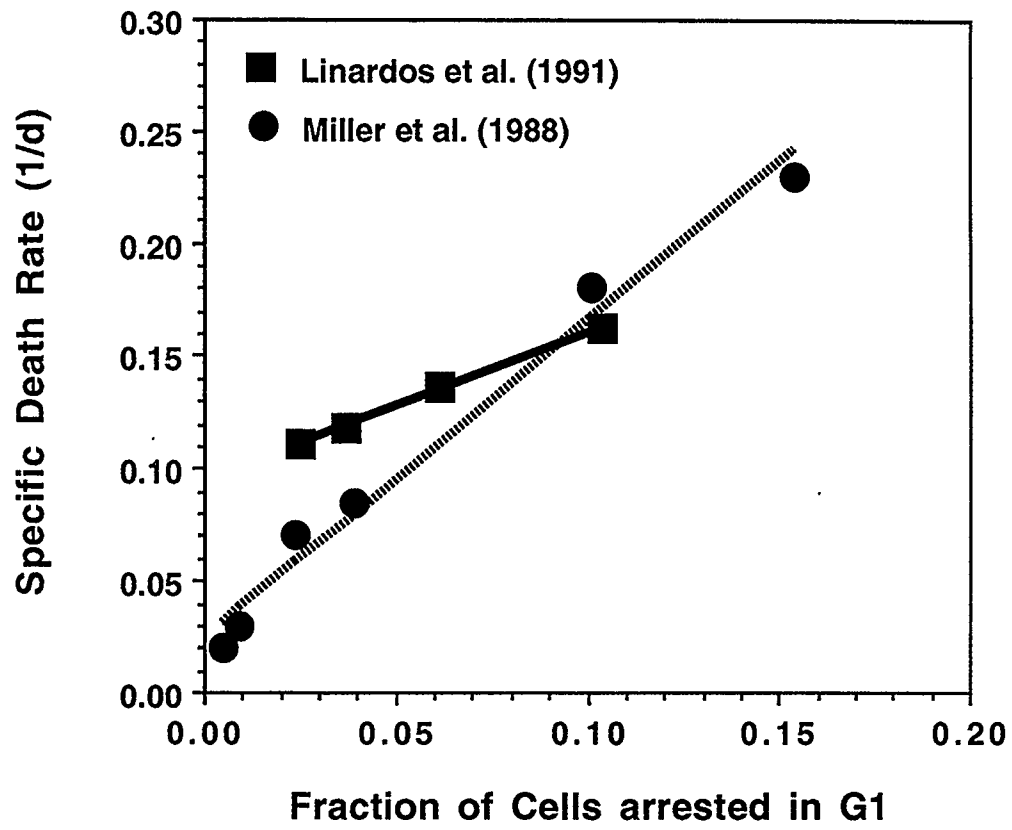


Figure 9.2 Experimental values of specific death rate in a steady state chemostat culture versus the fraction f_0 of cells arrested in the G_1 phase of the cell cycle.

9.3.3. Calculation of t_B

The constant duration of phase B, t_B , is approximately equal to the minimum time required for a cell to traverse the entire cycle (Ronning and Seglen, 1982). The value of t_B was estimated as follows: At maximum growth rate practically all cells are cycling. Therefore, the non cycling fraction f_0 can be neglected. Furthermore, the average duration $t_A = 1/\lambda$ of state A is minimal and can also be neglected (Smith and Martin, 1974). Under these assumptions, Equation (9.16) becomes

$$t_B \approx \frac{\ln 2}{\mu_{max}} \quad (9.23)$$

where μ_{max} denotes the maximum specific growth rate. As seen in Table 9.1, a value of 0.46 d was obtained for t_B , for both sets of data.

9.3.4. Estimation of T_C and model predictions

The system of Equations (9.1), (9.10), (9.12), (9.14), (9.15) and (9.16) can be solved for f_1 , f_0 , λ , μ and k_d over a range of dilution rates from 0 to 1.4 d^{-1} . The critical time T_C which cannot be directly estimated from the experimental data, was taken as an adjustable parameter. Its value was obtained by non-linear least squares estimation whereby the sum of squares of the deviations between the model predictions and the experimental data was minimized. For our own experimental data a value of 0.60 d was estimated, whereas a value of 0.48 d was obtained for the Miller et al. (1988) data set.

9.4. RESULTS AND DISCUSSION

The cell age distribution in state A described by Equation (9.8) is shown in Figure 9.3 parametrically as a function of the dilution rate using the parameters from our data set. As seen, at higher dilution rates where the cell growth is rapid, most cells are distributed in the low age region. At lower dilution rates, the age of the cells is more evenly distributed over the G_1 phase with an increasing portion of cells having ages

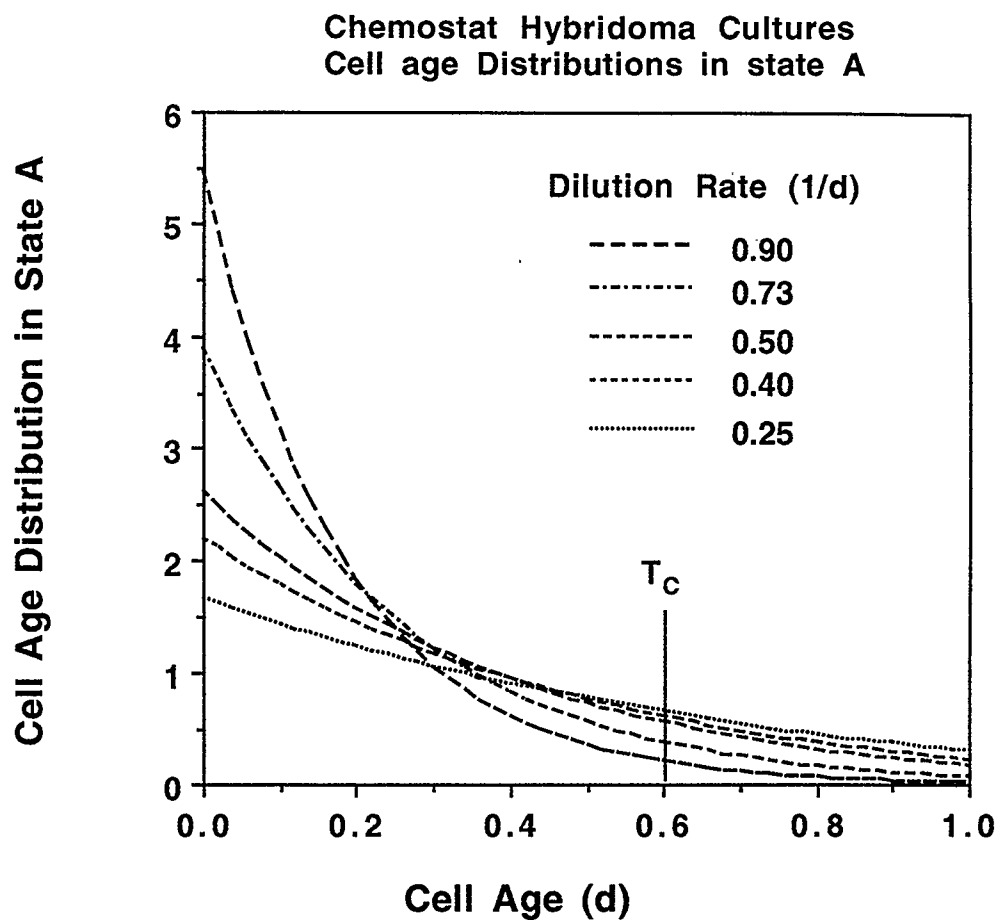


Figure 9.3 The calculated steady state cell age distributions in state A of the cell cycle as a function of the dilution rate in a chemostat culture.

higher than T_C , i.e. with a higher arrested cell fraction f_0 . The profiles of f_0 with respect to the specific growth rate are shown in Figure 9.4 for both data sets. The points represent the values estimated from the experimental MAb productivity values, using the Suzuki and Ollis (1989a) model of antibody production whereas the predictions of the proposed model are represented by the continuous lines. Evidently a very good agreement can be observed between the predicted and the estimated values of f_0 . The behavior of f_0 is similar to that observed by Suzuki and Ollis, namely a rapid increase in the arrested cell fraction at lower dilution rates.

The specific growth and death rate as a function of the dilution rate are shown in Figures 9.5 and 9.6 for our and the Miller et al. data sets respectively. The steady state death rate is related to the growth rate through Equation (9.14). The profile of growth rate increasingly deviates from the diagonal at lower dilution rates due to the increasing magnitude of the death rate. At the limit where the dilution rate becomes zero, the death rate is equal to the growth rate and the viability is practically zero.

The steady state viability can be calculated by solving the Equation (6.6) for v_x , namely

$$v_x = \frac{D}{D+k_d} = \frac{D}{\mu} \quad (9.24)$$

The viability values calculated using the above equation are shown in Figures 9.7 and 9.8. The model predictions are in excellent agreement with the experimental values in both cases. It can be readily observed that the steady state viability drops sharply at lower dilution rates. Steady state chemostat operation is in general very difficult when viability falls below 50%. Small fluctuations in growth rate can result in washout. Therefore, model predictions at low growth rate regions are of little significance for chemostat cultures, however, very important for perfusion cultures. This type of culture is not subject to washout and a very low quasi steady state growth rate can be achieved.

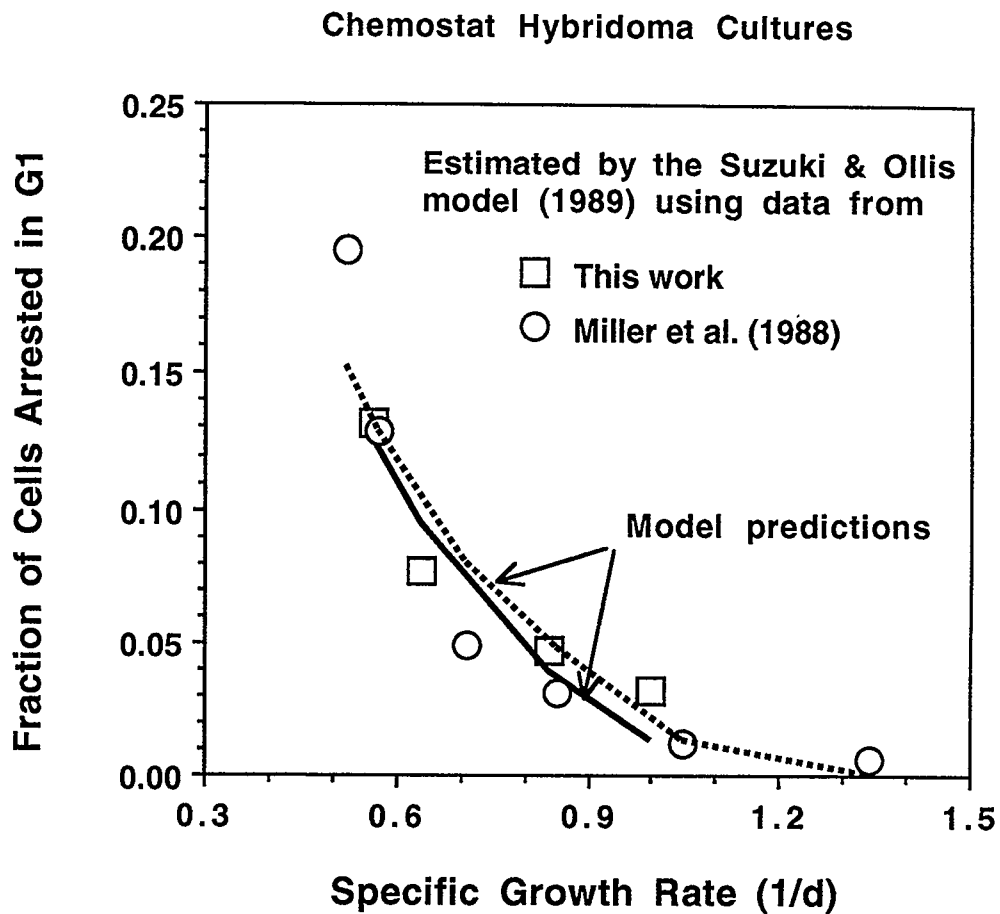


Figure 9.4 The profile of the fraction of G_1 arrested cells versus the specific growth rate in steady state chemostat cultures.

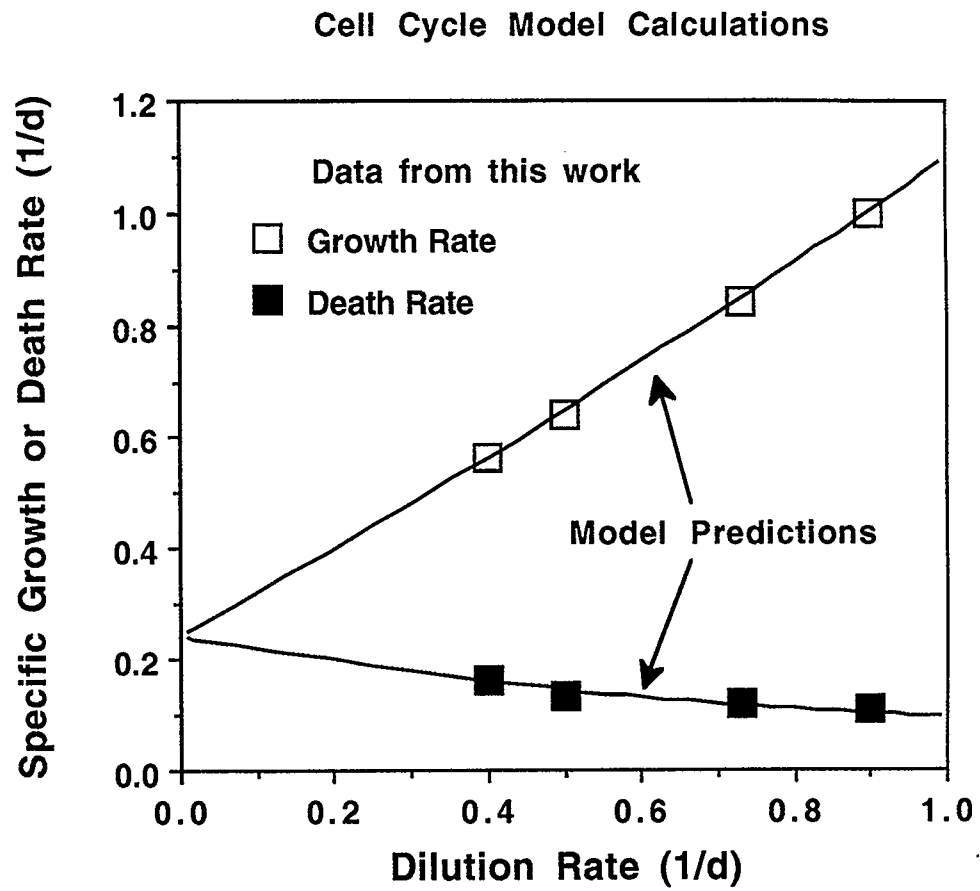


Figure 9.5 Comparison of the model predictions with experimental data of specific growth and death rates from this work.

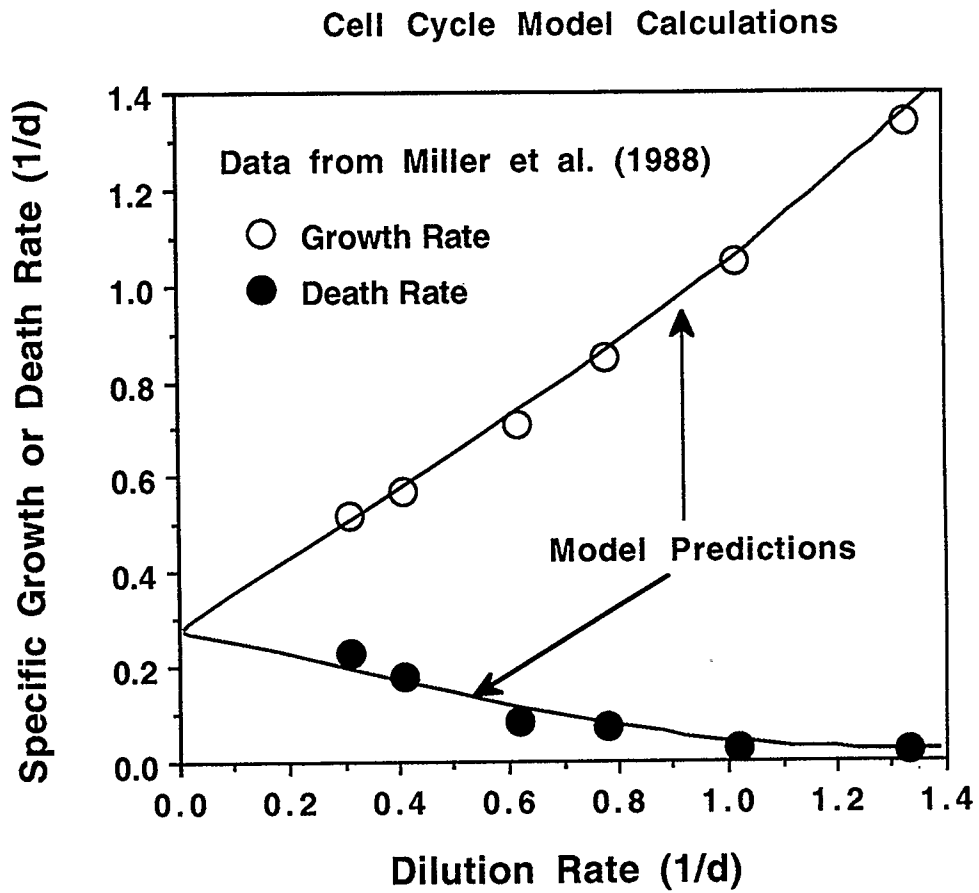


Figure 9.6 Comparison of the model predictions with experimental data of specific growth and death rates reported by Miller et al. (1988).

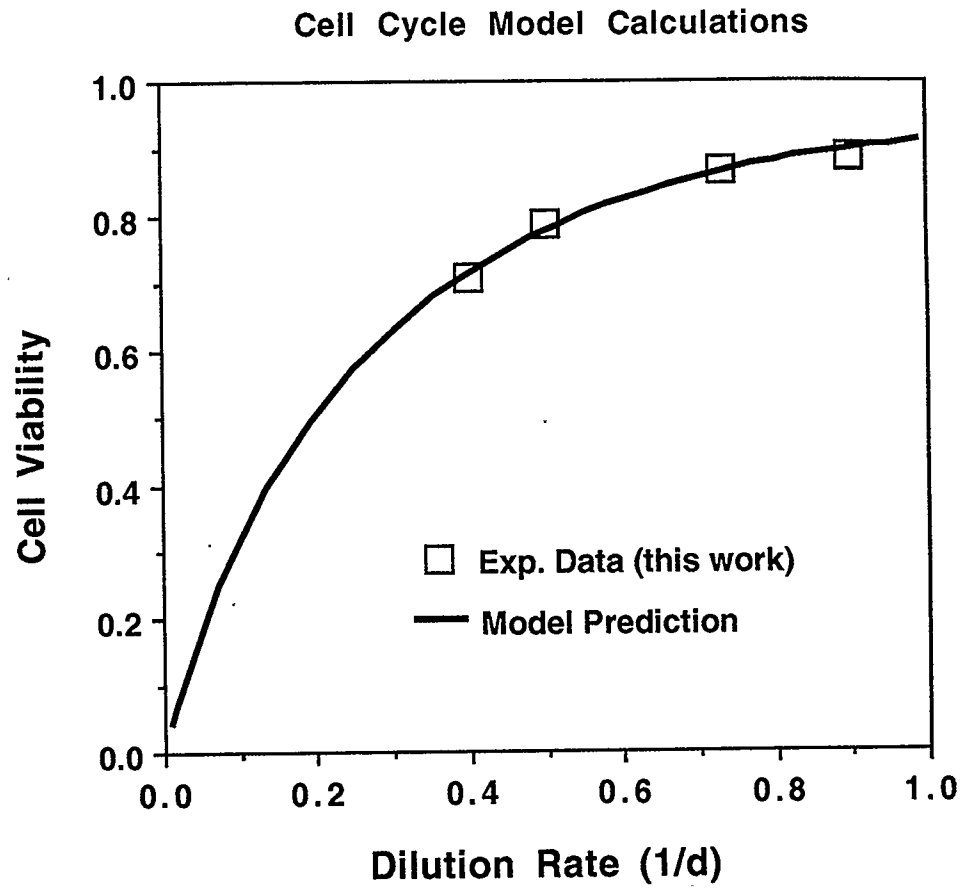


Figure 9.7 Comparison of the model predictions with experimental data of cell viability in steady state chemostat cultures.

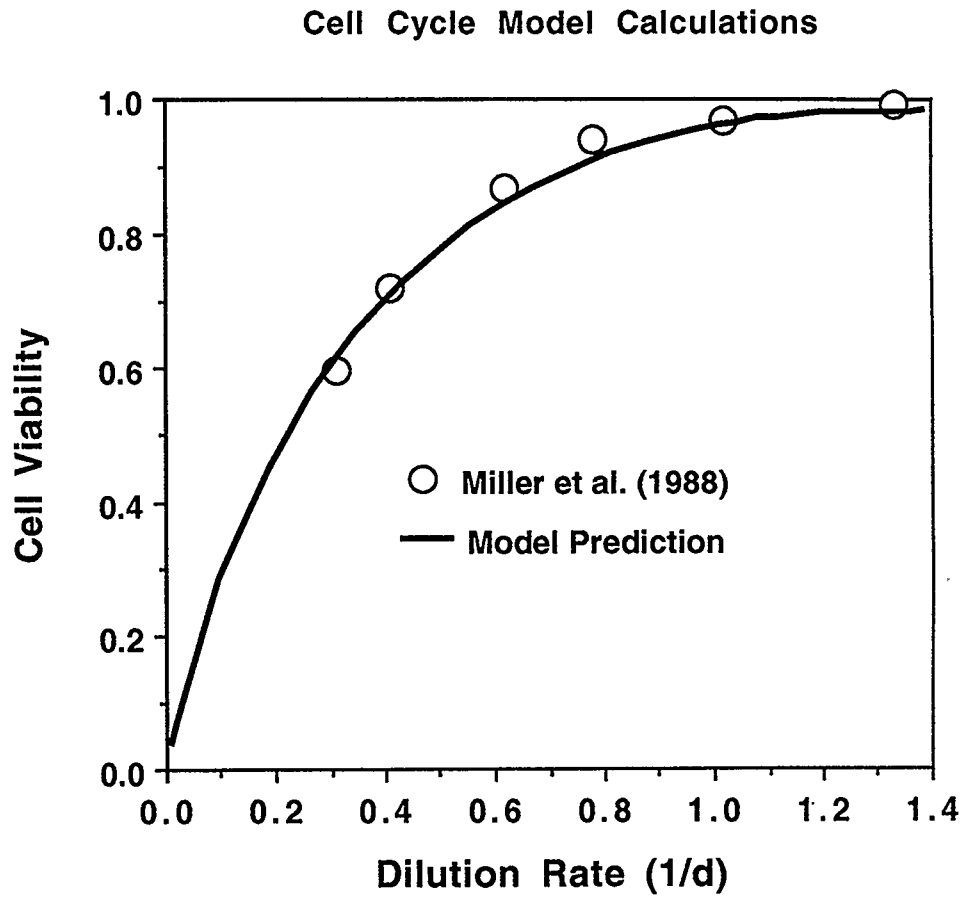


Figure 9.8 Comparison of the model predictions with experimental data of cell viability reported by Miller et al. (1988).

Figures 9.9 and 9.10 show the calculated profiles of the cell fractions f_0 , f_1 and f_B for the two data sets. As expected, the arrested cell fraction f_0 increases continuously with decreasing dilution (or growth) rate. The behavior of the fraction f_1 is, however, non monotonic. Initially f_1 increases with decreasing growth rates as the cells shift from phase B to state A but remain in the cycling fraction. A plateau is reached at an intermediate dilution rate and at very low dilution rates, as growth slows down, the cells become arrested and hence, the fraction of cycling state A cells, f_1 , decreases again. after the exponential phase of growth (data not shown).

Finally, Suzuki and Ollis (1989a) suggested that the average cycle time increases continuously with decreasing growth rate. Calculations using the proposed cell cycle model indicate the same type of behavior, as shown in Figure 9.11, where the model predictions are given for both data sets. In addition, the model predictions of t_c as a function of μ are identical for the two data sets. This was expected since for a given growth rate, t_c is only a function of f_0 and the difference in the estimated f_0 values is very small, as shown in Figure 9.4.

9.5. CONCLUDING REMARKS

Using experimental data reported in this thesis as well as data in the literature from chemostat hybridoma cultures it has been shown that the steady state specific death rate in chemostat hybridoma cultures is a function of the cell fraction arrested in the G_1 phase of the cell cycle.

A simple cell cycle model has been proposed that describes the steady state specific death and growth rates as well as the cell viability in chemostat hybridoma cultures. Furthermore, the proposed model is able to predict the steady state cell fractions in the cycling and arrested subcompartments of the cell cycle. The average cycle time can be readily estimated as a function of growth rate.

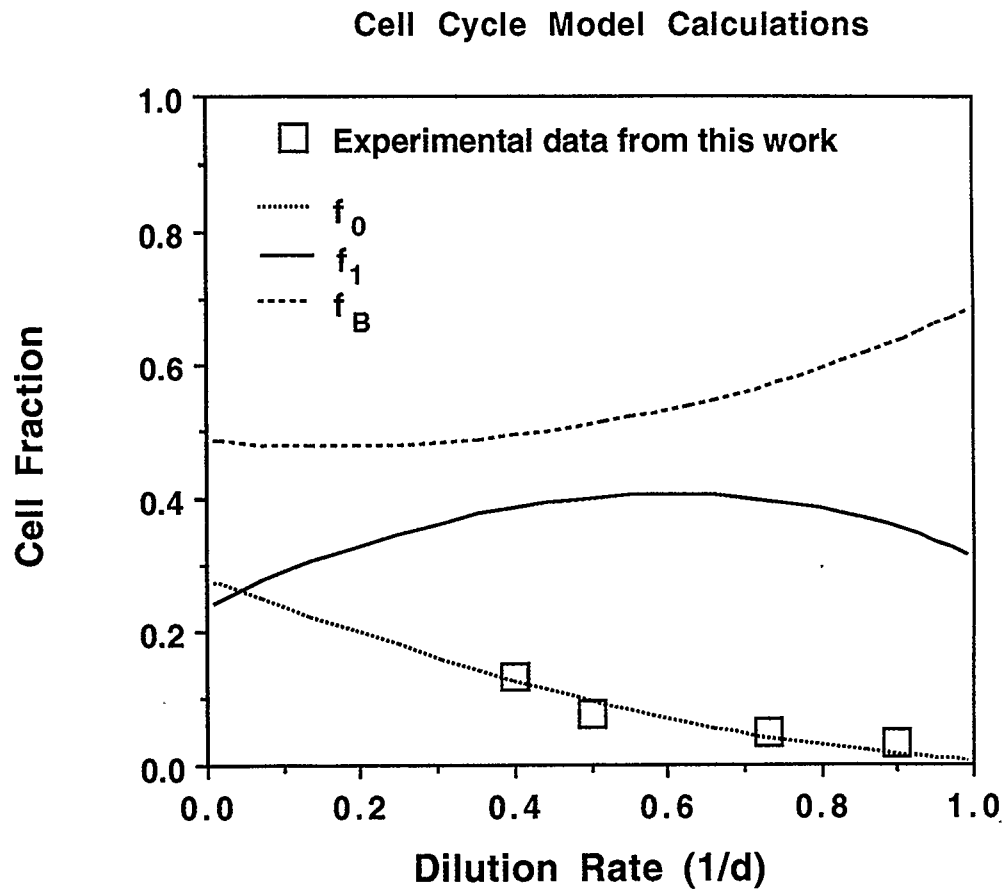


Figure 9.9 Model predictions of cell fractions in the division cycle for a range of dilution rates. The parameters used were computed from the chemostat data reported in this work.

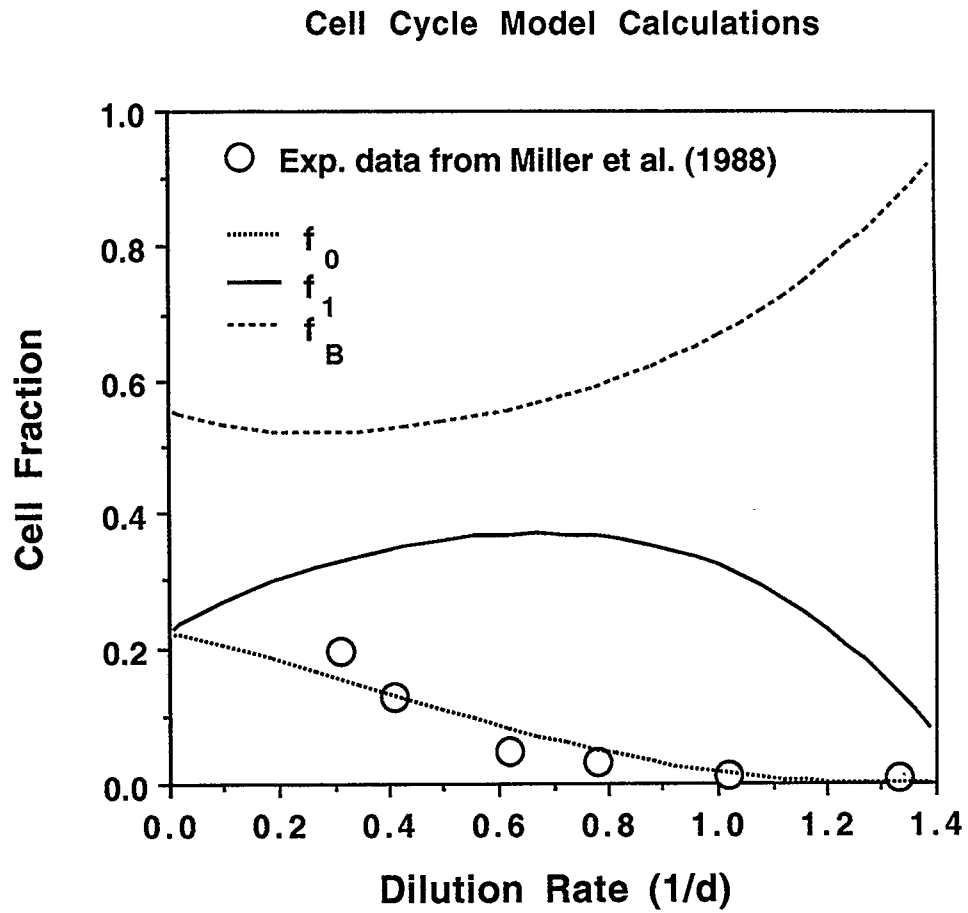


Figure 9.10 Model predictions of cell fractions in the division cycle for a range of dilution rates. The parameters used were computed from the chemostat reported by Miller et al. (1988).

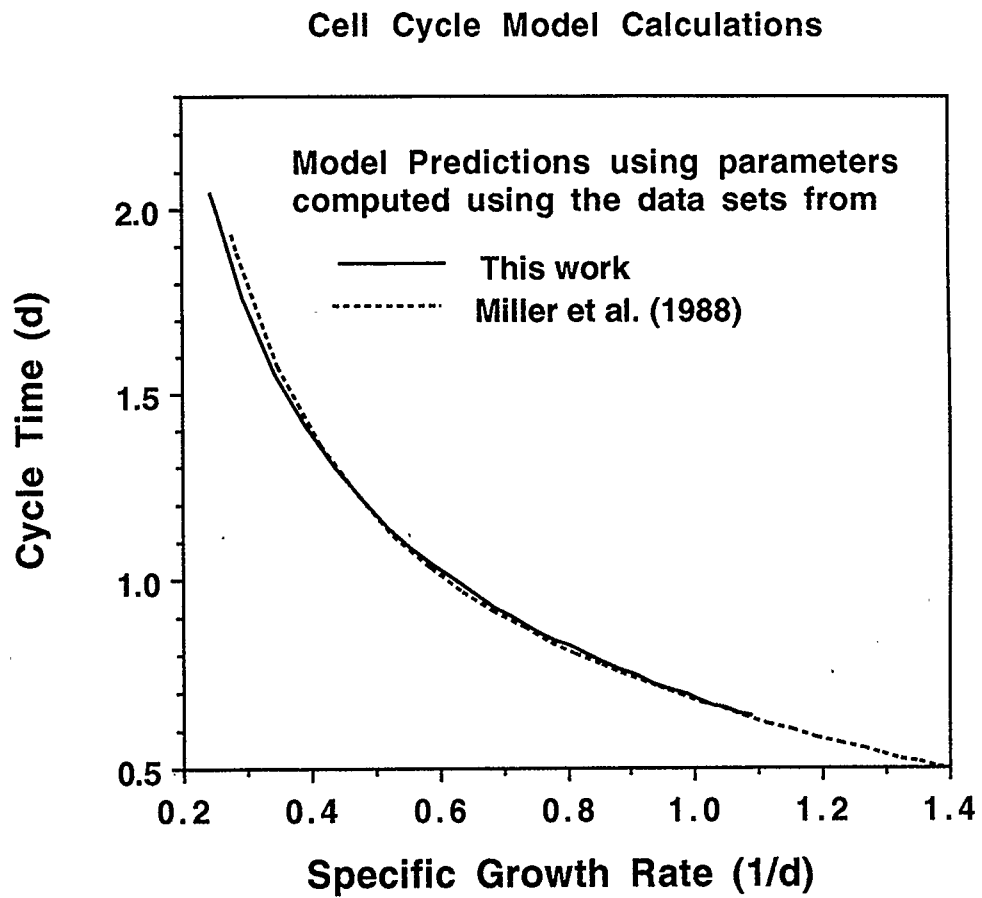


Figure 9.11 Model predictions of the average cycle time as a function of the specific growth rate in a chemostat bioreactor.

Overall, an excellent agreement was observed between the calculated and the experimental data from this work and from the literature.

10. CONCLUSIONS AND RECOMMENDATIONS

10.1 CONCLUSIONS

A series of batch and continuous (chemostat) experiments were performed using a commercially important anti-Lewis^b producing hybridoma cell line, property of Chembiomed Ltd. (Edmonton). The main objective of the experiments was to examine the kinetics of MAb production and at the same time investigate methods of overcoming production bottlenecks in bioreactor cultures. The inhibiting effect of the waste byproduct ammonia was the main target of our efforts.

Data from a large number of batch spinner flask cultures were used to examine the effect of glutamine content of the medium on ammonia production, cell growth and MAb production. It was shown that glutamine cannot be replaced either by a TCA cycle intermediate such as glutamate and ketoglutarate, or by glucose which is considered to be a nutrient complementary to glutamine. In addition, it was shown that media with an increased glutamine content could support a significantly higher cell density and MAb production in batch spinner flask cultures. An important inhibiting factor in stirred suspension cultures is the hydrodynamic shear stress. In contrast to growth inhibition by ammonia, growth inhibition by shear stress appeared easier to control. Addition of 0.1% (w/v) methylcellulose to the culture medium restored normal cell growth at stirrer speeds as high as 560 RPM.

Results from chemostat cultures were collected during many months of continuous operation of 1.5 L Celligen bioreactors. The uptake of nutrients, cell death and MAb production were determined as functions of the growth rate. The effect of culture pH, studied in a second set of chemostat runs, was found to be significant. The cell density, viability, MAb production and the specific glucose uptake rate were strong functions of the pH. This fact emphasizes the need for careful selection and accurate control of the operating conditions in cultures used for commercial MAb production. The DO on the other hand had no effect within a range from 15% to 60% of saturation. In the last

series of chemostat cultures glucose was partially replaced by glutamine in the feed medium. The objective was to compare the results with results from the corresponding batch experiment. Based on the batch culture results one would expect a positive effect on the culture. However, strong inhibition on cell growth was apparent and it was attributed to increased ammonia production due to the high concentration of glutamine. The interesting conclusion is that culture media optimized for one mode of operation (e.g. batch) may not be optimal for another (e.g. chemostat).

An important part of the experimental work was the development and operation of the dialyzed chemostat bioreactor. MAb productivity and cell density in the new reactor were 40% higher than in a conventional chemostat. It is believed that proper optimization of the feed and dialysis media can lead to much higher productivities, especially at low growth rates. Furthermore, the dialyzed chemostat shows promise as a tool for kinetic studies, since it allows independent manipulation of the growth rate on one hand and the nutrient and waste product concentrations on the other.

A simple empirical model was developed using steady state data from the chemostat cultures. The underlying idea in the model development was the use of the specific death rate to quantify the effect of stress on the culture. Our answer to the debate about the dependence of the specific MAb production rate on the growth rate was that the specific MAb production rate is actually a linear function of the specific death rate. Furthermore, it was shown that at steady state conditions an exponential relationship connected the death rate to the inverse of the growth rate. The effect of cell stress on the glucose uptake was also found to be important, especially at low growth rates. The Generalized Maintenance Energy equation that was proposed extended the maintenance energy model to take into account the effect of cell stress on the nutrient utilization. In general, excellent agreement was observed between the model predictions and chemostat data from this work and from the literature.

Finally, a cell cycle model was developed. A simple linear equation described the relationship between the specific death rate at steady state and the fraction of cells

arrested in the G_1 phase of the cycle. The cell age distributions in the indeterminate portion of the cycle were analytically calculated and were used to determine the cell fractions in various cycle compartments as functions of the dilution rate. Again, the predictions of the cell cycle model were in excellent agreement with chemostat data from this work and from the literature.

10.2 RECOMMENDATIONS

In the previous section the conclusion was reached that the optimum medium formulation depends strongly on the type of the culture. Therefore, common media used in continuous cultures are probably far from being optimum, since they were developed for batch cultures and for cell lines potentially very different than the ones they are used for. The above analysis implies that media optimization for continuous cultures will have very impressive results. Very positive results on batch cultures were published recently by Jo et al (1990).

The effects of glutamine substitution by glutamate and ketoglutaric acid should be studied in chemostat cultures. Addition of KGA had a positive effect in batch cultures and further investigation may be warranted. Furthermore, long term cell adaptation to the various glutamine replacements may produce a positive effect, as the conducted preliminary experiments seemed to indicate.

The dialyzed chemostat showed promise and effort should be devoted in optimizing both the feed and dialysis medium. Moreover, it is expected that low growth rates (i.e high specific MAb production rates) can be achieved without a significant drop in the viable cell density. Therefore, there is significant room for improvement with respect to the MAb production in the dialyzed chemostat.

Death rate was shown in this work to be a function of cell position in the cycle. The same effect was shown for the MAb production by many researchers. Cell cycle modeling is made simple and attractive by the recent popularization of flow cytometric techniques. It is expected that in the near future cell cycle modeling will encompass other important aspects of the cell behavior, mainly metabolism.

11. REFERENCES

1. Abu-Reesh I., Kargi F. 1989. Biological responses of hybridoma cells to defined hydrodynamic shear stress. *J. Biotechnol.* **9**: 167-178.
2. Adamson S.R., Fitzpatrick S.L., Behie L.A., Gaucher G.M., Lesser B.H. 1983. *In vitro* production of high titer monoclonal antibody by hybridoma cells in dialysis culture. *Biotechnol. Lett.* **5**: 573-578.
3. Alberghina L., Mariani L. 1978. Control of cell growth and division. p. 85-102 In: A.J. Valleron and P.D.M. Macdonald (ed.), *Biomathematics and Cell Kinetics*. Elsevier/North-Holland Biomedical Press.
4. Alberts B., Bray D., Lewis J., Raff M., Roberts K., Watson J.D. 1983. *Molecular Biology of the Cell*. Garland, New York.
5. Al-Rubeai M., Oh S.K.W., Musaheb R., Emery A.N. 1990. Modified cellular metabolism in hybridomas subjected to hydrodynamic and other stresses. *Biotechnol. Lett.* **12**: 323-328.
6. Augenstein D.C., Sinskey A.J., Wang D.I.C. 1971. Effect of shear on the death of two strains of mammalian tissue cells. *Biotechnol. Bioeng.* **13**: 409-418.
7. Backer M.P., Metzger L.S., Slaber P.L., Nevitt K.L., Boder G.B. 1988. Large-scale production of monoclonal antibodies in suspension culture. *Biotechnol. Bioeng.* **32**: 993-1000.
8. Balin A., Goodman D.B.P., Rasmussen H., Cristofalo V. 1976. The effect of oxygen tension on the growth and metabolism of WI-38 cells. *J. Cell. Physiol.* **89**: 235-250.
9. Baltzis B.C., Fredrickson A.G. 1988. Limitation of growth rate by two complementary nutrients: Some elementary but neglected considerations. *Biotechnol. Bioeng.* **31**: 75-86.
10. Batt B.C, Kompala D.S. 1987. Structured kinetic modeling of hybridoma growth and monoclonal antibody production in continuous suspension

- cultures. Paper presented at the ACS National Meeting, New Orleans.
11. Bibila T., Flickinger M.C. 1991. A structured model for monoclonal antibody synthesis in exponentially growing and stationary phase hybridoma cells . *Biotechnol. Bioeng.* **37**: 210-226.
 12. Birch J.R., Edwards D.J. 1980. The effect of pH on the growth and carbohydrate metabolism of a lymphoblastoid cell line. *Develop. Biol. Standard.* **46** : 59-63.
 13. Birch J.R., Thompson P.W., Lambert K., Boraston R. 1984. The large-scale cultivation of hybridoma cells producing monoclonal antibodies. Paper presented at the ACS Annual Meeting, Philadelphia.
 14. Blank L. 1980. *Statistical Procedures for Engineering, Management, and Science.* McGraw Hill, New York.
 15. Bole D.G., Hendershot L.M., Kearney J.F. 1986. Posttranslational association of immunoglobulin heavy chain binding protein with nascent heavy chains in nonsecreting and secreting hybridomas. *J. Cell Biol.* **102**: 1558-1566.
 16. Boraston R., Thompson P.W., Garland S., Birch J.R. 1984. Growth and oxygen requirements of antibody-producing mouse hybridoma cells in suspension culture. *Develop. Biol. Standard.* **55**: 103-111.
 17. Bowen I.D. 1981. Techniques for Demonstrating Cell Death. p. 379-444 In: I.D. Bowen and R.A. Lockshin (ed.), *Cell Death in Biology and Pathology.* Chapman and Hall, New York.
 18. Bree M., Dhurjati P., Geoghegan R.F., Robnett B. 1988. Kinetic modeling of hybridoma cell growth and immunoglobulin production in a large scale suspension culture. *Biotechnol. Bioeng.* **32**: 1067-1072.
 19. Brooks R.F. 1979. The cytoplasmic origin of variability in the timing of S phase in mammalian cells. *Cell Biol. Int. Rep.* **3**: 707-716.
 20. Brooks R.F. 1977. continuous protein synthesis is required to maintain the

- probability of entry into S phase. *Cell* **12**: 311-317.
21. Burill G.S., Lee K.B. Jr. 1990. *Biotech 91: A changing environment*. Ernst & Young. San Fransisco, California.
 22. Burns F.J., Tannock I.F. 1970. On the existence of a G_0 -phase in the cell cycle. *Cell Tissue Kinet.* **3**: 321-334.
 23. Cook J.R, James T.W. 1964. Age distribution of cells in logarithmically growing cell populations. p. 485-495 In: E. Zeuthen (ed.), *Synchrony in Cell Division and Growth*. Interscience Publishers, New York.
 24. Dalili M., Sayles G.D., Ollis D.F. 1990. Glutamine-limited batch hybridoma growth and antibody production: experiment and model. *Biotechnol. Bioeng.* **36**: 74-82.
 25. Darzynkiewicz Z., Sharpless T., Staiano-Coico L., Melamed M.R. 1980. Subcompartments of the G1 phase of cell cycle detected by flow cytometry. *Proc. Nat. Acad. Sci. USA* **77**: 6696-6699.
 26. Dodge T.S., Hu W.S. 1986. Growth of hybridoma cells under different agitation conditions. *Biotechnol. Lett.* **8**: 683-686.
 27. Dodge T.S., Ji G.Y., Hu W.S. 1987. Loss of viability in hybridoma cell culture - A kinetic study. *Enzyme Microb. Technol.* **9**: 607-611.
 28. Doyle C., Butler M. 1990. The effect of pH on the toxicity of ammonia to a murine hybridoma. *J. Biotechnol.* **15**: 91-100.
 29. Emery A.N., Lavery M., Williams B., Handa A. 1987. Large-scale hybridoma culture p. 137-146. In : C.Webb and F. Mavituna (ed.), *Plant and Animal Cells: Process Possibilities*. Ellis Horwood Ltd., Chichester.
 30. Flickinger M.C., Goebel N.K., McNeil D., Bergold A., Bohn M., Karl D.W. 1987. A total cell recycling reactor for investigation of hybridoma maintenance energy demand and monoclonal antibody modification. Paper presented at the 194th ACS National Meeting, New Orleans.
 31. Frame K.K., Hu W.-S. 1991. Kinetic Study of Hybridoma Cell Growth in Con-

- tinuous Culture. I. A model for non-producing cells. *Biotechnol. Bioeng.* **37**: 55-64.
32. Frame K.K., Hu W.-S. 1985. Oxygen uptake of mammalian cells in microcarrier culture. Response to changes in glucose concentration. *Biotechnol. Lett.* **7**: 147-152.
 33. Garatun-Tjeldsto O., Pryme I.F., Weltman J.K., Dowbe R.M. 1976. synthesis and secretion of light-chain immunoglobulin in two successive cycles of synchronized plasmacytoma cells. *J. Cell Biol.* **68**: 232-239.
 34. Glacken M.W., Adema E., Sinskey A.J. 1988. Mathematical description of hybridoma culture kinetics: I. initial metabolic rates. *Biotechnol. Bioeng.* **32**: 491-506.
 35. Glacken, M.W., Fleischaker R.J., Sinskey A.J. 1986. Reduction of waste product excretion via nutrient control: possible strategies for maximizing product and cell yields on serum in cultures of mammalian cells. *Biotechnol. Bioeng.* **28**: 1376-1389.
 36. Goding J.W. 1983. *Monoclonal antibodies: Principles and Practice.* Academic Press Inc. London.
 37. Golding B., Pillemer S.R., Roussou P., Peter E.A., Tsokos G.C., Ballow J.E., Hoffman T. 1988. Inverse relationship between proliferation and differentiation in a human TNP-specific B cell line. Cell cycle dependence of antibody secretion. *J. Immunol.* **131**: 2564-2568.
 38. Goochee C.F., Passini C.A. 1988. Intracellular proteins produced by mammalian cells in response to environmental stress. *Biotechnol. Prog.* **4**: 189-201.
 39. Hagedorn J., Kargi F. 1990. Production of monoclonal antibodies by hybridoma cells in a flat sheet membrane bioreactor. *Biotechnol. Prog.* **6**: 220-224.
 40. Hecht V., Bischoff L., Gerth K. 1990. Hollow fiber supported gas membrane

- for in situ removal of ammonium during an antibiotic fermentation. *Biotechnol. Bioeng.* **35**: 1042-1050.
41. Hu W.S., Dodge T.C., Frame K.K., Himes V.B. 1987. Effect of glucose on the cultivation of mammalian cells. *Develop. Biol. Standard.* **66**: 279-290.
 42. Jo E.C., Park H.J., Park J.M., Kim K.H. 1990. Balanced nutrient fortification enables high density hybridoma cell culture in batch culture. *Biotechnol. Bioeng.* **37**: 717-722.
 43. Jöbses I., Martens D., Tramper J. 1991. Lethal events during gas sparging in animal cell culture. *Biotechnol. Bioeng.* **37**: 484-490.
 44. Kearns M. 1990. Integrated Design for Mammalian Cell Culture. *Bio/Technology* **8**: 409-413.
 45. Kilburn D.G., Webb F.C. 1968. The cultivation of animal cells at controlled dissolved oxygen partial pressure. *Biotechnol. Bioeng.* **10**: 801-814.
 46. Köhler G., Milstein C. (1975). Continuous cultures of fused cells secreting antibody of predefined specificity. *Nature* **256**: 495-497.
 47. Kunas K.T., Papoutsakis E.T. 1990. Damage mechanisms of suspended animal cells in agitated bioreactors with and without bubble entrainment. *Biotechnol. Bioeng.* **36**: 476-483.
 48. Lanks K.W., Li P.W. 1988. End products of glucose and glutamine metabolism by cultured cell lines. *J. Cell. Physiol.* **135**: 151-155.
 49. Lavery M., Kearns M.G., Price D.G., Emery A.N., Jefferis R., Nienow A.W. 1985. Physical conditions during batch culture of hybridomas in laboratory scale stirred tank reactors. *Develop. Biol. Standard.* **60**: 199-206.
 50. Lee G.M., Huard T.K., Kaminski M.S., Pallson B.O. 1988. Effect of mechanical agitation on hybridoma cell growth. *Biotechnol. Lett.* **10**: 625-628.
 51. Leist C.H., Meyer H.P., Fiechter A. 1990. Potential and problems of animal cells in suspension culture. *J. Biotechnol.* **15**: 1-46.
 52. Linardos T., Kalogerakis N., Behie L.A. 1991a. Cell cycle model for growth

- rate and death rate in hybridoma chemostat cultures. *Biotechnol. Bioeng.* submitted.
53. Linardos T., Kalogerakis N., Behie L.A., Lamontagne L.R. 1991b. Monoclonal antibody production in a dialyzed chemostat. *Biotechnol. Bioeng.* submitted.
 54. Linardos T., Kalogerakis N., Behie L.A., Lamontagne L.R. 1991c. The effect of Specific Growth Rate and Death Rate on Monoclonal Antibody Production in Hybridoma Chemostat Cultures. *Can. J. Chem. Eng.* **69**: 429-438.
 55. Linardos T., Kalogerakis N., Behie L.A. 1988. Monoclonal antibody production in a cost effective medium. Report submitted to Biotechnology Research Institute, Montreal.
 56. Lloyd D., Poole R.K., Edwards S. W. 1982. *The Cell Division Cycle. Temporal Organization and Control of Cellular Growth and Reproduction.* Academic Press, London.
 57. Low K., Harbour C. 1985. Growth kinetics of hybridoma cells: (2) The effects of varying energy source concentrations. *Develop. Biol. Standard.* **60**: 73-79.
 58. Luan Y.T., Mutharasan R., Magee W.E. 1987a. Factors Governing Lactic Acid Formation in Long Term Cultivation of Hybridoma Cells. *Biotechnol. Lett.* **9**: 751-756.
 59. Luan Y.T., Mutharasan R., Magee W.E. 1987b. Strategies to extend longevity of hybridomas in culture and promote yield of monoclonal antibodies. *Biotechnol. Lett.* **9**: 691-696.
 60. Luan Y.T., Mutharasan R., Magee W.E. 1987c. Effect of various glucose/glutamine ratios on hybridoma growth, viability and monoclonal antibody formation. *Biotechnol. Lett.* **9**: 535-538.
 61. deMaerteler V. 1978. Cell Loss from Germinative Cell Populations. p. 103-116 In: A.J. Valleron and P.D.M. Macdonald (ed.), *Biomathematics and Cell*

Kinetics. Elsevier/North-Holland Biomedical Press.

62. Marques-Pereira J.P., Leblond C.P. 1965. Mitosis and Differentiation in the Stratified Squamous Epithelium of the Rat Esophagus. *Amer. J. Anat.* **117**: 73-90.
63. McQueen A., Bailey J.E. 1990. Effect of ammonium ion and extracellular pH on hybridoma cell metabolism and antibody production. *Biotechnol. Bioeng.* **35**: 1067-1077.
64. McQueen A., Meilhoc E., Bailey J.E. 1987. Flow effects on the viability and lysis of suspended mammalian cells. *Biotechnol. Lett.* **9**: 831-836.
65. Miller W.M., Wilke C.R., Blanch H.W. 1989a. Transient Responses of Hybridoma Cells to Nutrient Additions in Continuous Culture: I. Glucose Pulse and Step Changes. *Biotechnol. Bioeng.* **33**: 477-486.
66. Miller W.M., Wilke C.R., Blanch H.W. 1989b. Transient Responses of Hybridoma Cells to Nutrient Additions in Continuous Culture: II. Glutamine Pulse and Step Changes. *Biotechnol. Bioeng.* **33**: 487-499.
67. Miller W.M., Blanch H.W., Wilke C.R. 1988. A Kinetic Analysis of Hybridoma Growth and Metabolism in Batch and Continuous Suspension Culture: Effect of Nutrient Concentration, Dilution Rate, and pH. *Biotechnol. Bioeng.* **32**: 947-965.
68. Miller W.M., Wilke C.R., Blanch H.W. 1987. Effects of Dissolved Oxygen Concentration on Hybridoma Growth and Metabolism in Continuous Culture. *J. Cell. Physiol.* **132**: 524-530.
69. Munro S., Pelham H.R.B. 1986. An Hsp70-like Protein in the ER: Identity with the 78 kd Glucose-Regulated Protein and Immunoglobulin Heavy Chain Binding Protein. *Cell* **46**: 291-30.
70. Ozturk S.S., Pallson B.O. 1990. Chemical decomposition of glutamine in cell culture media: Effect of media type, pH, and serum concentration. *Biotechnol. Prog.* **6**: 121-128.

71. Pardee A.B. 1989. G1 Events and Regulation of Cell Proliferation. *Science* **246**: 603-608.
72. Passini C.A., Goochee C.F. 1989. Response of a Mouse Hybridoma Cell Line to Heat Shock, Agitation and Sparging. *Biotechnol. Prog.* **5**: 175-18.
73. Petersen J.F., McIntire L.V., Papoutsakis T.E. 1988. Shear sensitivity of cultured hybridoma cells (CRL-8018) depends on mode of growth, culture age and metabolite concentration. *J. Biotechnol.* **7**: 229-246.
74. Pirt S.J. 1975. *Principles of Microbe and Cell Cultivation*. Blackwell Sc. Publications, Cambridge.
75. Prescott D.M. 1976. *Reproduction of Eukaryotic Cells*. Academic Press, New York.
76. Quastler H., Sherman F.G. 1959. Cell Population Kinetics in the Intestinal Epithelium of the Mouse. *Exp. Cell Res.* **17**: 420-438.
77. Rabinovitch P.S. 1983. Regulation of Human Fibroblast Growth Rate by both Noncycling Fraction and Transition Probability is Shown by Growth in 5-bromodeoxyuridine Followed by Hoechst 33258 Flow Cytometry. *Proc. Natl. Acad. Sci. U.S.A.* **80**: 2951-2955.
78. Ramirez O.T., Mutharasan R. 1990. Cell Cycle- and Growth Phase-Dependent Variations in Size Distribution, Antibody Productivity, and Oxygen Demand in Hybridoma Cultures. *Biotechnol. Bioeng.* **36**: 839-848.
79. Ramirez O.T., Mutharasan R. 1989. The role of plasma membrane fluidity on the shear sensitivity of hybridomas grown under hydrodynamic stress. Paper presented at the AIChE National Meeting, San Fransisco.
80. Reitzer L.J., Wice B.M., Kennell D. 1979. Evidence that Glutamine, not Sugar, is the Major Energy source for cultured He-La Cells. *J. Biol. Chem.* **254**: 2669-2676.
81. Reuveny S., Velez D., Riske F., Macmillan J.D., Miller L. 1987. Factors affecting Monoclonal Antibody Production in Culture. *Develop. biol. Stan-*

- dard. **66**: 169-175.
82. Reuveny S., Velez D., Macmillan J.D., Miller L. 1986. Factors affecting cell growth and monoclonal antibody production in stirred reactors. *J. Immunol. Meth.* **86**: 53-59.
 83. Reuveny S., Velez D., Riske F., Macmillan J.D., Miller L. 1985. Production of Monoclonal Antibodies in Culture. *Develop. biol. Standard.* **60**: 185-197.
 84. Ronning O.W., Seglen P.O. 1982. The Relation Between Protein Accumulation and Cell Cycle Traverse of Human NHIK 3025 Cells in Unbalanced Growth. *J. Cell. Physiol.* **112**: 19-26.
 85. Sanbrook J., Fritsch E.F., Maniatis T. 1989. *Molecular Cloning. A Laboratory Manual.* Cold Spring Harbor Laboratory Press, New York.
 86. Schliermann M., Beckers C., Miltenburger H.G. 1987. Cell cycle analysis by flow cytometry in an antibody secreting line. *Develop. biol. Standard.* **66**: 101-109.
 87. Schneiderman M.H., Dewey W.C., Highfield D.P. 1971. Inhibition of DNA synthesis in Synchronized Chinese Hamster Cells Treated in G1 with Cycloheximide. *Exp. Cell Res.* **67**: 147-155.
 88. Schürch U., Kramer H., Einsele A., Widmer F., Eppenberger H.M. 1988. Experimental evaluation of laminar shear stress on the behavior of hybridoma mass cell cultures, producing monoclonal antibodies against mitochondrial creatine kinase. *J. Biotechnol.* **7**: 179-184.
 89. Seaver S.S. (ed.) 1987. *Commercial Production of Monoclonal Antibodies. A Guide for Scale-Up.* Marcell Dekker Inc., New York.
 90. Shields R. 1979. Transition Probability and the Division Pattern of WI-38 Cells. *Cell Biol. Int. Rep.* **3**: 659-662.
 91. Shields R. 1978. Further Evidence for a Random Transition in the Cell Cycle. *Nature* **273**: 755-758.
 92. Shields R., Brooks R., Riddle P., Capellaro D., Delia D. 1978. Cell Size, Cell

- Cycle and Transition Probability in Mouse Fibroblasts. *Cell* **15**: 469-474.
93. Shields R., Smith J.A. 1977. Cells Regulate their Proliferation through Alterations in Transition Probability. *J. Cell. Physiol.* **91**: 345-356.
 94. Smith J.A., Martin L. 1974. Regulation of cell proliferation. p. 43-60 In: G.M.Padilla, I.L. Cameron and A. Zimmerman (ed.), *Cell Cycle Controls*. Academic Press, New York.
 95. Smith J.A., Martin L. 1973. Do cells cycle? *Proc. Nat. Acad. Sci. USA* **70**: 1263-1267.
 96. Stavroulakis D.A. 1990. Growth characteristics of a *Bombyx mori* cell line in stationary and suspension cultures. M.Sc. Thesis, University of Calgary.
 97. Sureshkumar G.K, Mutharasan R. 1991. The influence of temperature on a mouse-mouse hybridoma growth and monoclonal antibody production. *Biotechnol. Bioeng.* **37**: 292-295.
 98. Suzuki E., Ollis D.F. 1989a. Cell Cycle Model for Antibody Production Kinetics. *Biotechnol. Bioeng.* **34**: 1398-140.
 99. Suzuki E., Ollis D.F. 1989b. Antibody Production Kinetics of Hybridomas at Slow or Non-growth States. paper presented at the AIChE National Meeting, San Fransisco.
 100. Thayer A.M. 1991. Revenues grow for some biotech companies. *Chem. and Engin. News* **April 1** : 21-22.
 101. Thayer A.M. 1990. Emerging biotechnology products focus of patent disputes. *Chem. and Engin. News* **February 5**: 17-19.
 102. Tovey M., Brouty-Boye D. 1976. Characteristics of the Chemostat Culture of Murine Leukemia L1210 cells. *Exp. Cell. Res.* **101**: 346-354.
 103. Tritsch G.L., Moore G.E. 1962. Spontaneous Decomposition of Glutamine in Cell Culture Media. *Exp. Cell. Res.* **28**: 360-364.
 104. Truskey G.A., Nicolakis D.P., Dimasi D., Haberman A., Swartz R.W. 1990. Kinetic studies and unstructured models of lymphocyte metabolism in fed-

- batch culture. *Biotechnol. Bioeng.* **36**: 797-807.
105. Velez D., Reuveny S., Miller L., Macmillan J.D. 1986. Kinetics of monoclonal antibody production in low serum growth medium. *J. Immunol. Meth.* **86**: 45-52.
 106. Wiedemann C., Moser H.A. 1988. An elementary approach to cell cycle analysis. *Acta Biother.* **37**: 205-236.
 107. Wohlpart D., Kirwan D., Gainer J. 1990. Effects of cell density and glutamine levels on the respiration rates of hybridoma cells. *Biotechnol. Bioeng.* **36**: 630-635.
 108. Yang J.-D., Wang N.S., Chang K.-C., Calabrese R.V. 1989. Hybridoma Cell Inactivation by Air Sparging in a Mechanically Agitated Bioreactor. *Biotechnol. Bioeng.* to appear (obtained through personal communication, January 1991)
 109. Yen A., Pardee A.B. 1978. Exponential 3T3 Cells Escape in Mid-G1 from their High Serum Requirement. *Exp. Cell Res.* **116**: 103-113.
 110. Zielke H.R., Submilla C.M., Sevdalian D.A., Hawkins R.L., Ozand P.T. 1980. Lactate: A major product of glutamine metabolism by human diploid fibroblasts. *J. Cell. Physiol.* **104**: 433-441.
 111. Zielke H.R., Ozand P.T., Tildon J.T., Sevdalian D.A., Cornblath M. 1978. Reciprocal regulation of glucose and glutamine utilization by human diploid fibroblasts. *J. Cell. Physiol.* **95**: 41-48.

12. APPENDIX A: DMEM Composition

The composition of the powdered medium used (Sigma D2902) is given below.

Component	<i>g/L</i>
L-Arginine · HCl	0.084
L-Cysteine · 2HCl	0.0626
L-Glutamine	0.729
Glycine free base	0.030
L-Histidine · HCl · H ₂ O	0.042
L-Isoleucine	0.105
L-Leucine	0.105
L-Lysine · HCl	0.146
L-Methionine	0.030
L-Phenylalanine	0.066
L-Serine	0.042
L-Threonine	0.095
L-Tryptophan	0.016
L-Tyrosine (2Na)	0.1038
L-Valine	0.094
Choline Chloride	0.004
Folic acid	0.004
Myo-Inositol	0.0072
Niacinamide	0.004
D-Pantothenic acid Ca	0.004
Pyridoxal HCl	0.004
Na Pyruvate	0.110
Riboflavin	0.004

Thiamine HCl	0.04
Calcium Chloride · 2H ₂ O	0.265
Ferric Nitrate · 9H ₂ O	0.0001
Magnesium Sulphate (Anhydrous)	0.09767
Potassium Chloride	0.400
Sodium Chloride	6.400
Sodium Phosphate Monobasic (Anhydrous)	0.109
Glucose	1.000

The standard medium we used in most experiments was supplemented with an extra 3.5 *g/L* of glucose. Therefore, the glucose concentration in the standard DMEM was 4.5 *g/L*.